PACIFIC EARTHQUAKE ENGINEERING
RESEARCH CENTER

Numerical Modeling of the Nonlinear Cyclic Response of Shallow Foundations

Chad Harden and Tara Hutchinson
Department of Civil and Environmental Engineering
University of California, Irvine

Geoffrey R. Martin
Department of Civil Engineering
University of Southern California

Bruce L. Kutter
Department of Civil and Environmental Engineering
University of California, Davis

PEER 2005/04
AUGUST 2005

Numerical Modeling of the Nonlinear Cyclic Response of Shallow Foundations

Chad Harden and Tara Hutchinson
Department of Civil and Environmental Engineering
University of California, Irvine

Geoffrey R. Martin
Department of Civil Engineering
University of Southern California

Bruce L. Kutter
Department of Civil and Environmental Engineering
University of California, Davis

PEER Report 2005/04
Pacific Earthquake Engineering Research Center
College of Engineering
University of California, Berkeley

August 2005

ABSTRACT

Understanding the nonlinear behavior of shallow building foundations under large-amplitude loading is an important aspect of performance-based earthquake engineering (PBEE). Soil yielding beneath foundations can be an effective energy-dissipation mechanism; however, this yielding may lead to excessive permanent deformations. The objective of this report is to develop and test procedures to account for foundation nonlinearity and uplift in PBEE.

In order to accurately represent PBEE in current design, a Winkler-type finite element mesh generator is written to simulate a shallow strip footing, and nonlinear springs are used to capture permanent displacements. The beam-on-nonlinear-Winkler foundation (BNWF) is chosen due to the familiarity of current engineering practice with the simplified Winkler approach. The model parameters, including material models and varying pressure and stiffness distributions, are calibrated against a suite of model centrifuge and one-g tests with a broad range of design vertical safety factors and by considering both clay and sand soil mediums. Numerical results show that a reasonable comparison between the nonlinear Winkler-based approach and the experimental data (moment, settlement, lateral displacement) can be obtained, given appropriate selection of soil properties.

Simulations using the Winkler model are extended to current code simplified design methods. Current methods account for increased displacement of an equivalent SDOF system relative to the reduced design strength, but not explicitly for the case of foundation uplift. Suggestions are made to account for foundation uplift in simplified design, as well as for incorporating Housner's rocking block model and empirical test data to estimate settlement.

ACKNOWLEDGMENTS

This research was supported primarily by the Pacific Earthquake Engineering Research Center's Program of the National Science Foundation under award number EEC-9701568 and PEER project number 2272001.2.

Any opinions, findings, and conclusions or recommendations expressed in this material are those of the authors and do not necessarily reflect those of the National Science Foundation.

Data for this study were provided by centrifuge experiments described in Rosebrook and Kutter (2001a, b, c) and Gajan et al. (2003a, b). In addition, Professor Paolo Negro at the European Laboratory for Structural Assessment (ELSA) in Italy provided one-g data sets from his experiments. Helpful suggestions by practicing engineers, Craig Comartin, of Comartin-Reis, and Mark Moore, of Rutherford and Chekene, were provided throughout the study. The above support is greatly appreciated.

CONTENTS

LIST OF FIGURES

LIST OF TABLES

LIST OF SYMBOLS

a	Moment arm
a_o	Vertical dashpot coefficient
c_u	Undrained shear strength
c, n	Constants that control the shape of the $q - z^p$ curve
C_{R-V}^K	Rotational stiffness deficit ratio
c_{Z1}	Vertical dashpot coefficient
COV	Coefficient of variation
C_1	Modification factor to relate expected maximum inelastic displacements to displacements calculated for linear elastic response
C_{1-ave}	Average value of C_1
C_2	Modification factor to represent the effects of pinched hysteresis shape, stiffness degradation, and strength deterioration on maximum displacement response (equal to 1 for linear procedure)
C_3	Modification factor to represent increased displacements due to dynamic $P-\Delta$ effects
C_m	Effective mass factor to account for higher mode participation
D_r	Relative density
D_{top}	Top displacement
d	Depth of footing
E	Elastic modulus
E_D	Hysteretic energy
E_s	Elastic strain energy
E_D^r	Energy associated with moment-rotational rocking
E_D^{LT}	Energy associated with lateral translation
E_D^{VT}	Energy associated with vertical vibration
F_H	Normalized horizontal load

F_M	Normalized moment
F_V	Normalized vertical load
FS_V	Vertical factor of safety
F_{qi}	Edge tip resistance ratio
g	Acceleration due to gravity
H	Horizontal load
H_y	Yield force of lateral system
I	Moment of inertia
I_y'	End region moment of inertia
K_{PE}	Seismic passive earth pressure
$K_{\theta x}$	Global rotational stiffness
$K_{\theta y}$	Global rotational stiffness
K_z	Global vertical stiffness
K_L	Lateral stiffness
k	subgrade modulus
$k_{\theta y}$	Subgrade rotational stiffness
k_z	Subgrade vertical stiffness
$k_{\theta x}$	Subgrade rotational stiffness
k_{mid}	Subgrade modulus, middle region
k_{end}	Subgrade modulus, end region
L_e	End region length
M	Moment
M_{cr}	Critical moment at incipient uplift
$M_{\max}$	Maximum moment
m	Mass
N_{qE}	Seismic bearing capacity factor, overburden
$N_{\gamma E}$	Seismic bearing capacity factor, unit weight

N_{cE}	Seismic bearing capacity factor, cohesion
PGA	Peak ground acceleration
PGV	Peak ground velocity
PGD	Peak ground displacement
p_{LE}	Seismic critical angle of rupture
Qred	Seismic bearing capacity reduction factor
q	Bearing pressure
q_{ult}	Ultimate bearing pressure
q_o	q at the start of the current plastic loading cycle
$q_{i-\exp}$	End tip contact pressure, from experiment
q_{i-calc}	End tip contact pressure, calculated
q_{ave}	Average bearing pressure
R	Ratio of elastic strength demand to calculated yield strength
SA	Spectrum acceleration
s	Settlement
T	Period
T_S	Characteristic period of the response spectrum
T_e	Effective fundamental period of the building
TP	Tension percentage
U_H	Normalized horizontal displacement
U_M	Rotation
U_V	Normalized vertical displacement (settlement)
u	Lateral base displacement
V	Pseudo lateral load
V_S	Shear wave velocity
W	Effective seismic weight
ZPA	Zero Period Acceleration
z_{50}	Displacement at which 50% of q_{ult} is mobilized during monotonic loading
z_o^p	z^p at the start of the current loading cycle

β	Constant in the solution of an infinite elastic beam under a distributed load
Δ	Top story displacement
γ	Unit weight
θ	Rotation
θ_{cr}	Critical rotation at incipient uplift
$\theta_{\max}$	Maximum rotation
v	Bearing capacity reduction
v_h	Bearing capacity reduction, due to horizontal load
v_i	Bearing capacity reduction, due to load inclination
v_e	Bearing capacity reduction, due to load eccentricity
ω	Circular frequency
ψ_{SA}	Ratio of nonlinear system spectral acceleration to elastic system spectral acceleration
ξ_{eff}	Effective damping ratio
ξ_v	Viscous damping ratio
ξ_{eq}	Equivalent viscous damping ratio

1 Introduction and Background

1.1 BACKGROUND AND MOTIVATION

The nonlinear load-displacement behavior of soil provides an opportunity for energy to dissipate from a structural system at the soil-structure interface. This has been recognized for some time; for example, Housner (1963) assumed that a structure (block) allowed to rock would be an effective means of dissipating energy, and presented fundamental equations describing the loss of kinetic energy per impact as the system radiates energy. In addition, using these relations, one can determine the peak displacement as a function of the number of impacts. A scale effect was found that defined why taller structures might not topple where a more squat structure would. This study is applicable to the case of stiff structures such as shear walls, which are commonly used in earthquake-prone regions.

The consequences of allowing a shallow foundation to rock (or in some cases accurately representing an existing structure which *may* rock), which include permanent settlement and rotation, must be reasonably estimated and accounted for. This balance of benefit and consequence is the basis for performance-based earthquake engineering (PBEE), such that the desired structure (e.g., building or bridge) has a specific performance for a defined hazard level. The benefits of a rocking shallow foundation (energy dissipation) are well documented, though there is much uncertainty in modeling these systems. Therefore, this report investigates the applicability of a beam-on-nonlinear-Winkler-foundation (BNWF) model to reasonably predict the benefits and consequences of PBEE for shallow foundations.

Generally, one may anticipate that a more rigorous model representing any real system with a detailed representation of all observed physical mechanisms would lead to better results of the system response. However, the uncertainty in determining the input parameters of the more rigorous model is often contrary to such anticipation. Therefore, the intent of using subgrade type models (springs, gap elements and dashpots) has always been to strike a balance between

theoretically more rigorous solutions and practicality and ease of use in routine geotechnical engineering practice. By now there are numerous publications discussing BNWF approaches applied to pile or pile group foundations, correlating parameter selection assumptions in the model development (spring constitutive relations, modeling of gap or drag resistance, solution algorithms, etc.). For shallow foundations, however, largely due to the limited experimental data, there are fewer Winkler-based numerical studies. This study will answer some important parameters specific to the Winkler-based model.

PBEE measures important to quantifying the performance or suitability of a design specific to shallow foundations are the moment absorbed into the soil-structure interface versus rotation of the foundation, the settlement of the foundation and (if allowed) the horizontal sliding of the foundation. Any of the degrees of freedom of the foundation (rotation, settlement, or horizontal sliding) are generally represented as a function of stiffness. It follows that these degrees of freedom if accurately represented are all possible modes of energy dissipation (benefit), but are therefore susceptible to permanent displacements (consequence).

A nonlinear Winkler-based model can be used to study PBEE implications for shallow foundations, as both the benefits and consequences of allowing the structure to rock can be reasonably represented. However, important parameters specific to the shallow foundation problem must first be addressed, including representative foundation stiffness and capacity, spacing of the Winkler springs and distribution of the spring strengths. ATC-40 (1996) presents an example of this case where a shear wall is connected to a flexible frame, as shown in Figure 1.1. Since the shear wall is sensitive to loads and the frame is sensitive to displacement, selection of the foundation stiffness is important to determine which structural component is the "weakest-link" in the load path.

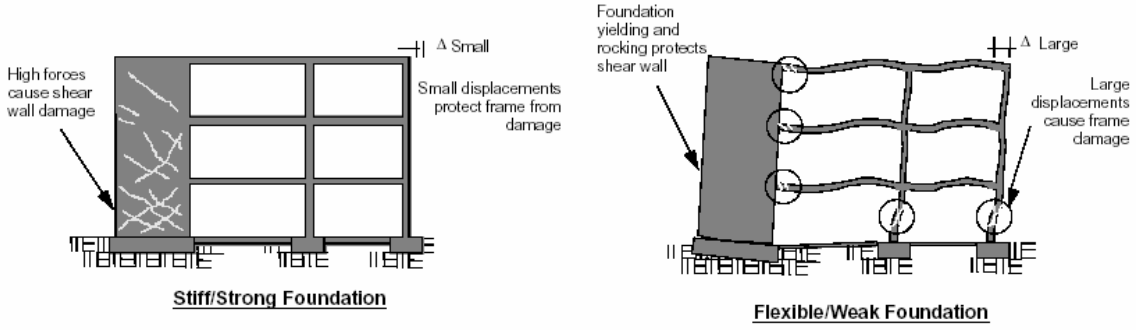

Fig. 1.1 Comparison between response of a structural system, considering stiff/strong or flexible/weak foundation (after ATC-40, 1996)

Present codes, such as ATC-40 (1996) and FEMA 356 (2000) recommend using a Winkler-based model to represent the stiffness of the soil-structure interface and the nonlinearity associated with foundation uplift, in conjunction with a range of soil stiffness and capacity to capture the uncertainty of the soil properties and to provide a best estimate of the most sensitive structural elements. With the popularity in design of the Winkler-based model, regularly used to model the capacity and stiffness of the soil-structure interface, further research is warranted to also provide recommendations for estimating settlement and rotation of the rocking shallow foundation.

1.2 COLLABORATIVE RESEARCH PROJECT

The work presented in this report was coordinated as part of a multidisciplinary, multi-university collaboration between the University of California at Davis (UCD), the University of California at Irvine (UCI), and the University of Southern California (USC), through funding by the Pacific Earthquake Engineering Research Center (PEER). Professor Geoff Martin (USC) initiated the project in 2000 with a background study defining the significance of nonlinear load-deformation behavior and the scope of needed research, and has provided oversight throughout. Model testing of shallow foundations followed at the UC Davis Center for Geotechnical Modeling centrifuge with studies by Rosebrook and Kutter (2001a, b, c), and further model tests by Gajan et al. (2003a,b) (also described in Phalen 2003) in parallel with the Winkler-based analytical modeling presented in this report. In addition, UC Davis is currently investigating the application of a macro-element to represent the nonlinear response of a rocking shallow foundation, integrating the concepts of Nova and Montrasio (1991), Cremer et al. (2001) and Houlsby and Cassidy (2002). For more information on this collaborative research project, see Kutter et al. (2003).

1.3 WINKLER-BASED MODELING

Perhaps the most popular method used in design practice when modeling soil-foundation-interaction (SFSI), is the BNWF approach. The BNWF generalization originates from Winkler's (1867) early representation of the physical soil medium, which assumes a system of discrete, closely spaced independent linear elastic springs as shown in Figure 1.2 Such an approach assumes that a lateral reaction in the soil q per unit length at a given distance along the foundation is related only to the foundation deflection δ at that distance. Based on this assumption, displacements of the foundation are confined to only the loaded regions of the footing. Heyenti (1946) provided an important extension to this by considering the deformation of the beam element by accounting for its flexibility. This general approach has become popular in the analysis of pile and pile group systems, whereby individual spring elements are simply placed horizontally (rather than vertically) and used to represent the lateral resistance of the soil and the soil-pile interaction forces. In each case (the shallow or deep foundation), the discretely placed springs result in a lack of coupling between individually placed spring elements; however, the continuum effect provided by the soil may be implicitly included if the resistance curves are back-calculated from monotonic or cyclic loading experiments.

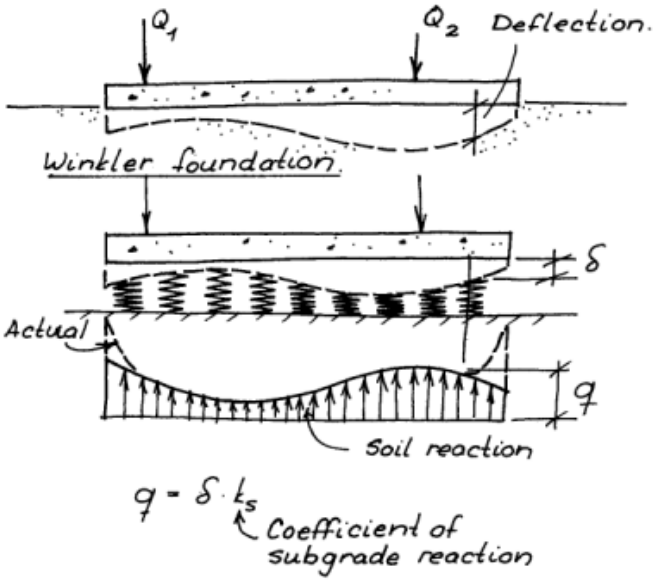

Fig. 1.2 Winkler foundation concepts (after Broms 2003)

1.4 PREVIOUS WORK USING WINKLER-BASED MODELS

Several publications in the literature describe various Winkler-based approaches used for modeling the rocking response of shallow foundations resting on either an elastic or inelastic soil medium, and which consider the inelastic actions through the effect of uplifting of the foundation. Upon uplifting of the foundation, however, the equations of motion describing the system response become highly nonlinear. Therefore, various researchers have also considered simple symmetric two-spring models to allow for linearization of the system of equations. Such an approach is generally more applicable for rigid structural systems. Descriptions of some of these previous works are provided in this section.

Weissing (1979) used elastic-plastic springs coupled with Coulomb slider elements and subdivided the foundation into finite strips. This work considered two-dimensions of loading (moment and vertical loading with horizontal movement restrained), modeled after his experimental studies. Elastic-plastic springs were considered to only have compression capacity, while Coulomb slider elements captured the uplifting of the foundation. Results from this numerical study provided good comparison with experimental studies for the range of soil-foundations considered [also conducted by Weissing (1979)]. Four out of five tests considered the strong direction of loading, with vertical factors of safety, FS_V, ranging from two to ten. A small plate footing was used, 0.5 m by 0.25 m, and the loading protocol was generally five cycles each for three sets 0.001, 0.005, and 0.02 radians.

Prior to Weissing's work, Bartlett (1976) completed similar tests on a clay soil, with the same size footings and range of factors of safety. Analytical work was also performed, using a Winkler-based model with elastic perfectly-plastic springs allowed to uplift. Three out of four tests considered the weak direction of loading, and FS_v ranged from 1.5 to 8. A small plate footing was used, 0.5 m by 0.25 m, and the loading protocol was generally five cycles each for three sets 0.005, 0.01, and 0.02 radians. Good qualitative comparisons were made between the analytical and experimental results, with the following key observations: (1) general degradation of the soil modulus occurs with increasing loading amplitude, (2) the majority of the permanent deformation occurs in the first large cycle of a set of similar amplitude cycles, and (3) increasing energy dissipation occurs with increasing rotation.

Psycharis (1982) considered two types of soil modeling using base springs: (1) the two-spring model and (2) the distributed Winkler (system) of springs. Nonlinearity at the foundation

interface was considered through three mechanisms: (1) viscous dampers, (2) elastic-perfectly-plastic nonlinear springs, and (3) an impact mechanism allowing dissipation of energy at impact. Comparison of the solutions from theoretical equations developed on the basis of the two spring and distributed spring system were provided using response results from the Milliken Library building and a ground motion recording from the 1971 San Fernando earthquake. The primary conclusion from this numerical study was that a two-spring model was much simpler and provided reasonable enough response results for practical design. In a later publication by Psycharis (1983), a simplified two-spring system is used for studying the response of a multi-story building system.

Two separate but similar studies by Chopra and Yim (1985) and Yim and Chopra (1985) evaluated the rocking response of single-degree-of-freedom (SDOF) and multi-degree-of-freedom (MDOF) systems. In follow-up work (Yim and Chopra 1985), the model was extended to an MDOF system supported on a two-spring dashpot system. The selected system of base supports is shown in Figure 1.3. In each of these studies, the individual spring elements were considered linear elastic. Resulting moment-rotation envelope response with the different base idealizations are shown in Figure 1.4. A primary conclusion from this work was that foundation flexibility and uplift has little affect on higher modes of vibration and for a multi-story building structure, these effects can be incorporated only by inclusion in the fundamental mode of response. In the SDOF study, the authors develop simplified expressions for determining the base shear resistance of flexible structures allowed to uplift.

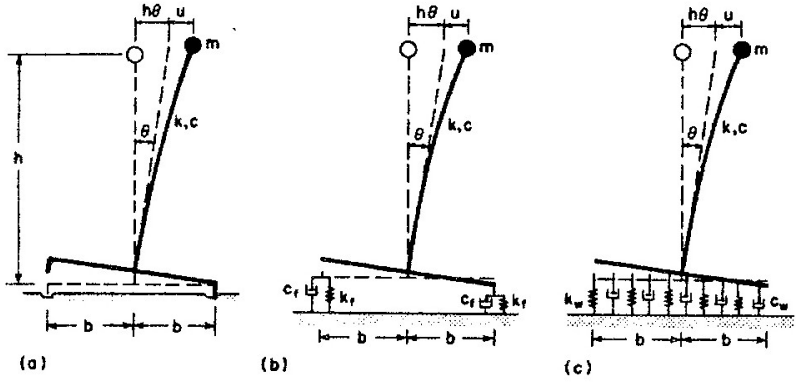

Fig. 1.3 Idealized foundation system by Chopra and Yim (1985): (a) rigid foundation, (b) two-element (spring-dashpot) system, and (c) distributed Winkler (spring-dashpot) system

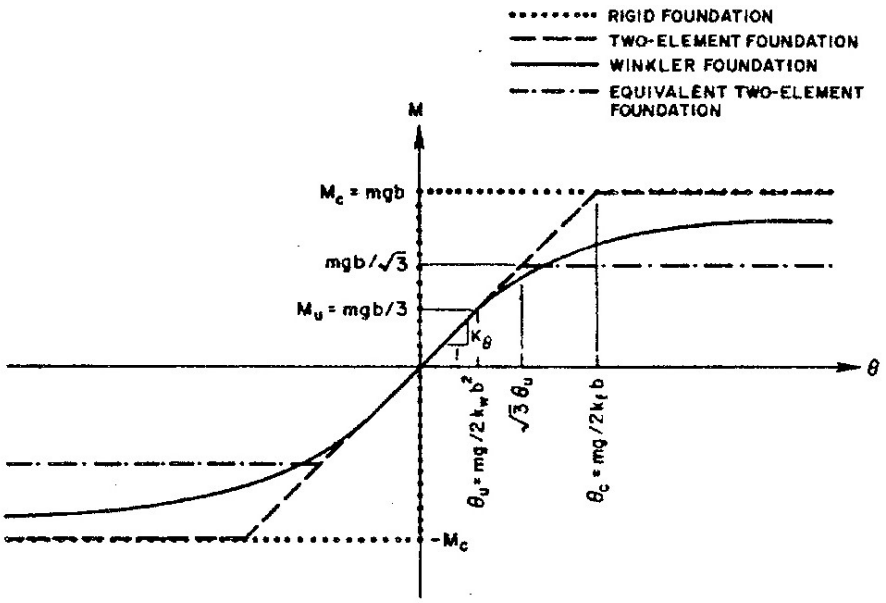

Fig. 1.4 Moment-rotation envelope assuming different idealized foundations (after Chopra and Yim 1985)

In an application specific to the system considered in this report, Nakaki and Hart (1987) used discretely placed vertical elastic springs with viscous dampers at the base of a shear wall structure to illustrate the benefits of uplifting of the foundation supporting shear wall systems during earthquake loading. The Winkler springs had zero tension capacity and provided only elastic compressive resistance. The inelastic shear wall structure was modeled using a nonlinear stiffness-degrading hysteretic model. Figure 1.5 shows the schematic of the base spring configuration and the structural model considered. Nonlinear time history analyses were performed on this system considering two different ground motions: (1) a long-duration motion from the 1940 El Centro earthquake and (2) a short, impulsive type motion measured at Pacoima Dam. Important findings from this study included the illustration, through the numerical results, that uplifting of the foundation results in a significant reduction in structural ductility demands as shown in Figure 1.6. This is primarily because the rocking system has a longer period than that of the fixed-base system. It was also observed that the frequency content of the ground motion has a significant effect on the system ductility demand. In select cases, allowing uplift of the foundation caused greater ductility demands on the structure.

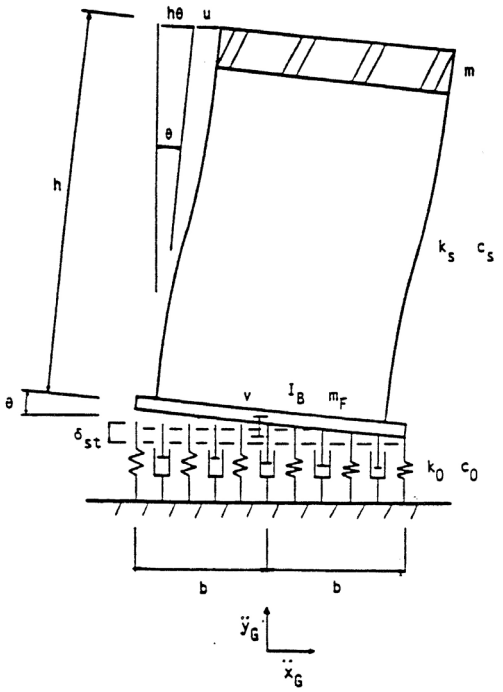

Fig. 1.5 Winkler-foundation system below a model inelastic shear wall (after Nakaki and Hart 1987)

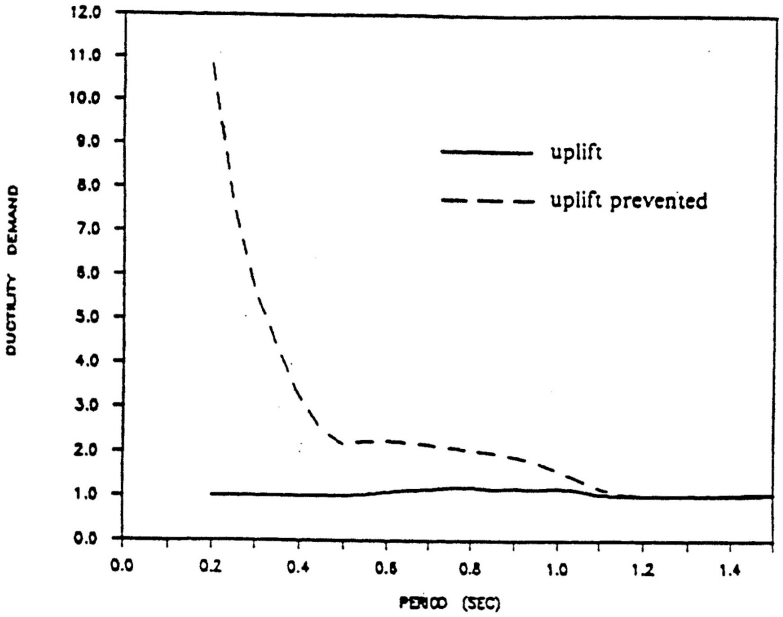

Fig. 1.6 Ductility demand vs. period relation for structures allowing and preventing uplift (results from analyses using the El Centro earthquake) (after Nakaki and Hart 1987)

Although these and other studies were able to reasonably capture the dissipation of energy through numerical Winkler-based foundation modeling, few previous works have focused on capturing the ramifications of this dissipation of energy. The associated accrued settlement through the cumulative strain development within the soil near to the foundation is an important part of the overall performance-based design of the structure with consideration of the soil-structure system.

Fenves (1998) models uplift of pile caps using a composite element of multiple elastic perfectly-plastic elements (bilinear) in the computer code DRAIN-3DX. The compression and tension sides of the load-displacement curves are nonsymmetrical to model the reduced capacity under uplift, and gapping elements are used that have the ability to capture permanent settlement. The vertical factor of safety was found to significantly influence the moment capacity and the vertical settlement. Accordingly, the vertical factor of safety influences the amount of moment-rotation energy which may be dissipated, as a larger factor of safety will have a moment capacity which may not be reached and therefore exhibit more pinched hysteresis.

Nova and Montrasio (1991), Houlsby and Cassidy (2002) and Cremer et al. (2001) have provided theoretical work and numerical simulations to capture shallow-foundation soil-structure interaction using a macro-element through empirical, yield surface, hardening law and plastic potential models. The envisioned macro-element would be implemented into a model through a single element at the base of a structural system. Sivapalan at UC Davis is currently working to implement a similar, but expanded approach in OpenSees. For more information see Kutter et al. (2003).

1.4.1 Case Studies

Several interesting case studies have used Winkler-based modeling to compare with field measured structural response, as obtained during earthquake events. For example, Rutenberg et al. (1982) presents an analytical study of the response of the Veterans Administration Hospital Building subjected to the 1971 San Fernando earthquake. Foundation modeling was incorporated using a distributed nonlinear Winkler spring system. The primary conclusion from this analysis was that the structure performed well in part due to the unanticipated benefits of the nonlinear soil-structure interaction.

Similarly, Wallace et al. (1990) present a case study comparing the numerical and measured response of two shear wall type buildings, one subjected to the 1984 Morgan Hill earthquake and the other to the 1987 Whittier earthquake. These structures were instrumented as part of the California Strong Motion Instrumentation Program (CSMIP). Foundation compliance was modeled using ATC 3-06 elastic spring concepts. Poor correlations between measured response and computed response were observed when soil flexibility was ignored in the modeling.

1.4.2 Summary of Observations and Scope of Report

From the previous literature review, it appears there are a number of opportunities and challenges in providing a suitable base foundation model to capture shallow foundation rocking behavior. With respect to the Winkler-based approach, issues of model discretization, material model selection, the geometric and loading details, and perhaps the numerical solution scheme, to name a few, become very important. The level of rigor applied and the evaluation of the overall robustness of the numerical model require proper balance in estimation of the important performance measures of the rocking shallow foundation, such as the monotonic and cyclic moment capacity, rotational demand at the base, and the cyclic and permanent settlement of the foundation. Each of these parameters is evaluated in the context of the Winkler-based numerical modeling approach in this report.

2 Experimental Data

A suite of model tests have been performed that can be used to develop numerical models, study parameters, and provide recommendations for Winkler-based approaches. These experiments were collected from the literature review and are briefly described here. They have been classified into either model centrifuge experiments or one-gravity ("one-g") experiments. The experimental data described in this chapter will be modeled and the results presented in Chapters 3 and 4.

2.1 CENTRIFUGE EXPERIMENTS

Scale centrifuge testing provides a unique opportunity to test scaled, model specimens while retaining the proper prototype soil stresses. Centrifuge scaling laws are discussed in Kutter (1997); however, based on similitude between model and prototype stresses for a model tested at an N-g level, the prototype length may be obtained by multiplying the model length by N. Similarly, prototype mass may be obtained by multiplying model mass by N^3. The 9-meter radius geotechnical centrifuge at UC Davis provided this opportunity for this joint research project. Two series of experiments were performed at UC Davis as part of this project, and will be discussed in the following section. Table 2.1 describes the primary variables of these tests.

Table 2.1 Summary of test series at UC Davis (after Phalen 2003)

Test Series	Soil Type	FS_v Range	Embed [m]	Wall Type
KRR01	Dry Sand	1.6-6.5	0.3	Double
KRR02	Dry Sand	1.6-4.1	0	Double
KRR03	Sat Clay	2.8-4.8	0	Double
SSG02	Dry Sand	3.4-9.6	0	Single
SSG03	Dry Sand	1.3-11.5	0.7	Single

2.1.1 Rosebrook and Kutter Experiments (KRR Series)

Centrifuge experiments by Rosebrook and Kutter (2001a, b, c) (also summarized in Rosebrook 2001) incorporate a range of footing sizes, static vertical factors of safety (from FS_v = 1.6-8) and both clay and sand soil types. In these experiments, series KRR01 consider sandy soils of relative density 60% and 80%, while KRR02 considers sandy (dry) soils of relative density 60%. Series KRR03 considers systems resting on stiff saturated clay. Estimation of the undrained shear strength of the model clay ranged from 63–107 kPa for the KRR03 experiments, based on review of Torvane measurements, sample compression tests, and bearing experiments (Phalen 2003). An average value of 103 kPa was determined by back-calculation from compression tests. The KRR series centrifuge model experiments were all conducted at 20 g's; each series was subjected to pure compression, lateral cyclic (moment) loading and base excitation.

For the KRR01 series, the friction angle ϕ' of the sand ranged from 39–40 degrees. This range was determined by back-calculating from the ultimate load of the vertical compression tests using conventional bearing capacity theory. For the KRR02 series, the friction angle ϕ' ranged from 41–44 degrees. All model tests were surface footings, with the exception of KRR01, which had embedments of ½B and 1B (where B = width of footing). The sand medium used throughout the test series was Nevada sand. Strip footings were used with three different sizes (length x width) selected: 2.54 m by 0.38m (small), 2.67 m by 0.69 m (medium), and 3.94 m by 1.08 m (large).

The general displacement history applied to the KRR01, KRR02 and KRR03 series experiments consisted of between three and six cycles of symmetric reversed cyclic loading each to a target constant displacement followed by increasing (typically by 50% or 100%) of the previous step displacement amplitude and application of another series of reversed cycles of constant amplitude. This loading protocol was termed "slow cyclic" and this terminology will be followed in this thesis. In addition, dynamic base excitation of step waves and tapered cosine waves were used with frequencies of 1.25–2 Hz. This loading protocol was termed "dynamic cyclic" and will be adopted in this report.

Figure 2.1(a) shows the general construction of the KRR models for a slow cyclic test. Model structures consisted of double shearwall systems connected by a rigid floor.

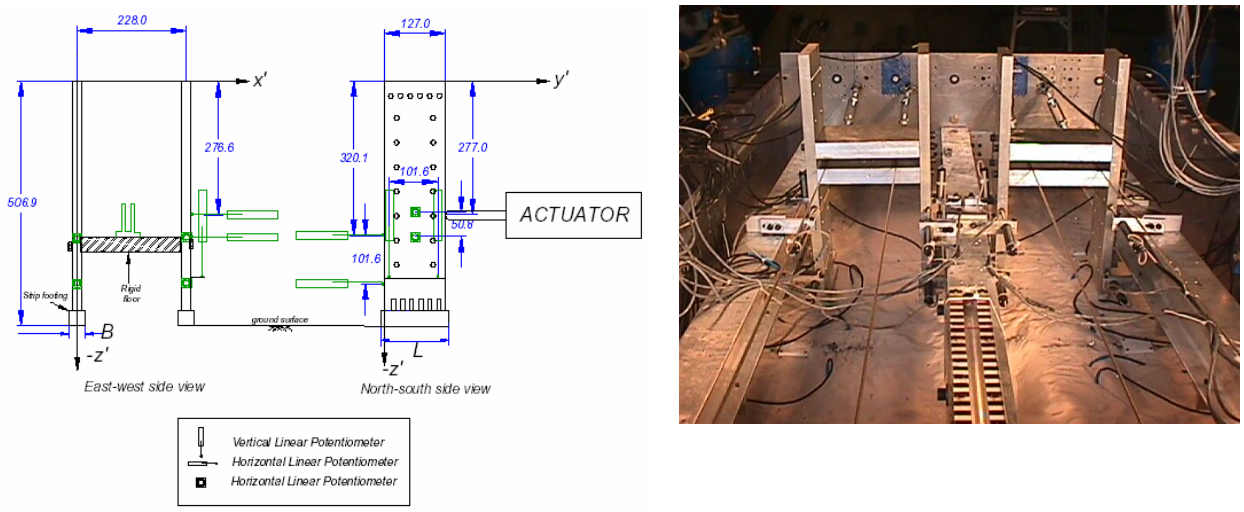

(a) **(b)**

Fig. 2.1 Double-wall test configuration for KRR series; (a) schematic (after Rosebrook and Kutter 2001b), (b) photograph (Rosebrook 2001). (All units in model scale, mm).

2.1.2 Gajan et al. Experiments (SSG Series)

Recent centrifuge experiments by Gajan et al. (2003a, b) (also summarized in Phalen 2003), performed at UC Davis, also incorporate a range of footing sizes and design vertical factors of safety (from FS_v = 1.3 to 11.5). The primary difference in the SSG series were the inclusion of more tests with embedment and a lower horizontal push height to allow study of the horizontal displacement–shear relationship. Embedments of one B were considered (where B = footing width). Tests were performed on only 80% relative density (dry) sand.

The general displacement history applied to the SSG02 and SSG03 series experiments consists of various sets of three cycle step sinewaves, with increasing amplitudes (typically double the previous amplitude). Dynamic tests included time histories of various amplitudes of a tapered cosine wave. In addition, vertical cyclic loading (rather than monotonic as applied in the KRR series) was applied.

The SSG02 and SSG03 series implement a single shear wall system, as shown in Figure 2.2. Stability in the out-of-plane loading direction was provided by Teflon supports to minimize friction.

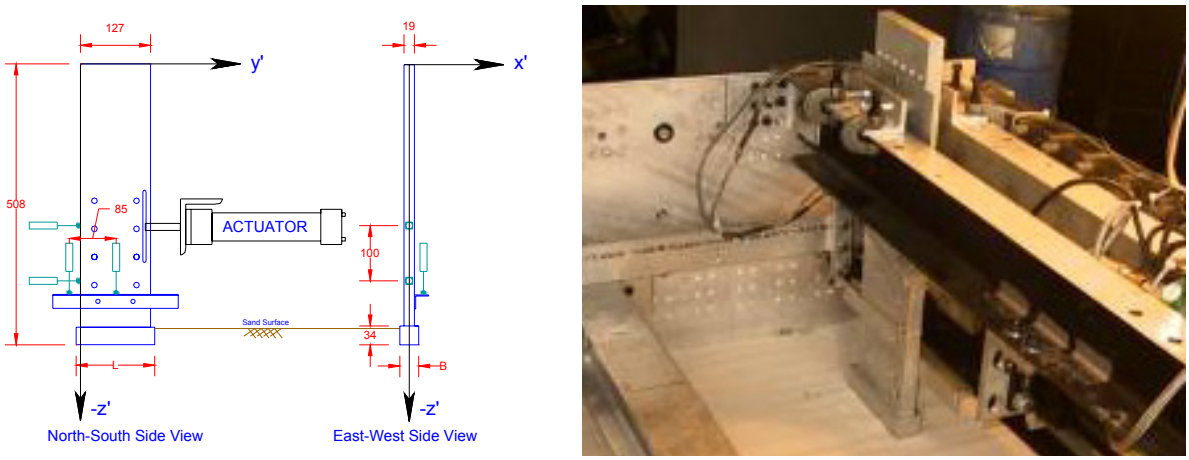

(a) (b)

Fig. 2.2 Single-wall configuration for SSG series (a) schematic (all units in model scale, mm), (b) photograph (after Phalen 2003)

Both the SSG and KRR series experiments were heavily instrumented with displacement potentiometers, accelerometers and force transducers. Typically, at least 15–20 sensors were used for a given experiment. Figure 2.3 shows a plan view of the centrifuge box for the SSG series 2. A single series, e.g., KRR01, SSG02, etc., will have multiple footing experiments, typically named with the series, station letter (A, B, e.g.) and test number.

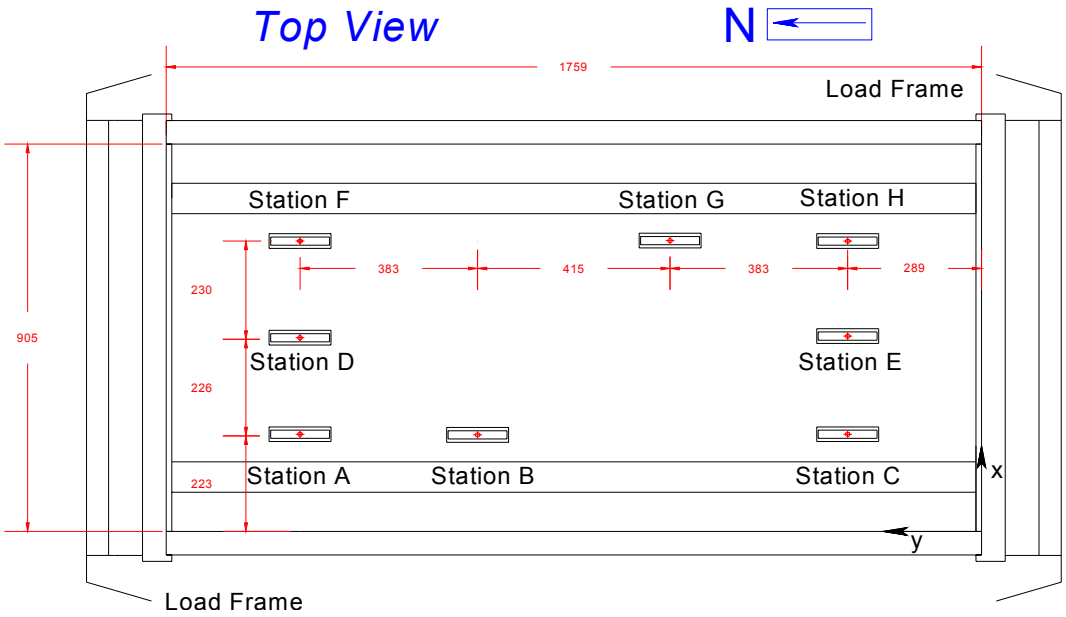

Fig. 2.3 Centrifuge station plan view (after Phalen 2003)

2.2 ONE-g EXPERIMENTS

Test data are also available from experiments performed at one-g, where model and prototype are one and the same.

2.2.1 TRISEE Laboratory Experiments

One-g experiments were recently completed at the ELSA (European Laboratory for Structural Assessment) in Italy. Results from these experiments are reported in Negro et al. (1998) and Faccioli et al. (2001). The system considered consisted of a one meter square foundation, placed on a saturated Ticino sand base, subjected to static vertical, slow cyclic, and dynamic cyclic events. Saturation was achieved by flushing water from the base of a large concrete caisson in which the foundation and soil were placed for testing. Two relative densities were considered in these experiments, D_r = 85% (high density, denoted "HD") and 45% (low density, denoted "LD"). A constant vertical load is sustained by an air cushion system throughout the test, at 300 kN for the HD test and 100 kN for the LD test. The experimental setup is shown in Figure 2.4.

The friction angle is recommended as the peak shear resistance of Ticino sand (after Bolton 1986), corresponding to values of 42 and 38 degrees, respectively, for the HD and LD cases. Using the surcharge loading around the footing, the calculated friction angles and conventional bearing capacity theory (with bearing capacity factors after De Beer (1970), Hansen (1970), and Hanna and Meyerhoff (1981)), the approximate design vertical factors of safety are found to be 12.5 and 20.7 for the HD and LD cases, respectively. Rotation was applied to the foundation through a hydraulic actuator placed 0.9 m above the foundation. The loading protocol consisted of single reversed (symmetric) cycles of increasing amplitude.

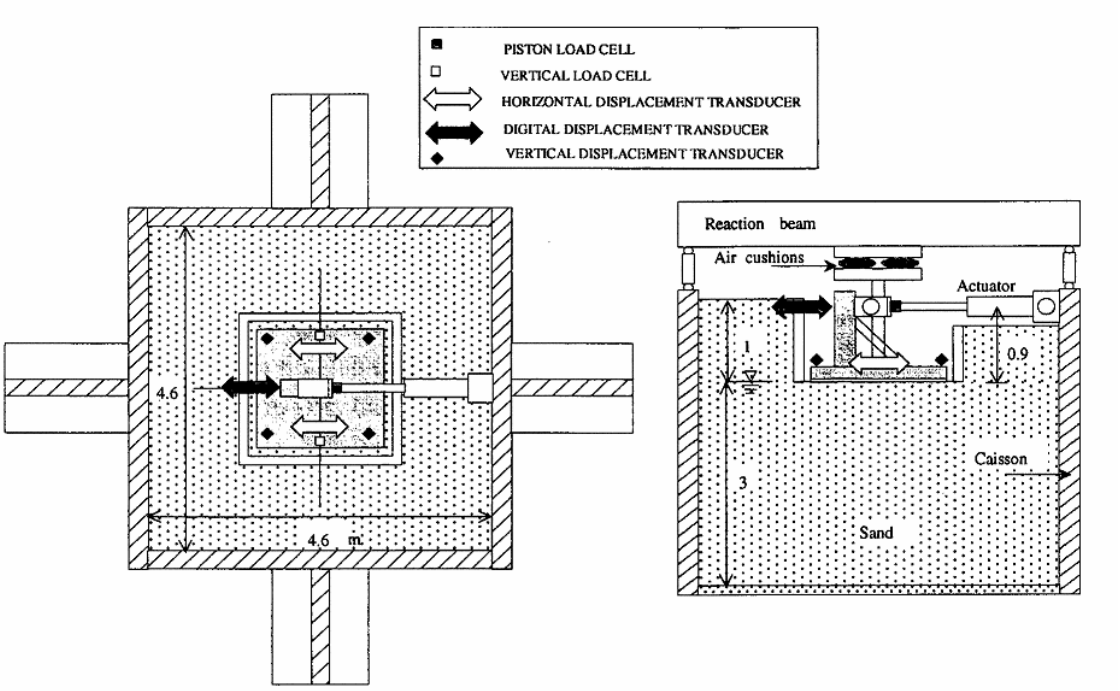

Fig. 2.4 ELSA test series experimental setup (after Negro et al. 1998)

2.2.2 New Zealand Experiments

Model footing experiments were conducted at the University of New Zealand [described in Taylor et al. (1981), Weissing (1979), and Bartlett (1976)]. The focus of these experiments was to investigate the nonlinearity developed in the soil and the uplift at the interface of the soil and footing upon large-amplitude moment loading. Studies by Weissing (1979) considered the rocking response of foundations resting on dry sand, while studies by Bartlett (1976) considered foundations resting on clay. In these experiments, horizontal movement of the footing was restrained through the use of a steel tie-rod system. Each experiment consisted of five loading cycles to each of three increasing amplitude levels. Only the first, second, and fifth loading cycles from these experiments were reported; therefore only these could be simulated due to limited available data. The test configuration for the tests on sand by Weissing (1979) are shown in Figure 2.5. The setup for experiments by Bartlett (1976) were similar.

For Weissing's experiments, four out of five tests considered the strong direction of loading, with vertical factors of safety, FS_V, ranging from two to ten. A small plate footing was used, 0.5 m by 0.25 m, resting on dry clean quartz sand. The friction angle was estimated from triaxial test data, shear box tests, and plate bearing tests to be 43 degrees. Bartlett's experiments

consisted of three out of four tests conducted in the weak direction of loading. A similar sized footing was used.

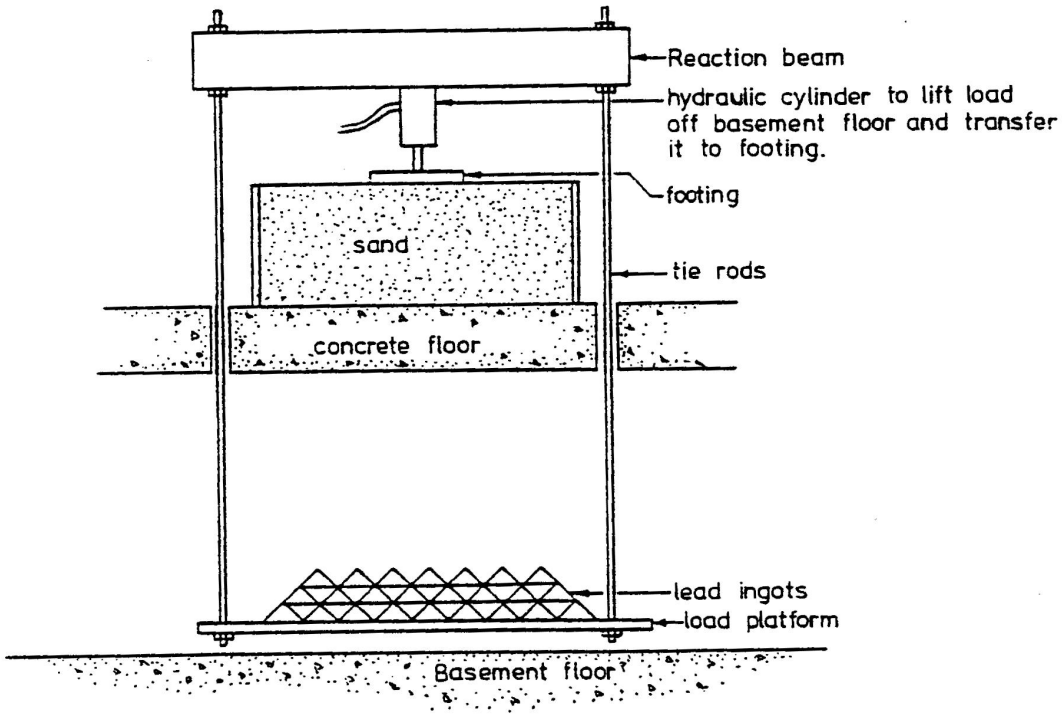

Fig. 2.5 Test setup for New Zealand experiments (after Weissing 1979)

2.3 ANALYSIS OF EXPERIMENTAL DATA

Prior to analytical modeling of a rocking system, some simple analyses of the moment-rotation and settlement-rotation data collected from the experimental literature were performed. The objective was to study the rocking foundation as an energy-dissipating mechanism. Although the moment-rotation response of the rocking system is capable of dissipating much energy, the consequence of permanent structural deformations should be observed.

2.3.1 Energy Dissipation and Equivalent Viscous Damping

Soil-foundation interaction is highly nonlinear. The moment-rotation hysteresis curves from the previously described experimental results display excellent ductility and good potential to dissipate energy that may otherwise damage the superstructure. A side effect of this nonlinearity is the permanent settlement of the footing. As expected, the amount of settlement depends on the

magnitude of the axial load and the cyclic rotation. Data available from experiments that isolate the nonlinear contributions of the foundation of a soil-structure system provide the opportunity to determine the energy that has been dissipated and the associate consequences of such energy dissipation. Such information will be valuable to the assessment of systems using nonlinear static procedures (NSPs), since many of these methods have their basis in the substitute structure approach.

The substitute structure approach (Chopra and Goel 1999), diagramed in Figure 2.6, relies on idealizing the behavior of an inelastic system with that of an equivalent linear system using secant stiffness and equivalent viscous damping properties representative of the global behavior of the structure at an anticipated peak (or design) displacement level. Early works by Hudson (1965) and Jennings (1968) have provided the general approach. Subsequent modifications by Gulkan and Sozen (1974) describe the method applied to reinforced concrete frame structures. Kowalsky et al. (1995) describe a displacement-based design procedure for reinforced concrete bridge columns, which is based on the substitute structure method. Recent code procedures, for example ACT-40 (1996), adopt the approach in combination with the capacity spectrum approach (Freeman 1978) to provide an alternative design procedure for retrofit of reinforced concrete buildings.

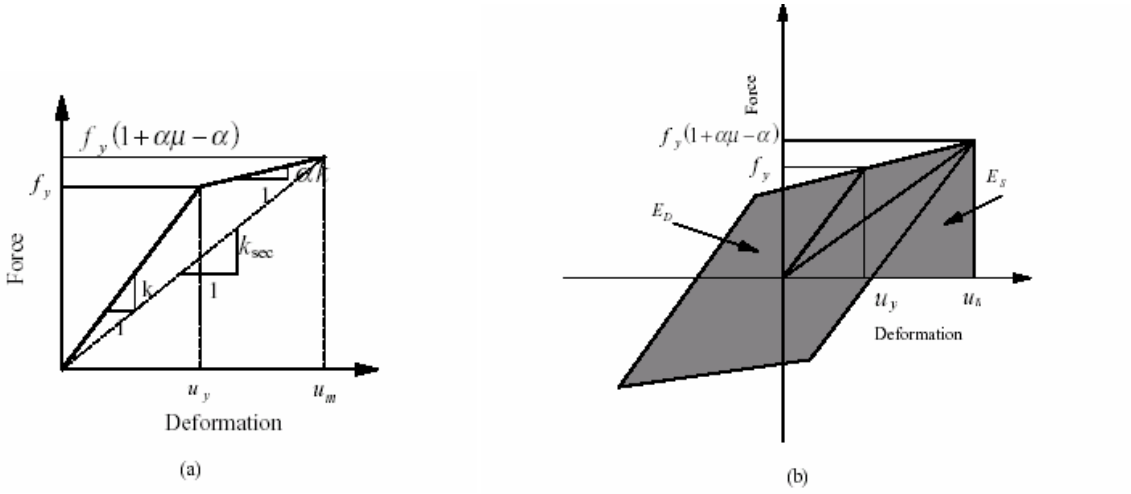

Fig. 2.6 Equivalent linear system approach: (a) inelastic system bilinear response and (b) determination of equivalent viscous damping due to hysteretic energy dissipation (after Chopra and Goel 1999)

To use the method in the context of the systems studied herein, the effective damping ratio versus demand relation needs to be determined for the rocking foundation system. The effective damping ratio ξ_{eff} is equivalent to the sum of the hysteretic damping of the system represented as an equivalent viscous damping term ξ_{eq} and a viscous damping component ξ_v, i.e.,

$$\xi_{eff} = \xi_v + \xi_{eq} \tag{2.1}$$

The equivalent viscous damping may be determined by equating the energy dissipated in a vibrational cycle (of the inelastic system) with that of the equivalent linear system (Chopra 1995):

$$\xi_{eq} = \frac{1}{4\pi} \cdot \frac{E_D}{E_s} \tag{2.2}$$

where E_D = the hysteretic energy dissipated by the shallow foundation system during one cycle of loading and E_s = the elastic strain energy associated with that cycle of motion, at a peak displacement. The hysteretic energy E_D for this system is a combination of the cyclic lateral and vertical translation and rocking energy, i.e.,

$$E_D = E_D^{\theta} + E_D^{u} + E_D^{s} = \int M(t) \cdot d\theta(t) + \int H(t) \cdot du(t) + \int V(t) \cdot ds(t) \tag{2.3}$$

where E_D^{θ} = energy associated with moment-rotational rocking (defined as the integral of moment M with respect to rotation θ), E_D^{u} = energy associated with horizontal translation (defined as the integral of horizontal load H with respect to horizontal displacement u), and E_D^{s} = energy associated with vertical vibration (defined as the integral of vertical load V with respect to vertical displacement s). For this exercise, it is assumed that the rocking contribution to system energy dissipation dominates the calculation of E_D. The elastic strain energy (from Fig. 2.7) may be determined as:

$$E_S = \frac{M_{max} \cdot \theta_{max}}{2} \tag{2.4}$$

where M_{max} = the average (of positive and negative) maximum moment of the system and θ_{max} = the associated (average) maximum rotation. E_D and E_S may be determined, for example by using the M-θ data shown in Figure 2.7, averaged over three cycles of uniform loading to the same target displacement level.

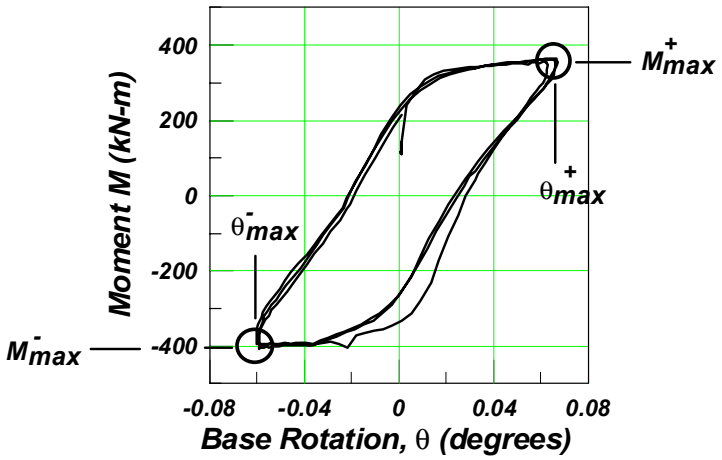

Fig. 2.7 Example of estimation of equivalent damping using experimental M-θ data

For the static cyclic experimental test data sets, Figure 2.8 shows the equivalent viscous damping versus distortion (average settlement normalized by the foundation length) per cycle, where (a) shows data from sand experiments and (b) shows data from clay experiments. These data are shown for all experiments available with reversed slow-cyclic loading (KRR series data, SSG series, TRISEE data, and Bartlett and Weissing data). Suggested distortion levels for various types of common structural systems are also shown (by Duncan and Buchignon 1987). The results indicate that high levels of equivalent viscous damping are obtained within tolerable distortion levels (maximum values indicate approximately up to $\xi_{eq} \sim 30\%$ for tolerable distortions for load-bearing walls). For a lower factor of safety it appears that a larger amount of damping is mobilized. This makes intuitive sense, as a lower factor of safety will allow additional densification and softening, and higher energy dissipation.

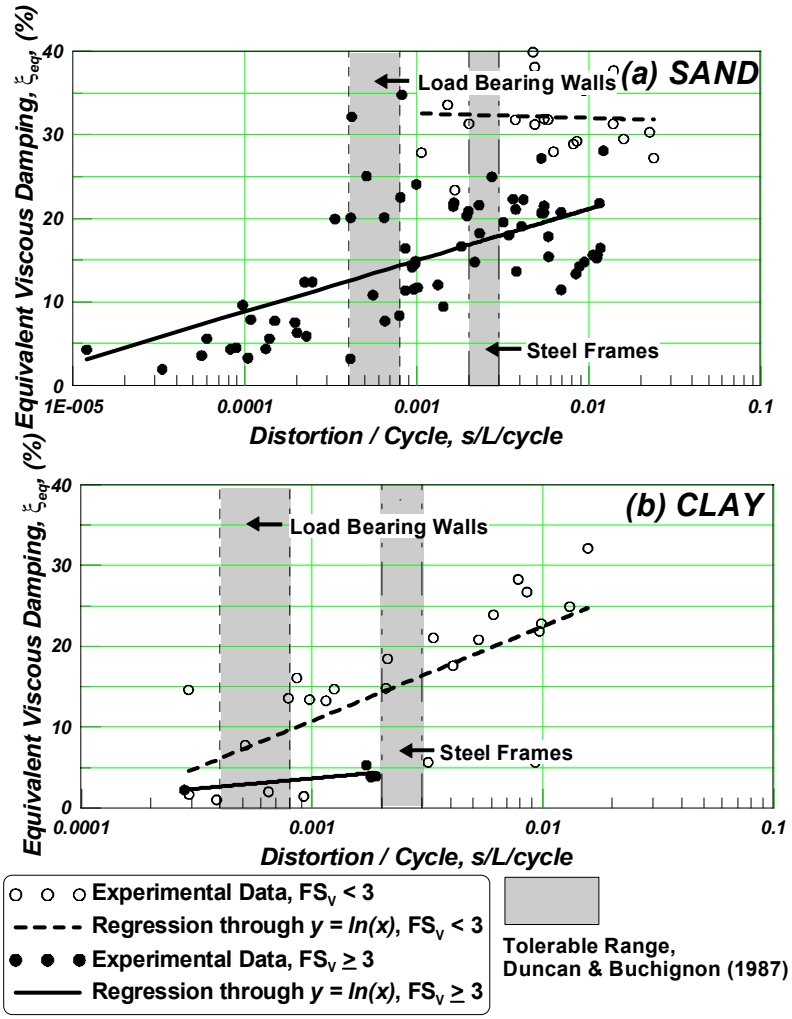

Fig. 2.8 Equivalent viscous damping vs. maximum footing distortion (settlement normalized by footing length) per cycle for slow cyclic tests: (a) sand data and (b) clay data

For the dynamic test data, shown in Figure 2.9, very large values of equivalent viscous damping are obtained. There is a large scatter in the data, particularly at low distortion levels (Note that the y-axis scale in Fig. 2.9 is different than in Fig. 2.8). In the case of sand, it appears that the trend is fairly similar for low and higher factors of safety. For tests on clay, initially large values of damping are found for relatively small values of distortion, with little data to interpret a trend. However, large equivalent viscous damping levels are attained within tolerable distortion levels. This plot includes only KRR series, SSG series, and ELSA series data, as Weissing and Bartlett did not perform dynamic tests. For the dynamic data, 65% of the data points shown in Figure 2.9(a) "Sand" below a distortion per cycle (s/L/cycle) of 0.003 have ξ_{eq}

between 10 – 30%; in Figure 2.9(b) "Clay," this value is 74%. For the static data, 30% of the data points shown in Figure 2.8(a) "Sand" below a distortion per cycle (s/L/cycle) of 0.003 have ξ_{eq} between 10 – 30%; in Figure 2.8(b) "Clay," this value is 19%.

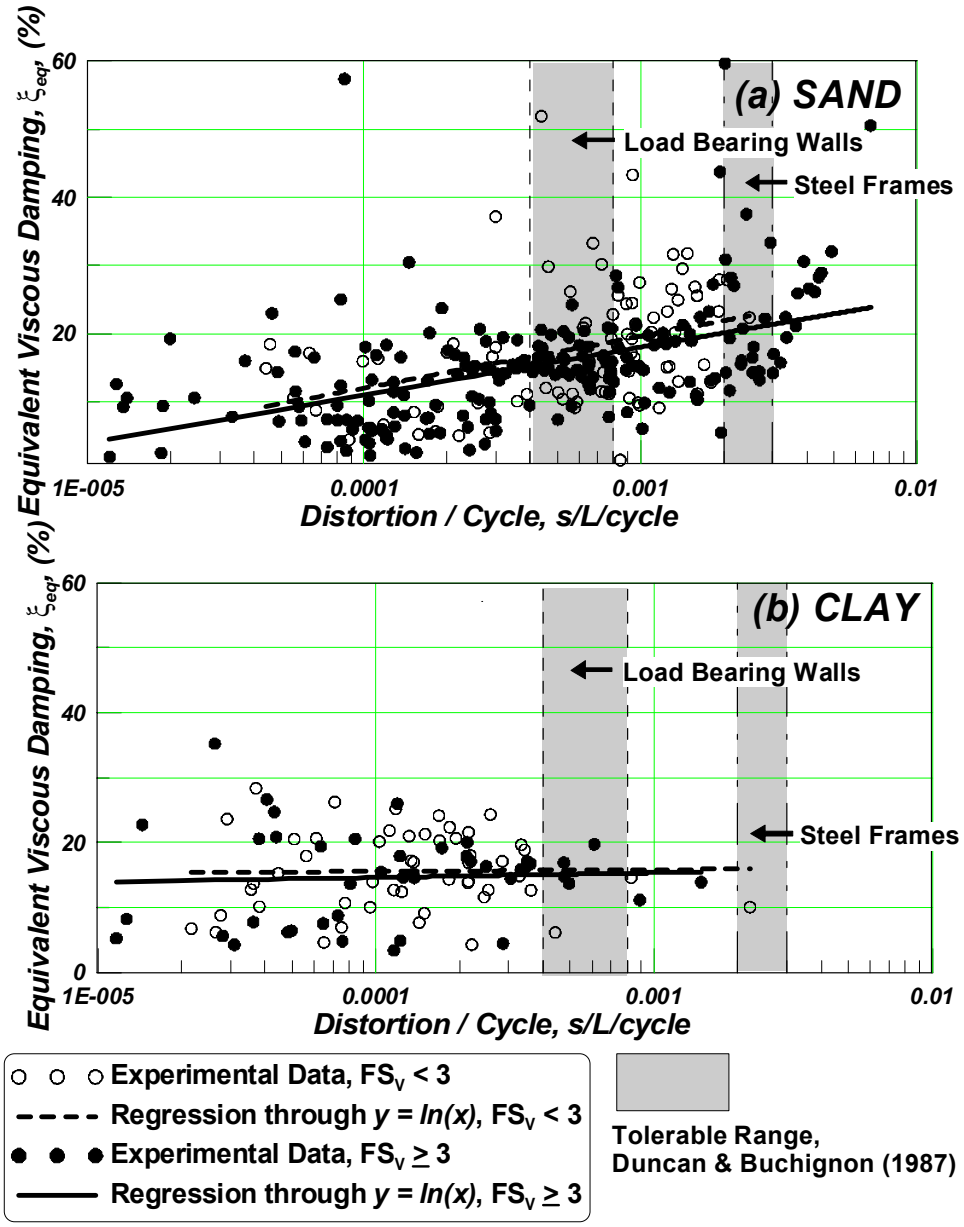

Fig. 2.9 Equivalent viscous damping vs. maximum footing distortion (settlement normalized by footing length) per cycle for dynamic cyclic tests: (a) sand data and (b) clay data

The relation between rotation and equivalent viscous damping is also investigated, since this is an equally important damage measure in terms of footing performance. For static test data, Figure 2.10 plots equivalent viscous damping versus the half amplitude of rotation (the maximum value of rotation) per cycle, where (a) shows data from sand experiments and (b) data from clay experiments. These data are shown for all experiments available with reversed slow-cyclic loading (KRR series data, SSG series, ELSA data, and Bartlett and Weissing data). High levels of equivalent viscous damping are obtained for even the smallest amounts of rotation, starting at approximately $\xi_{eq} \sim 10\%$ and mobilizing up to 20% – 30% for large rotations. The results show that for the lower FS_V (< 3.0) a larger amount of damping is mobilized, and in general a greater amount for larger rotations. This follows the conclusion from the investigation of ξ_{eq} versus distortion.

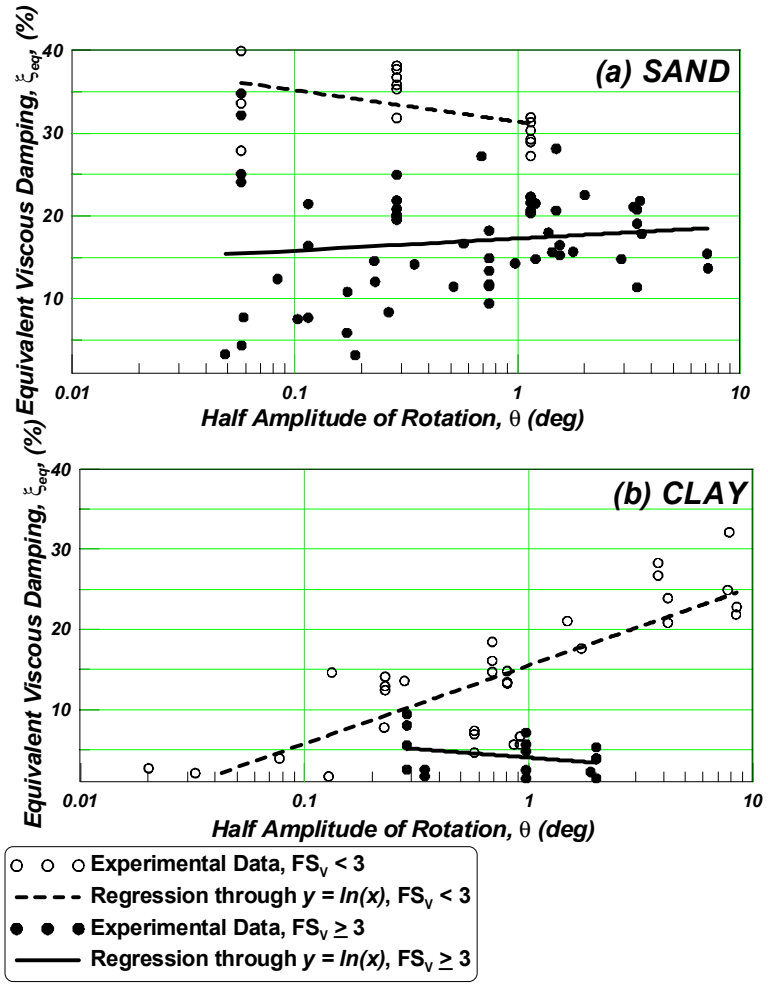

Figure 2.10 Equivalent viscous damping vs. rotation for slow cyclic tests: (a) sand data and (b) clay data

For dynamic test data, Figure 2.11 plots equivalent viscous damping versus the half amplitude of rotation, where (a) shows data from sand experiments and (b) shows data from clay experiments. Similar to the ξ_{eq} versus distortion plots for dynamic data, very large values of equivalent viscous damping are obtained, in addition to a large scatter in the data at low rotation levels. Additionally, for both sand and clay, the trend is fairly similar for low and higher factors of safety. This plot includes only KRR series, SSG series and ELSA series data, as Weissing and Bartlett did not perform dynamic tests.

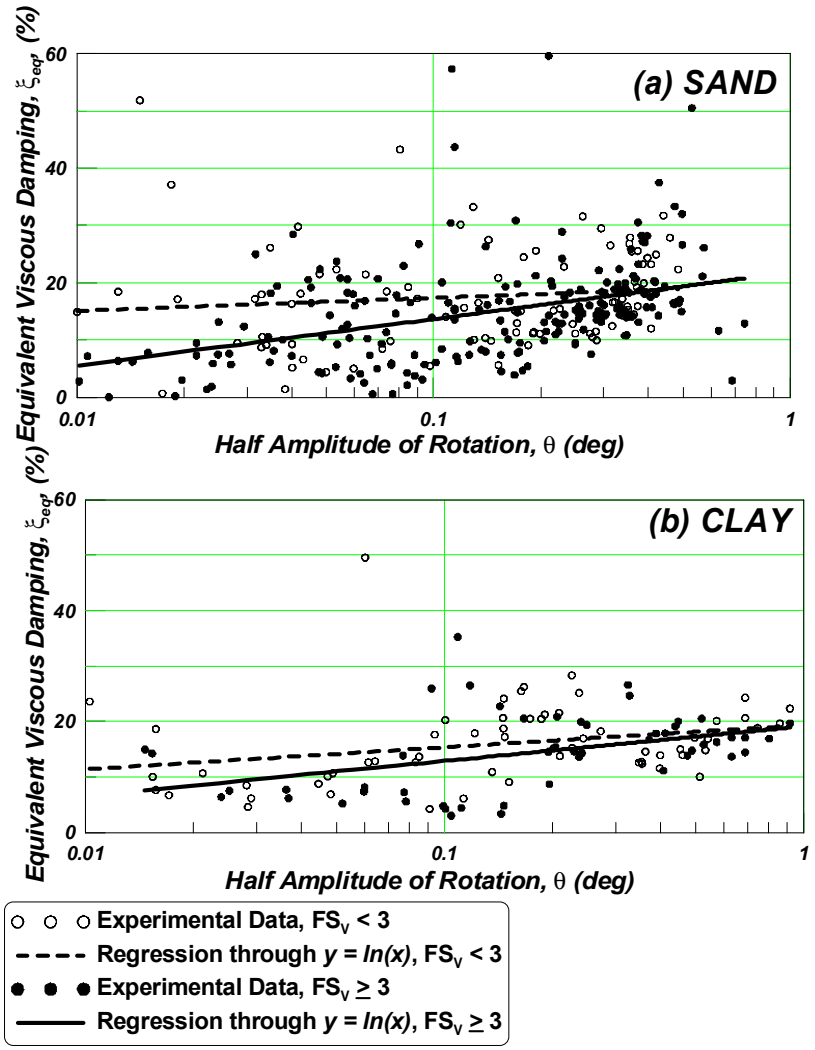

Figure 2.11 Equivalent viscous damping vs. rotation for dynamic cyclic tests: (a) sand data and (b) clay data

3 Beam-on-Nonlinear-Winkler-Foundation (BNWF) Modeling

A BNWF mesh generator was developed to model the various experimental systems described in Chapter 2 and to study the sensitivity of parameter selection. Prior to discussing this, it is helpful to establish common notation for use throughout modeling and presentation of results.

3.1 NOMENCLATURE

The notation for forces and displacements throughout the report are clearly defined. The following notation will be used as shown in Figure 3.1.

Vertical Displacement (settlement):	s
Lateral Displacement:	u
Rotation:	θ
Vertical Load:	V
Horizontal Load:	H
Moment	M

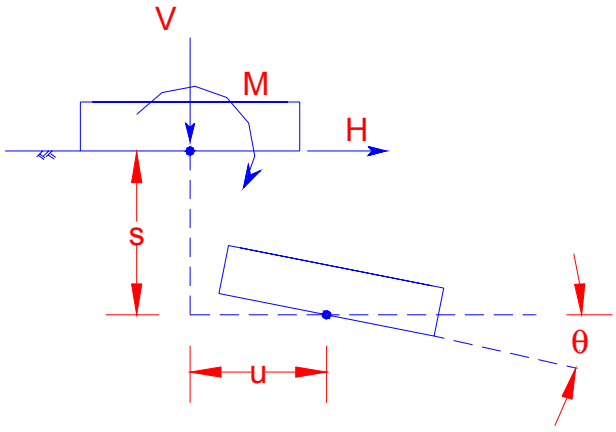

Fig. 3.1 Force and displacement notation for a displaced footing (after Phalen 2003)

Normalized parameters are also defined, such that one could compare any displacement or force measurement against a similar system with different aspect ratios and/or capacities:

Normalized Vertical Displacement (settlement): $U_V = s / L$
Normalized Horizontal Displacement: $U_H = u / L$
Normalized Rotation: $U_M = \theta$
Normalized Vertical Load: $F_V = V / V_{MAX}$
Normalized Horizontal Load: $F_H = H / V_{MAX}$
Normalized Moment: $F_M = M / V_{MAX}L$
Vertical Factor of Safety: $FS_V = V_{MAX} / V$
where L = footing length and V_{MAX} = ultimate bearing capacity

3.2 OPENSEES IMPLEMENTATION

The application of a Winkler-model for studying the nonlinear cyclic response of shallow foundations has been implemented into the OpenSees[1] platform. OpenSees is an open source numerical modeling platform being developed by the Pacific Earthquake Engineering Research (PEER) Center. There are a number of technical documents describing the OpenSees framework, commands, and examples; e.g., Mazzoni et al. (2003). OpenSees has been developed in C^{++} with a scripting language wrapper, Tk/Tcl, for model input (for more information, see Welch 2000). There are a variety of elements and material libraries available as well as a number of solution

[1] (Open System for Earthquake Engineering Simulation http://opensees.berkeley.edu/)

algorithms implemented for programmers, developers and users. The approach adopted herein is to study the applicability of using the materials and element models readily available in OpenSees. First, suitable material models were considered and subsequently various representative numerical models are constructed of the various physical models described in Chapter 2. A best approximation of the measured response is attempted. Both static and dynamic analyses were performed using OpenSees and the parameters discussed herein.

Static analyses were run with a linear algorithm of ten load steps per load increment using a load control integrator; a single point (sp) constraint to force the correct (target) displacement of the shear wall was used. The solution algorithm used a reverse Cuthill McKee (RCM) numberer, banded symmetric positive definite system of equations (BandGeneral), plain constraints, and a normal displacement increment test (test NormDispIncr) with a convergence tolerance of 1.0E–12 over a maximum of 100 iterations.

Transient analyses were run with a Newton algorithm, reverse Cuthill McKee (RCM) numberer, a general sparse system (UmfPack) of equations, a Newmark integrator with parameters of $\gamma = 0.5$ and $\beta = 0.25$, and a normal displacement increment test (test NormDispIncr) with a convergence tolerance of 1.0E–12 over a maximum of 100 interactions. A uniform excitation pattern was used to input the accelerations to the structure.

3.3 ONE-DIMENSIONAL MATERIAL RESPONSE AND CONSTITUTIVE LAWS

A variety of uniaxial material models currently available in OpenSees were evaluated for their applicability to model the shallow foundation-soil-structure interaction, including the effects of uplift. Elastic-perfectly-plastic materials combined with gap elements, general hysteretic materials and a QzSimple1 material developed by Boulanger et al. (1999) were studied. Three observed physical aspects are particularly important to capturing the overall response of the rocking shallow foundation and must be represented in the Winkler mesh: (1) the footing may uplift on the opposing loading side; (2) soil beneath the footing may yield; and (3) upon continued reversal of loading, settlement may accrue below the foundation. These properties should be represented in the individual material element response.

3.3.1 ElasticPPGap Material

The *elastic-perfectly-plastic* (EPP) material linearly follows an elastic tangent defined by Young's Modulus E. At a specified yield strain the material enters the plastic state, where further deformations are sustained without an increase in stress. The unloading stiffness is identical to the original loading stiffness. Different yield strains may be assumed in tension and compression. However, the material does not retain permanent deformations, thus may not capture accrued settlements below a rocking foundation. The *elastic-perfectly-plastic-gap* material follows the same behavior as the *elastic-perfectly-plastic* material, with the exception of a defined gap placed in parallel with the EPP response. The gap offsets the starting point of the material behavior beginning with a certain amount of material strain; thus this would be suitable for capturing uplifting on the load reversal side of the foundation. However, this material also does not have strain growth features, which is important for accrued settlement.

3.3.2 General Hysteretic Material

A *general hysteretic* material is available, whereby the user specifies two to three points on the compression and tension backbones in order to define bilinear or trilinear compression and tension backbone curves, respectively. Options are available to define pinching of the hysteresis in load or displacement directions, damage due to ductility, damage due to energy dissipation, and degraded unloading stiffness based on ductility. The generalized form of this material is shown in Figure 3.2. Combining multiple materials in parallel as shown in Figure 3.3 is useful for capturing any generalized backbone response using multiple bilinear materials. The algorithm presented in this figure was implemented in FLAC by Martin et al. (1997) to model bridge abutment soil-structure interaction, and could be reproduced in most finite element programs. The generality of the hysteretic material allows one to capture gap growth features as well.

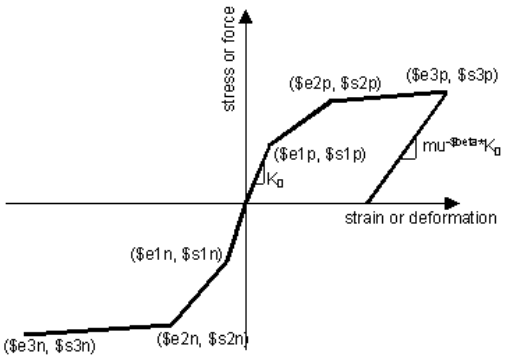

Fig. 3.2 Hysteretic material backbone curve (after Mazzoni et al. 2003)

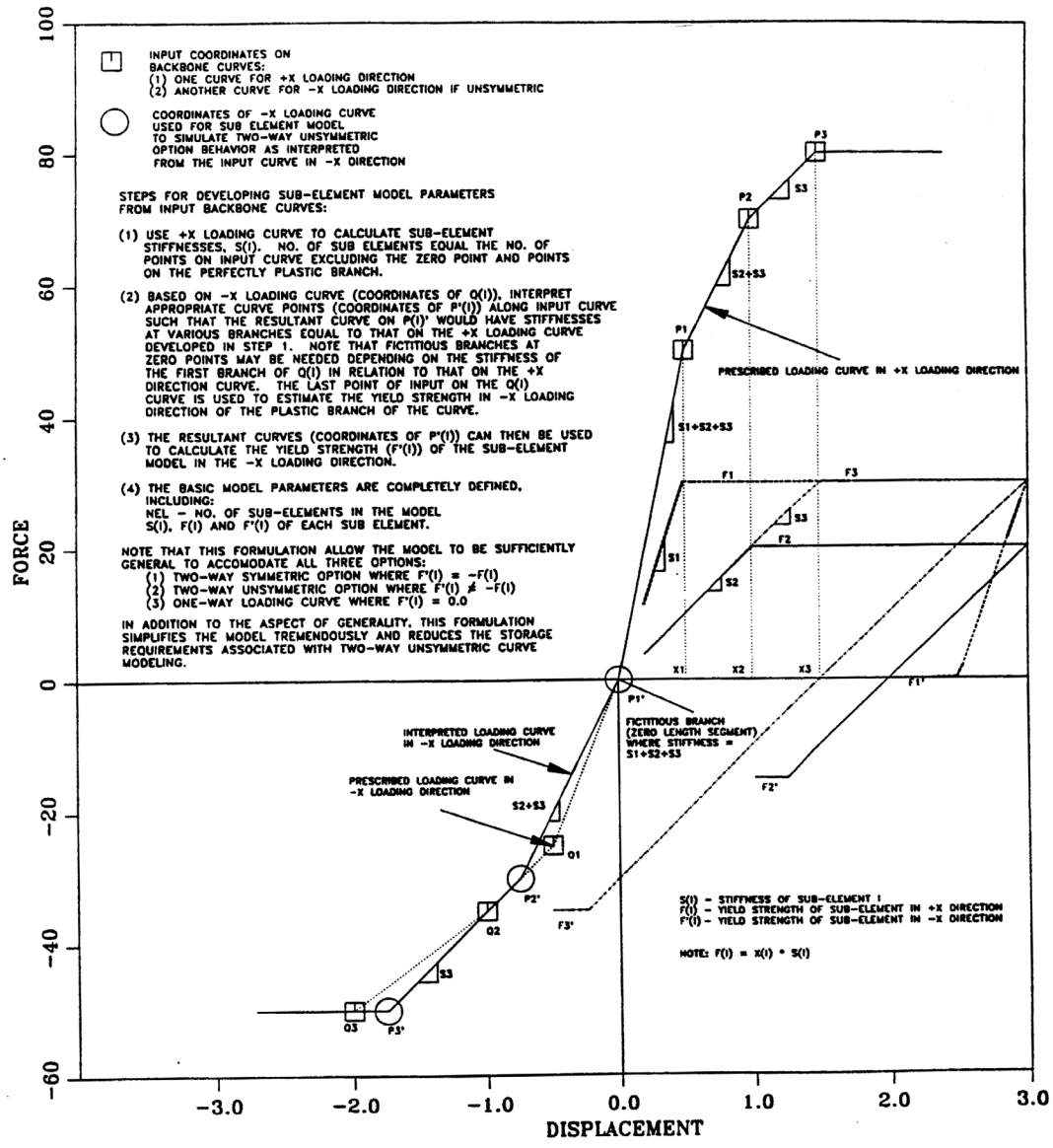

Fig. 3.3 Creation of backbone response by adding materials in parallel (after Martin et al. 1997)

3.3.3 QzSimple1 Material

The QzSimple1 material was recently implemented into OpenSees based on the formulation described in Boulanger et al. (1999). Although this material was intended to model the behavior of a pile tip under cyclic loading, the mechanisms of local response below the shallow foundation are quite similar.

Of the materials reviewed, the Q-z material is most applicable to the shallow foundation problem because it has a non-symmetric backbone defined by an ultimate load on the compression side and a reduced strength in tension as the soil separates from the footing (in tension). Uplift (geometric nonlinearities) are provided by adding an additional gapping component in series with the elastic and plastic components.

In addition, under cyclic loading, the material does not attain full stiffness until the strain reaches the previous cycle's unloading strain. In this sense, the material has a gap that grows with each cycle, such that settlement is cumulative. The element utilizes an elastic, plastic, and gap component in series as generally shown in Figure 3.4. Radiation damping may be modeled through a dashpot added in parallel to the elastic component of the material. Wang et al. (1998) showed that providing rate-dependent damping in parallel with plastic (hysteretic) elements overestimates damping forces; therefore placing dashpots in parallel with elastic components is preferred. The behavior modeled either follows Reese and O'Neill's (1987) relation for drilled shafts in clay or Vijayvergiya's (1977) relation for piles in sand. The material is used with one-dimensional zero length elements. The inputs to this material are the type of material, clay (1) or sand (2), the ultimate load capacity q_{ult}, the displacement, z50, at which 50% of the ultimate load is mobilized, the amount of suction (tension capacity) *suction*, and viscous damping, *c*.

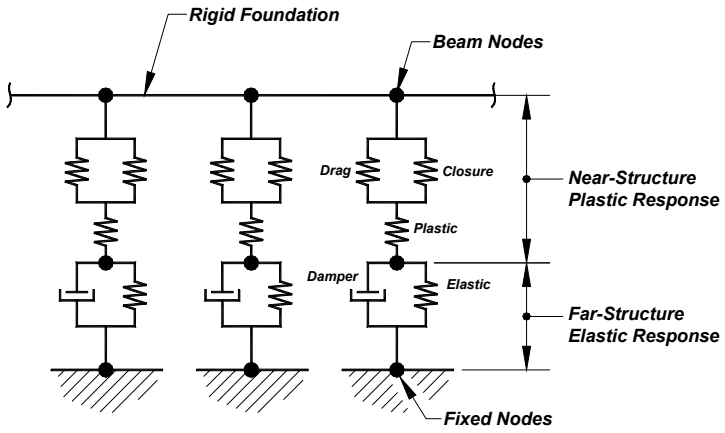

Fig. 3.4 Example series of Winkler springs below a rigid foundation represented by one-dimensional finite elements

The QzSimple1 material, however, may not be readily found in other platforms, although one may easily reproduce the characteristic curve by placing several general hysteretic materials in parallel. The advantage of the hysteretic material is its ease of implementation within readily available analysis platforms (e.g., DRAIN-3DX (2002), RAM Perform-3D (2003)). The material behavior of both the parallel hysteretic material and the QzSimple1 material applied to a single zero-length one-dimensional element and subjected to ramped sinusoidal displacement are shown in Figure 3.5 with a tension capacity of 10% q_{ult}.

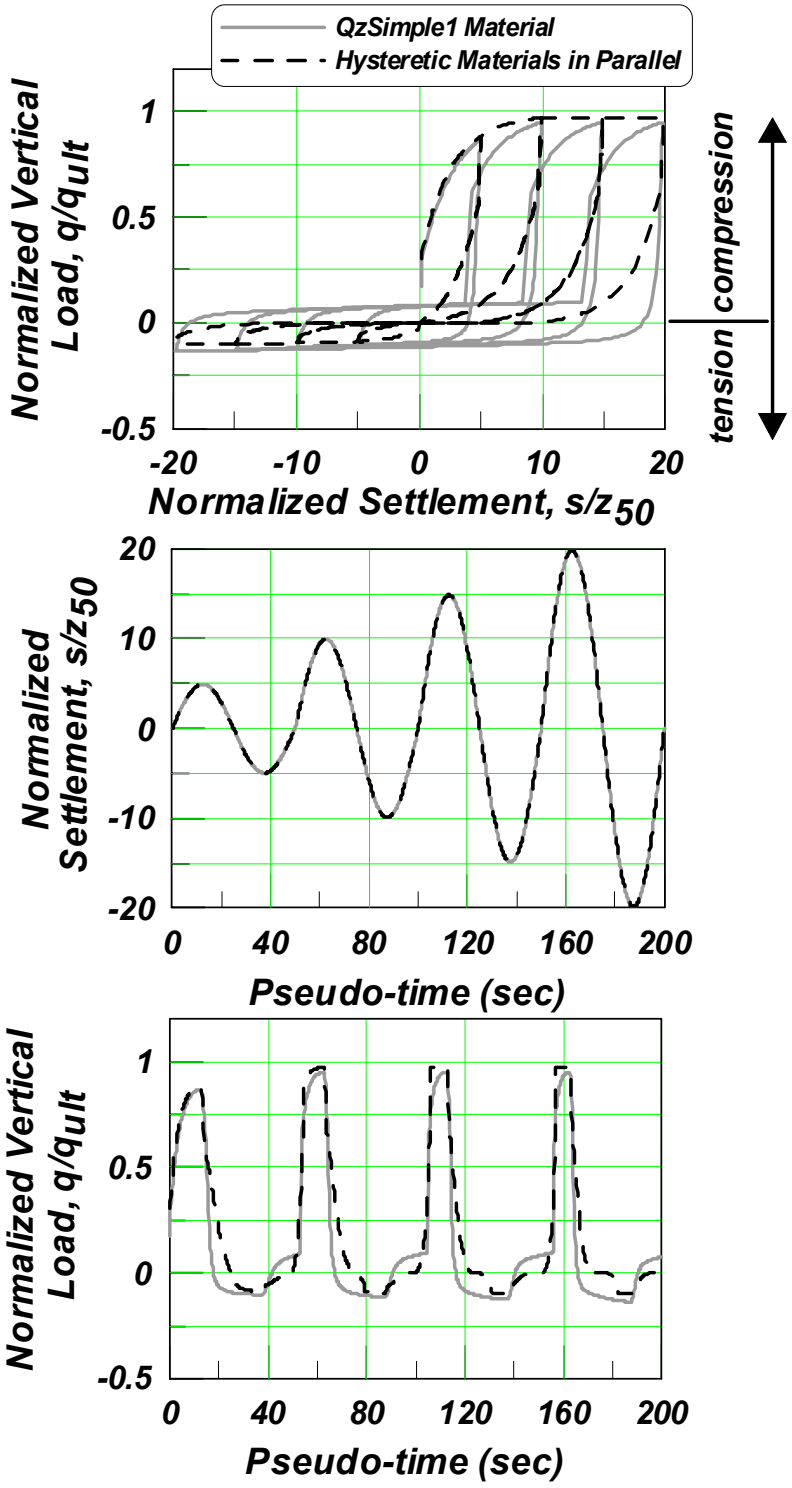

Fig. 3.5 Comparison of QzSimple1 and hysteretic materials placed in parallel

Perhaps the most visible difference between the two materials is the unloading from the compression region, i.e., approaching zero load (into tension zone). At this interface, the parallel hysteretic material unloads only to approximately zero strength, while the QzSimple1 material unloads until mobilization of nominal tension capacity. The former would imply a material with zero resistance through a range of strain accumulation. The later is more representative of the backside suctioning that may occur upon compression unloading due to the any adhesion of the soil to the foundation element. Given their similar nature, the QzSimple1 material is used throughout these analyses.

In OpenSees, two other materials are available for modeling the soil-foundation interface using one-D elements; the P-y and T-z materials. Originally intended to simulate the horizontal (P-y) and skin resistance (T-z) components against a pile, these materials are useful to the study of broader soil-structure interaction problems because they have been evaluated using a range of pile-test data and they are formed using basic mechanisms anticipated at the interface. All three materials are similar in nature, in that they consist of an elastic and plastic material in series. The elastic material captures the "far-field" behavior, while the plastic component captures the "near-field" permanent displacements, as illustrated in Figure 3.4.

The OpenSees implementation of the P-y, T-z and Q-z materials are described in Boulanger (2000b) and are based on earlier work by Boulanger et al. (1999). For the Q-z material, the plastic component is initially very rigid in the range of $-C_r \cdot q_{ult} < q < C_r \cdot q_{ult}$, where C_r is the ratio of q / q_{ult} when plastic yielding first occurs in virgin loading. After this initially rigid range, which grows with plastic yielding, the plastic response is described by:

$$q = q_{ult} - (q_{ult} - q_o) \cdot \left[\frac{cz_{50}}{cz_{50} + \left| z^p - z_o^p \right|} \right]^n \tag{3.5}$$

where

q = load on the plastic component

q_{ult} = ultimate resistance of the q-z material in compression

q_o = q at the start of the current plastic loading cycle

z_{50} = the displacement at which 50% of q_{ult} is mobilized during monotonic loading

z_o^p = z^p at the start of the current loading cycle

c, n = constants that control the shape of the $q - z^p$ curve

The plastic region of the uplift, or tension, side of the response is controlled by:

$$q_d = C_d q_{ult} - \left(C_d q_{ult} - q_o^d\right) \cdot \left[\frac{z_{50}}{z_{50} + 2\left|z^g - z_o^g\right|}\right] \tag{3.6}$$

where

q^d = drag force on the closure component

q_{ult} = ultimate resistance of the q-z material in compression

q_o^d = q^d at the start of the current loading cycle

z_{50} = the displacement at which 50% of q_{ult} is mobilized during monotonic loading

z_o^g = z^g at the start of the current loading cycle

C_d = Ratio of the maximum drag (suction) force to the ultimate resistance of the q-z material

The constants c, n and C_r are recommended in Boulanger (2000b). For a clay material, c = 0.35, n = 1.2, and C_r = 0.2 in order to follow Reese and O'Neill's (1987) recommended backbone for drilled shafts in clay. For a sand material, c = 12.3, n = 5.5, and C_r = 0.3 in order to follow Vijayvergiya's (1977) recommended backbone for piles in sand. In the current OpenSees implementation of the Q-z material (named "QzSimple1"), the constants c, n, and C_r are pre-programmed such that the user only specifies the material type, either sand or clay and follows the backbone curve prescribed. The user also specifies the values of q_{ult}, z_{50}, and C_d. The recommended value of z_{50} for piles in sand is given as $0.125 z_{crit}$ by Vijayvergiya (1977), where z_{crit} = displacement at which q_{ult} is fully mobilized.

The initially rigid portion of the QzSimple1 material can be set to any stiffness K_{el} by inputting the z_{50} value as:

$$z_{50} = \frac{1.39 q_{ult}}{K_{el}} \text{ for sand, and } z_{50} = \frac{0.525 q_{ult}}{K_{el}} \text{ for clay} \tag{3.7}$$

where the coefficients 1.39 and 0.525 were found from an investigation of the OpenSees source code. These values are based on an approximation of the recommended backbones described.

3.3.4 PySimple1 Material

Similar to the QzSimple1 material, the PzSimple1 material was originally intended to model horizontal soil resistance against piles. This material may also be useful for embedded shallow foundations, for example, to capture horizontal passive earth pressure and stiffness that develops as the foundation slides, densifies, and possibly creates gaps. Under cyclic loading, the material does not reload until the strain reaches the previous cycle's unloading strain, thus a gap develops that grows with each cycle.

For the P-y material the plastic component is initially very rigid in the range of $-C_r p_{ult} < q < C_r p_{ult}$, where C_r is the ratio of p/p_{ult} when plastic yielding first occurs in virgin loading. After this initially rigid range, which grows with plastic yielding, the plastic response is described by (Boulanger et al. 1999):

$$p = p_{ult} - (p_{ult} - p_o) \cdot \left[\frac{c y_{50}}{c y_{50} + \left| y^p - y_o^p \right|} \right]^n \tag{3.8}$$

where

p = load on the plastic component
p_{ult} = ultimate resistance of the q-z material in compression
p_o = p at the start of the current plastic loading cycle
y_{50} = the displacement at which 50% of p_{ult} is mobilized during monotonic loading
y_o^p = y^p at the start of the current loading cycle
c, n = constants that control the shape of the $p - y^p$ curve

The closure spring, $p - y^g$ is described by:

$$p^c = 1.8 p_{ult} \left[\frac{y_{50}}{y_{50} + 50\left| y_o^+ - y^g \right|} - \frac{y_{50}}{y_{50} - 50\left| y_o^- - y^g \right|} \right] \tag{3.9}$$

where

p^c = drag force on the closure component
$y_o^{+,-}$ = memory terms for the positive and negative side of the gaps

The nonlinear drag spring is described by:

$$p^d = C_d\, p_{ult} - \left(C_d\, p_{ult} - p_o^d\right) \cdot \left[\frac{y_{50}}{c y_{50} + 2\left| y^p - y_o^g \right|} \right] \tag{3.10}$$

The constants c, n, and C_r are recommended in Boulanger (2000a) as c = 10, n = 5, and C_r = 0.35 in order to follow Matlock's (1970) recommended backbone for soft clay and c = 0.5, n = 2, and C_r = 0.2 to approximate API's (1993) backbone for drained sand. P-y springs are generally placed in multiple locations along the length of a pile to account for varying soil properties with depth. However, for the shallow foundation modeling discussed here, it is assumed that the soil properties are not changing from the top of the footing to the base; thus all properties are lumped at a single spring. Additionally, it is assumed that the shape of the footing (rectangular) does not affect the load-displacement response of the soil, since the elevation cross sections of a footing of base B and a pile of diameter B, both of the same embedment, would have the same effective area against the soil. However, it is arguable that the zone of disturbance may be different between a square and circular cross section. In the current OpenSees implementation of the P-y material (named "PySimple1"), the constants c, n, and C_r are pre-programmed such that the user only specifies the material type, either sand or clay. The user also specifies the values of p_{ult}, y_{50}, and C_d. The response of the PySimple1 material is shown in Figure 3.6.

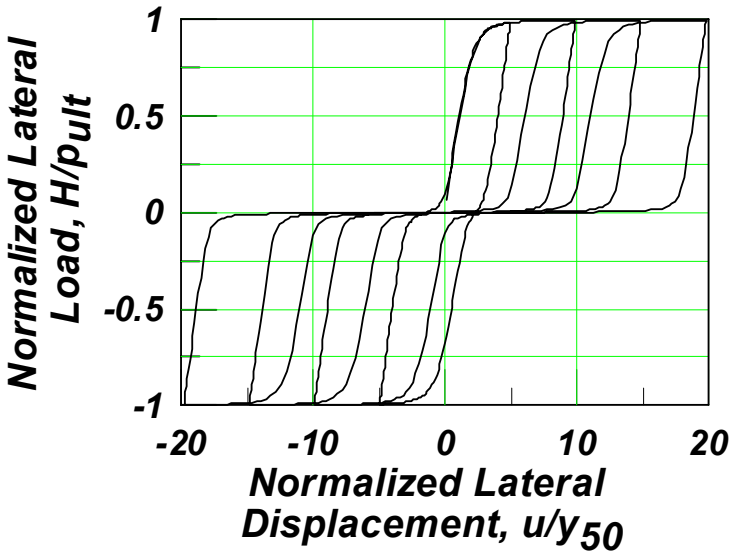

Fig. 3.6 PySimple1 material normalized load-displacement behavior

The initially rigid portion of the PySimple1 material can be set to any stiffness K_{el} by inputting the y_{50} value as:

$$y_{50} = \frac{0.542\, p_{ult}}{K_{el}} \text{ for sand, and } y_{50} = \frac{8.0\, p_{ult}}{K_{el}} \text{ for clay} \tag{3.11}$$

where the coefficients 0.542 and 8.0 were found from an investigation of the OpenSees source code. These values are based on an approximation of the recommended backbones described.

3.3.5 TzSimple1 Material

The TzSimple1 material was intended to capture the frictional component of load and displacement as axial displacement develops along the pile length. Although this material was implemented to model the behavior of a pile moving vertically, the mechanisms of a surface sliding over a frictional material are quite similar. The element uses an elastic and plastic component in series.

The behavior and equations controlling the T-z material are described in Boulanger (2000c), and generally follow the P-y material discussed by Boulanger et al. (1999). For the T-z material the plastic component is described by:

$$t^p = t_{ult} - \left(t_{ult} - t_o^p\right) \cdot \left[\frac{cz_{50}}{cz_{50} + \left|z^p - z_o^p\right|}\right]^n \tag{3.12}$$

where

t = load on the plastic component
t_{ult} = ultimate resistance of the t-z material in the current loading direction
t_o^p = t^p at the start of the current plastic loading cycle
z_{50} = the displacement at which 50% of q_{ult} is mobilized during monotonic loading
z_o^p = z^p at the start of the current loading cycle
c, n = constants that control the shape of the t-z^p curve

The elastic component is defined by:

$$t^e = C_e \frac{t_{ult}}{z_{50}} \cdot z^e \tag{3.13}$$

where

C_e = Constant that defines the normalized elastic stiffness

The constants *c, n,* and C_e are recommended in Boulanger (2000c), c = 0.5, n = 1.5, and C_e = 0.708 for drilled shafts following Reese and O'Neil's (1987) backbone, and to follow Mosher's (1984) recommendation for axially loaded piles in sand, c = 0.6, n = 0.85 and C_e = 2.05. In the current OpenSees implementation of the T-z material (named "TzSimple1"), the constants *c, n*, and C_e are pre-programmed such that the user specifies only the material type, either sand or clay. The user also specifies the values of t_{ult}, and z_{50}. The response of the TzSimple1 material is shown in Figure 3.7.

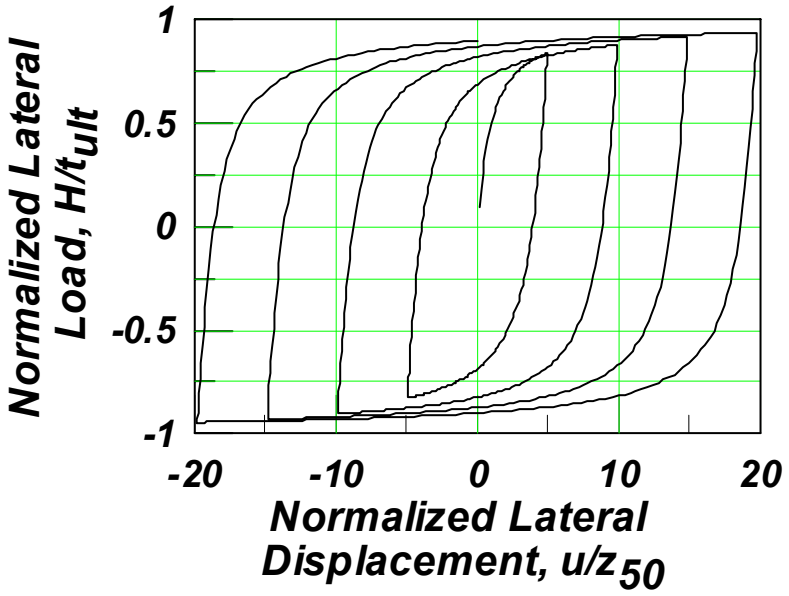

Fig. 3.7 TzSimple1 material normalized load-displacement behavior

The elastic stiffness of the TzSimple1 material can be set to any stiffness K_{el} by inputting the z_{50} value as:

$$z_{50} = C_e \frac{t_{ult}}{K_{el}} \tag{3.14}$$

3.4 ELASTIC STIFFNESS COMPARISON

Gazetas (1991) elastic stiffness recommendations are widely adopted in several recent design documents [e.g., ATC-40 (1996) and FEMA 356 (2000)]. These equations will be used for preliminary stiffness estimation and compared with experimentally observed values of vertical, sliding, and rotational stiffness.

For a footing with the dimensions as shown in Figure 3.8, Gazetas (1991) presents the global stiffness (or uncoupled total embedded stiffness) of a foundation K_i as a product of the stiffness of a footing resting on the surface K_i' and an embedment factor e_i :

$$K_i = K_i' e_i \tag{3.15}$$

where

K_i = Uncoupled Total Surface Stiffness for a rigid plate on a semi-infinite homogeneous elastic half-space

e_i = Stiffness Embedment Factor for a rigid plate on a semi-infinite homogeneous elastic half-space

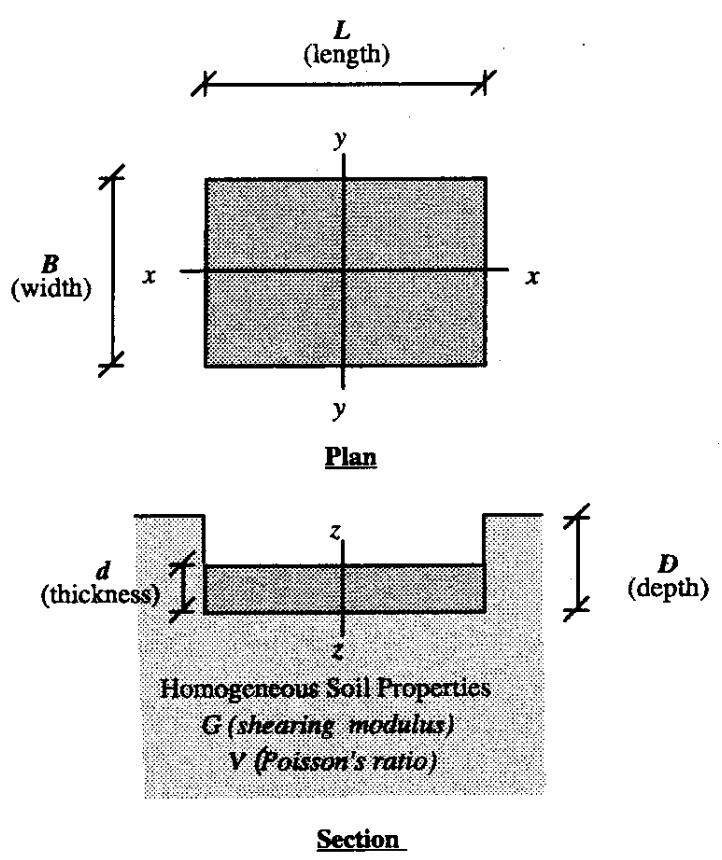

Fig. 3.8 Foundation dimensions for use with Gazetas' elastic stiffness equations, as presented in ATC-40 (1996). Table 3.1 presents the generalized stiffness equations for horizontal and vertical translation and rocking about both planar axes.

Table 3.1 Gazetas' equations for shallow footing stiffness [after Gazetas (1991), as summarized in ATC-40 (1996)]

Stiffness Parameter	Equation
	Surface Stiffnesses
Vertical Translation	$K_Z' = \frac{GL}{1-\nu}\left[0.73 + 1.54\left(\frac{B}{L}\right)^{0.75}\right]$
Horizontal Translation (toward long side)	$K_Y' = \frac{GL}{2-\nu}\left[2 + 2.5\left(\frac{B}{L}\right)^{0.85}\right]$
Horizontal Translation (toward short side)	$K_X' = \frac{GL}{2-\nu}\left[2 + 2.5\left(\frac{B}{L}\right)^{0.85}\right] + \frac{GL}{0.75-\nu}\left[0.1\left(1-\frac{B}{L}\right)\right]$
Rotation about x-axis	$K_{\theta x}' = \frac{G}{1-\nu} I_X^{0.75}\left(\frac{L}{B}\right)^{0.25}\left(2.4 + 0.5\frac{B}{L}\right)$
Rotation about y-axis	$K_{\theta y}' = \frac{G}{1-\nu} I_Y^{0.75}\left[3\left(\frac{L}{B}\right)^{0.15}\right]$
	Stiffness Embedment Factors
Embedment Factor, Vertical Translation	$e_Z = \left[1 + 0.095\frac{D}{B}\left(1 + 1.3\frac{B}{L}\right)\right]\left[1 + 0.2\left(\frac{2L+2B}{LB}d\right)^{0.67}\right]$
Embedment Factor, Horizontal Translation (toward long side)	$e_Y = \left[1 + 0.15\left(\frac{2D}{B}\right)^{0.5}\right]\left\{1 + 0.52\left[\frac{\left(D-\frac{d}{2}\right)16(L+B)d}{BL^2}\right]^{0.4}\right\}$
Embedment Factor, Horizontal Translation (toward short side)	$e_X = \left[1 + 0.15\left(\frac{2D}{L}\right)^{0.5}\right]\left\{1 + 0.52\left[\frac{\left(D-\frac{d}{2}\right)16(L+B)d}{LB^2}\right]^{0.4}\right\}$
Embedment Factor, Rotation about x axis	$e_{\theta X} = 1 + 2.52\frac{d}{B}\left(1 + \frac{2d}{B}\left(\frac{d}{D}\right)^{-0.2}\left(\frac{B}{L}\right)^{0.5}\right)$
Embedment Factor, Rotation about y axis	$e_{\theta Y} = 1 + 0.92\left(\frac{2d}{L}\right)^{0.60}\left(1.5 + \left(\frac{2d}{L}\right)^{1.9}\left(\frac{d}{D}\right)^{-0.60}\right)$

For the comparison with experimental shallow foundation systems, Gazetas stiffnesses will be calculated using relations from the EPRI manual (1990) of shear modulus and Poisson's ratio according to soil type. The specifics of these estimates are described in Chapter 3.8.1.

3.5 SELECTION OF WINKLER SPRING PROPERTIES

In the selection of properties for the BNWF mesh generator, there exist two types of parameters that could benefit from investigation; inherent properties such as strength and stiffness and modeling parameters. Inherent soil properties are well investigated but have a great amount of uncertainty associated with them. Soil properties generally vary quite a bit, so an attempt is made to justify a range of values. Model parameters are those which are specific to the type of model (e.g., Winkler, continuum). In this study these parameters include the type of bearing pressure distribution to use and an end region length to better capture densification and rounding of the soil medium at the edge of the foundation.

3.5.1 Vertical Stiffness

Stiffness of the Winkler springs is an important characteristic of the material model that must be specified to a reasonable degree of accuracy. In this case, both the vertical and rotational stiffness of the shallow foundation system are investigated using experimental data and equations available in the literature. In the Winkler framework, summing the individual spring contributions provides the vertical stiffness of the system, whereas contributions to rotational stiffness are accounted for by the springs along the length of the foundation and through varying the vertical spring element properties.

The appropriate stiffness to use in modeling any foundation system is widely open to debate, based on the typically wide range found for soil properties, as well as the wide variety of simulation methods and their assumptions. Based on the uncertainty of soil properties alone, ATC-40 states that unless detailed geotechnical data are available, a factor of two should be applied to the component capacity and stiffness in order to capture the effects of soil-structure interaction on the superstructure. If the soil is stronger than the design assumption, larger loads

may potentially be transmitted to the superstructure, while if the soil is weaker than the design assumption, larger displacements may occur. The safest design would anticipate both cases.

Vertical push-test data of model shallow-foundation footings are available for the experimental data of Rosebrook and Kutter (2001a, b, c), Negro et al. (1998), and Gajan et al. (2003a, b). From these tests, linear stiffnesses can be determined at different loading locations.

Allotey and Naggar (2003) recently compared theoretical moment rotation curves with experimental results from the TRISEE test series. Initial, unloading, and secant stiffnesses were obtained from the vertical push test data, and moment-rotation envelopes were constructed. A good comparison with the experimental envelope was found when the unloading stiffness was used in the analytical model. A similar approach was attempted here, where an initial stiffness K_{int} was fit to the straight line portion of the curve, and an unloading stiffness K_{unl} was extracted if unloading was performed. For vertical push test KRR02 S12, the variation of unloading stiffness with settlement was investigated. Figure 3.9(a) shows the unloading stiffness at various points along the compression vertical push test, and Figure 3.9(b) shows the variation of the unloading stiffness from the mean of the sample unloading stiffnesses as a function of the values available. Of the data shown in Figure 3.9(b), 81% fall within $\pm$ 1σ of the mean of the data analyzed.

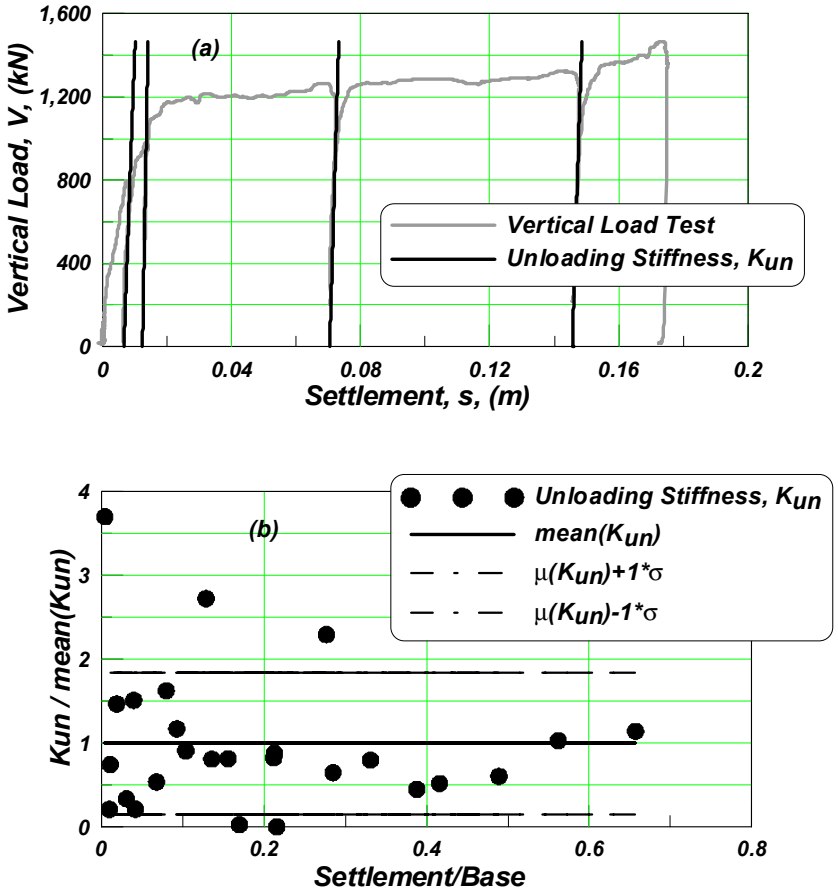

Fig. 3.9 (a) Unloading stiffness shown graphically on a vertical load vs. settlement plot and (b) variation of unloading stiffness with settlement (KRR02-S12, Rosebrook and Kutter 2001b)

An example M-θ envelope using the initial and unloading stiffness is shown in Figure 3.10. The vertical unloading stiffness appears to provide a reasonable estimate of the initial rotational stiffness.

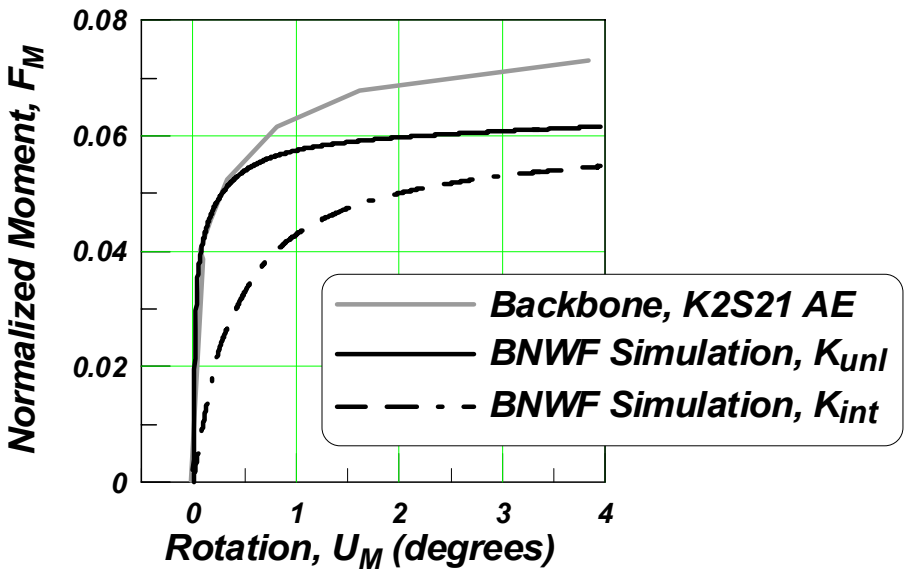

Fig. 3.10 Normalized backbones for comparison of unloading to initial stiffness (test K2S21 AE)

By setting the initially elastic portion of the Qzsimple1 model (as defined in Chapter 3.3.3) to the unloading stiffness, the comparison between vertical push tests and the QzSimple1 behavior generally agrees well, as shown in Figures 3.11–3.12. In some cases the unloading stiffness is much larger than the initial stiffness due to the densification that may occur upon cycling, and the Q-z relation based on Kunl input does not give reasonable comparison. This is true particularly for softer specimens, such as KRR02-S54 (medium dense sand, medium size footing), and the specimen is loaded with repeated vertical cycles at early settlement levels.

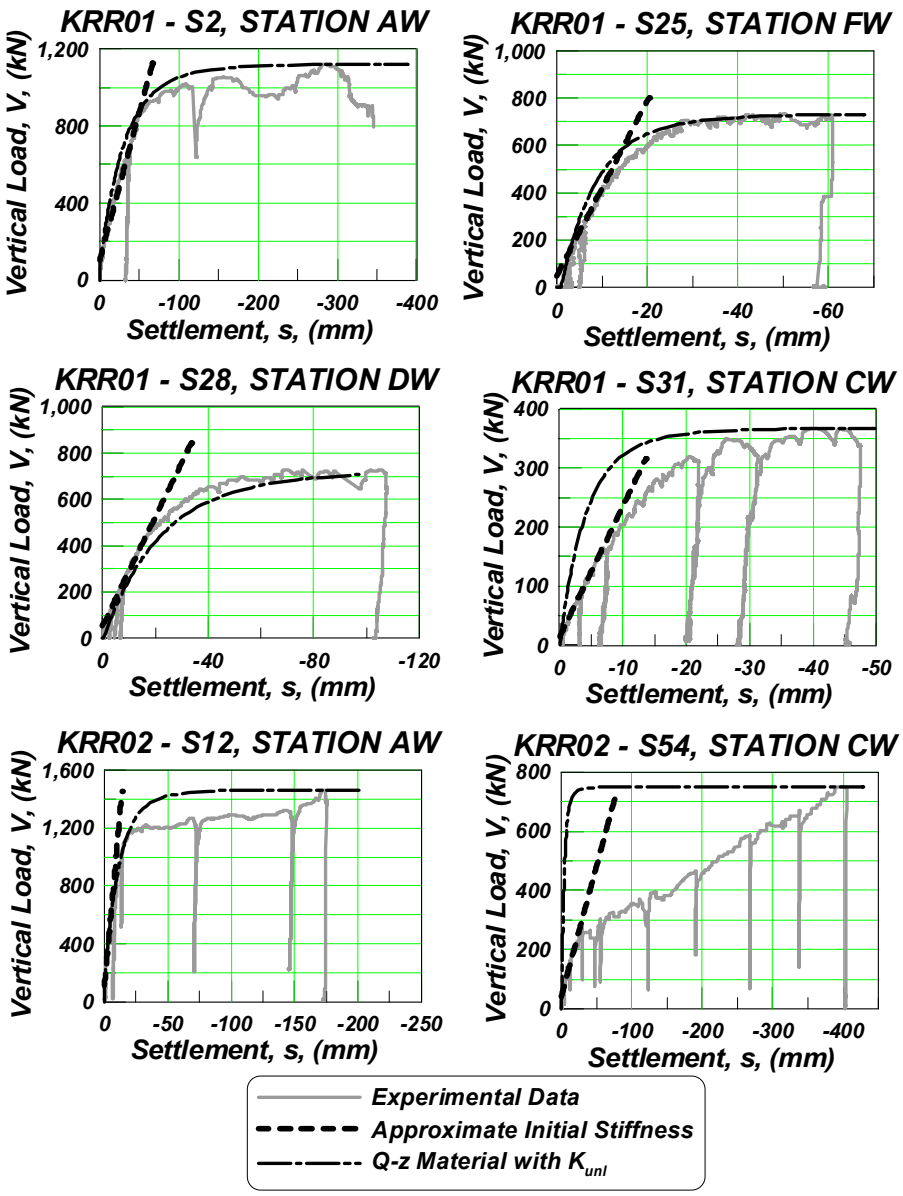

Fig. 3.11 Vertical push test data from centrifuge testing on sand

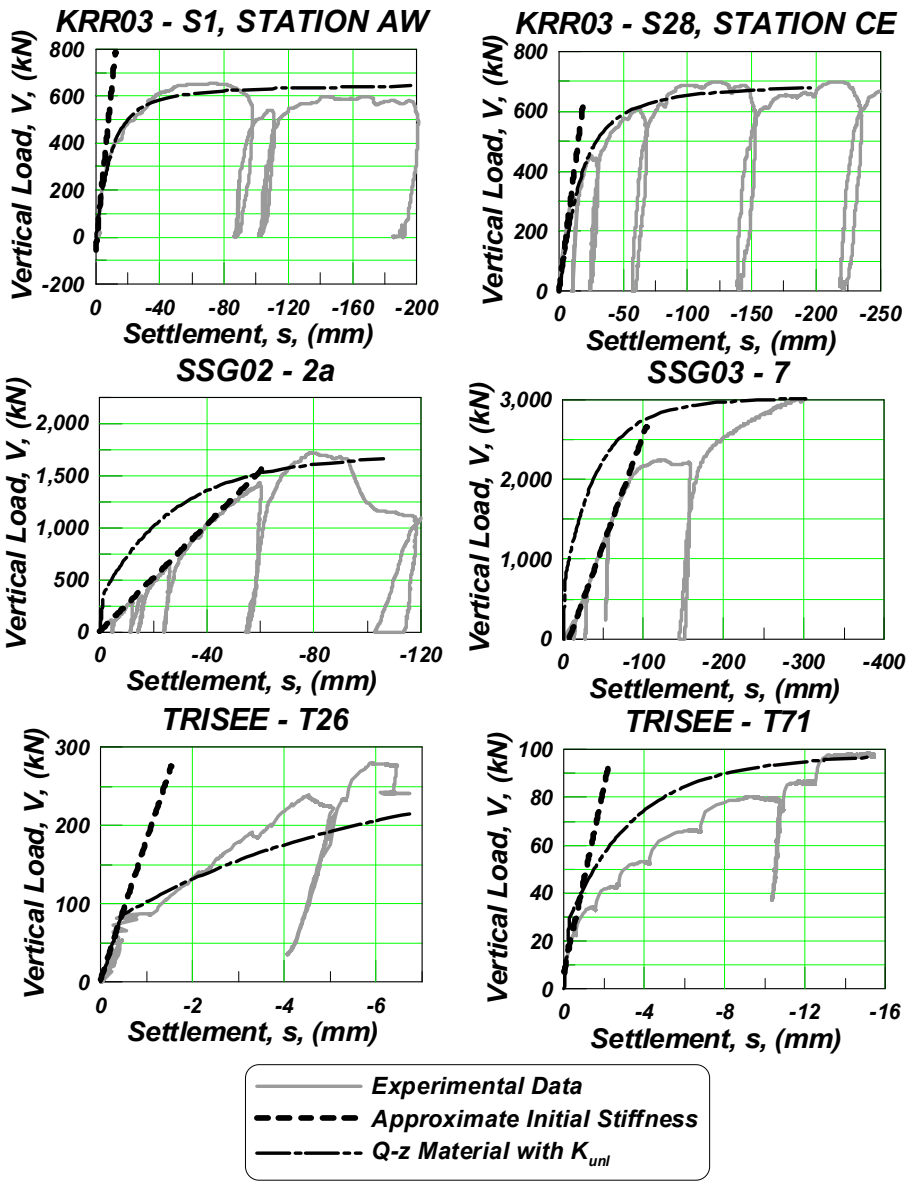

Fig. 3.12 Vertical push test data on clay (KRR03) and sand (TRISEE) testing

3.5.2 Horizontal Load Capacity and Stiffness

Horizontal strength and stiffness is provided to the shallow foundation through sliding at the base (and sides if the foundation is embedded) and passive earth pressure at the front of the foundation (if embedded).

3.5.2.1 Horizontal Frictional Sliding

Similar to the manner in which the vertical load-displacement relationship was evaluated from vertical load capacity tests, the horizontal load-displacement sliding capacity relationship is evaluated using tests where horizontal loading was isolated (or a primary contributor) from moment loading. For these analyses, it is reasonable to assume the largest contribution of horizontal resistance is transmitted through interface (base) friction, (since footings are either lightly embedded or resting on the surface). Therefore, springs are placed horizontally in the BNWF model, parallel to the level ground surface, to account for sliding resistance. Three test series on sand provide such data, including two tests in a series conducted by Gadre and Dobry (1998) at the 100-g RPI geotechnical centrifuge, and one test each for two test series SSG02 and SSG03 on the UC Davis Geotechnical centrifuge by Gajan et al. (2003 a,b). Tests by Gadre and Dobry are performed on a rigid square foundation of length 1.14 m, on a dry sand of relative density 75%. Figure 3.13(a) shows the prototype structure test setup and (b) the configuration of two tests B and BL, where sliding is isolated by separation from the confining soil walls. Test BL has an additional weight added to the structure. Figures 3.13(c)–(d) show the horizontal load versus sliding displacement for tests B and BL, respectively.

An inspection of the experimental plots shows that for both tests B and BL, the load gradually increases toward a maximum value. The maximum horizontal loads for tests B and BL are the peak values of 44 and 88 kN, respectively.

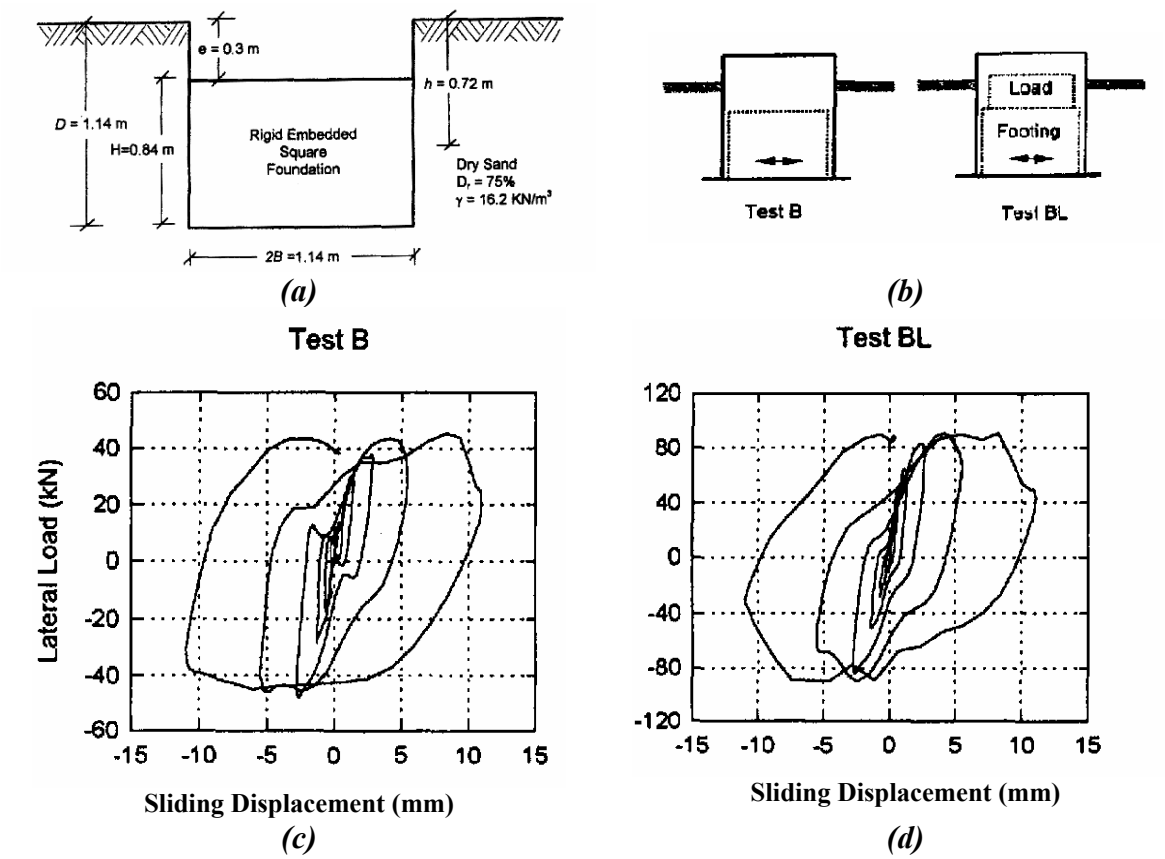

Fig. 3.13 Tests B and BL by Gadre and Dobry (1998), (a) prototype structure test setup, (b) sliding-isolated tests B and BL, horizontal load vs. sliding displacement for (c) test B and (d) BL

The horizontal load tests by Gajan et al. (2003a, b) are performed on 80% relative density sand, on a footing 2.84 m by 0.69 m resting on the ground surface. Figure 3.14(a) shows results for test SSG02 6a (station H), and Figure 3.14(c) shows test SSG03 1a (station A). In test SSG02 6a, both load and displacement are unsymmetrical (i.e., significantly larger forces and displacements are observed in the positive direction than in the negative direction). For test SSG03 1a, the maximum load and displacement is more symmetric but continues to increase with cycling, which may be attributed to accumulation of passive earth pressure as the footing settles. For both tests, permanent rotations develop as the footing settles more to one side. However, at small amplitude cycles, these permanent settlements and rotations are very small, so any contribution to the horizontal resistance from passive earth pressure is very small. For these two tests, the maximum load corresponding to the base frictional resistance is taken at the point where sliding resistance is first broken; it is assumed as the largest load on the negative axis (first

loading cycle) of 115 kN for test SSG02 6a (Fig. 3.14(b), and the first constant of 187 kN for test SSG03 1a (Figs. 3.14(b)–(d) show the low amplitude, early cycles of these tests with the backbone overlain for each.

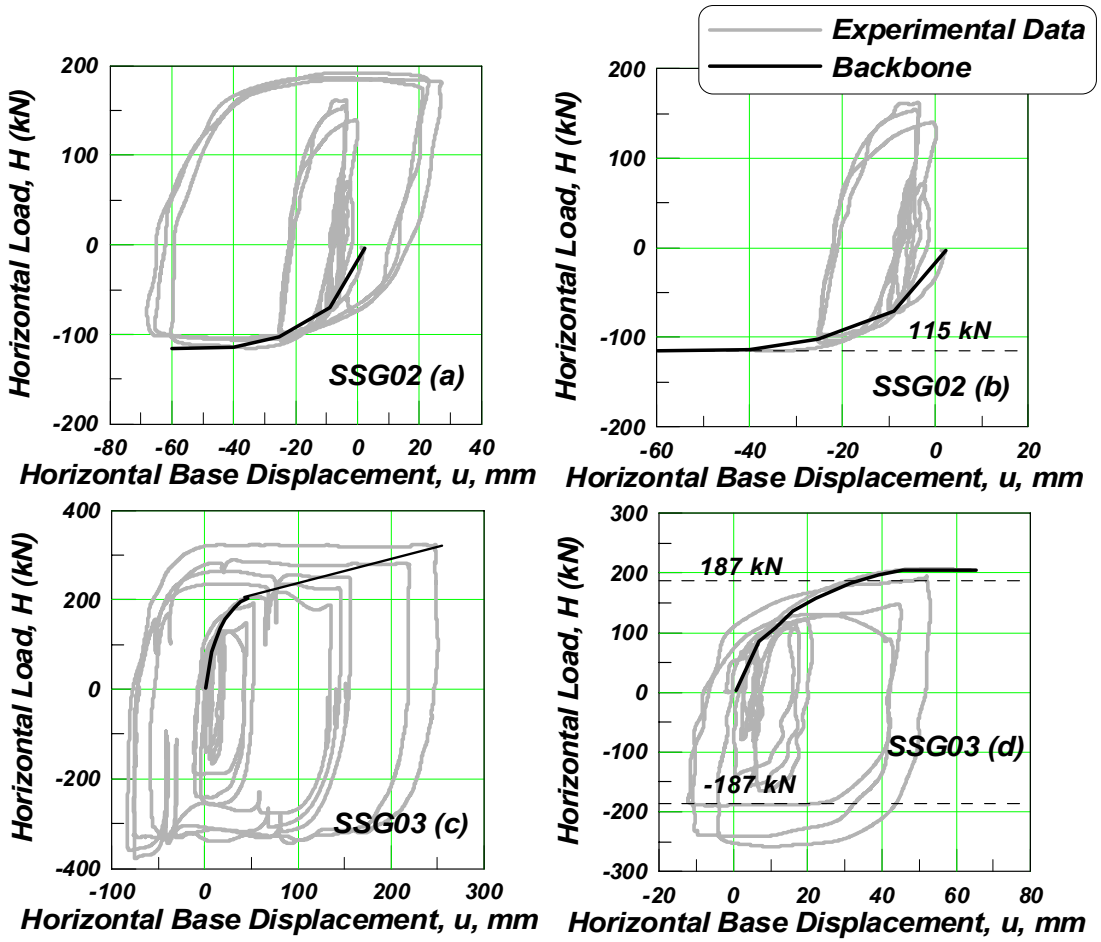

Fig. 3.14 Horizontal load vs. sliding displacement, (a) complete horizontal load vs. displacement of SSG02 Test 6a, (b) early cycles of (a), (c) complete horizontal load vs. displacement of SSG03 Test 1a, (d) early cycles of (c)

In conventional design practice, the frictional resistance of an interface shearing a cohesionless material is estimated as $\tan(k\phi')$ times overburden, where k varies from 1/3 to 2/3. Alternatively, one may assume the critical state friction angle is attained upon full shearing, since this represents the final strength of the system when it has either degraded past the peak value or increased to a maximum, depending on its density, at large strains. EPRI (1990) provides an empirical relation of the critical state friction angle after Bolton (1986):

$$\phi_{cs} = \phi' - 3(Dr[10 - \ln(q_u / p_a)] - 1) \tag{3.16}$$

where ϕ' is the friction angle calculated by triaxial compression, Dr is the relative density, q_u is the mean principal effective stress at failure, and p_a is atmospheric pressure. For the tests by Gadre and Dobry (1998), the reported friction angle was determined from the inverse tangent of the friction coefficient at failure, so this is in fact the critical state friction angle. The proposed expression for the critical state friction angle slightly overestimates the coefficient of friction for the SSG test series, as shown in Table 3.2.

Table 3.2 Comparison of static coefficient of friction for horizontal sliding tests

Ref	test	Dr	ϕ	ϕ_{cs}	L	B	H	$\mu_{\exp}$	μ_{cs}
		(%)	(deg)	(deg)	(m)	(m)	(kN)	-	-
(1)	(2)	(3)	(4)	(5)	(6)	(7)	(8)	(9)	(10)
G&D	"B"	75	39	39	1.14	1.14	44	0.82	NA
G&D	"BL"	75	39	39	1.14	1.14	88	0.82	NA
SSG02	6a	80	43.2	27.7	2.84	0.69	115	0.41	0.52
SSG03	1a	80	37.9	22.2	2.84	0.69	188	0.32	0.41

Column Notes:
(1) G&D refers to tests by Gadre and Dobry (1998); SSG refers to tests by Gajan et al. (2003 a,b).
(2) For tests by Gadre and Dobry, "B" denotes Base shear, "L" denotes additional vertical load at base.
(4) Friction angle for Gadre and Dobry (1998) calculated by laboratory triaxial tests from Arulmoli et al. (1992). Friction angle for SSG back-calculated from vertical load test data.
(6), (7) Length parameters for foundation are presented at prototype scale.
(8) H = Horizontal load at observed sliding initiation
(9) $\mu_{\exp}$ = Friction coefficient from experiment, calculated by dividing the vertical load by the maximum horizontal load (as reported in Gadre and Dobry (1998))
(10) μ_{cs} = Critical state friction coefficient, calculated by $\tan(\phi_{cs})$

Using the T-z material discussed in Section 3.3.3 shows good agreement with the backbone of the sliding tests available, as shown in Figure 3.15. The backbone of the T-z material is empirically calculated based on pile tests, but the load-displacement mechanisms of the friction force developed by a foundation structure sliding over a cohesionless base appear to give reasonable results. For the tests by Gajan et al. (2003a, b) the critical state friction coefficient is approximately 1.27 times the experimentally observed value.

In summary, using ϕ_{cs} to estimate sliding capacity gives a reasonable approximation, calculating a friction coefficient within 20% compared with experimental data. Additionally, the

T-z style horizontal spring has a reasonably shaped nonlinear response for use with the BNWF simulations for representing the sliding resistance.

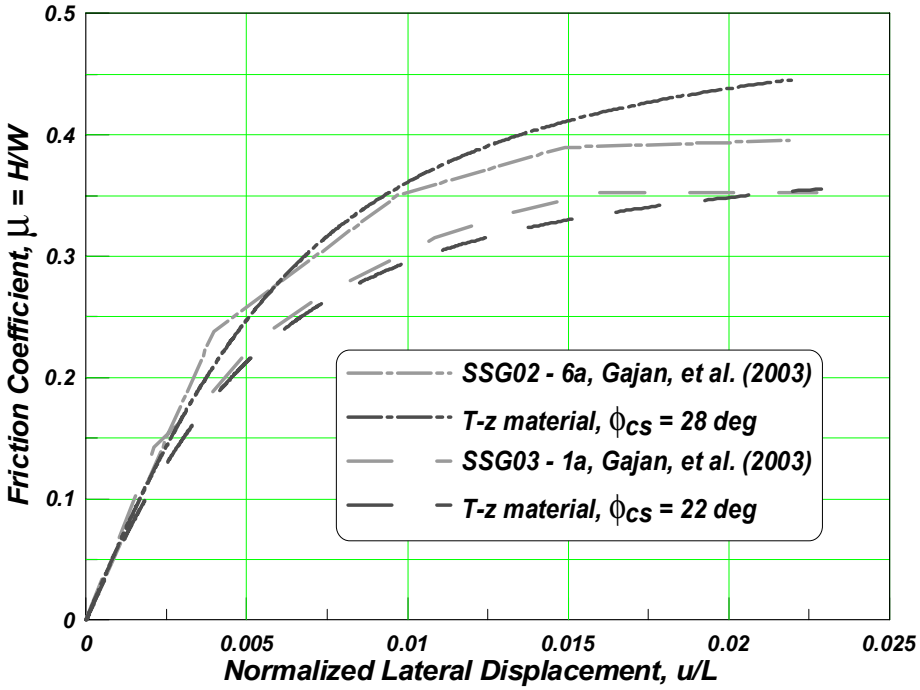

Fig. 3.15 Normalized load-displacement backbone; comparison between experimental tests and the T-z material formulation

3.5.2.2 Lateral Earth Pressure Capacity and Stiffness

The lateral earth pressure resistance for embedded footings is an important aspect in the modeling of shallow foundations. Generally, a foundation should be designed such that the passive earth pressure prevents sliding from becoming a significant consideration. However, passive pressure will develop at very low horizontal movements (on the order of 0.01–0.04 times the depth of embedment).

Referring to tests by Gadre and Dobry (1998), Test P of this test series isolated the effect of passive earth pressure, as shown in Figure 3.16.

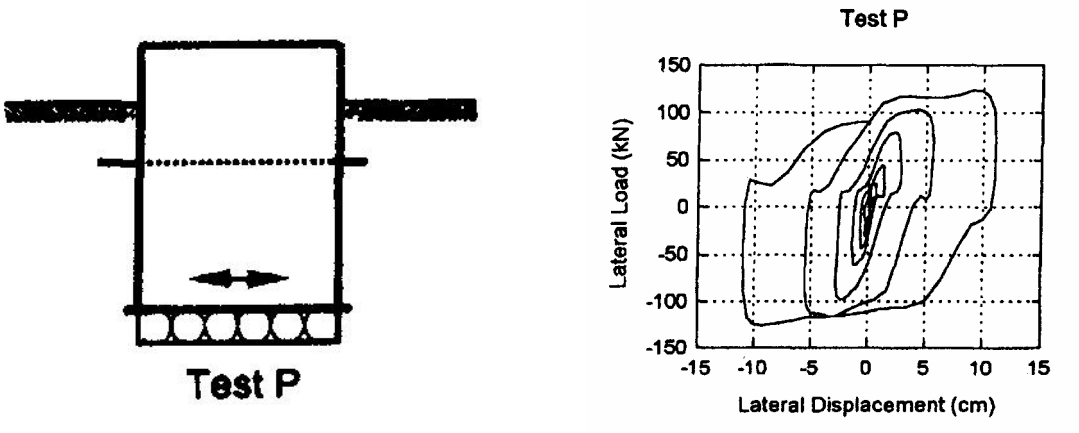

(a) *(b)*

Fig. 3.16 Tests by Gadre and Dobry (1998): (a) prototype structure test setup, (b) Test P load vs. displacement

For this case, a passive earth pressure coefficient of K_p = 11.1 was found using the experimental maximum horizontal load observed. It was assumed that active earth pressure (on the back face of the footing) did not contribute to this value. Gadre and Dobry compare this value to an estimated value of 14.1 for a soil friction angle of 39 and an identical wall-soil interface angle, using the trial wedge method with curved boundaries as presented by Terzaghi (1943), Terzaghi and Peck (1967) and Caquot and Kérisel (1949) (Fig. 3.17). Note that a calculation of passive earth pressure by the Rankine method would give a passive earth pressure coefficient of 4.4, and a value of 10.6 by the Coulomb method.

Comparing the backbone of the model Test P by Gadre and Dobry (1998) to the PySimple1 material shows a good comparison, as shown in Figure 3.18. The fit shown is for PySimple1 type 2 (API recommendation for drained sand), and a y50 taken from the backbone of Test P, which is approximately 0.015*B*. All simulations where the model footing is embedded will use a PySimple1 material with capacity estimated using the figure of Caquot and Kérisel (1949).

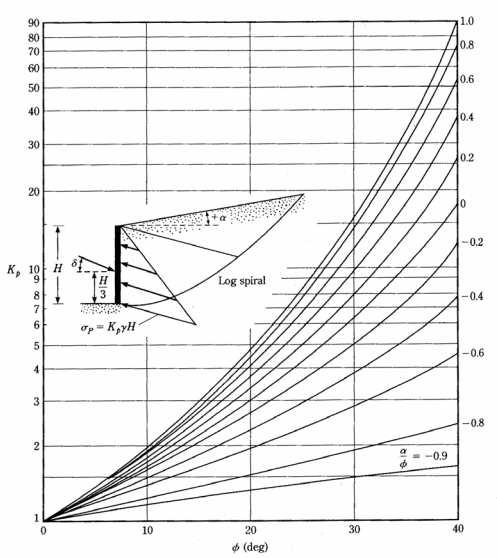

Fig. 3.17 Calculation of passive earth pressure coefficient vs. friction angle from Caquot and Kerisel (1949) (after Das 1999)

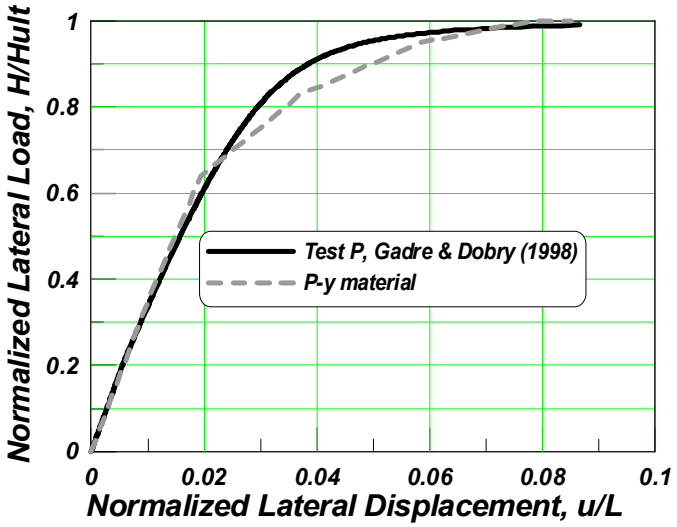

Fig. 3.18 Backbone comparison of model test by Gadre and Dobry (1998), with the PySimple1 material

3.5.2.3 Horizontal Sliding — Separation of Frictional Sliding and Passive Earth Pressure Stiffness

The model tests performed by Gadre and Dobry (1998) systematically separated the capacity and stiffness effects of sliding and embedment. They found that the stiffness embedment factors presented by Gazetas and Tassoulas (1987) for a square embedded footing give good prediction

for the effect of embedment on a square foundation. The prediction was within 21% maximum. These embedment factors are the same as presented by Gazetas (1991) and ATC-40 (1996). Therefore, for each BNWF simulation, if the foundation is embedded the stiffness of the frictional sliding component K_{fr} and the stiffness of the passive earth pressure component K_{PEP} can be separated from the observed experimental global horizontal stiffness K_{exp} by:

$$K_{fr} = \frac{K_{\exp}}{e_x} \tag{3.17}$$

$$K_{PEP} = K_{\exp}\left(1 - \frac{1}{e_x}\right) \tag{3.18}$$

Additionally, in order to validate the comparison of Gazetas' stiffness equations to observed model stiffnesses, reference is again made to the tests by Gadre and Dobry (1998). Gadre and Dobry compared the horizontal stiffness to the analytical stiffness of a square foundation as given by Pais and Kausel (1988):

$$K_{sur} = \frac{9.2BG}{2-\nu} \tag{3.19}$$

The shear modulus was back-calculated for tests B and BL where surface sliding was the only component of load transfer. Then, computed stiffnesses for tests where side friction and passive earth pressure were allowed were compared to observed values of initial horizontal secant stiffness, and the superposition of these effects showed that the analytical stiffness was within 5%. Recall that the horizontal stiffness using Gazetas' stiffness equations collapses to:

$$K_{sur} = \frac{9BG}{2-\nu} \tag{3.20}$$

Therefore, using the equations of Gazetas for nonsquare foundations should be a reasonable estimate of the elastic stiffness (associated with friction and passive earth pressure).

3.5.3 Bearing Pressure Distribution and End Tip Resistance

A realistic distribution of pressure beneath a shallow foundation is desirable to capture the nonlinear (reversed) cyclic loading behavior. This is particularly important when estimating settlement, since during repeated cyclic moment loading the selected distribution of ultimate pressure will dictate the magnitude of cumulative settlement that occurs. Using the Winkler

approach, individual springs are provided with an ultimate pressure q_{ult} and the distribution is naturally defined by value at each spring (distributed horizontally below the footing)

3.5.3.1 Review of the Literature on Bearing Capacity

Terzaghi (1943) formulated the contact pressure distribution below the base of a continuous footing by superimposing the separate contributions of cohesion, surcharge and unit weight. To determine the bearing capacity factors, three cases are considered: (1) a surface footing with ϕ' = 0 and γ = 0 to compute N_c, (2) a surface footing with $c = 0$ and γ = 0 to compute N_q, and (3) $c = 0$ and overburden = 0 to compute N_γ. Considering the equilibrium of forces about one-half the elastic soil wedge beneath the foundation, shown in Figures 3.19(a)–(b), the passive earth pressure acting against the soil wedge provides the bearing capacity. Since N_c and N_q are computed by assuming the unit weight is zero, the passive earth pressure is constant with depth. Therefore, the bearing stress must be uniform for the contribution of these two factors. Since N_γ is calculated with a nonzero unit weight, the passive earth pressure must increase linearly with depth. Therefore, the contact pressure distribution must also increase from zero at the tip of the footing to some maximum value at the center of the footing. Terzaghi showed that, for the N_γ contribution the force on the soil wedge increases linearly with depth. Therefore, the contact pressure distribution must also increase linearly from zero to some maximum value.

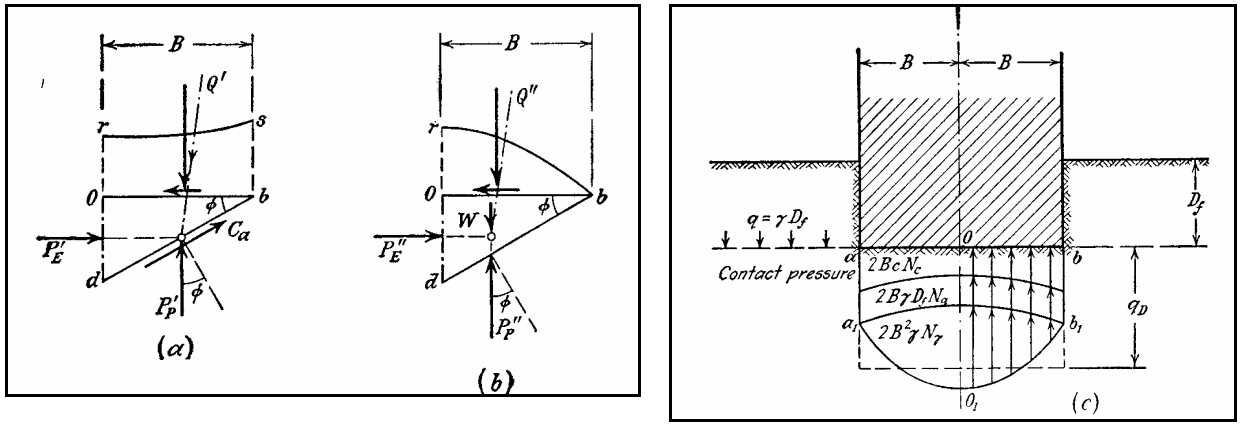

Fig. 3.19 Bearing pressure distribution under vertical loading proposed by Terzaghi (1943)

Meyerhoff (1951) continued Terzaghi's bearing capacity equations, but with the assumption that the failure surface extends to the free surface. He also discusses the contributions considered in resisting pressure, similar to Terzaghi's, as shown in Figure 3.20.

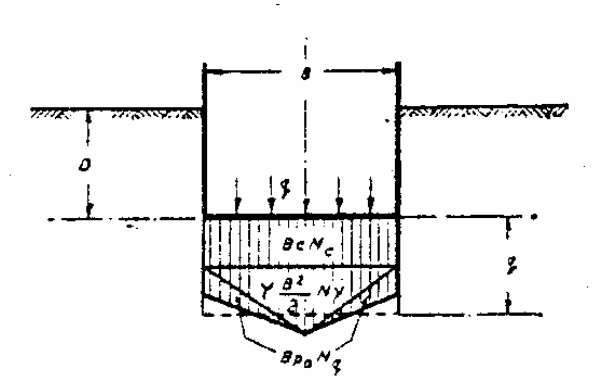

Fig. 3.20 Superposition of contact stresses due to the contributions of cohesion, unit weight, and overburden (after Meyerhoff 1951)

Schultz (1961) combines Boussinesq's elastic method with plastic flow along the edges defined by the methods of Terzaghi and Meyerhoff to determine a triangular ultimate pressure distribution. For loads less than ultimate, a saddle-shaped contact pressure distribution is observed, while at ultimate load a full plastic envelope results. Schultz gives the following equation for the contact pressure on a rigid footing assuming the soil behaves elastically:

$$q_e(x) = \frac{2q_{ave}}{\pi B} \cdot \frac{1}{\sqrt{1-(2x/B)^2}} \tag{3.21}$$

where q_{ave} = average contact pressure, and x is the distance horizontally from the center of the footing.

From this equation, it can be seen that at the edges of the footing an infinite stress develops for the elastic case. Using the previously described method of superimposing the contributions of cohesion, surcharge, and unit weight for a soil at shear failure, the following equation describes the contact stresses for a soil behaving plastically (corrected from Schultz (1961), who finds a coefficient of 4 before x):

$$q_p(x) = cN_c + \gamma N_q \cdot D + B\gamma N_\gamma \left(1 - \frac{2x}{B}\right) \tag{3.22}$$

Schultz combines these two equations to solve for the state of contact stress, given the factor of safety of the foundation system, as shown in Figures 3.21(a)–(c). Figure 3.21(b) shows the contact stress distribution for a cohesionless soil on the left side and a cohesive soil with a

small friction angle on the right, with a less than ultimate load in both cases. The fully plastic case is shown in Figure 3.21(c).

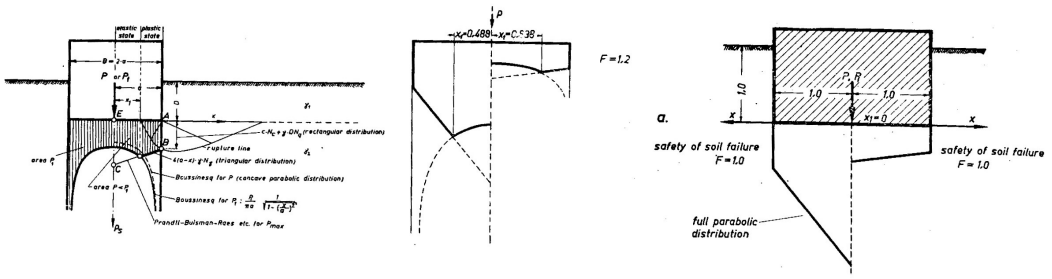

(a) elastic (b) elastic and plastic $FS_V > 1$ (c) fully plastic $FS_V = 1$

Fig. 3.21 Combination of elastic and plastic contact stress distribution (after Schultz 1961)

Schultz compared his theoretical approach with eleven case histories of actual foundations which, in general, qualitatively showed good agreement under working loads for the theoretical contact pressure distribution presented.

Lazebnik and Smirnov (1965) performed tests on a 60 cm surface footing on sand and loess-like loam. As shown in Figure 3.22, the saddle shaped distribution was observed for varying load levels in the case of sand with nonzero end tip pressures. The footings were not tested to failure, but vertical load test data were provided such that an ultimate bearing pressure could be estimated. The friction angle of the sand tested was 32 degrees, with a field unit weight of approximately 1.70 ton/m^3 and 1.8% water content. The dry unit weight is then 1.67 ton/m^3 for the sand. From conventional bearing capacity theory, the ultimate bearing pressure for the sand case is 150 kPa.

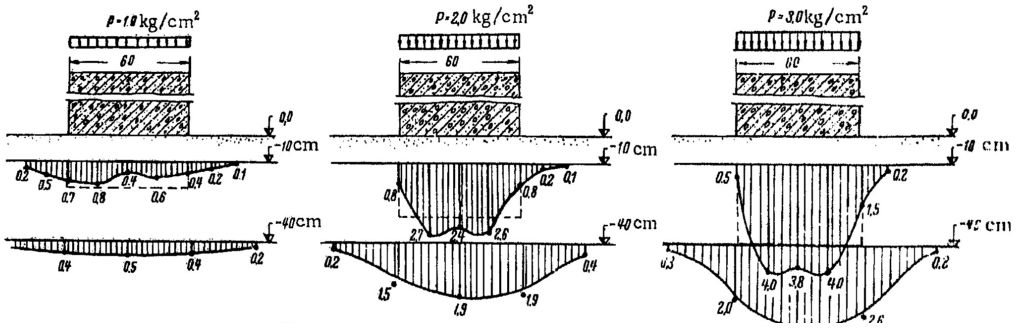

Fig. 3.22 Contact pressure distribution for sand (after Lazebnik and Smirnov 1965)

Merzenko (1965) observed the saddle shaped distribution of pressure on a dense sand and for repeated axial loadings to increasing levels of pressure, as shown in Figure 3.23. Additionally, the peaks moved closer together for larger magnitude loads, toward a parabolic shape. It should be noted that the pressure meters are not placed exactly at the foundation edge, so an edge pressure of zero cannot be inferred from the graph.

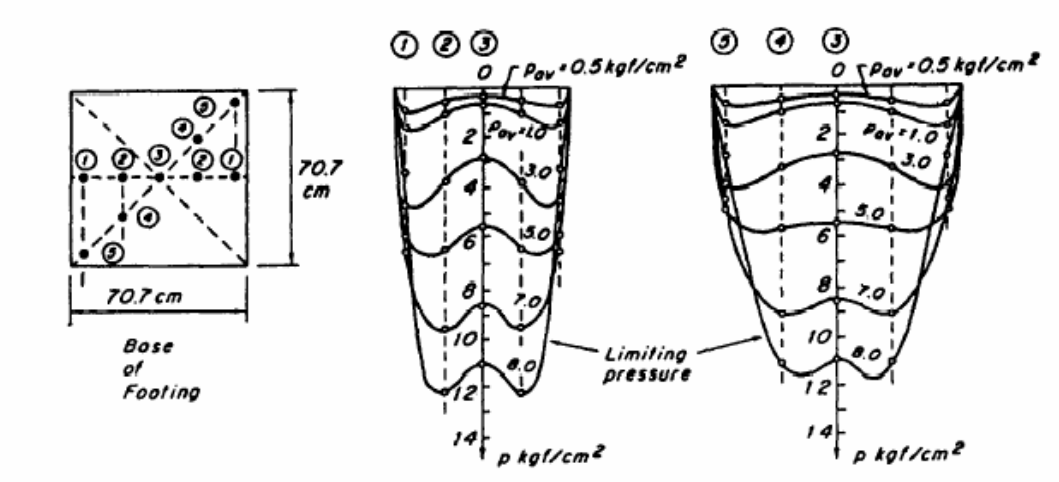

Fig. 3.23 Saddle-shaped contact pressure distribution observed by Murzenko (1965) (after Kerr 1989)

Smoltczyk (1967) presents an analytical solution that defines the foundation contact pressure as a function of depth and in the six tensorial components, computing stresses on a statistical pattern. For a simplified two-dimensional case, the contact pressure distribution in Figure 3.24 is plotted for varying levels of load intensity. It is interesting to note that for relatively lower load levels the distribution is "saddle-shaped," while at the highest load level the distribution becomes parabolic. In addition, for all load levels the end tip bearing pressure is zero.

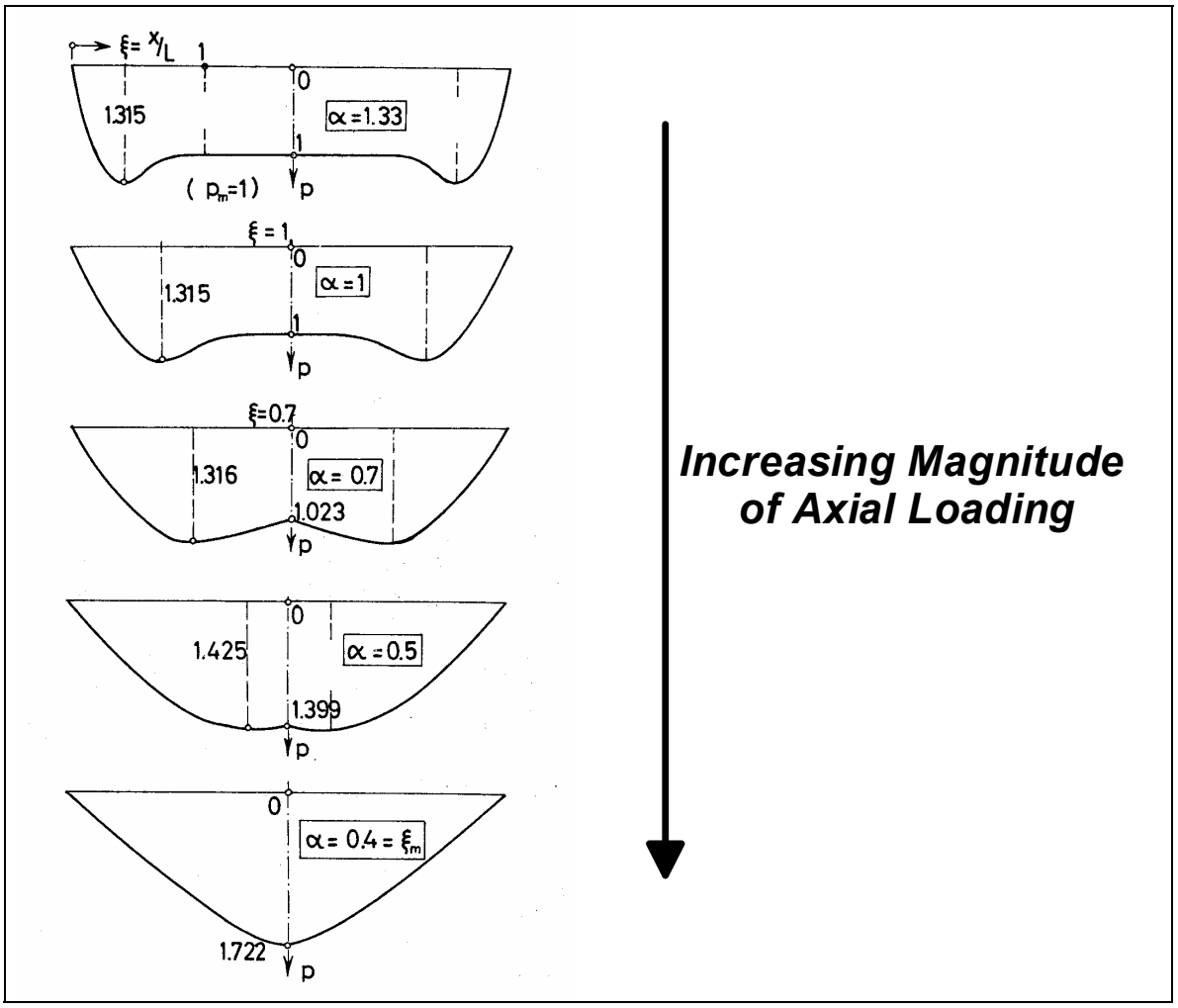

Fig. 3.24 Varying pressure distribution with increasing load (after Smoltczyk 1967)

Ho and Lopes (1969) performed experiments on a rigid circular foundation resting on a dry uniform Ottawa sand ($\phi' = 41°$). Figure 3.25 shows the measured contact pressure distribution from these experiments for various depths of embedment. The top of the figure is for a footing on the surface, while the last figure has the greatest embedment of two times the footing diameter. The saddle-shaped distribution is evident for the surface footing, with an increasingly uniform distribution as the embedment increases. The effect of vertical load-cycling was observed to flatten the distribution of bearing pressure after the first two cycles of loading. However, it is not clear how the edge contact pressure is determined, as presented in the figure, since pressure sensors were not placed near the edge of the footing. Therefore, the conclusion of zero edge pressure for the footings cannot be inferred from the figure.

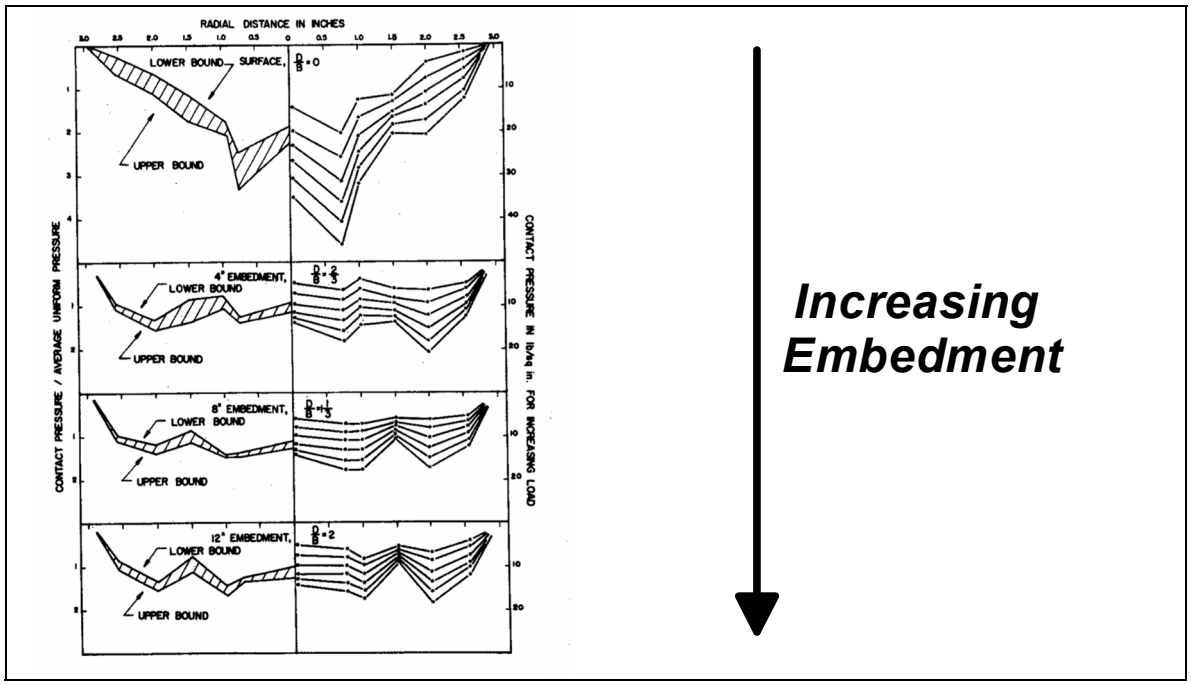

Fig. 3.25 Contact bearing pressure distribution for increasing levels of embedment (after Ho and Lopes 1969)

Bauer et al. (1979) observed the parabolic shape for increasing load intensities in two test cases on sand with varying relative densities under a 30.5 cm by 61 cm surface footing, as shown in Figure 3.26. The footing "Test 1" is on a 90% relative density sand, with $\phi' = 45°$ and $\gamma = 15.7$ kN/m3. The ultimate bearing capacity of this footing is taken from load settlement curves as 391 kN, or an ultimate bearing pressure of 2102 kPa. "Test 4" is on a 55% relative density sand, with $\phi' = 38°$ and $\gamma = 14.2$ kN/m3. The ultimate capacity is reported as 24kN, or an ultimate bearing pressure of 129 kPa. For Test 1, it appears that all lines are approximated as zero at the ends, while Test 4 shows nonzero edge stresses. However, simply interpolating the trend between the nearest two data points at each edge of the foundation gives better agreement with Test 4 for nonzero edge stresses. These results are tabulated in Table 3.3, for use in approximating the edge stresses for the Winkler modeling. The measurement error was reported to be within 20%.

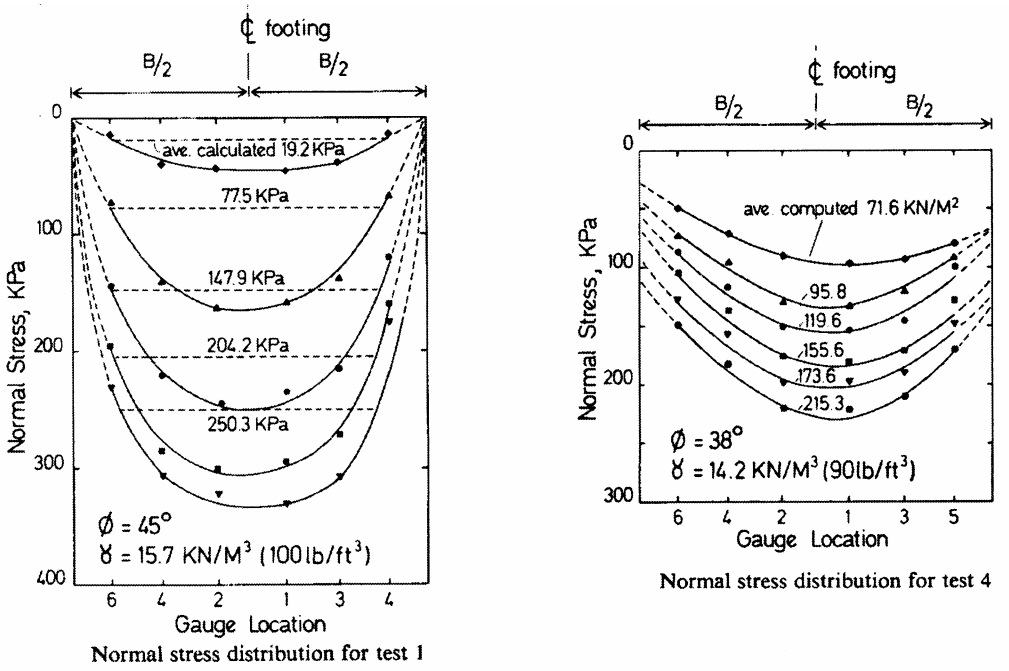

Fig. 3.26 Stress distribution in sand (after Bauer et al. 1979)

Weissing (1979) performed experimental tests of a small rectangular footing in addition to an analytical model. Weissing assumed, after Meyerhoff (1951), that for a surface footing on a cohesionless soil the distribution of contact pressure at failure can be assumed to be triangular based on the passive earth pressure acting on the elastic wedge beneath the footing. Based on the weight of the structure, if the system is at a load less than failure, the distribution is trapezoidal as shown in Figure 3.27, such that the soil is behaving plastically along the edges of the trapezoidal distribution and elastically along the horizontal portion of the distribution. Therefore, the pressure distribution is entirely based on the vertical factor of safety, FS_V.

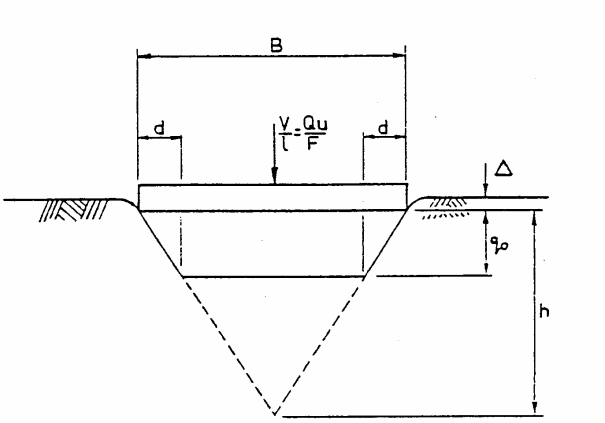

Fig. 3.27 Plastic end region by Weissing (1979)

Selvadurai and Rabbaa (1983) performed experiments to explore the effects of adjacent footing interaction. Spacing (S) ratios of S/B = 1, 2, 3, and 4 were conducted on an apparatus which tested small footings (378 mm square) on a long strip of sand ($\phi' = 41°, D_r \approx 90\%$) in order to create a plane strain condition. The footings are loaded to 1/3 of the computed maximum bearing capacity, estimated by conventional theory. Figure 3.28 shows the varying pressure distribution as the distance between the two footings is increased. In all cases the distribution is parabolic, as opposed to a saddle or uniform, and changes as a function of the relative distance between footings. Of practical interest to this study is the case of S/B = 1, where the two footings are directly touching. The following equation is used to define the maximum and minimum contact pressure as a function of the spacing between footings:

$$\left.\begin{matrix} q_1 \\ q_2 \end{matrix}\right\} = q_a\left[1 \pm \left(0.6 - 0.15\frac{S}{B}\right)\right] \tag{3.23}$$

where q_1 = contact pressure beneath the confined edge, q_2 = contact pressure beneath the free edge, and q_a = average applied pressure on a single footing. Therefore, for S/B = 1, the pressure beneath the footing varies parabolically from $1.45q_a$ at the center to $0.55q_a$ at the edge.

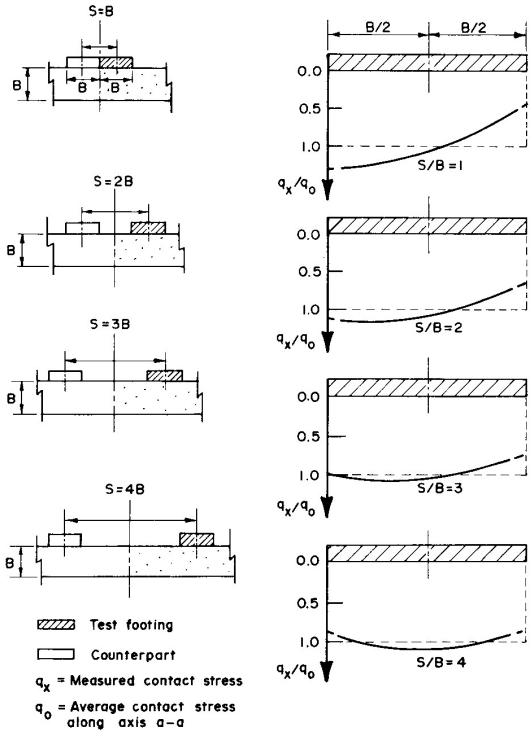

Fig. 3.28 Observed relation between contact bearing pressure distribution and footing spacing ratio (after Selvadurai and Rabbaa 1983). The dark line shows the measured contact pressure distribution normalized by the average contact pressure (dashed line).

Kerr (1989) presents a method to model the saddle-shaped distribution using a Winkler approach, where the springs are in series with an additional spring layer and displacements are forced at the edges of the foundation. This approach captures the saddle-shaped distribution of pressure for large footings at low load levels as well as the full parabolic shape observed for small footings. Kerr observes from review of the literature that early work on contact bearing pressure distribution using small plate samples on a sand base found the contact pressure distribution to be parabolic. However, later results of full-scale footings on sand documented the saddle-shaped distribution, potentially because only working load levels were applied.

Muller (1996) captures the contact pressure distribution under a foundation through experiments with a photoelastic material on sand. The contact pressure distribution was found to be roughly parabolic with zero pressure at the ends of the foundation for relatively small loads and with larger nonzero pressures at the corners of the foundation for higher loads. Figure 3.29 depicts the observed contact pressure under the foundation.

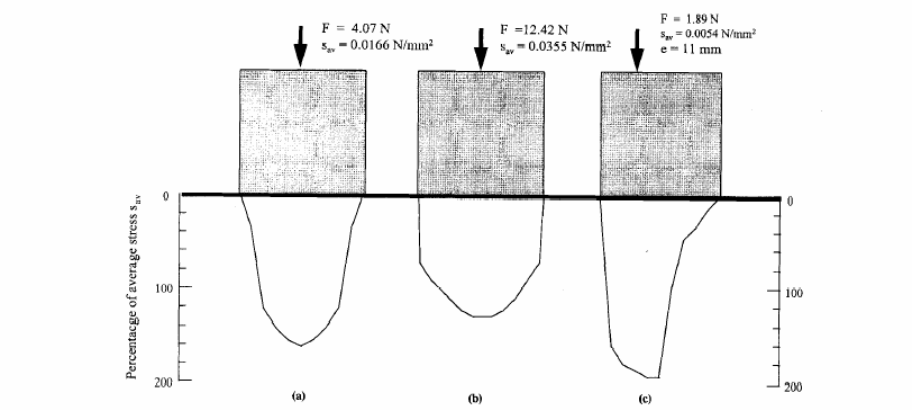

FIG. 5. Contact Stress Distribution from Photoelastic Experiments: (a) Central Load, Load = 4.07 N; (b) Central Load, Load = 12.42 N; (c) Eccentric Load

Fig. 3.29 Bearing contact pressure distribution on cohesionless sand, captured by a photoelastic material (after Muller 1996)

3.5.3.2 Summary Remarks from Literature Review

From these and other research on footings loaded under pure compression, it is observed that small model footings generally have a parabolic distribution of contact pressure, while large footings have a parabolic distribution at ultimate load and a saddle-shaped distribution for lower working loads. Several suggested functions were provided to describe these two shapes, each generally assuming that the soil is behaving either perfectly elastic or perfectly plastic. Since the soil springs will define the maximum stress after which plastic deformations occur, it is reasonable to model the ultimate load state of the system. Therefore, the parabolic contact pressure distribution is appropriate, since it captures the shape observed for shallow foundations at the ultimate bearing capacity.

Assuming a parabolic distribution, the bearing pressure at the ends of the footing needs to be determined. The theoretical presentations of the bearing pressure distribution fail to predict the nonzero edge stresses observed by Selvadurai and Rabbaa (1983) and Muller (1996) unless some overburden or cohesion exists. The models proposed by Terzaghi (1943), Meyerhoff (1951), and Schultz (1961) capture the observed pressure distribution well as discussed by Schultz, and provide the conventional bearing capacity used in practice today. These models, as described earlier, superimpose the contributions of cohesion, overburden, and unit weight, and predict a linear distribution of contact stress due to the counterpart of unit weight.

In this study, the ultimate bearing pressure will be defined as a parabola using the observations from the literature review for the contribution of soil weight, and a uniform distribution for the parts of cohesion and overburden. This distribution of ultimate pressures does not change throughout the analysis, although working load contact pressures will obviously constantly redistribute as the footing rocks and the resistance provided by the individual springs varies.

The trapezoidal shape (N_γ component) as defined by Schultz can easily be converted to a parabolic shape in order to approximate the observed pressure distribution by equating the areas of the triangular distribution to the parabolic distribution,

$$q_\gamma(x) = \frac{3\gamma N_\gamma}{B}\left(\frac{B^2}{4} - x^2\right) \tag{3.24}$$

The drawback to this approach is that for a cohesionless soil with no overburden, the contact stress at failure is zero at the edges of the foundation, which is contradictory to experimental observations.

To provide a more realistic approximation for the edge bearing pressure, experimental data are investigated. Table 3.3 lists the experimental data on the distribution of contact stresses for which the edge stresses were measured and not assumed to be zero.

In Table 3.3, columns 2 and 3 list the friction angle and vertical safety factor of each test. Columns 4 and 5 list the average and end tip contact pressures, while column 6 lists the ratio of these two values to facilitate comparison among different sized footings. Column 7 lists a calculated end tip ratio based on equation 3.29 (normalized by an average bearing pressure q_{ave}), the development of which is discussed below.

Table 3.3 Estimation of foundation pressure at edge for surface footings on sand

Reference	ϕ' (deg)	FS_V	q_{ave} (kPa)	$q_{i-\exp}$ (kPa)	$\frac{q_{i-\exp}}{q_{ave}}$	$\frac{q_{i-calc}}{q_{ave}}$
(1)	(2)	(3)	(4)	(5)	(6)	(7)
L and S (1965)	32	1.5	98	56	0.57	0.44
	32	0.8	196	78	0.40	0.68
	32	0.5	294	98	0.33	1.00
Bauer et al. (1979)	45	109.5	19	0	0.00	0.30
	45	27.1	78	17	0.22	0.32
	45	14.2	148	68	0.46	0.34
	45	10.3	204	99	0.48	0.35
	45	8.4	250	121	0.48	0.36
	38	1.8	72	48	0.67	0.41
	38	1.3	96	56	0.58	0.51
	38	1.1	120	68	0.57	0.58
	38	0.8	156	90	0.58	0.74
	38	0.7	174	108	0.62	0.81
	38	0.6	215	107	0.50	0.96
S and R (1983)	41	3.0	NR	NR	0.55	0.36
Muller (1996)	34	15.4	NR	NR	0	0.09
Muller (1996)	34	5.0	NR	NR	0.8	0.15
	34	11.8	NR	NR	0.37	0.10

Column notes:

(1) "L" and "S" (1965) refer to tests by Lazebnick and Smirnov (1965), "S" and "R" (1983) refer to tests by Salvadurai and Rabaa (1983).

(3) Design vertical factor of safety, FS_V, defined as the bearing failure over the load. *Note: in some cases the footings were loaded past this design value.*

(4) q_{ave} = average bearing pressure

(5) $q_{i-\exp}$ = end tip pressure measured from experiment

(6) $\frac{q_{i-\exp}}{q_{ave}}$ = ratio of the measured end tip pressure to the average bearing pressure

(7) $\frac{q_{i-calc}}{q_{ave}}$ = ratio of the calculated end tip pressure (Equation 3.29) to the average bearing pressure

From the data in Table 3.3, where mostly nonzero end tip contact pressure was found for surface footings on sand, comparison of the value of edge tip resistance reveals there may be some relation to the shear strength of the soil and the safety factor of the foundation. This makes sense intuitively because the shear strength would control the dispersion of stresses at the

discontinuity at the foundation edge, and the safety factor is a measure of stress intensity given the weight of the structure and the bearing capacity of the soil.

Considering a linear failure surface, and the Mohr-Coulomb failure criteria ($s = c' + \sigma' \tan\phi'$), a simple approximation for the edge tip resistance at failure for a $c'=0$ material may be taken as:

$$F_{qi} = \frac{q_i}{q_{ave}} = \frac{s}{\sigma'} = \tan(\phi) \tag{3.25}$$

where F_{qi} = edge tip resistance ratio, q_i = edge tip resistance, and q_{ave} = average bearing pressure.

This assumes the edge pressure is due to the discontinuity of the footing edge, thus only a function of the normal pressure on the soil failure surface. Physically, this expression defines the edge contact pressure as a ratio of the shear stress to the normal force.

From Table 3.3 data, it is observed that at higher vertical factors of safety FS_V, the distribution becomes more uniform. For the extreme cases, at an infinite FS_V, the pressure at the edge is zero, and at FS_V unity the edge pressure is equal to the average pressure. Therefore it seems a plausible that $F_{qi} \propto 1/FS_V$.

Averaging the proposed functions of shear strength and safety factor gives a fairly good fit to the data, such that the following equation for the edge tip resistance results:

$$F_{qi} = 0.5\left(\tan(\phi') + \frac{1}{FS_V} \right) \tag{3.26}$$

It appears that the friction angle and vertical footing safety factor alone provide a fairly reasonable estimate of the end tip resistance. For a FS_v of one, the proposed equation is higher than observed; however, this is acceptable considering the good fit for higher FS_v, which are appropriate for design levels. Figure 3.30 plots the measured edge contact pressure data in Table 3.3, overlain with Equation 3.29.

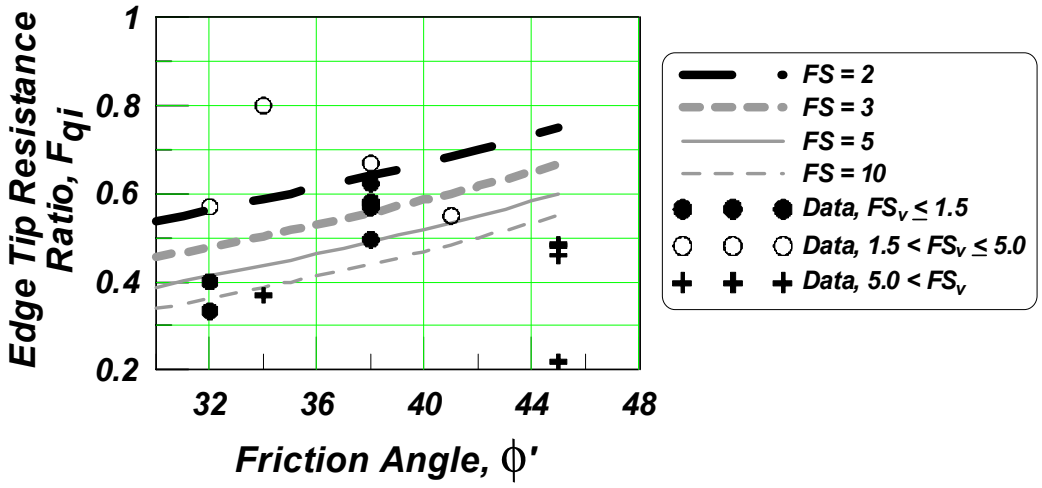

Fig. 3.30 Measured contact pressure data and proposed function of contact pressure given the friction angle and safety factor

The following revision to Equation 3.24 is suggested, such that the contribution of unit weight to the overall bearing pressure distribution is also a function of the end tip resistance q_i:

$$q_\gamma(x) = q_i + \frac{6}{B^2}\left(\frac{1}{2}\gamma B N_\gamma - q_i\right)\left(\frac{B^2}{4} - x^2\right) \tag{3.27}$$

Finally, the ultimate bearing capacity distribution is given by superimposing all terms:

$q(x) = cN_c + \gamma N_q D + q_\gamma(x)$

where

$$q_\gamma(x) = q_i + \frac{6}{B^2}\left(\frac{1}{2}\gamma B N_\gamma - q_i\right)\left(\frac{B^2}{4} - x^2\right) \text{ and} \tag{3.28}$$

$$q_i = F_{qi} q_\gamma = 0.5\left(\tan(\phi') + \frac{1}{FS_V}\right)\frac{1}{2}\gamma B N_\gamma$$

3.5.4 End Length Ratio

Experimental observation of shallow rocking footings has shown rounding of the soil medium below the edges of the foundation. Foundation profiles computed from plaster casts of the KRR02 tests series are shown in Figure 3.31. These figures show that significant permanent rounding along the base has occurred after slow cyclic tests. This rounding occurs because the edges are more heavily loaded as the opposite end lifts up and high compressive stiffness

develops on one end to maintain stability. This leads to densification and plastic development first on the ends. Since soil at the edge of the footing compresses more than in the center during rotation, the stiffness in the end region may increase due to densification.

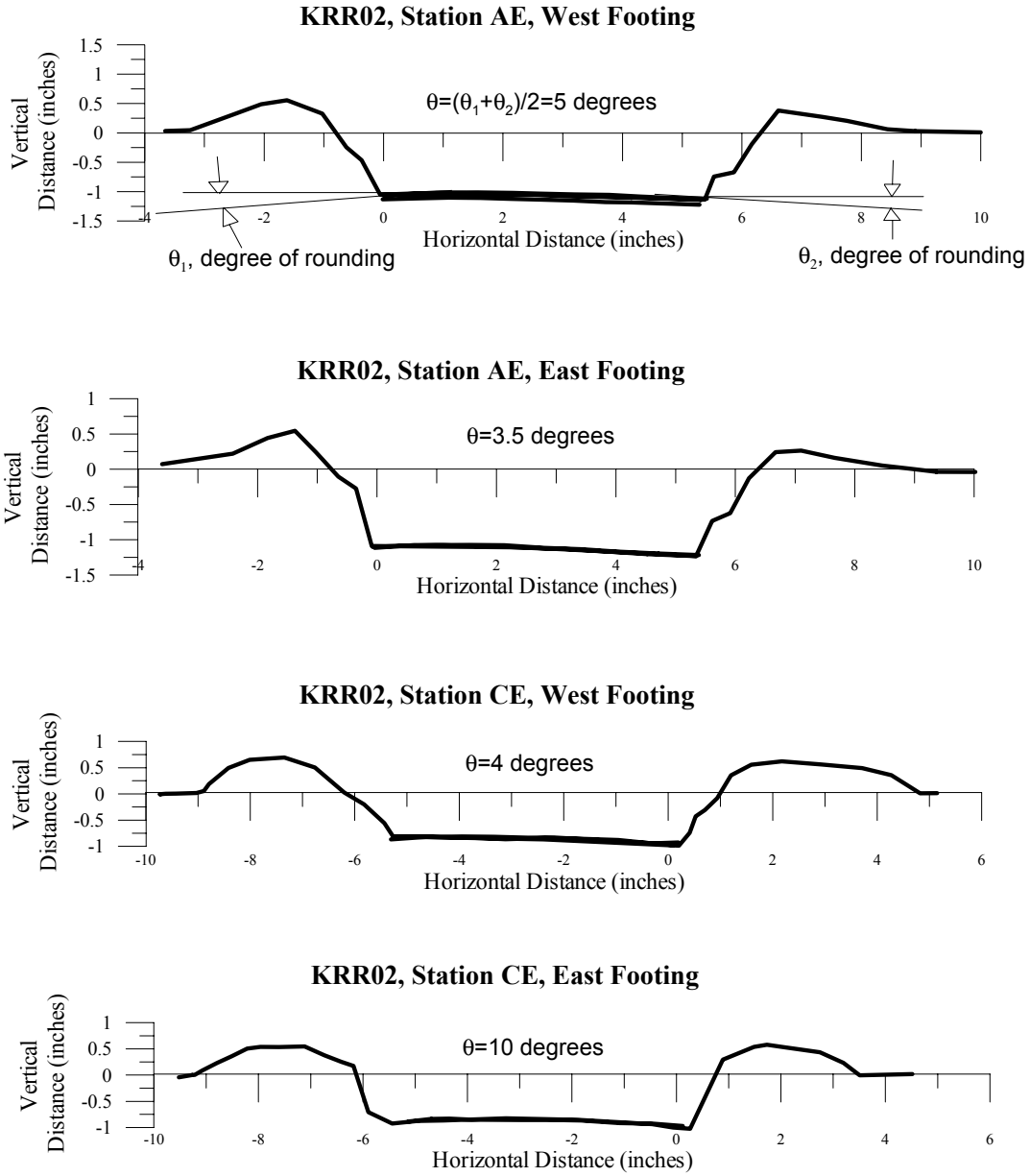

Fig. 3.31 Permanent displacement profiles taken from post-test plaster casts of shallow rocking strip footings (after Rosebrook and Kutter 2001b)

To capture this behavior using the Winkler model, the degree of rounding can be associated with the degree of coupling between the vertical and rotational stiffness. To account for a larger degree of coupling, ATC-40 (1996) presents a simplified approach, first converting

global vertical (K_Z) and global rotational ($K_{\theta x}$ or $K_{\theta y}$) stiffnesses into vertical stiffness intensities:

$$k_{\theta x} = \frac{K_{\theta x}}{I_x},\ k_{\theta y} = \frac{K_{\theta y}}{I_y} \text{ and } k_z = \frac{K_z}{LB} \tag{3.29}$$

where I_x = moment of inertia about the weak axis and I_y = moment of inertia about the strong axis.

If the difference between the stiffness intensities ($k_z - k_{\theta x}$ or $k_z - k_{\theta y}$) is small, then the larger calculated stiffness intensity is used. Alternatively, if the difference is large and the stiffness intensities are highly coupled, a modified vertical stiffness distribution is suggested where the model footing is divided into two regions: an end region to capture the effect of rotational stiffness and a middle region to capture the vertical stiffness. The middle region stiffness intensity is taken as that for an infinitely long strip footing (i.e. $L/B \to \infty$). The end region vertical stiffness intensity is based on the vertical stiffness of an isolated plate with an area of $B \cdot B/6$. The resulting stiffness intensities, using Gazetas' equations are:

$$k_{mid} = \frac{0.73G}{(1-\nu)B} \text{ and } k_{end} = \frac{6.8G}{(1-\nu)B} \tag{3.30}$$

The rotational stiffness may be implicitly provided by either varying the load-deflection characteristics of the individual springs along the length or providing variations in the vertical stiffness of the laterally placed springs. ATC-40 suggests varying the magnitude of stiffness and distribution of the individual spring elements, as shown in Figure 3.32. In this case, the end stiffness is approximately nine times that of the middle region stiffness. This approach was adopted in these numerical simulations, using suggested middle and end stiffness values and tighter spring spacing in the end region in which stiffness is increased, since the systems studied are highly dominated by the rotational degree of freedom.

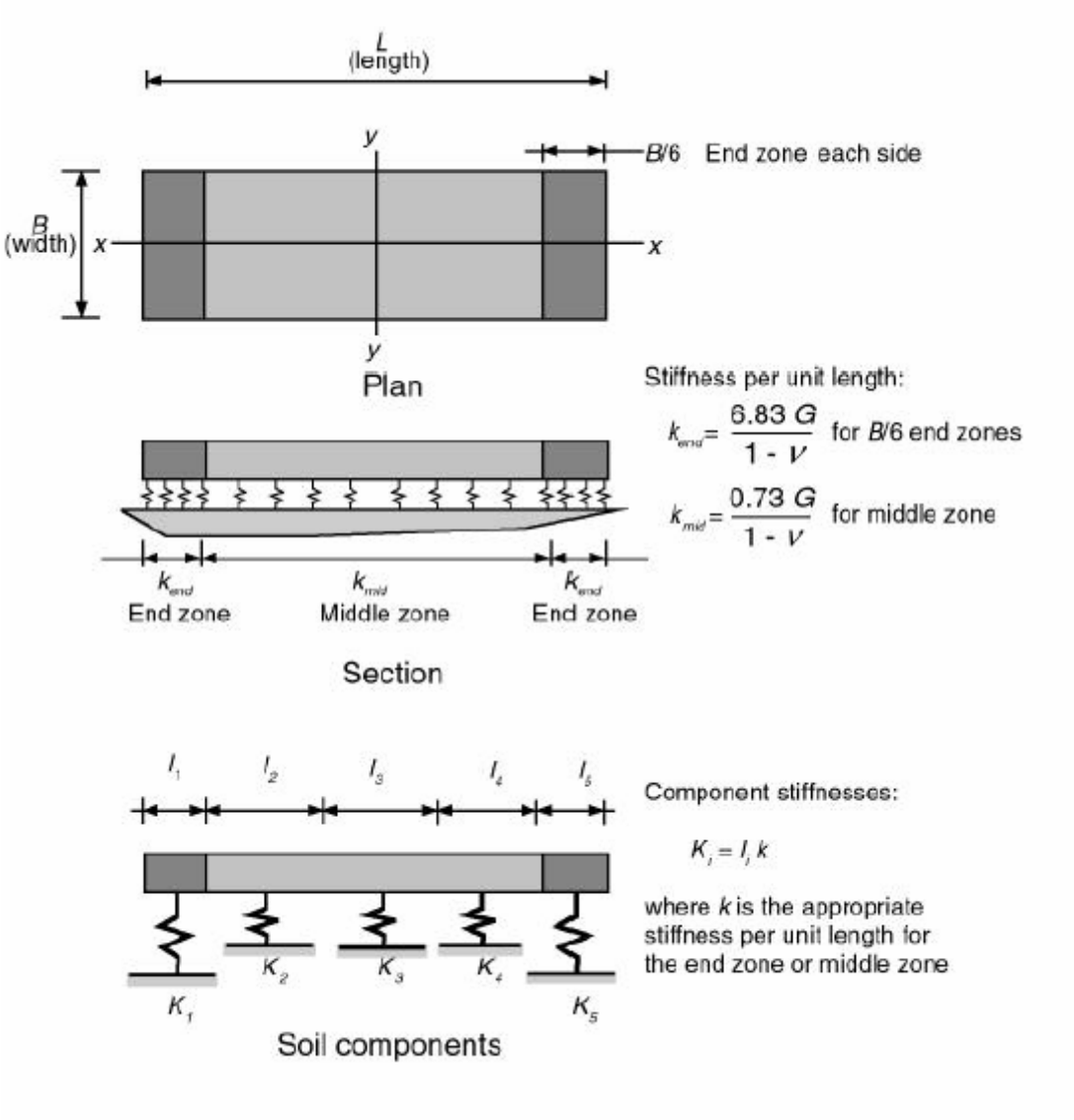

Fig. 3.32 ATC-40 recommendation when vertical and rotational stiffnesses are highly coupled (after ATC-40, 1996)

A more refined estimation of k_z and k_θ (accounting for their coupling) may be derived by equating the vertical to the vertical rotational stiffness intensities. Assuming the end region length (over which k_{end} occurs) L_e is an unknown variable, then setting the vertical stiffness intensity of a B x L_e plate equal to the rotational stiffness intensity of a footing with plan dimensions B x L:

$$k_z = k_{\theta y} \tag{3.31}$$

$$\frac{K_z}{BL} = \frac{K_{\theta y}}{I_y} \tag{3.32}$$

$$\frac{G}{(1-\nu)B}\left[0.73 + 1.54\left(\frac{B}{L_e}\right)^{0.75}\right] = \frac{G}{1-\nu} I_Y{}^{-0.25}\left[3\left(\frac{L}{B}\right)^{0.15}\right] \tag{3.33}$$

solving for $\frac{L_e}{B}$,

$$\frac{L_e}{B} = \left[\left(\frac{3B}{I_y^{0.25}}\left(\frac{L}{B}\right)^{0.15} - 0.73\right)\frac{1}{1.54}\right]^{\frac{-4}{3}} \tag{3.34}$$

where $I_y = \frac{1}{12}BL^3$ for a rectangular foundation with full contact. If $B = L$, this function is equal to 0.216, a L_e/B ratio of approximately 1/5. A ratio of 1/6 (as suggested by ATC-40) therefore seems reasonable so that the end length is not overestimated.

It is reasonable to assume that L_e and the resulting degree of rotational and vertical stiffness coupling is sensitive to not only *B,* but the ratio of *B/L*. ATC-40 gives a recommendation for L_e only as a function of *B,* and Weissing does not account for rotational stiffness. An improvement is suggested whereby the length and base of the footing are incorporated as well as the degree of coupling between vertical and rotational stiffness. Similar to the approach suggested in ATC-40, the known or calculated global stiffnesses are converted to stiffness intensities, and it is assumed that there is some relationship between the vertical stiffness intensity and the vertical rotational stiffness intensity:

$$\frac{K_{\theta y}}{I_y} \propto \frac{K_z}{BL} \tag{3.35}$$

In order to determine this relationship, a parameter is defined which indicates the degree of coupling between vertical and rotational stiffness, which is represented as a ratio of the difference in rotational stiffness capacities. This assumes that the difference in global rotational stiffness and the rotational stiffness due to the vertical stiffness intensity will control the magnitude of the end length region. The rotational stiffness deficit ratio, C_{R-V}^K, is defined as the ratio of the rotational stiffness capacity difference to the rotational stiffness:

$$C_{R-V}^{K} = \frac{K_{\theta y} - \frac{K_z}{A} I_y}{K_{\theta y}} \tag{3.36}$$

If C_{R-V}^{K} is greater than zero, then a larger stiffness is required at the end region to compensate for the difference in vertical and rotational stiffness and the coupling between them.

In order to define an end length ratio for a footing simply in terms of the length, base and uncoupled global vertical and rotational stiffnesses, the problem can be simplified by lumping the coupling of stiffness into geometry. Applying the newly defined rotational stiffness deficit ratio, the moment of inertia of the end length region is equal to C_{R-V}^{K} times the moment of inertia of the entire footing ($I_y^{*} = C_{R-V}^{K} I_y$). This is reasonable if one assumes that the rotational and vertical stiffnesses can be transformed to vertical stiffness intensities to assist in defining stiffnesses of the Winkler model springs. The moment of inertia of the end region, I_y^{*}, is given by:

$$I_y^{*} = 2\left[\frac{1}{12} B L_e^{3} + B L_e \left(\frac{L - L_e}{2}\right)^2\right] \text{ (end region moment of inertia)} \tag{3.37}$$

Setting I_y^{*} as a function of the rotational stiffness deficit ratio and the moment of inertia of the footing:

$$I_y^{*} = C_{R-V}^{K} I_y \tag{3.38}$$

$$2 \cdot \left[\frac{1}{12} B L_e^{3} + B L_e \left(\frac{L - L_e}{2}\right)^2\right] = C_{R-V}^{K} I_y \tag{3.39}$$

collecting terms:

$$L_e^{3} - \frac{3L}{2} L_e^{2} + \frac{3L^2}{4} \cdot L_e - \frac{3C_{R-V}^{K}}{2B} I_y = 0 \tag{3.40}$$

After Spanier and Oldham (1987), the characteristic cubic equation

$$x^3 + ax^2 + bx + c = 0 \tag{3.41}$$

has the discriminate D defined by:

$$D = Q^2 - P^3, \text{ where } Q = \frac{ab}{6} - \frac{c}{2} - \frac{a^3}{27} \text{ and } P = \frac{a^2}{9} - \frac{b}{3} \tag{3.42}$$

If D is greater than zero, there is one real root:

$$r = \left(Q + \sqrt{D}\right)^{1/3} + \left(Q - \sqrt{D}\right)^{1/3} - \frac{a}{3} \tag{3.43}$$

If D is less than zero, there are three real roots:

$$\begin{aligned} r_1 &= 2\sqrt{|P|}\cos(\phi) - \frac{a}{3} \\ r_2 &= -2\sqrt{|P|}\cos\left(\phi + \frac{\pi}{3}\right) - \frac{a}{3} \text{ where, } \phi = 3 \cdot \arccos\left(\frac{Q}{\sqrt{|P|^3}}\right) \\ r_3 &= 2\sqrt{|P|}\cos\left(\phi - \frac{\pi}{3}\right) - \frac{a}{3} \end{aligned} \tag{3.44}$$

If D is equal to zero, there are two real roots:

$$\begin{aligned} r_1 &= 2Q - \frac{a}{3} \\ r_2 &= -Q - \frac{a}{3} \end{aligned} \tag{3.45}$$

For Equation 3.40:

$$Q = \frac{3C_{R-V}^{K} I_y}{4B} - \frac{L^3}{16}, \; P = 0, \text{ and } D = Q^2 \tag{3.46}$$

Since D is always greater than zero for this system, there is always one real solution given by:

$$L_e = \frac{L}{2} - \left[2\left(\frac{L^3}{16} - \frac{3C_{R-V}^{K} I_y}{4B}\right)\right]^{1/3} \tag{3.47}$$

For a rectangular footing, this equation can be simplified to:

$$L_e = \frac{L}{2} - \left[\frac{L^3}{8}\left(1 - C_{R-V}^{K}\right)\right]^{1/3} = 0.5L - L\left[\frac{1}{8}\left(1 - C_{R-V}^{K}\right)\right]^{\frac{1}{3}} \tag{3.48}$$

In comparison to the recommendation by ATC-40, Figure 3.33 plots the end length normalized by both the foundation width (*B)* and length (*L)* versus the aspect ratio B/L, for a foundation with uncoupled vertical and rotational stiffnesses defined by Gazetas' equations. The trend is independent of any physical length or shear moduli (the variables in Gazetas' (1991) equations). For a *B/L* ratio of 1, Equation 3.48 reasonably converges with ATC-40 recommendations. Notice that for an infinite length, $B/L = 0$, the required end length drops

below zero as expected, such that an end length of higher stiffness is not required. ATC-40 presents the end length region as a function of the foundation width, and Equation 3.48 is also very sensitive to this parameter.

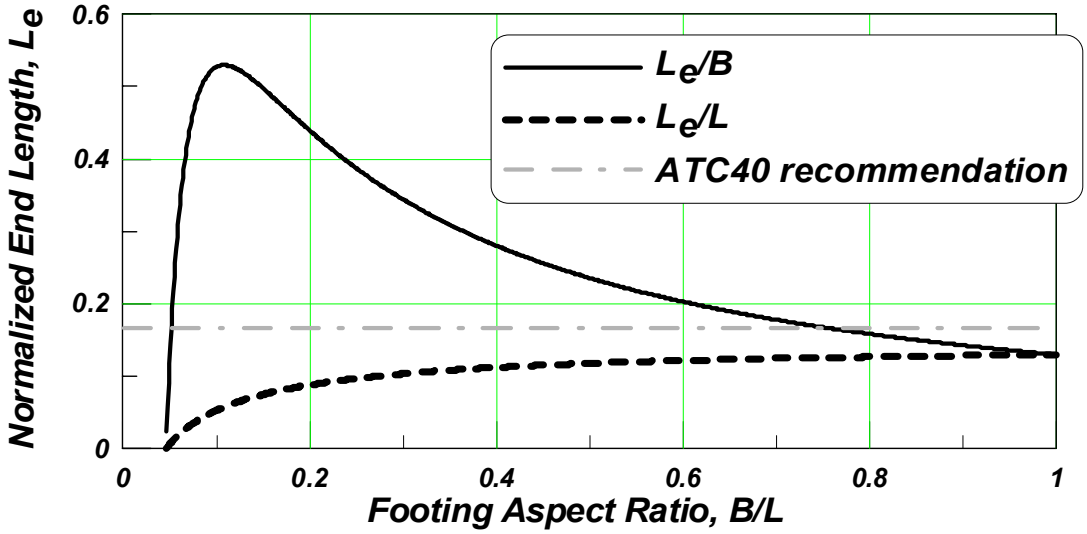

Fig. 3.33 Normalized end length region for system defined by Gazetas' stiffnesses

Once the end length region is defined, the vertical stiffness intensities of the middle and end regions of the Winkler model can be recomputed so that the global vertical and rotational stiffnesses are matched.

The stiffness intensity of the middle region k_{mid} is simply set to the uncoupled vertical stiffness intensity:

$$k_{mid} = \frac{K_z}{BL} \tag{3.49}$$

The stiffness intensity of the end region that defined the end region length is simply the addition of the middle zone stiffness intensity and any required rotational stiffness not provided by the vertical stiffness of the system, or

$$\begin{aligned} k_{end} &= k_{mid} + \frac{K_{\theta y}}{I_y} C_{R-V}^K \\ k_{end} &= \frac{K_z}{LB} + \frac{K_{\theta y}}{I_y} C_{R-V}^K \end{aligned} \tag{3.50}$$

The ratio of the end to middle region stiffness intensities versus the footing aspect ratio *B/L* is plotted in Figure 3.34. The value reaches unity as *B/L* approaches zero, in which case the

middle and end regions would have the same stiffness. Note that for a footing with *B/L = 1*, the ratio of the end to middle region stiffness intensities is approximately five, much lower than the ATC-40 recommendation of approximately nine. Recall that the ATC-40 recommendation assumes a middle region stiffness intensity based on an infinite footing, and an end region stiffness intensity of a *B x B/6* plate. These two assumptions will no doubt have a large spread; the proposed method takes into account footing geometry and defines an end region, if required, to account for degree of coupling between the vertical and rotational global stiffnesses.

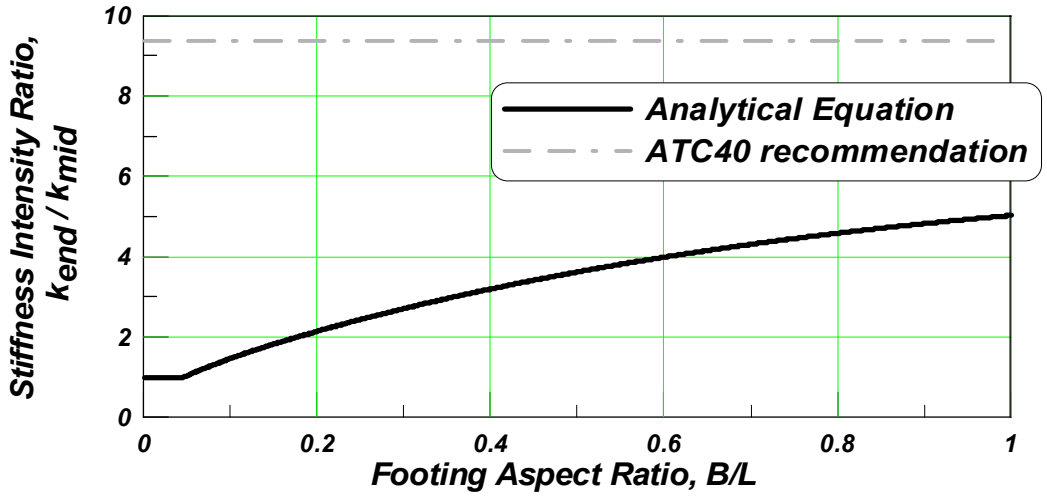

Fig. 3.34 Ratio of stiffness intensity, k_{end}/k_{mid}, vs. footing aspect ratio *B/L*

3.5.5 Radiation Damping

Gazetas (1991) provides convenient graphs and equations to estimate radiation damping due to vertical oscillation of an surface footing resting on an elastic half-space. This set of equations is generally accepted in common practice and will be used in the analysis of dynamically loaded shallow foundations (for the dynamic dashpot coefficients).

The dashpot coefficient for vertical vibrations is given by $C_z = \rho V_{La} A_b \tilde{c}_z$, where ρ is the unit density, V_{La} is Lysmer's analog wave velocity equal to 3.4 V_s /(π(1-ν)), A_b is the area of the foundation base, and $\tilde{c}_z$ is given in Gazetas (1991), also shown in Figure 3.35.

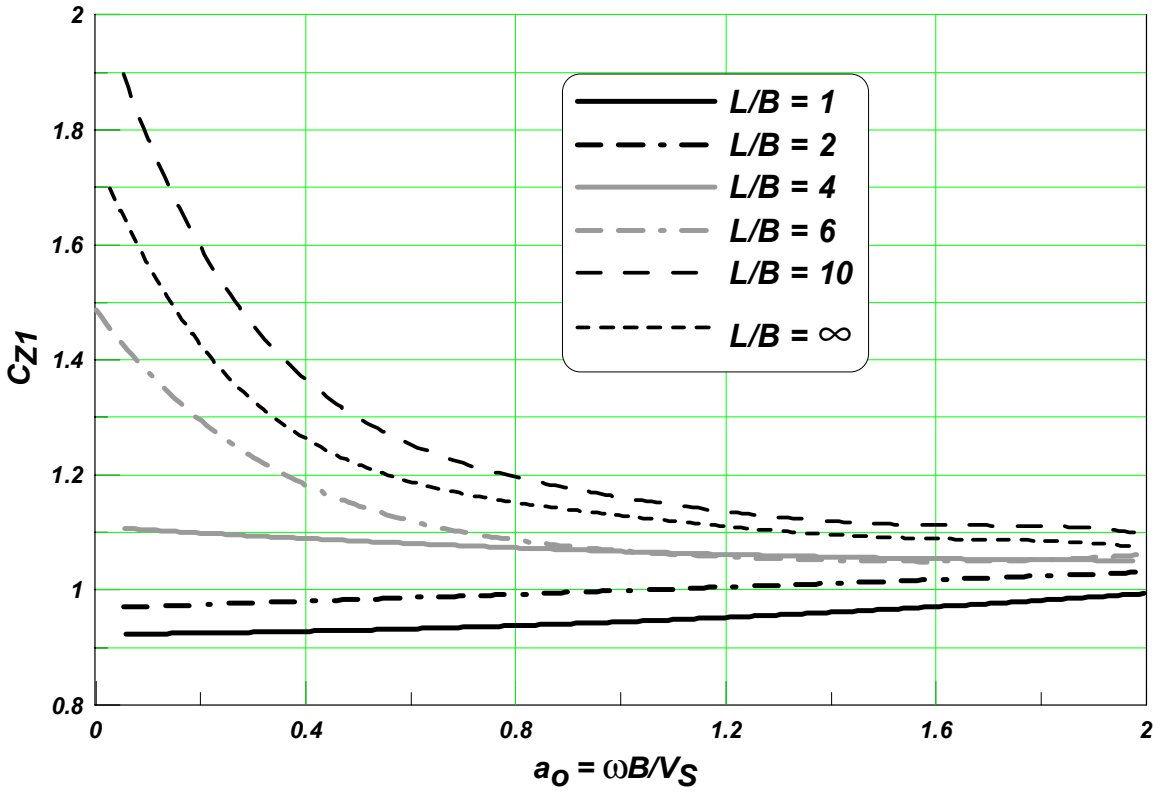

Fig. 3.35 Gazetas' (1991) vertical dashpot coefficient

Radiation damping through horizontal sliding oscillation is assumed to be negligible with respect to the Winkler elements. Damping due to the rotational mode is assumed to be incorporated through the vertical Winkler springs, since rotation stiffness is captured in the same manner.

3.6 BNWFSHALLOW MESH GENERATOR

A mesh generator *BNWFShallow* is used to study the sensitivity of the Winkler model parameters for capturing the salient features of the rocking strip foundation. Currently, *BNWFShallow* is implemented in the TCL scripting language, which wraps the OpenSees platform. *BNWFShallow* allows the user to consider different (1) lateral spring distributions, (2) bearing pressure distributions, and (3) variable material models and model parameters.

Appendix A contains the text files BNWFShallow.txt and BNWF_MAT.txt, which build the BNWF mesh for the static and dynamic simulations. The user would source the BNWFShallow file into the tcl script, and then input the variables through the procedure called

"BNWFShallow." These files could easily be implemented to act within an existing tcl script describing a much larger structural system.

(1) Lateral Spring Distribution — Base spring lateral distributions of interest include both the number of springs (as a function of the footing length), the type of spacing of the springs, and the stiffness of the different springs. A nonuniform lateral distribution is suggested in ATC-40 (1996) and uses closer spacing at the ends to compensate for the heavily loaded edges of the footing, which may cause more densification at the edges. In *BNWFShallow*, the user can specify either uniformly distributed spring spacing or variable spring spacing along the length of the foundation, as shown in Figure 3.36.

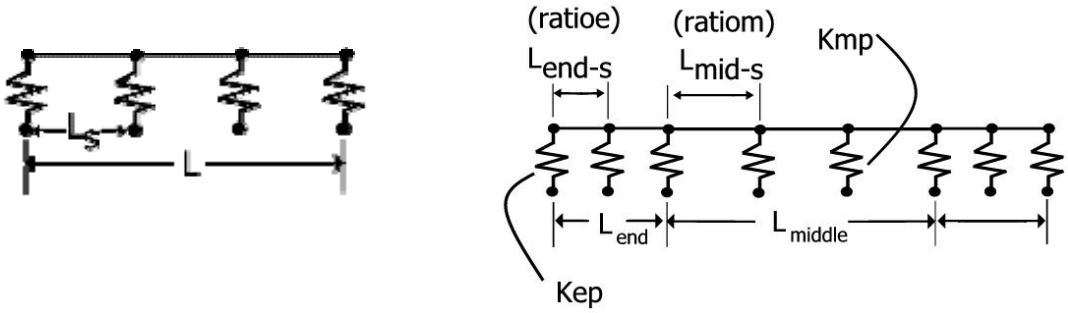

(a) Uniform lateral spring spacing **(b) Variable lateral spring spacing**

Fig. 3.36 Lateral spring distributions in *BNWFShallow* mesh generator

For the variable spring spacing, a distribution symmetric about the centerline of the footing element is assumed. By this option, the user specifies the end region length percentage (L_{end}) as a percentage of the entire footing length (L). End and middle spring spacing and stiffness can then be independently specified using the variables (2) and (3) following:

(2) Middle Length Ratio, (ratiom) — This value specifies the length ratio in the middle region of the foundation, defined as the value of the length between nodes divided by the length of the middle region (L_{mid}*L).

(3) End Length Ratio, (ratioe) — This value specifies the length ratio in the end region of the foundation, defined as the value of the length between nodes divided by the length of one end of the foundation outside of the middle region *($[(1- L_{mid})*L]/2$).*

(4) End Stiffness, (K_{ze}) — This stiffness is a global vertical stiffness of the foundation, which will be applied to the individual springs at the ends of the footing through a tributary area calculation.

(5) Middle Stiffness, (K_{zm}) — This stiffness is a global vertical stiffness of the foundation, which will be applied to the individual springs in the middle region of the footing through a tributary area calculation.

(6) Bearing Pressure Distribution — Applying the Winkler-based approach, perhaps the most important parameter for accurately modeling the system is the contact pressure distribution. This variation will depend upon the flexibility of the foundation and the nature of the soil below the foundation. Therefore, in the mesh generator, the user can specify different bearing pressure distributions to represent the ultimate soil capacity approximated by the Winkler spring system. The different distributions, uniform, triangular, trapezoidal, and parabolic are termed "Type I" through "Type–IV," respectively (Fig. 3.37).

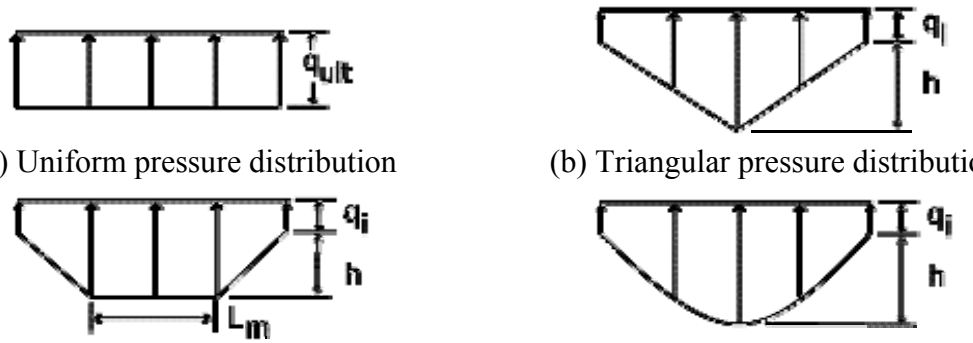

(a) Uniform pressure distribution (b) Triangular pressure distribution

(c) Trapezoidal pressure distribution (d) Parabolic pressure distribution

Fig. 3.37 Bearing capacity distributions available in *BNWFShallow* mesh generator

Other variables available for input into *BNWFShallow* include the end tip resistance of the spring system, q_i, the suction (suction or TP), and the initial pre-compression (id). The tip resistance q_i defines the amount of soil pressure to be placed at the ends (last springs) of the bearing pressure distribution shown in Figure 3.37. for a nonuniform distribution. The mesh generator then calculates the curve of the distribution such that the system still retains the global bearing capacity similar to the uniform distribution. The suction (variable *TP)* defines the amount of ultimate tension capacity of the individual springs. Initial pre-compression "*id"* is the value of settlement accrued prior to cyclic loading. For comparison with centrifuge experimental data this includes the settlement accrued during spin up (from one to 20 g's for example) and any

tests not modeled in the sequence up to the current test. However, during spin up the value of settlement is lost because of the sensitivity and calibration of the linear potentiometers. Therefore, the best estimate of this settlement can be taken from the weight of the configuration modeled and the corresponding initial stiffness from the vertical push test data.

3.7 BNWF PARAMETER SENSITIVITY

This section aims to investigate the sensitivity of the proposed BNWF parameters on the system response, for a range of vertical factors of safety from two to ten, in increments of $\Delta FS_V = 1$. The parameters previously discussed were varied while keeping all others constant to study the isolated effect of each. The constant variables used are listed in Table 3.4. A representative surface footing is modeled with an aspect ratio B/L = 3.9, a vertical stiffness of $Kz = 325\ MN/m$ (representative of dense sand for the tests considered), and a loading protocol of two cycles each of one, two, and four degrees of rotation, as shown in Figure 3.38.

Table 3.4 Constant factors for sensitivity study

Variable	Value
Bearing Capacity Uncertainty, *FQ*	1
Vertical Stiffness Factor, *FK*	1
End Tip Resistance Ratio, F_{qi}	1
Ultimate Bearing Capacity distribution	uniform
End Length, L_e/L	0%
Tension Capacity, *TP*	0%
ratio	0.01

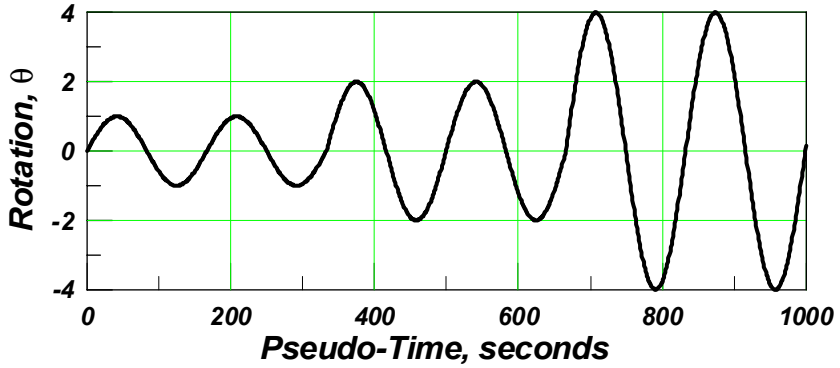

Fig. 3.38 Loading protocol for sensitivity study

The results are shown graphically in normalized format, such that a researcher or designer could easily interpret the effects of these parameters for a BNWF mesh to a particular study.

Figure 3.39 shows the result for varying the bearing capacity by the factor *FQ*; as the ultimate bearing capacity is reduced from 100% to 75%, the magnitude of moment capacity reduces by approximately 25% for the lowest factor of safety. Settlement magnitude intuitively decreases with increasing FS_V, though the reduction in bearing capacity does not seem to significantly affect the overall settlement. For a larger reduction of bearing capacity and a lower value of FS_V, it appears that the magnitude of horizontal sliding is decreased, as more energy is dissipated into the nonlinear soil springs.

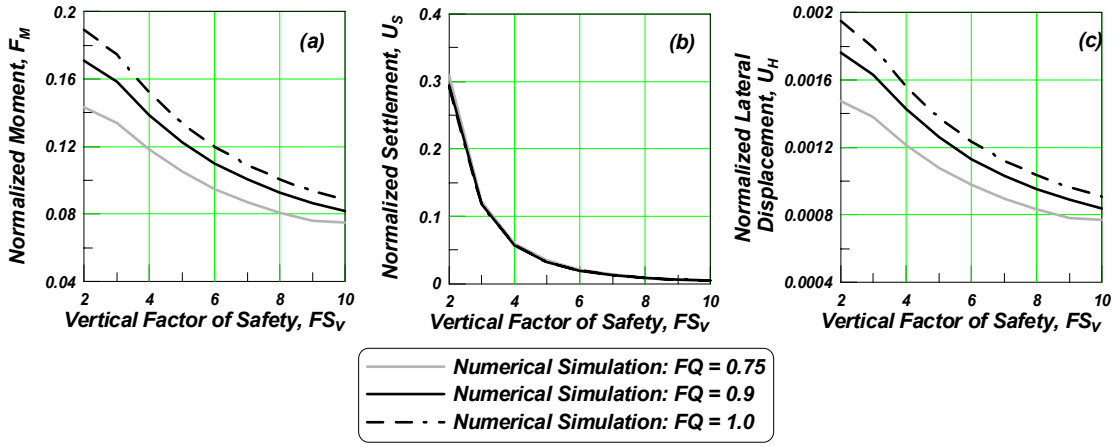

Fig. 3.39 Influence of bearing capacity reduction factor on BNWF simulation response (a) normalized moment, (b) normalized settlement and (c) normalized horizontal displacement vs. vertical factor of safety

Figure 3.40 shows that increasing or decreasing the vertical stiffness by a factor of two has an intuitive effect consistent with the findings of Allotey and Naggar (2003); a larger stiffness value gives a larger moment capacity. Also, a plateau is evident in the range of relatively large FS_V, whereby no additional moment capacity can be mobilized. The difference in normalized moment between different values of *FQ* is also larger for higher FS_V. Additionally, a softer stiffness gives a slightly increased value of settlement. A stiffer subgrade appears to transfer more energy into sliding, as evident in the larger sliding displacement. Overall, the factor most affected by variation in subgrade stiffness is the moment capacity.

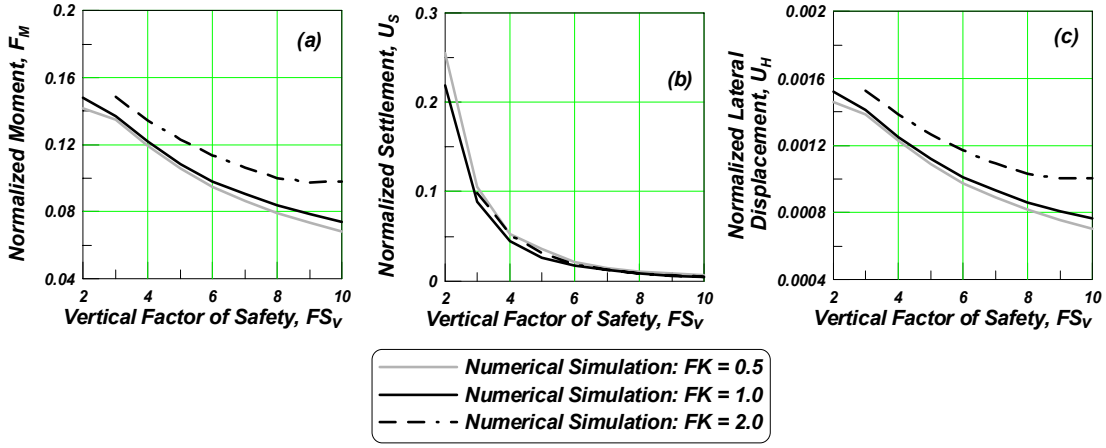

Fig. 3.40 Influence of variable stiffness on BNWF simulation response (a) normalized moment, (b) normalized settlement and (c) normalized horizontal displacement vs. vertical factor of safety

Figure 3.41 shows the result for the effect of varied end tip resistance on moment capacity. As the end tip resistance is decreased, the moment capacity is decreased; however, settlement is consistently less for a lower end tip resistance. Base sliding appears to be generally greater for a larger end tip resistance.

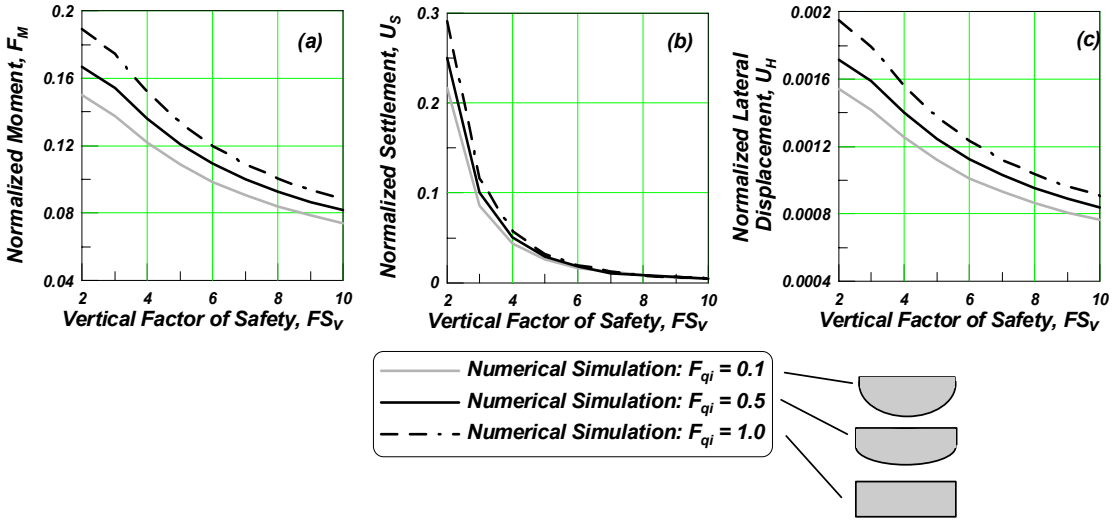

Fig. 3.41 Influence of variable end tip resistance on BNWF simulation response (a) normalized moment, (b) normalized settlement, and (c) normalized horizontal displacement vs. vertical factor of safety

Figure 3.42 shows that the difference between a triangular and parabolic (F_{qi} = 0) distribution is small, but the affect of a uniform to either a triangular or parabolic distribution is large. For moment, settlement, and horizontal displacement, the uniform distribution is consistently larger for all factors of safety.

Figure 3.43 shows that increasing the end length ratio increases the moment capacity for all FS_V , and significantly increases the horizontal displacement for increasing FS_V. This makes sense, since with higher L_e, K_θ is larger, and with higher FS_V, the rocking mode contribution is larger. Settlement was less affected for FS_V smaller than four, but increasing FS_V after this point shows more settlement for a smaller end region. For the simulation studying the end length ratio only, the ratio of stiffness between the end and middle region was taken as the recommendations in ATC-40 (1996).

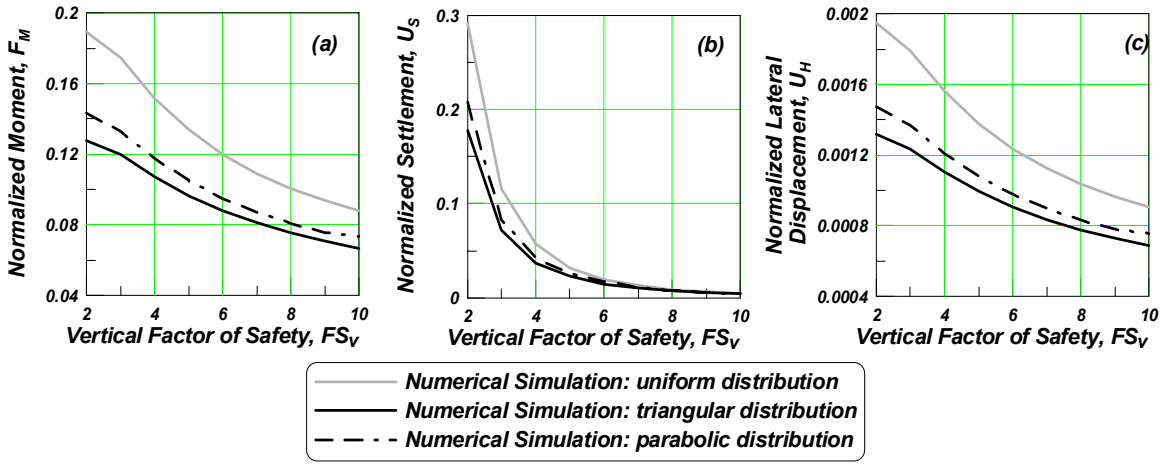

Fig. 3.42 Influence of ultimate bearing capacity distribution on BNWF simulation response (a) normalized moment, (b) normalized settlement and (c) normalized horizontal displacement vs. vertical factor of safety

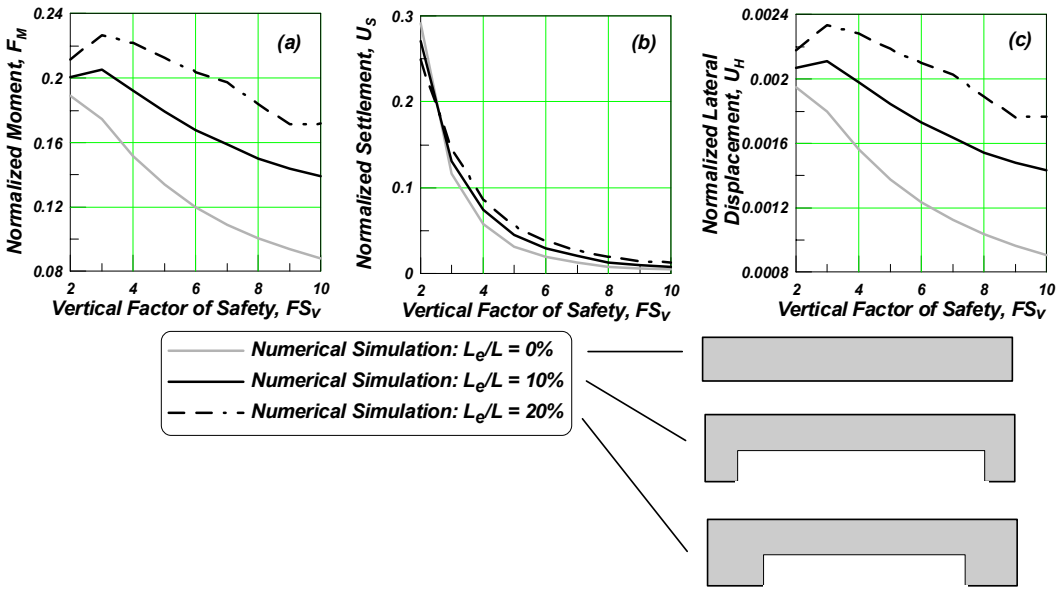

Fig. 3.43 Influence of variable end length ratio on BNWF simulation response (a) normalized moment, (b) normalized settlement and (c) normalized horizontal displacement vs. vertical factor of safety

A larger tension capacity as shown in Figure 3.44 appears to increase the moment capacity for all FS_V. Settlement is slightly increased for the smaller tension capacity, though this is the least affected parameter. Horizontal displacement increases with tension percent and FS_V, since the moment is larger with higher tension percent and more load will be absorbed by the system.

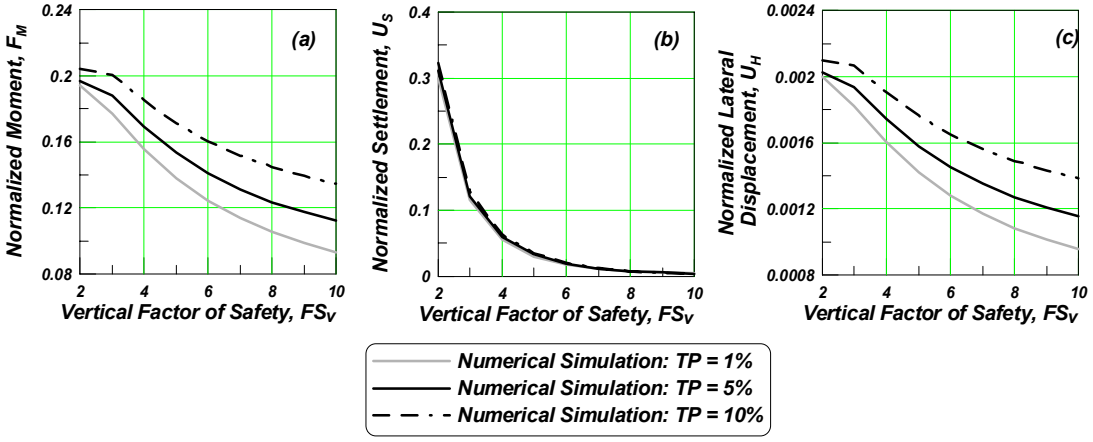

Fig. 3.44 Influence of variable tension capacity on BNWF simulation response (a) normalized moment, (b) normalized settlement, and (c) normalized horizontal displacement vs. vertical factor of safety

In general, it appears that the least sensitive parameter is the spring spacing ratio, evident in the small difference in sensitivity between results for simulations of 10 and 100 nodes, as illustrated in Figure 3.45; however, a significant difference can be seen for simulations with only 4 nodes. This difference is due to "lumping" the soil properties at relatively large steps along the footing. Overall, the global parameters may be not be significantly affected by the spring spacing ratio, but as the simulations will later show, a "stepped" effect occurs for a coarser spring spacing due to a redistribution of forces, and thus the overall energy dissipation will be affected.

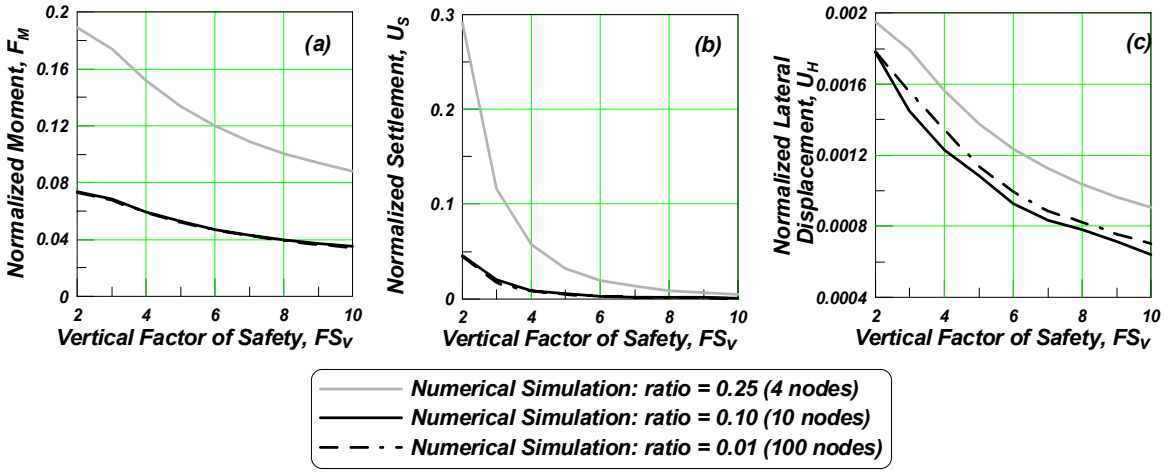

Fig. 3.45 Influence of spring spacing ratio*n* on BNWF simulation response (a) normalized moment, (b) normalized settlement, and (c) normalized horizontal displacement vs. vertical factor of safety

From this qualitative analysis, it appears that all of the studied variables have a direct and significant impact on the response of the BNWF model, and should not be neglected. However, one exception to this statement should be made in the case of tension capacity. No data were found by the author to suggest that any tension capacity should be warranted in the Winkler springs, so this value component will be neglected in the model.

3.8 SUMMARY AND SELECTION OF PROPERTIES

The following sections detail the known, assumed, and calculated geotechnical data for the suite of vertical, slow cyclic, and dynamic test data modeled from those experiments described in Chapter 2.

3.8.1 Vertical Test Data

Table 3.5 lists all the known and calculated parameters used for the simulations of experiments analyzed where vertical compression experiments were performed and BNWF models generated. Both centrifuge and one-g tests are modeled and all data in these sections are presented at prototype scale. There are seven broad categories of data and information in Table 3.5. The first is "Soil Data," the most basic parameters that describe the soil, either recommended by the authors or calculated through derived relations. The next category of data is "Footing Geometry" and is presented in prototype units. "Derived Properties" are those that were required for particular calculations and were estimated using engineering judgment and the basic soil parameters in "Soil Data." "Gazetas Stiffness" presents the stiffness calculated using the equations presented in Gazetas (1991) and ATC-40 (1996) (reproduced in Table 3.1). The calculated "Gazetas" stiffness values are based on recommendations in the EPRI manual (1990). Specifically, an elastic modulus is estimated from EPRI Table 5.2 for clays and EPRI Table 5.5 for sands. These tables present a range of values given the description of the soil (i.e., loose sand, medium sand, stiff clay, etc.), so the basic strength characteristics of relative density and cohesion are used to interpolate a specific value for sands and clays, respectively. The shear modulus is then calculated based on the Poisson ratio of the soil, as given in EPRI Table 5.1, and the estimated elastic modulus (see Notes B, C, and D to Table 3.5). "Winkler Model Input" lists the values of capacity and stiffness that were obtained from the vertical test data. Finally, "Notes" corresponds to a detailed list of comments following the table that clarify specific and general calculations and assumptions.

Table 3.5 Soil properties for modeling of experimental test data

	EXPERIMENTAL DATA SET			SOIL DATA					FOOTING GEOMETRY				DERIVED PROPERTIES			GAZETAS' STIFFNESS				WINKLER MODEL INPUT			NOTES
	REF	TEST	STA	Description	Dr	ϕ	c_u	γ_d	L	B	d	D	ν	E_{EPRI}	G	e_z	e_θ	Kv_{GAZ}	$K\theta_{GAZ}$	Qult	Kv-int	Kv-unl	
		Units			(%)	(deg)	(kN/m^2)	(kN/m^3)	(m)	(m)	(m)	(m)		(MN/m^2)	(MN/m^3)			(MN/m)	(MNm/rad)	(kN)	(MN/m)	(MN/m)	
CENTRIFUGE		***KRR01, KRR02 - Uniform, Fine Sand, SP (Nevada Sand)***																					
	17	KRR01	AW (V) S2	Dense / Very Dense	80	38.9	0	16	2.67	0.69	0.64	0.30	0.36	71	26	1.28	1.59	180	255	1479	15	171	1
	17	KRR01	FW (V) S25	Medium / Dense	60	37.2	0	16	2.67	0.69	0.64	0.30	0.32	45	17	1.28	1.59	110	156	1092	37	507	1
	17	KRR01	DW (V) S28	Medium / Dense	60	37.2	0	16	2.67	0.69	0.64	0.30	0.32	45	17	1.28	1.59	110	156	1103	23	180	1
	17	KRR01	S31 CW (V)	Dense / Very Dense	80	40.2	0	16	2.54	0.38	0.64	0.30	0.36	71	26	1.41	1.61	162	161	725	22	638	1
	18	KRR02	AW (V) S12	Dense / Very Dense	60	43.4	0	16	2.67	0.69	0.64	0.00	0.32	45	17	1.00	1.00	86	98	1822	98	565	1
	18	KRR02	CW (V) S54	Dense / Very Dense	60	40.6	0	16	2.67	0.69	0.64	0.00	0.32	45	17	1.00	1.00	86	98	1107	9	1008	1
	18	KRR02	CE S38-50	Dense / Very Dense	60	40.6	0	16	3.94	1.08	0.64	0.00	0.32	45	17	1.00	1.00	130	329	4019			4
		KRR03 - Stiff Clay (Bay Mud)																					
	19	KRR03	AW (V) S01	Very Stiff Clay			103	17	2.67	0.69	0.64	0.26	0.3	10	4	1.25	1.53	24	33	1012	70	87	5,10
	19	KRR03	CW (V) S28	Very Stiff Clay			103	17	2.67	0.69	0.64	0.26	0.3	10	4	1.25	1.53	24	33	1059	33	52	5,10
		SSG02, SSG03 - Uniform, Fine Sand, SP (Nevada Sand)																					
	8	SSG02	V02, B-G	Dense / Very Dense	80	42.3	0	16	2.84	0.69	0.70	0.00	0.36	71	26	1.00	1.00	147	187	1930	26	255	1
	9	SSG03	V03, C-E,G	Dense / Very Dense	80	37.0	0	16	2.84	0.69	0.70	0.70	0.36	71	26	1.55	2.06	227	385	2320	28	278	1
		Bartlett - Clay - water content = 34%, LL = 67, PL = 31, %clay sizes = 48, S.G. = 2.64																					
	2	Bartlett	3.4-4,6,8	Medium Clay			49	18	0.25	0.50	0.00	0.00	0.4	8	3	1.00	1.00	4	0.2	44			4,6,7,10
	2	Bartlett	3.4-11	Medium Clay			49	18	0.50	0.25	0.00	0.00	0.4	8	3	1.00	1.00	4	0.2	35			4,6,7,10
		Weissing - Clean Quartz Sand																					
	22	W Type A	5.10 (FS = 5)	Very Dense	93	42.7	0	17	0.50	0.25	0.00	0.00	0.39	93	33	1.00	1.00	45	2	37			3,4,8
ONE-G	22	W Type A	5.11 (FS = 2)	Very Dense	93	42.7	0	17	0.50	0.25	0.00	0.00	0.39	93	33	1.00	1.00	45	2	37			3,4,8
	22	W Type A	5.12 (FS = 10)	Very Dense	93	42.7	0	17	0.50	0.25	0.00	0.00	0.39	93	33	1.00	1.00	45	2	37			3,4,8
	22	W Type A	5.15 (FS = 2)	Sand	NR	33.2	0	14	0.50	0.25	0.00	0.00	0.1	10	5	1.00	1.00	4	0	6			3,4,8
	22	W Type B	5.17 (FS = 5)	Very Dense	93	42.7	0	17	0.25	0.50	0.00	0.00	0.39	93	33	1.00	1.00	45	2	19			3,4,8
		TRISEE - Ticino Sand - Uniform, course to medium silica sand (Cu = 1.6, D50 = 0.55mm, F200 < 5%, Cz < 1 --> SP). Saturated																					
	15	TRISEE T26	HD	Very Dense	85	41.8	0	16	1.00	1.00	1.00	1.00	0.37	79	29	1.84	8.30	190	176	3742	178	189	2,11
	15	TRISEE T71	LD	Medium	45	38.5	0	15	1.00	1.00	1.00	1.00	0.28	30	12	1.84	8.30	68	63	2071	39	73	2,11

COMMON NOTES

A. For sands, dry unit weight calculated as a function of minimum and maximum dry unit wieght and the relative density.
   For clays, dry unit weight assumed from Das (Table 1.5)
B. Poisson's Ratio for sands determined by range of values from EPRI Manual (Table 5-1), where Dr used to classify soil as loose or dense.
C. Elastic Modulus determined from EPRI manual (Table 5-2 for clays and Table 5-5 by Poulos for sands)
   For sands, Dr used to classify soil as loose, medium, etc. For clays, su used to classify soil as stiff, medium, etc.
D. G calculated from Elastic modulus and poisson's ratio: G = E / 2*(1+v)
E. Kv and Kr calculated from Gazetas' equations reported in Foundation Engineering Handbook (comparable to ATC-40)
F. Soil Descriptions based on relative density range reported in DAS for sand Table 1.6 pg 12, and Table 3.8 pg 89 in Coduto for clay

SPECIFIC NOTES

1 Friction Angle "Back-Calculated" from vertical load test

2

Friction Angle equal to the peak shear resistance of Ticino Sand (Bolton, 1986)	Recommended Eo and Go (Lo Presti, et al.)
Recommended: HD = 41.8, LD = 38.47	Eo, HD = 392 MN/m2, LD = 166 MN/m2
Back-Calculated: HD = 41, LD = 20	Go, HD = 140 MN/m2, LD = 67 MN/m3

3 Weissing reports friction angle versus relative density, based on a composite of shear box test, triaxial test, and plate bearing tests. Those values are used in this table.
4 Bearing Capacity calculated by conventional bearing capacity theory, bearing capacity factors used are those defined by De Beer (1970), Hansen (1970) and Hanna and Meyerhoff (1981)
5 Cohesion back-calcualted from vertical load tests, as recommended in Kutter, et al.
6 Cohesion as recommended in Bartlett (1976) from unconfined compression tests
7 Bartlett observes a soil modulus ks of 340 MPa/m, where ks = Kr/lo. Kv = 340 Mpa/m *0.5m*0.25m = 43MN/m (see pages 89-93)
8 Weissing reports an observed subgrade modulus of 2300 MN/m3 (page 72)
10 Unit Weight of clay for KRR03 test series referenced from DAS Table 1.5 page 11 and Liping Yan (1998) uses 18 kN/m3 for Bartlett test data.
11 For TRISEE tests, thickness of footing is estimated from report drawings (required for Gazetas stiffness values)

REFERENCES

1 Applied Technolgy Council (ATC) (1996). "Seismic Evaluation and Retrofit of Concrete Buildings ATC-40." Volume 1 and 2 November.
2 Bartlett, P.E. (1976), "Foundation Rocking on a Clay Soil," M. E. Thesis, University of Auckland, New Zealand.
3 Coduto, Donald P.(2001). *Foundation Design: Principles and Practices*. Prentice Hall, New Jersey.
4 Das, Braja M. (1999). *Principles of Foundation Engineering* . Brooks/Cole Publishing Company, California
5 DeBeer, E.E. (1970). "Experimental Determination of the Shape Factors and Bearing Equation Factores of Sand, "Geotechnique, Vol. 20, No. 4, pp 387-411.
6 Duncan, J. M., Byrne, P., Wong, K. S., and Mabry, P. (1980). *Strength, Stress-Strain and Bulk Modulus Parameters for Finite Element Analyses of Stresses and Movements in Soil Masses,* Report No. UCB/GT/80-01, August, Department of Civil engineering, University of California, Berkeley, California.
7 EPRI (1990) Manual on Estimating Soil Properties for Foundation Design. Electric Power Research Institute, Palo Alto, California.
8 Gajan, S., Phalen, J.D. and Kutter, B.L. (2003a). "Soil-Foundation Structure Interaction: Shallow Foundations. Centrifuge Data Report for the SSG02 Test Series," Center for Geotechnical Modeling Data Report UCD/CGMDR-03/01.
9 Gajan, S., Phalen, J.D. and Kutter, B.L. (2003a). "Soil-Foundation Structure Interaction: Shallow Foundations. Centrifuge Data Report for the SSG02 Test Series," Center for Geotechnical Modeling Data Report UCD/CGMDR-03/01.
10 Gazetas, G. (1991). *Foundation Engineering handbook* , Fang, H.Y. edit. Van Nostrand Rienhold, 40 pp.
11 Hanna, A. M. and Meyerhoff, G.G. (1981). "Experimental Evaluation of Bearing Capacity of Footings Subjected to Inclined Loads," *Canadian Geotechnical Journal,* Vol. 18, No. 4, pp. 599-603
12 Hansen, J. B. (1970). "A Revised and Extended Formula for Bearing Capacity," Danish Geotechnical Institute, *Bulletin* 28, Copenhagen.
13 Hausmann M. R. (1990). *Engineering Principles of Ground Modification,* McGraw-Hill Publishing Company.
14 Kutter, B., Martin, G., Hutchinson, T., Harden, C., Sivapalan, G., Phalen, J. "Status Report on Study of Modeling of Nonlinear Cyclic Load-Deformation Behavior of Shallow Foundations" PEER Workshop March 5, 2003 Documentation
15 Negro, P., Verzeletti, G., Molina, J., Pedretti, S., Presti, D. Lo, Pedroni, S. "Large-Scale Geotechnical Experiments On Soil-Foundation Interaction (TRISEE Task 3)," Ispra, Italy: Joint Research Center. 1998. (Special Publication I.98.73). 1 v.
16 Poulos, H. G., "Settlement of Isolated Foundations", in Soil Mechanics - Recent Developments, Eds. S. Valliapan, S. Hain, and I. K. Lee, William H. Sellen Pty., Zetland, 1975, pp. 181-212.
17 Rosebrook, K. R. and Kutter, B. L. (2001a.) "Soil-Foundation Structure Interaction: Shallow Foundations. Centrifuge Data Report for the KRR01 Test Series," Center for Geotechnical Modeling Data Report UCD/CGMDR-01/01.
18 Rosebrook, K. R. and Kutter, B. L. (2001b.) "Soil-Foundation Structure Interaction: Shallow Foundations. Centrifuge Data Report for the KRR02 Test Series," Center for Geotechnical Modeling Data Report UCD/CGMDR-01/01.
19 Rosebrook, K. R. and Kutter, B. L. (2001c.) "Soil-Foundation Structure Interaction: Shallow Foundations. Centrifuge Data Report for the KRR03 Test Series," Center for Geotechnical Modeling Data Report UCD/CGMDR-01/01.
20 Rosebrook, K. R. "Moment Loading on Shallow Foundations: Centrifuge Test Data Archives, M.S. Thesis, University of California, Berkeley.
21 Gajan, S., Phalen, J. and Kutter, B. (2003a) "
22 Wiessing, P. R. (1979), "Foundation Rocking on Sand," School of Engineering Report No. 203, Universtiy of Auckland, New Zealand.
23 Yan, Liping (1998) "Nonlinear Load-Deformation Characteristics of Bridge Abutments and Footings under Cyclic Loading." Ph.D Dissertation, University of Southern California, December.

3.8.2 Static Lateral Test Data

The properties obtained, assumed and calculated from the vertical test data are applied to the static lateral tests. Only the pertinent information required as input for the simulation is presented in the following tables.

In order to present as much useful information for the vertical load test data available, and in as concise a manner as possible, Table 3.6 lists all the known and calculated parameters used for the simulation of experiments analyzed. The presentation of information is similar to that in Table 3.5. "Test Data" indicates information taken directly from the model test data files. The abbreviations used in the table are as follows,

Abbreviation	Definition
FQ	Bearing capacity reduction factor
FS2	Reduced FS_V (for reference), $FS2 = FQ^* FS_V$
μ	Coefficient of friction
Qs	Frictional sliding capacity
e_x	Gazetas (1991) embedment factor, used to separate the contributions of friction and passive earth pressure on sliding stiffness
K_{fr}	Sliding stiffness due to base friction
Kp	Passive earth pressure coefficient
Pp	Passive earth pressure capacity
K_{PEP}	Sliding stiffness due to embedment .
id	Initial displacement prior to start of model test

Table 3.6 Static lateral test data

EXPERIMENTAL DATA SET						FOOTING GEOMETRY							SOIL DATA						TEST DATA							WINKLER MODEL INPUT													NOTES
REF	TEST	STA	STA-V	Description	FS_V	L	B	d	D	mass	cg	PL	Dr	ϕ'	ϕ'_{cs}	γ_d	FK	Kv-eq	$K\theta$	Klat	Hmax	Mmax	FQ	Qult	FS2	Qult	qi	Le/L	ke	km	cz	Fu	u	Qs	ex	$K_{x\text{-}f}$	Kp	Pp	$K_{x\text{-}pass}$	id	
	Units					m	m	m	m	kg	m	m	%	deg	deg	(kN/m^3)		(MN/m)	MNm/r	kN	kN	kN-m	kN	kN		kN	%	%	MN/m	MN/m	Mg/s			kN		MN/m		kN	MN/m	mm	
	KRR01, KRR02 - Uniform, Fine Sand, SP (Nevada Sand)																																							
17	KRR01	FE S18	FW (V) S25	Medium / Der	3.1	2.67	0.69	0.64	0.30	36480	4.52	6.8	60	37	25	15.56	1.00	507.1	71	7	44	316	1.00	1092	3.1	1092	79	0	277	277	0	0.30	0.13	48	1.8	8	12	2	3.2	9.7	
18	KRR02	AE S21-35	AW (V) S12	Dense / Very	5.1	2.67	0.69	0.64	0.00	36480	4.52	4.6	60	43	32	16.15	0.50	564.9	152	19	81	414	0.57	1822	2.9	1032	65	0	154	154	0	1.0	0.64	228	1.0	55	25	0	0.0	3.7	
18	KRR02	CE S38-50	CE S38-50	Dense / Very	8.2	3.94	1.08	0.64	0.00	49840	7.01	4.6	60	41	30	16.15	0.10	2343.0	180	21	110	826	0.45	4019	3.7	1809	56	0	55	55	0	0.75	0.41	200	1.0	39	19	0	0.0	8.5	1
	KRR03 - Stiff Clay (Bay Mud)																																							
19	KRR03	CE S18	CW (V) S28	Very Stiff Clay	3.0	2.67	0.69	0.64	0.26	36480	4.52	4.6	0	0		17.00	1.00	51.7	61	7	96	568	1.00	1059	3.0	1059	100	10	56	28	0	1.0	0.29	103	1.7	8	22	9	3.1	10.7	
	SSG02, SSG03 - Uniform, Fine Sand, SP (Nevada Sand)																																							
8	SSG02	G, test7a,b	V02, B-G	Dense / Very	3.4	2.84	0.69	0.70	0.00	58480	5.14	5.1	80	42	27	16.15	2.00	254.6	163	20	135	721	0.64	1930	2.2	1238	69	0	260	260	0	1.00	0.50	289	1.0	43	22	0	0.0	22.4	
9	SSG03	E, test4a-c	V03, C-E,G	Dense / Very	4.0	2.84	0.69	0.70	0.70	58480	4.54	4.5	80	37	22	16.15	3.00	277.7	348	42	121	714	1.00	2320	4.0	2320	84	9	792	425	0	1.0	0.40	231	2.6	81	12	33	25.8	20.7	
9	SSG03	D, test2a-c	V03, C-E,G	Dense / Very	8.2	2.84	0.69	0.70	0.70	28880	4.54	5.0	80	37	22	16.15	2.00	277.7	76	38	83	443	0.60	2320	4.9	1392	200	0	283	283	0	1.0	0.40	114	1.0	53	12	0	0.0	10.2	
	Bartlett - Clay - water content = 34%, LL = 67, PL = 31, %clay sizes = 48, S.G. = 2.64																																							
2	B Type A	3.4-12 (FS = 3)	3.4-11	Medium Clay	3.0	0.50	0.25	0.00	0.00	1190	0.70	0.7		0		18.00	1.00	43.0	1	31	3	2	1.00	35	3.0	35	100	0	349	344	0			0	1.0	0	1	0	0.0	0.2	3
2	B Type B	3.4-6 (FS = 1.5)	3.4-4,6,8	Medium Clay	1.9	0.25	0.50	0.00	0.00	2379	0.70	0.7		0		18.00	1.00	43.0	0	34	1	1	0.81	44	1.5	35	100	0	344	344	0			0	1.0	0	1	0	0.0	0.4	3
	Weissing - Clean Quartz Sand																																							
22	W Type A	5.11 (FS = 2)	5.11 (FS = 2)	Very Dense	1.9	0.50	0.25	0.00	0.00	1977	0.70	0.7		43		16.68	1.00	287.5	12	209	4	3	1.10	37	2.1	41	70	11	4788	2300	0			0	1.0	0	23	0	0.0	0.0	2
22	W Type A	5.10 (FS = 5)	5.10 (FS = 5)	Very Dense	4.8	0.50	0.25	0.00	0.00	791	0.70	0.7		43		16.68	2.00	287.5	3	209	2	1	0.70	37	3.3	26	61	0	4600	4600	0			0	1.0	0	23	0	0.0	0.0	2
22	**W Type B**	5.17 (FS = 5)	5.17 (FS = 5)	Very Dense	2.5	0.25	0.50	0.00	0.00	744	0.70	0.7		43		16.68	**0.50**	287.5	1	228	1	1	0.80	19	2.0	15	200	0	1150	1150	0			0	1.0	0	23	0	0.0	0.0	2
	TRISEE - Ticino Sand - Uniform, course to medium silica sand (Cu = 1.6, D50 = 0.55mm, F200 < 5%, Cz < 1 --> SP). Saturated																																							
15	TRISEE	25	HD	Very Dense	12.5	1.00	1.00	1.00	1.00	30590	0.90	0.9	85	42	29	16.04	1.50	189.1	39	81	126	122	0.30	3742	3.7	1123	139	13	707	284	0	0.20	0.10	30	1.0	19	21	0	0.0	10.2	2,4
15	TRISEE	83	LD	Medium	20.7	1.00	1.00	1.00	1.00	10197	0.90	0.9	45	38	32	14.79	0.50	73.0	16	40	44	42	0.10	2071	2.1	207	146	14	195	73	0	1.0	0.63	63	1.0	57	14	0	0.0	27.1	2,4

COMMON NOTES

A. All references in "REF" column correspond to the references in Table 3.5.
B. "STA-V" indicates corresponding vertical load test from Table 3.5 from which the footing geometry and Winkler Model Inputs are taken.
C. All ultimate bearing capacities are from a vertical push test, unless otherwise indicated.
D. Initial displacement determined from weight and initial stiffness, unless otherwise indicated.

SPECIFIC NOTES

1. Ultimate bearing capacity calculated from a back-calculated friction angle.
2. Ultimate bearing capacity calculated from a "researcher-specific" recommended friction angle.
3. Ultimate bearing capacity calculated from a "researcher-specific" recommended value of cohesion.
4. Initial displacement determined from weight and initial stiffness plus the previous test history data file.

3.8.3 Dynamic Lateral Test Data

The properties obtained, assumed, and calculated from the vertical test data are applied to the dynamic lateral tests. Only the pertinent information required as input for the simulation is presented in the following tables.

In order to present as much useful information for the vertical load test data available, and in as concise a manner as possible, Table 3.7 lists all the known and calculated parameters used for the simulation of experiments analyzed. The presentation of information is similar to that in Table 3.5. "Test Data" indicates information taken directly from the model test data files.

Table 3.7 Dynamic lateral test data

EXPERIMENTAL DATA SET					FS_V	FOOTING GEOMETRY							SOIL PROPERTIES						TEST DATA							WINKLER MODEL INPUT													NOTES
REF	TEST	STA	STA-V	Description		L	B	d	D	mass	cg	PL	Dr	ϕ'	ϕ'_{cs}	γ_d	FK	Kv-eq	$K\theta$	Klat	Hmax	Mmax	FQ	Qult	FS2	Qult	qi	Le/L	ke	km	cz	Fu	u	Qs	ex	$K_{x\text{-}f}$	Kp	Pp	$K_{x\text{-}pass}$	id	
	Units					m	m	m	m	kg	m	m		deg	deg	kN/m^3		(MN/m)	MN-m/r	MN/m	kN	kN-m		kN		(kN)	(%)	(%)	(MN/m)	(MN/m)	kN-s/m			kN		MN/m		(kN)	(MN/m)	mm	
	KRR01, KRR02 - Uniform, Fine Sand, SP (Nevada Sand)																																						
17	KRR01	EW D7,13-14	FW (V) S25	Medium / Den	3.1	2.67	0.69	0.64	0.30	36480	5.38	NA	60	37.2	25.4	15.56	1.00	428.0	84	12	69	384	1.00	1092	3.05	1092	79	0	233	233	301.8	1.00	0.47	170	1.8	28	12	5.9	12.3	13.8	4
17	KRR01	BW D36	S31 CW (V)	Dense / Very	1.7	2.54	0.38	0.64	0.30	42720	5.46	NA	80	40.2	24.0	16.15	1.00	379.3	344	13	59	337	1.40	725	2.42	1016	121	8	1054	392	166.6	1.00	0.45	187	2.2	40	13	3.7	17.8	20.8	4
18	KRR02	BE D5,9-12	AW (V) S12, CW (V) S54	Dense / Very	4.1	2.67	0.69	0.64	0.00	36480	4.66	NA	60	42.0	30.7	16.15	0.25	109	386	24	69	333	0.80	1465	3.28	1172	60	22	92	15	418.2	1.00	0.59	212	1.0	72	25	0.0	0.0	30.2	4
18	KRR02	BW D5,9-12	CE S38-50	Dense / Very	8.2	3.94	1.08	0.64	0.00	49840	3.13	NA	60	40.6	29.6	16.15	0.30	70.7	238	36	133	441	0.20	4019	1.64	804	73	14	14	5	483.6	1.40	0.88	432	1.0	118	19	0.0	0.0	45.1	1,4
	KRR03 - Stiff Clay (Bay Mud)																																						
19	KRR03	BE D4,8-11	AW (V) S01, CW (V) S28	Very Stiff Clay	2.9	2.67	0.69	0.64	0.26	36480	3.13	NA		0.0		17	1	69.491	159	10	102	328	1.00	1035	2.89	1035	100	18	184	38	377.4	1.00	0.29	103	1.7	10	22	8.8	4.0	10.2	4
	SSG02, SSG03 - Uniform, Fine Sand, SP (Nevada Sand)																																						
9	SSG03	H test8c-e (SW)	V03, C-E,G	Dense / Very	4.0	2.84	0.69	0.70	0.70	58480	5.14	NA	80	37.0	21.9	16.15	2.00	115.3	310	18	115	592	0.50	2320	2.02	1160	96	18	706	118	264.5	1.00	0.40	231	2.6	36	12	33.1	11.0	42.2	1,4
9	SSG03	I test8c-e (DW)	V03, C-E,G	Dense / Very	6.4	2.84	0.69	0.70	0.70	36800	4.78	NA	80	37.0	21.9	16.15	1	109	421	37	84	403	0.30	2320	1.93	696	98	22	375	56	263.1	1.00	0.40	145	2.6	63	12	33.1	22.3	34.5	1,4
	TRISEE - Ticino Sand - Uniform, course to medium silica sand (Cu = 1.6, D50 = 0.55mm, F200 < 5%, Cz < 1 --> SP). Saturated																																						
15	TRISEE	24	HD	Very Dense	12.5	1.00	1.00	1.00	1.00	30590	0.90	0.90	85	41.8	28.5	16.04	1.00	382.8	30	106	65	59	0.16	3742	2.00	599	150	0	383	383	335.8	0.75	0.39	117	1.0	193	21	0.0	0.0	7.4	2,4
15	TRISEE	82	LD	Medium	20.7	1.00	1.00	1.00	1.00	10197	0.90	0.90	45	38.5	32.0	14.79	0.25	54.8	17	43	19	17	0.08	2071	1.66	166	152	18	55	14	142.7	1.00	0.63	63	1.0	139	14	0.0	0.0	16.5	2,4

COMMON NOTES

A. All references in "REF" column correspond to the references in Table 3.5.
B. "STA-V" indicates corresponding vertical load test from Table 3.5 from which the footing geometry and Winkler modelinputs are taken.
C. All ultimate bearing capacities are from a vertical push test, unless otherwise indicated.
D. Initial displacement determined from weight and initial stiffness, unless otherwise indicated.

SPECIFIC NOTES

1. Ultimate bearing capacity calculated from a back-calculated friction angle.
2. Ultimate bearing capacity calculated from a "researcher-specific" recommended friction angle.
3. Ultimate bearing capacity calculated from a "researcher-specific" recommended value of cohesion.
4. Initial displacement determined from weight and initial stiffness plus the previous test history data file.

3.9 STRENGTH AND STIFFNESS UNCERTAINTY

Strength and stiffness of the soil media are highly uncertain. To estimate the uncertainty of strength characteristics, specifically the ultimate bearing capacity q_{ult}, reference is made to a literature review. To estimate the uncertainty in stiffness, the model test data are investigated. All simulations of the model tests will include additional runs to incorporate the uncertainties of strength and stiffness discussed.

3.9.1 Variation in Strength

Strength properties of soil are highly uncertain; work by Jones et al. (2001) addresses the potential range of strength which may be anticipated, given the testing method and soil property under consideration. Coefficient of variation (COV) values are provided to represent the uncertainty characteristics of density, plasticity, strength, consolidation and permeability, stiffness and damping. Each of these are broken down into either in-situ or laboratory measurements.

For the sand tests considered in this report, ultimate strength is known from either a direct vertical bearing push test or calculated from the friction angle, which is recommended from triaxial test data in the corresponding test's literature. Therefore, the primary strength characteristic is the friction angle, since for tests where a vertical push test was performed, the friction angle can be back-calculated. For clay tests, the undrained shear strength is either back-calculated from a vertical push test or inferred from triaxial test data. Therefore, the undrained shear strength is the primary strength characteristic. Additionally, the COV given by Jones et al. (2001) for field-determined strength characteristics apply to tests such as the SPT and CPT. Therefore, since a vertical push test is most similar to a triaxial test, only COV's associated with laboratory uncertainty will be considered. Table 3.8 lists the most applicable uncertainty values associated with the strength characteristics corresponding to the type of soil considered.

Table 3.8 Uncertainty in strength characteristics [(a)]

Strength Characteristic	Soil Type	Property Value Range	Property Value Mean	COV Range (%)	COV Mean (%)
ϕ' (deg)	Sand	35–41	37.6	5–11	9
c_u (kPa)[(b)]	Clay, silt	15–363	276	11–49	22

Notes:
(a) Reference: Jones et al. (2001). Data after Phoon and Kulhawy (1999).
(b) Uncertainty based on data for unconsolidated undrained triaxial compression test.

Using these COV values to calculate bearing capacity, applied to the ϕ' and c_u values, the final capacity varies by about a factor of two. This generally coincides with the recommendation in ATC-40 (1996), which states that a best estimate is first performed and subsequently this estimate is multiplied and divided by a factor of two to envelope a possible range of uncertainty. For example, using the soil properties and foundation measurements of KRR02-S21AE, gives q_u = 989 kPa (FS_V = 5.1). Assuming $\pm$ 11% on ϕ', gives qu ranging from q_u = 460 kPa (FS_V = 2.4) to q_u = 2260 kPa (FS_V=11.7), which is about a factor of 2 from the first estimate.

3.9.2 Variation in Stiffness

3.9.2.1 Vertical Stiffness

To study the range of potential vertical stiffness values for input into the BNWF mesh, a normalized parameter is calculated. The normalized parameter is taken as the initial stiffness K_{int} determined based on appropriate compression test results presented in Figures 3.11–3.12, divided by an estimate of elastic stiffness $K_{GAZ\text{-}EPRI}$ as presented in Table 3.5. Recall that this value is defined as the elastic stiffness after Gazetas (1991), using a shear modulus estimated from the EPRI manual (1990). Since the vertical load tests do not have a factor of safety (each is tested to failure, $FS_V = 1$), the stiffness ratio is plotted against the ultimate load normalized by an initial shear modulus, G_{int}, times the foundation base area. Here the initial shear modulus is back calculated using Gazetas' equations from the known initial stiffness. As shown in Figure 3.46 the trend is well fit by a power regression (natural logarithm), and the actual stiffness appears to vary with the ultimate load, shear modulus, and dimensions of the footing. For practical design,

if the ultimate load and shear modulus for a shallow foundation are known and the Gazetas stiffness is calculated, a more representative vertical stiffness could easily be interpreted from the graph. It appears that the initial stiffness K_{int} varies from approximately 0.2–2 times the estimated elastic stiffness values $K_{GAZ\text{-}EPRI}$.

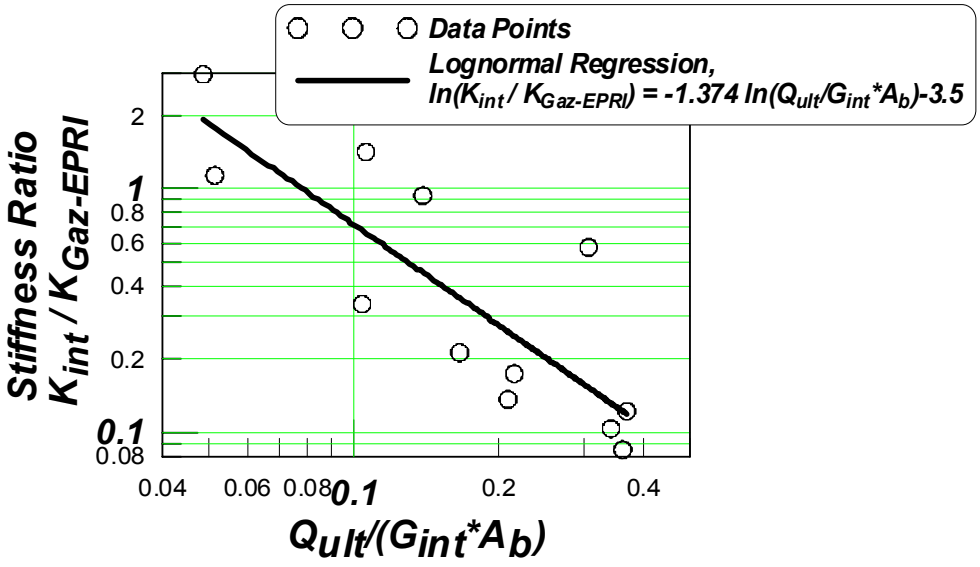

Fig. 3.46 Comparison of observed initial stiffness to elastic half space stiffness

Similarly plotted in Figure 3.47 is the normalized unloading stiffness versus the normalized ultimate load, again with values from the vertical load tests as presented in Table 3.5. Here, G_{unl} is the shear modulus back-calculated using the unloading stiffness and Gazetas' equations. A lognormal regression is applied and the regression equation presented in the legend. It is interesting to note that when the capacity of the system is relatively large compared to the stiffness of the soil medium, the stiffness ratio nears unity. This makes intuitive sense, since the recommendations by Gazetas (1991) are for an elastic system, and a system with a large reserve of capacity is more likely to behave elastically than a system close to failure. It appears that the unloading stiffness varies across a larger range than the initial stiffness, from approximately 1–12 times the estimated elastic stiffness values. However, in general a range of 0.9–2.2 times the elastic stiffness captures 58% of the foundation capacities, with larger deviations for relatively smaller foundation capacities.

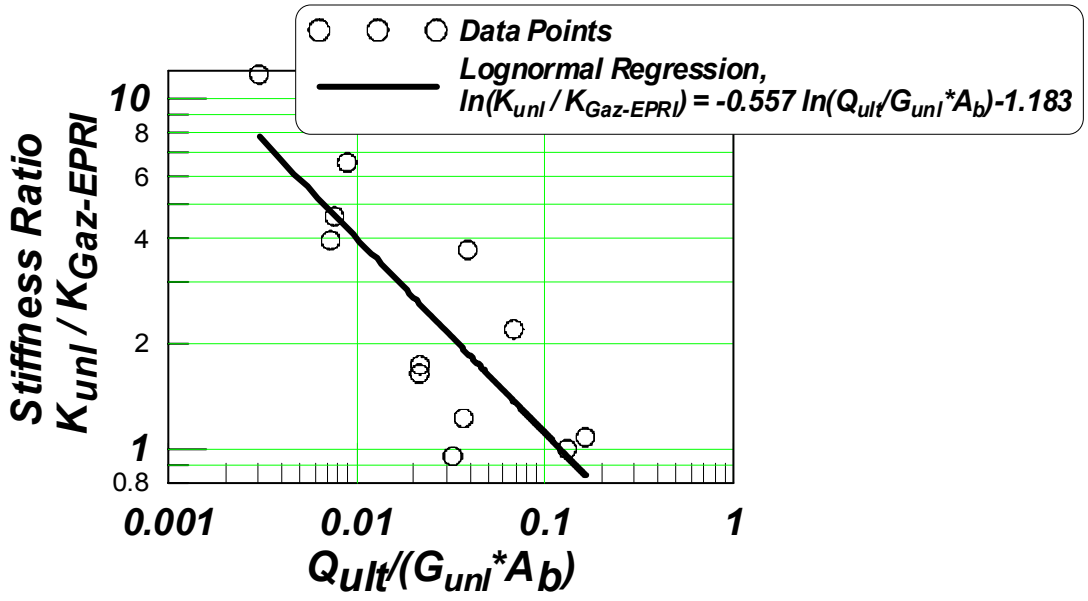

Fig. 3.47 Comparison of observed unloading stiffness divided by elastic stiffness vs. ultimate strength divided by the unloading shear modulus times the footing area

3.9.2.2 Rotational Stiffness

Unlike the vertical push test data, as shown previously in Figures 3.11–3.12, the rotational unloading stiffness tends to degrade with larger and larger magnitudes of rotation, as described in Phalen (2003). Therefore, it makes sense to use an initial stiffness, as shown in Figure 3.48 for both static and dynamic cases, from the moment-rotation response of the model. The rotational stiffness is taken as the average of the stiffnesses (determined from experimental M-θ curves) in each direction for the initial cycles of rotation.

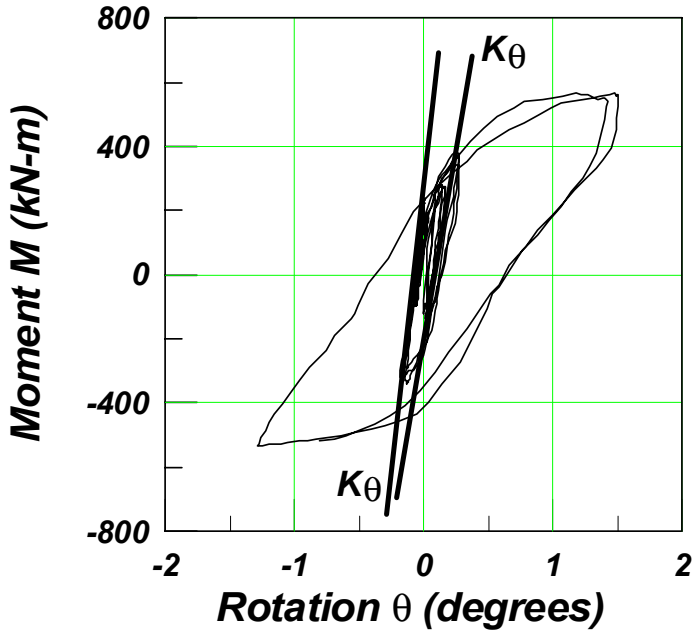

Fig. 3.48 Initial rotational stiffness: KRR02-S38, Station CE

The rotational stiffness from the experimental results K_θ is compared to the analytical rotational stiffness suggested by Gazetas (1991), $K_{GAZ\text{-}EPRI}$, in Figure 3.49. In this case, the rotational stiffness ratio is plotted against the vertical factor of safety FS_V.

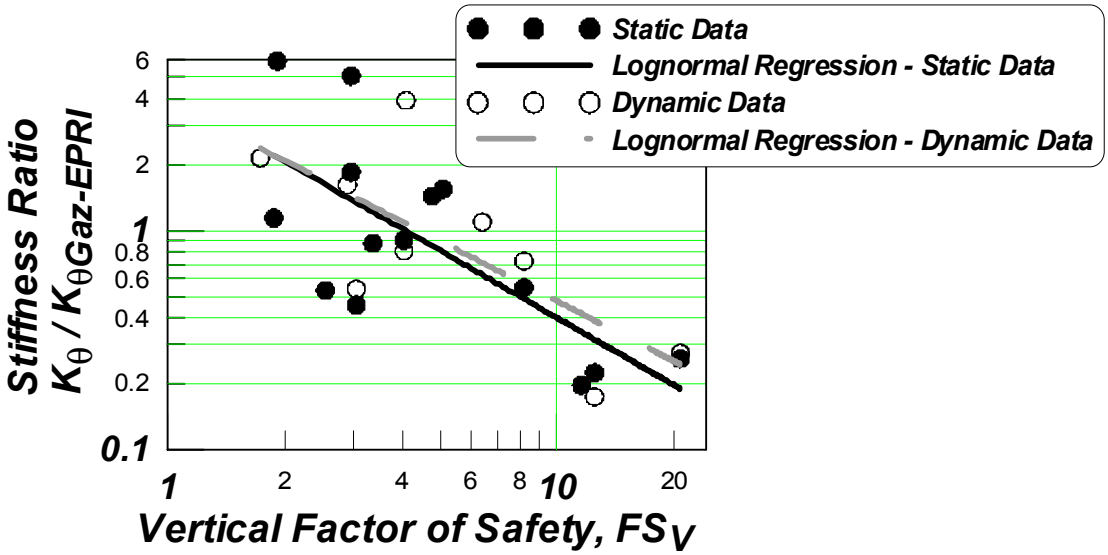

Fig. 3.49 Rotational stiffness ratio vs. vertical factor of safety

The rotational stiffness determined from the M-θ plots is between 0.5–6 times that determined using Gazetas' equations. For lower FS_V, the variation is larger. However, for FS_V > 4.0 the range of the rotational stiffness ratio is much less, varying between approximately 0.5–1.5. Overall, 57% of the cases can be bounded by 0.5–2.0 times Gazetas' estimate.

3.9.2.3 Horizontal Stiffness

The normalized horizontal stiffness K_X / $K_{GAZ\text{-}EPRI}$ of the system is shown versus the vertical factor of safety in Figure 3.50. Similar to the rotational stiffness, the horizontal stiffness is taken as the average stiffness from initial cycles of loading. In this case, both the dynamic and static test data are included and the difference in stiffness between them is significant. The dynamic stiffness is generally four times greater than the static stiffness for all factors of safety. The static stiffness compares reasonably well with the recommendations of Gazetas (1991), being within a factor of two, and generally increasing for larger factors of safety. The fact that the horizontal stiffness ratio K_X / $K_{GAZ\text{-}EPRI}$ increases with increasing FS_V is interesting (all other trends opposite). This points to the fact that systems with higher FS_V transfer load into the rotational degree of freedom, rather than into translation.

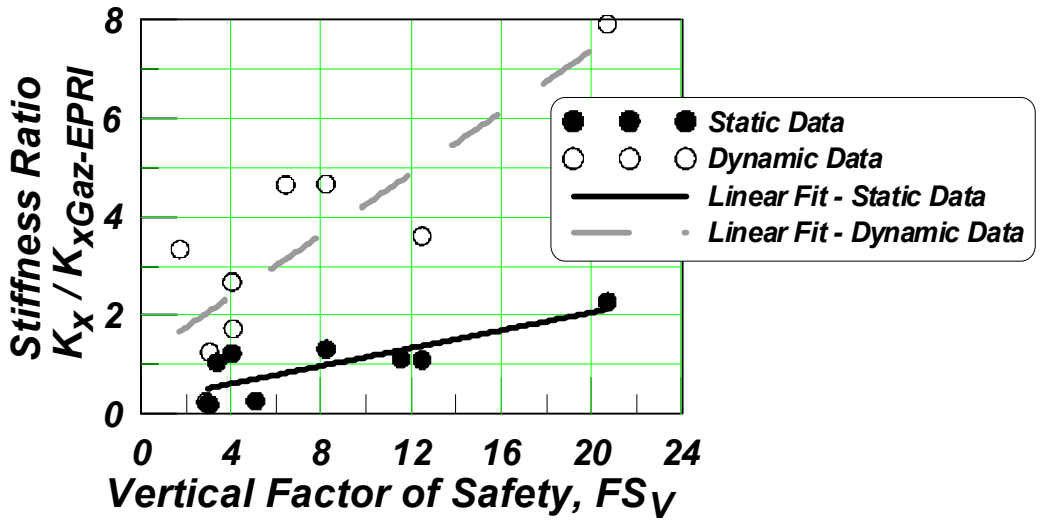

Fig. 3.50 Comparison of observed horizontal stiffness to continuum-based elastic stiffness

3.9.2.4 Summary of Stiffness Uncertainty

From an investigation of the model test data, it was found that in general the uncertainty of stiffness is within a factor of two for vertical, horizontal, and rotational stiffness. This compares with suggestions in ATC-40 (1996), which recommends a factor of 0.5–2.0 times to account for uncertainty in the soil medium. However, larger deviations were observed in static vertical unloading stiffness for stiffer systems and dynamic sliding stiffness for higher FS_V systems. Additionally, all data sets had values beyond a factor of two.

4 Simulation Results

Using the recommendations of the previous chapters for BNWF parameters, simulations are performed with these considerations and compared to the experimental data. Select figures which graphically compare the model response to the simulation response with respect to capacity, settlement, and horizontal sliding are presented in this chapter, and the remaining test simulations are presented in Appendix B for static tests and Appendix C for dynamic tests. The quantitative comparisons are further discussed in this chapter.

4.1 DECISION VARIABLES

In order to quantify the results of the simulations, with respect to the large number of tests considered and the simulations using uncertainty in soil properties, four decision variables are considered that capture and compare the salient features of the model data to the simulation data. These values of interest are the maximum absolute positive $|+M_{max}|$ and maximum absolute negative moment $|-M_{sim}|$, maximum settlement s_{max}, and maximum absolute sliding displacement u_{max}. In order to compare the observed value to the simulation value for any of these four quantities, a decision variable is defined as the absolute value of the simulation divided by the observed experiment value, or $|X_{sim}/X_{exp}|$ where X is the quantity of interest and the subscript indicates from simulation or experiment (e.g., $|(+M_{max})_{sim}/(+M_{max})_{exp}|$ constitutes one decision variable).

4.2 STATIC TESTS

Example simulation results for experiments KRR02-S38 Station C East and SSG03 test 2, Station D are shown in Figure 4.1 and Figure 4.2, respectively. These figures show (a) moment versus rotation, (b) settlement versus rotation, and (c) lateral base displacement versus pseudo time. These comparisons show that the Winkler model does a reasonable job capturing the

results for these hysteretic features. The shape, peaks, unloading, and reloading are reasonably captured for both of these example simulations. Figure 4.1 does show some difficulty in following the full sliding displacement, e.g. at pseudo-time ~8000 seconds, the simulation begins to drift, whereas this was not observed in the experimental results. Figure 4.2 shows a better comparison of overall sliding history; however, with a compromise in capturing peak moment (capacity) in the positive moment direction ($+M_{max}$ = 443 kN-m for the experiment and $+M_{max}$ = 383 kN-m for the simulation). However, the simulation is able to capture the pinched M-θ hysteresis in Figure 4.2(a) and the "U"-shaped settlement in Figure 4.2(b), even modeling the lifting above the ground surface (as positive s is observed).

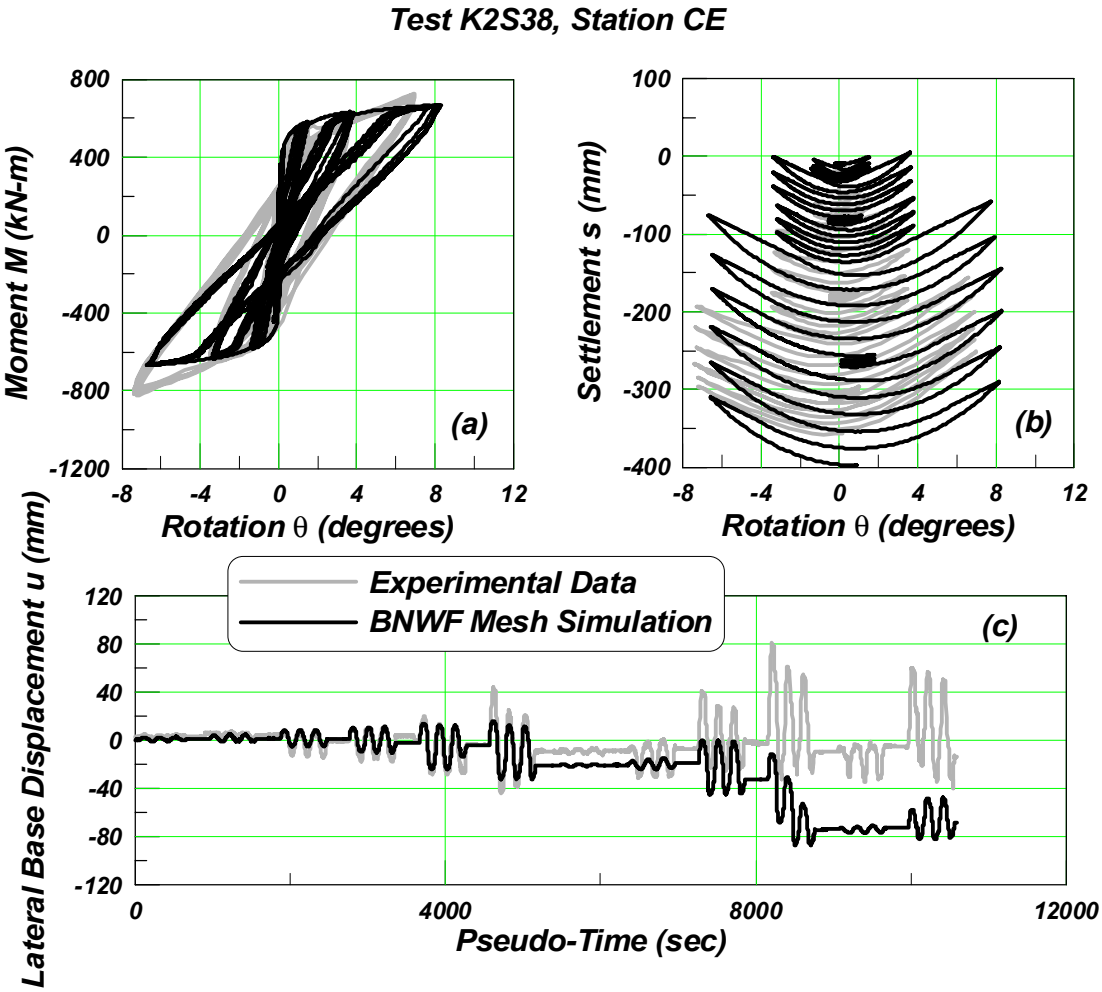

Fig. 4.1 Comparison of simulation to slow cyclic experiment for (a) moment vs. rotation, (b) settlement vs. rotation, and (c) lateral base displacement vs. pseudo-time: test KRR02-S38

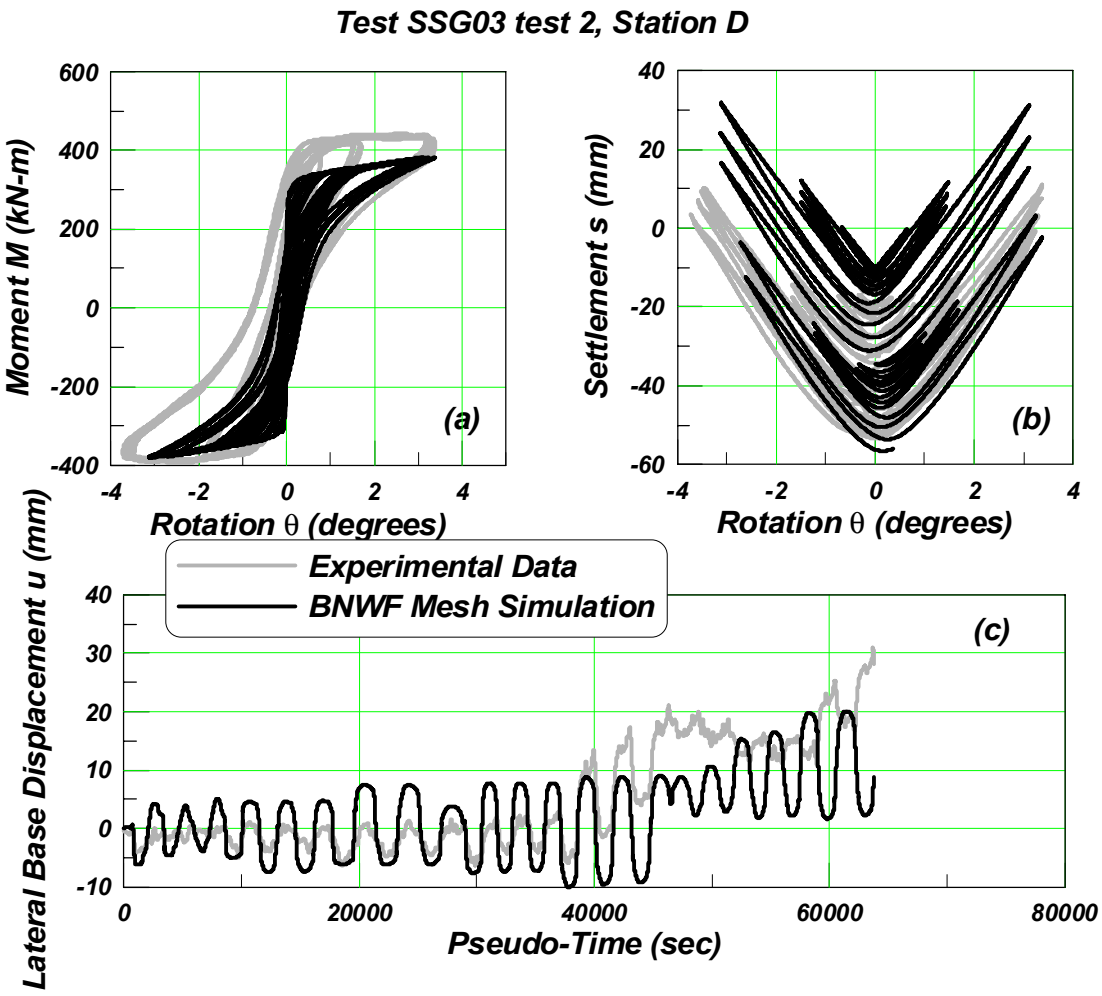

Fig. 4.2 Comparison of simulation to slow cyclic experiment for (a) moment vs. rotation, (b) settlement vs. rotation, and (c) lateral base displacement vs. pseudo-time: SSG03 test 2, Station D

Additional static test simulations are presented in Appendix B, and decision variables of interest are plotted in Figure 4.3. In some cases, it was necessary to apply a factor to the input bearing capacity (*FQ),* vertical stiffness (*FK),* and/or sliding coefficient (*Fu),* as listed in Table 3.6, in order to find good comparison with the experimental data. It was determined that the most important feature to capture in the BNWF simulation was the moment capacity of the model experiment. The second most important feature to capture was the maximum settlement. Once the moment and settlement were reasonably estimated in the BNWF model by applying factors to the capacity and stiffness input parameters, the sliding displacement was observed. The factors used are presented, thoroughly investigated, and interpreted in following sections. Once the BNWF simulations provided a reasonable comparison with model test data (best

estimate of input parameters), the values were adjusted to account for uncertainty in strength and stiffness in order to observe the possible range in decision variables. Therefore in Figure 4.3, "System Capacity & Stiffness + 1σ" indicates the best estimate of input parameters for the BNWF model, with the affect of uncertainty creating a "stiff-strong" foundation case. Alternatively, System Capacity & Stiffness - 1σ" indicates the best estimate of input parameters for the BNWF model, with the affect of uncertainty creating the "flexible-weak" foundation case.

Figure 4.3 shows good comparison of the baseline decision variables in general, and a conservative envelope when uncertainty in the predicted spring strength and stiffness is included through additional simulation runs. This envelope appears to encompass both the (a) maximum positive and (b) maximum negative, though the baseline (using the measured values presented in Table 3.6) seems to slightly underestimate these values, varying from 0.8–1.2 times for $+M$ and $-M$ across the broad range of FS_V considered.

Maximum settlement is matched quite well in general, and including a lower bound of strength and stiffness can overestimate this value by approximately two to six times.

Sliding displacement is generally underestimated, with a few large overestimations; approximately 5 times overestimated in select cases. Approximately 45% of cases predict sliding displacement within one-half to two times the experimental value.

Some special test cases that should be noted are the Weissing (1979) and Bartlett (1976) test series. These model tests were fixed against horizontal movement, thus the model footing was allowed only to rotate and settle. These simulations compare in general very well with the model tests.

Additionally, an elastic horizontal spring was used for simulation of TRISEE Test 25, as inspection of the experimental results showed there are no permanent horizontal displacements accrued. In this case, modeling the sliding component with an elastic spring gave a much better comparison of the simulation to the model test.

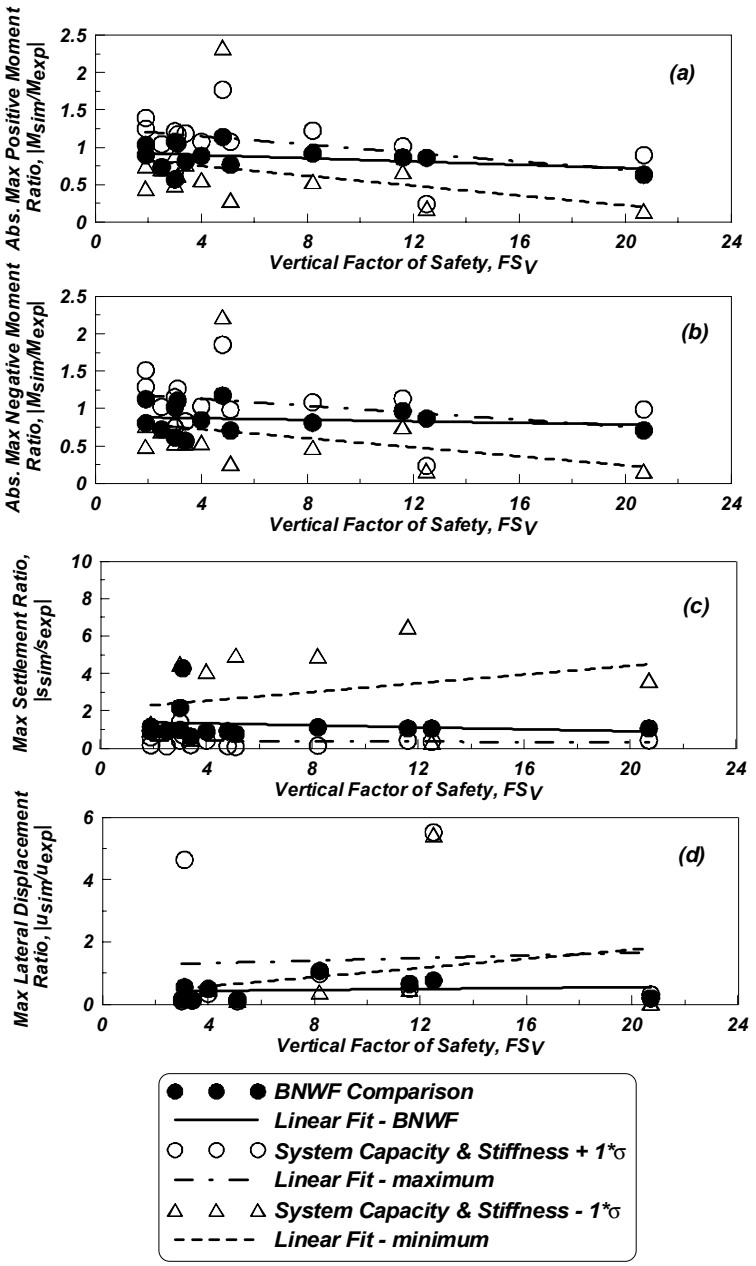

Fig. 4.3 Comparison variables vs. vertical factor of safety for static simulations

4.3 DYNAMIC TESTS

Example simulation results for experiments KRR01-D36 Station B West and KRR02-D5, 9-12 test 2, Station B West are shown in Figures 4.4.and 4.5, respectively. These figures show (a) moment versus rotation, (b) settlement versus rotation, and (c) lateral base displacement versus time. These comparisons show that the Winkler model does a reasonable job capturing the

results for these hysteretic features. The shape, peaks, unloading, and reloading are reasonably captured for both of these example simulations. Again, the full sliding displacement is difficult to capture, as evident in Figure 4.4, where after approximately 22 seconds the model test begins to accrue permanent displacements while the simulation does not. This trend is also observed in Figure 4.5. However, both simulations indicate that permanent rotations are accrued, and in comparable magnitudes to the model tests. Again, moment capacity is slightly underestimated, a seemingly computational expense of capturing realistic settlement in the Winkler framework.

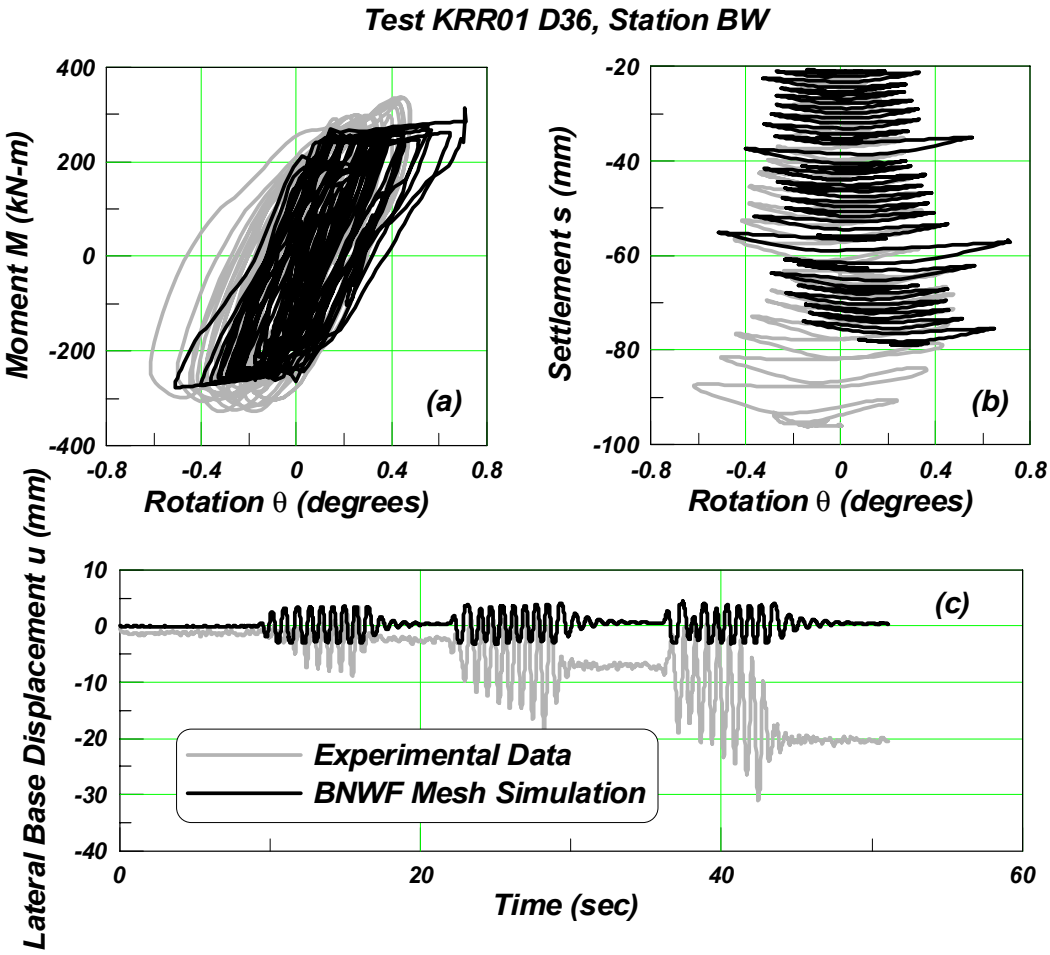

Fig. 4.4 Comparison of simulation to dynamic cyclic experiment for (a) moment vs. rotation, (b) settlement vs. rotation, and (c) lateral base displacement vs. time: test KRR01-D36

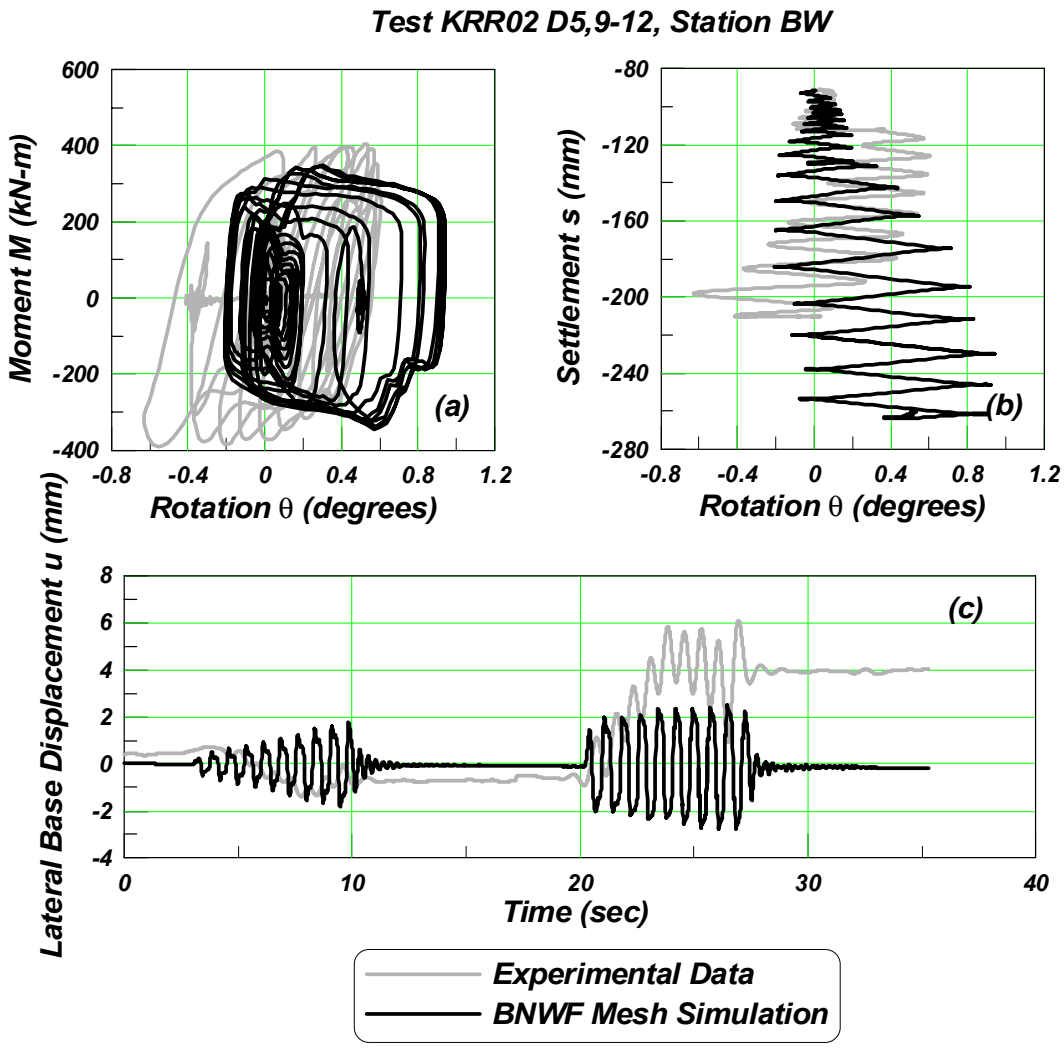

Fig. 4.5 Comparison of simulation to dynamic cyclic experiment for (a) moment vs. rotation, (b) settlement vs. rotation, and (c) lateral base displacement vs. time: test KRR02-D5

The procedure of additional modeling of uncertainty in the soil input parameters, as discussed in the cases of static simulations, is similarly followed for the dynamic simulations once the best model estimate is made. Figure 4.6 shows good comparison of the baseline decision variables in general, and a conservative envelope when uncertainty in the predicted spring strength and stiffness is included.

For vertical factors of safety less than ten, both the (a) maximum positive and (b) maximum negative moment are captured within the results produced by the envelope of uncertainty associated with strength and stiffness. An increase or decrease in strength and stiffness for footings with vertical factor of safety greater than ten (exclusively the TRISEE test

data by Negro et al. 1998) has little effect on the simulation results and underestimates the observed values by approximately a factor of two.

Maximum settlement is matched fairly well in general, and including a lower bound of strength and stiffness can overestimate this value by approximately two times.

Sliding displacement is generally underestimated, with approximately 55 % of the cases between 0.25–1 times the experimental value.

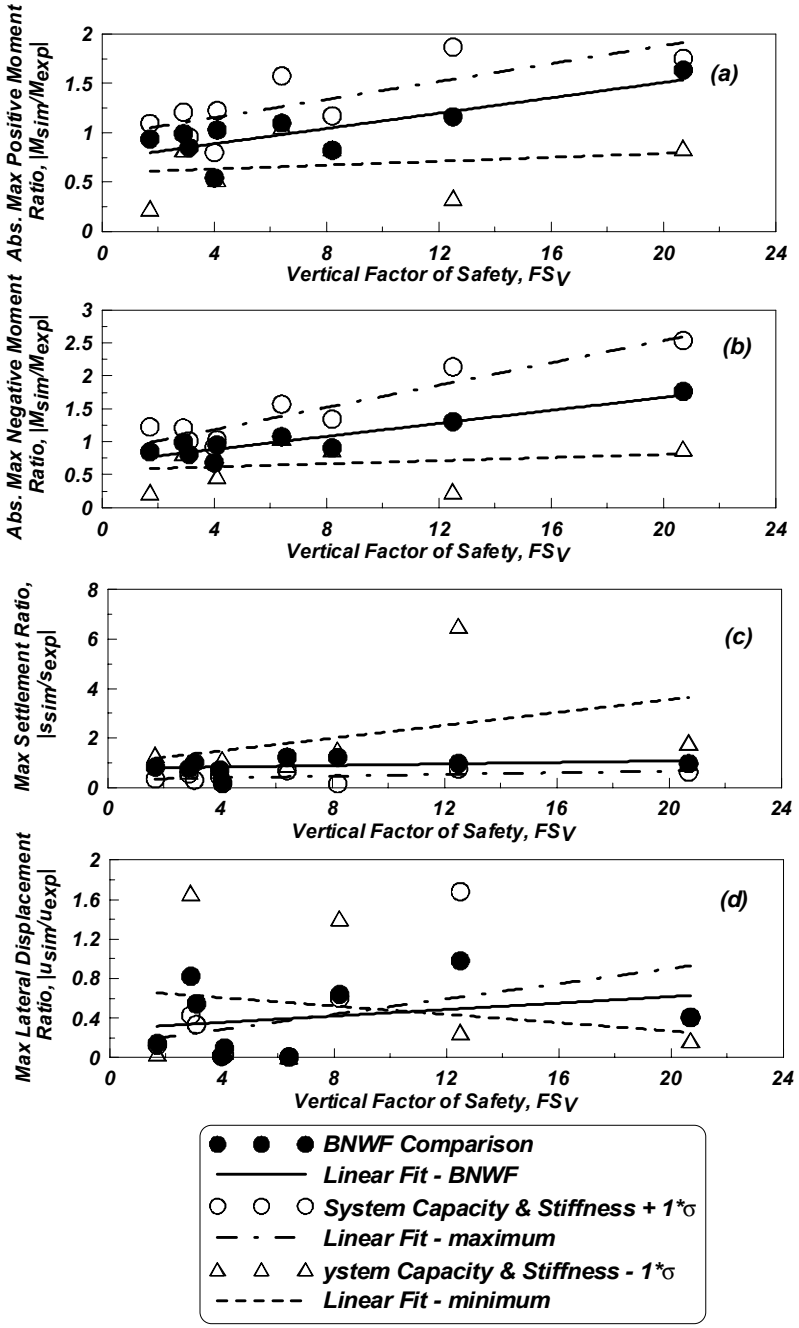

Fig. 4.6 Decision variables vs. vertical factor of safety for dynamic simulations

4.4 DISCUSSION OF RESULTS

Running a BNWF simulation with the recommended Winkler parameters can provide reasonable estimates of moment, settlement, and sliding if the uncertainty in soil properties is included to bound the estimate. The Winkler parameters for horizontal and vertical springs discussed previously and recommended are listed in Table 4.1.

Table 4.1 Recommended BNWF parameters

BNWF parameter	Section	value
Elastic vertical stiffness, K_z: Elastic Unloading Stiffness is suggested, K_{unl} (Normalized by Gazetas, 1991 with properties from EPRI, 1990)	3.9.2	$\ln\left(\frac{K_{unl}}{K_{Gaz-EPRI}}\right) = -0.557\ln\left(\frac{Q_{ult}}{G_{unl}A_b}\right) - 1.183$
End tip contact pressure	3.5.3	$q_i = 0.5\left(\tan(\phi') + \frac{1}{FS_V}\right)$
End length	3.5.4	$L_e = 0.5L - L\left[\frac{1}{8}\left(1 - C_{R-V}^K\right)\right]^{\frac{1}{3}}$, $C_{R-V}^K = \frac{K_{\theta y} - \frac{K_z}{A} I_y}{K_{\theta y}}$
Middle region subgrade reaction	3.5.4	$k_{mid} = \frac{K_z}{BL}$
End region subgrade reaction	3.5.4	$k_{end} = \frac{K_z}{LB} + \frac{K_{\theta y}}{I_y} C_{R-V}^K$
Passive Earth Pressure	3.5.2	K_p estimated using Caquot and Kérisel (1949)
Friction Coefficient	3.5.2	$\mu_{cs} = \tan(\phi_{cs})$, $\phi_{cs} = \phi' - 3(Dr[10 - \ln(q_u / p_a)] - 1)$
Sliding Stiffness (Normalized by Gazetas, 1991 with properties from EPRI, 1990)	3.5.2	$\frac{K_X}{K_{X,Gaz-EPRI}} = 0.091(FS_V) + 0.245$ (static); $\frac{K_X}{K_{X,Gaz-EPRI}} = 0.312(FS_V) + 1.134$ (dynamic)
If sliding stiffness is separated, frictional and passive earth pressure stiffness components	3.5.2	$K_{fr} = \frac{K_{\exp}}{e_x}$, $K_{PEP} = K_{\exp}\left(1 - \frac{1}{e_x}\right)$
Tension Capacity		0% (no data to support a recommendation)

Figure 4.7 shows a graphical representation of the BNWF model and the parameters investigated corresponding to Table 4.1.

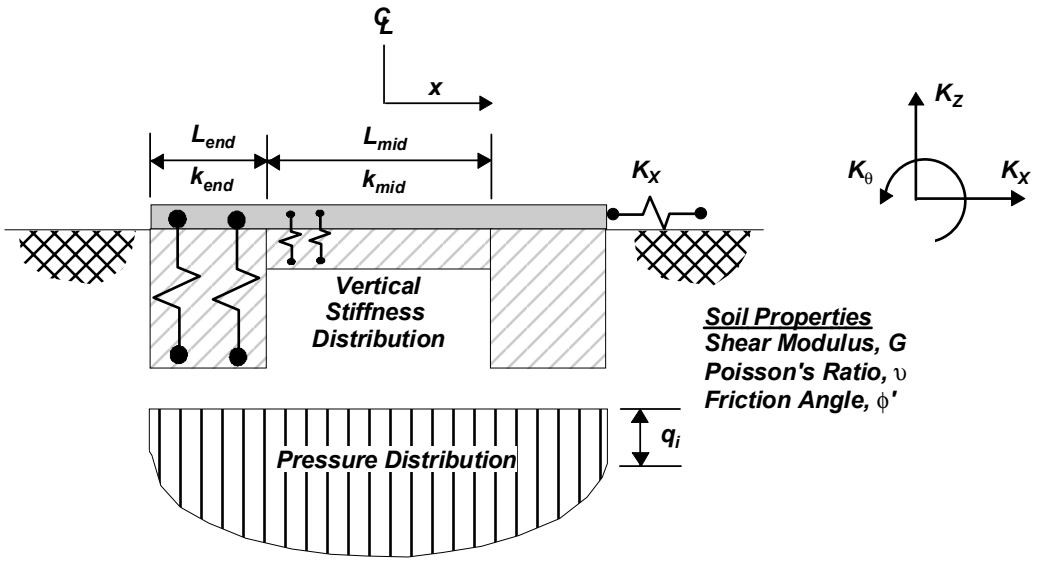

Fig. 4.7 Graphical representation BNWF model and associated study parameters

With regard to the moment capacity of the shallow foundation systems investigated, the BNWF model estimates, when the soil uncertainty in soil properties is considered, a comparable maximum absolute positive moment and maximum absolute negative moment for both static and dynamic cases; however, these targets are underestimated for FS_v greater than 12 in the dynamic case. The baseline (using the average value) seems to slightly underestimate the system moment capacity. Yan and Martin (1999) found similar results modeling the tests by Bartlett (1976), but using a hypoplasticity model in the framework of a half-space continuum on the FLAC platform.

Settlement is bound by approximately one-half to three times. Again, Martin (1999) also found that settlement was overestimated by approximately 1.3 to 5 times, using a hypoplasticity model and 2-D elements. Since the quantitative results compare reasonably well, an engineer could use these recommendations and find a solution which agrees fairly well with a more rigorous approach.

Maximum horizontal displacement is generally predicted within 0.1 (or smaller) to 1 times the model test observation, though considering the uncertainty of the soil properties produced values at approximately 1.6 times in some static cases and up to approximately 5 times in some dynamic cases.

The energy-dissipation capabilities of the BNWF simulations are apparent in the permanent settlements accrued, the permanent horizontal displacements, and in the nonlinear behavior of the moment-rotation plots. These three characteristics are important in design, with respect to the (reduced) loads transmitted to a superstructure and at a specific magnitude of permanent displacement. This global behavior is introduced into the system by the individual Winkler spring components, which have nonlinear, hysteretic properties.

4.4.1 Comparison of Bearing Capacity Reduction to Seismic Bearing Capacity

The mechanism controlling the bearing capacity of a shallow foundation resting on a frictional and cohesive material is generally accepted as some form of a failure surface that transfers frictional, cohesive, and normal forces to the adjacent soil. One possible reduction in the bearing capacity of the footing, in terms of this failure surface, is due to eccentricity of the loading. Given some rotation and uplift to the footing, the bearing area is reduced and therefore the failure surface is reduced, such that the ultimate bearing capacity is reduced for that specific amount of uplift. The BNWF model should capture this behavior naturally, as load is redistributed away from springs which have "gapped" in uplift and therefore provide no reaction.

Recent analytical solutions propose various methods that account for a footing's reduced vertical bearing capacity due to seismic vertical and lateral accelerations. From a mechanistic viewpoint, horizontal and vertical accelerations place additional demands on the failure plane below the footing, thereby reducing the capacity reserved for purely vertical loads, as shown in Figure 4.8. Recall that for both the static and dynamic BNWF simulations, in some cases it was necessary to introduce a bearing capacity factor, *FQ,* in order to allow a better agreement with the experimental results with respect to maximum moment and settlement. In cases with large vertical factors of safety, the bearing capacity from vertical push tests was too large for the model to behave plastically.

Because the Winkler model represents the vertical bearing capacity calculated by failure plane theory (i.e., Terzaghi 1943), it is plausible to make a comparison between the bearing factor *FQ* used in this study to "best fit" some cases to the seismic bearing capacity presented in resent papers. Two methods to estimate seismic bearing capacity are investigated; the methods of Paolucci and Pecker (1997) and Richards et al. (1993), briefly discussed herein.

4.4.1.1 Seismic Bearing Capacity (Richards, Elms, Budhu)

Richards, Elms, and Budhu (1993) propose a model based on Coulomb passive and active earth pressures. Prandtl first proposed the failure surface, shown in Figure 4.8, described by an active and passive soil region at the extreme sides of the foundation and a transition zone in between. An approximation to this surface is made using two smaller wedges which meet at a transition line. Using a Coulomb failure mechanism, which transfers shear force between the two wedges, seismic bearing capacity factors can be determined in terms of an earth pressure coefficient.

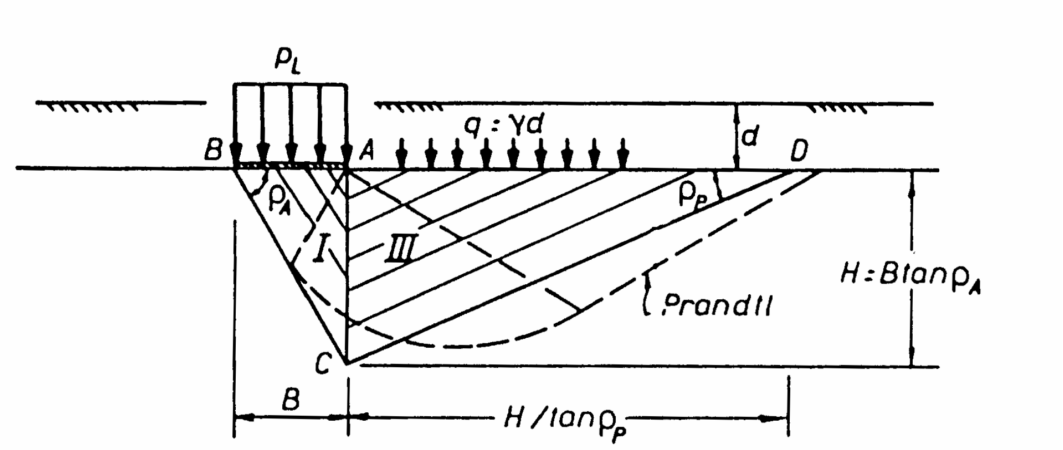

FIG. 2. Simplified Static Slip Field with Coulomb Wedges ($\delta \neq 0$)

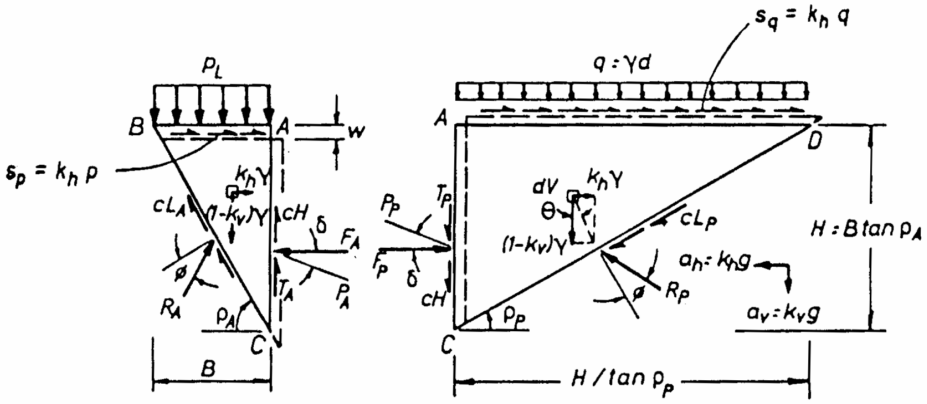

FIG. 3. Coulomb Mechanism (with Wall Friction, δ)

Fig. 4.8 Prandtl failure surface, with proposed simplification using Coulomb failure mechanism (after Richards et al. 1997)

The seismic bearing capacity is given by the following:

Seismic Bearing Capacity
$$q_E = cN_{cE} + \gamma dN_{qE} + \frac{1}{2}\gamma BN_{\gamma E} \tag{4.51}$$

Seismic Bearing Capacity Factor
$$N_{qE} = e^{\pi \tan\phi'} \tan^2\left(\frac{\pi}{4} + \frac{\phi'}{2}\right) = e^{\pi \tan\phi'} K_{pE} \tag{4.52}$$

$$N_{cE} = (N_{qE} - 1)\cot\phi' \tag{4.53}$$

$$N_{\gamma E} = 2(N_{qE} + 1)\tan\phi' \tag{4.54}$$

Seismic Passive Earth Pressure Coefficient
$$K_{PE} = \frac{\cos^2(\phi' - \theta)}{\cos\theta\cos(\delta + \theta)\left\{1 - \sqrt{\frac{\sin(\phi' + \delta)\sin(\phi' - \theta)}{\cos(\delta + \theta)}}\right\}} \tag{4.55}$$

where δ is taken as $\phi'/2, \theta = \tan^{-1}\left(k_h/(1 - k_v)\right)$, and k_h and k_v are the horizontal and vertical acceleration coefficients, respectively. For all analyses, k_v is assumed to be zero.

For the simulation data available, the ultimate bearing capacity is known, so the seismic bearing capacity is taken as the known bearing capacity times the ratio of the seismic bearing capacity for the given horizontal acceleration coefficient to the seismic bearing capacity for zero horizontal acceleration (maximum).

$$V_{seismic} = \frac{V_{calc}}{V_{calc(MAX)}} V_{\exp} \tag{4.56}$$

4.4.1.2 Seismic Bearing Capacity (Paolucci and Pecker)

Paolucci and Pecker (1997) propose a kinematic approach to reduce the known vertical bearing capacity based on a horizontal load applied, the horizontal load inclination and the load eccentricity. This is also based on the Prandtl type failure of a soil wedge beneath the foundation; useful formula are determined which match the kinematic approach.

Total Bearing Capacity Reduction
$$v = v_h v_i v_e \tag{4.57}$$

Bearing Capacity Reduction due to Horizontal Load
$$v_h = \left(1 - \frac{k_h}{0.85}\right)^3 \tag{4.58}$$

Bearing Capacity Reduction due to Load Inclination

for frictional soils:
$$v_i = \left(1 - \frac{k_h}{\tan\phi}\right)^{0.35} \tag{4.59}$$

or, for cohesive soils (Pecker, 1997):
$$v_i = \gamma k_h \frac{B}{c_u} \tag{4.60}$$

Bearing Capacity Reduction due to Load Eccentricity
$$v_e = \left(1 - \frac{2lk_h}{B}\right)^{1.8} \tag{4.61}$$

where k_h = pseudo-static seismic coefficient

Paolucci and Pecker (1997) find that good results are obtained if the effect of load eccentricity is neglected ($v_e = 1$), so only the effects of horizontal load and load inclination will be used in the simulations.

Figure 4.9 presents the comparison of the bearing capacity factor *FQ* used to best-fit static and dynamic model simulations to the seismic reductions after Richards et al. (1993) and Paolucci and Pecker (1997). The bearing reduction is taken as V_{calc} / $V_{calc(MAX)}$ for the method of Richards et al. (1993), and v for the method of Paolucci and Pecker (1997). The horizontal acceleration coefficient for these tests is calculated using the maximum horizontal force from the experimental test data.

From Figure 4.9, it is evident that the seismic bearing reduction after Richards et al. (1993) is an upper bound, and that the seismic bearing reduction after Paolucci and Pecker (1997) is a lower bound. For static tests in general, it appears that the bearing capacity reduction required in the simulations compares with the seismic bearing capacity reduction as follows: (a) for vertical factors of safety less than four, no reduction is required; (b) for $4 < FS_V \leq 12$ an average of the upper and lower bounds compares well; and (c) for $12 \leq FS_V$ the lower bound compares best. The tests that required no bearing capacity reduction were KRR01 FE S18, KRR03 CE S18, SSG03 E test 4, Bartlett test 3.4–12 and Weissing test 5.11. A general observation for modeling of static tests using a BNWF model is that a greater reduction in bearing capacity is required with larger factors of safety; generally an average of the upper and lower bounds of seismic bearing capacity reduction for FS_v less than 12, and an increasingly lower bound for higher factors of safety.

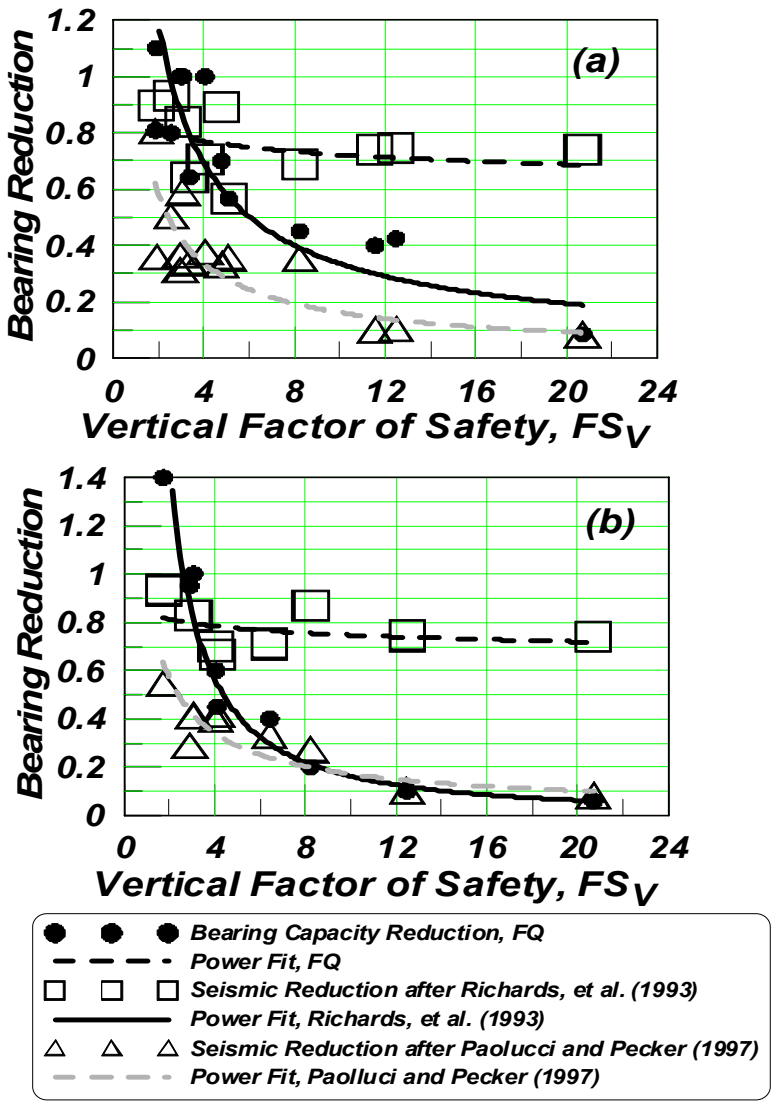

Fig. 4.9 Comparison of bearing capacity reduction *FQ* to seismic reduction for (a) static simulations and (b) dynamic simulations

For dynamic tests in general, it appears that the bearing capacity reduction required in the simulations compares with the seismic bearing capacity reduction as follows: (a) for vertical factors of safety less than four, no reduction is required; (b) for $4<FS_V<6$ an average of the upper and lower bounds compares well; and (c) for $6\leq FS_V$ the lower bound compares best. Therefore, a general observation for modeling of dynamic tests using a BNWF model is that a greater reduction in bearing capacity is required with larger factors of safety; generally an average of the upper and lower bound of seismic bearing capacity for FS_v less than six, and an increasingly lower bound for higher factors of safety.

The required seismic bearing capacity reductions, which were found to give the best results, appeared to vary with the vertical factor of safety, and are summarized in Tables 4.2–4.3.

Table 4.2 Bearing capacity reduction for static simulations

FS_v range	Bearing Capacity Reduction[1]
$FS_v \leq 4$	none ($FQ \sim 1$)
$4 < FS_v \leq 12$	average ($FQ \sim 0.4$ to 0.6)
$12 < FS_v$	maximum ($FQ \sim 0.1$ to 0.4)

Table 4.3 Bearing capacity reduction for dynamic simulations

FS_v range	Bearing Capacity Reduction[1]
$FS_v \leq 4$	none ($FQ \sim 1$)
$4 < FS_v \leq 6$	average ($FQ \sim 0.4$ to 0.7)
$6 < FS_v$	maximum ($FQ \sim 0.1$ to 0.4)

Note (1): indicates average, minimum, or maximum bearing capacity reduction according to the methods of Richards et al. (1993) and Paolucci and Pecker (1997).

4.4.2 Comparison of Stiffness and Sliding Factors

In order to get a best-fit solution for the model tests investigated, a factor *FK* in some cases was applied to the vertical subgrade stiffnesses *km* and *ke,* and / or a factor *Fu* was applied to the horizontal sliding coefficient μ. The values of these two factors are presented in Tables 3.6–3.7, for static and dynamic tests, respectively, and below in Figures 4.10 (a) and (b) versus vertical factor of safety. It can be seen that the required stiffness factor varied in general between a value of 2–0.25 for static and dynamic cases. The simulation was more sensitive to smaller changes in the sliding coefficient, which varied between 0.2–1.0 for static cases, and 0.75–1.4 for dynamic cases.

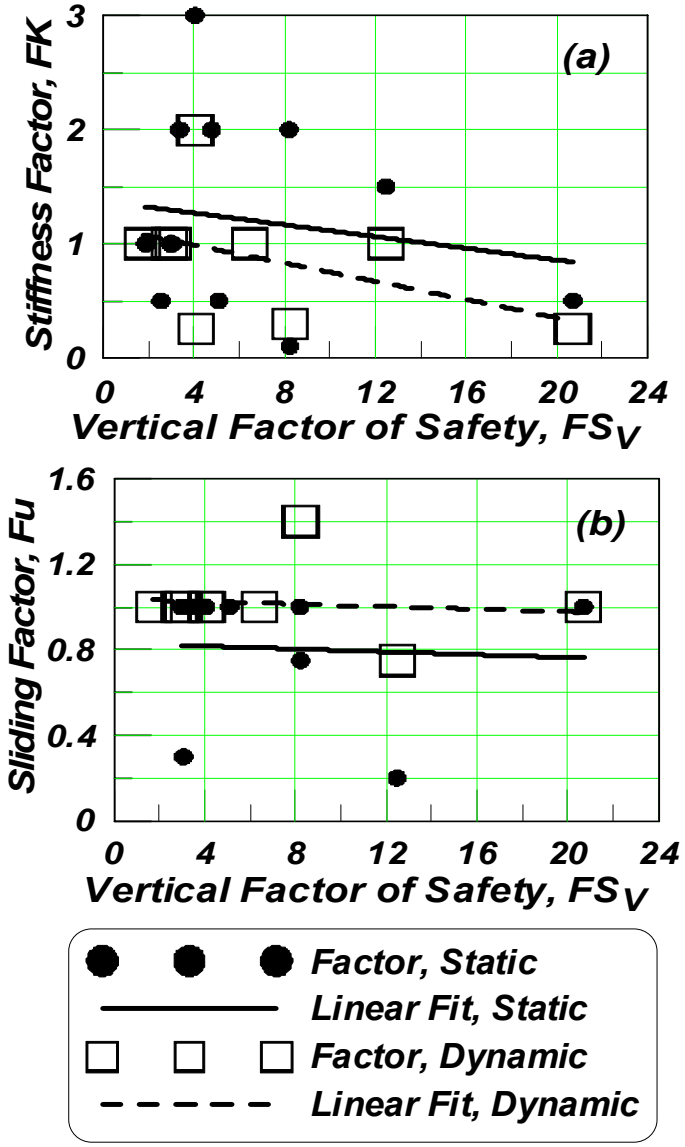

Fig. 4.10 Comparison of (a) stiffness factor *FK* and (b) sliding coefficient factor *Fu* vs. vertical factor of safety, required for best-fit solution

5 Investigation into the Effects of Uplift on Simplified Seismic Design Procedures

5.1 INTRODUCTION

It is well established that soil yielding beneath foundations can be an effective energy dissipation mechanism; however, this benefit may come with the expected costs of excessive transient and permanent deformations. To realistically account for the systems' performance, these consequences of permanent settlement and rotation must be reasonably estimated and accounted for. A practical example, where the propagation of the effects of a rocking foundation-superstructure becomes prominent is shown in Figure 5.1. The shearwall is typically stiffer than the frame and hence tends to attract load if the subgrade is stiff, while the more flexible frame may be damaged by large displacements due to a more compliant subgrade. Thus, selection of the foundation strength and stiffness is important to determine which structural component is the "weakest-link" in the load-path. Incorporating a bed of Winkler foundation springs below each of these footings and modeling the system, as a whole, would provide a reasonable account for the demands into both the frame and the shearwall. In recognition of this, present design guidelines such as ATC-40 (1996) and FEMA 356 (2000) recommend using such a Winkler-based model to represent the stiffness of the soil-structure interface, and provide methods to estimate stiffness of the individual vertical springs. Moreover, a nonlinear Winkler-based model can be used to more accurately conduct a performance-based design (PBD), through incorporation of the shallow foundation, as both the benefits and consequences of allowing the structure to rock can be reasonably represented. However, in design practice, more simplified procedures are often desired, without fully modeling some aspects of the system (such as the foundation).

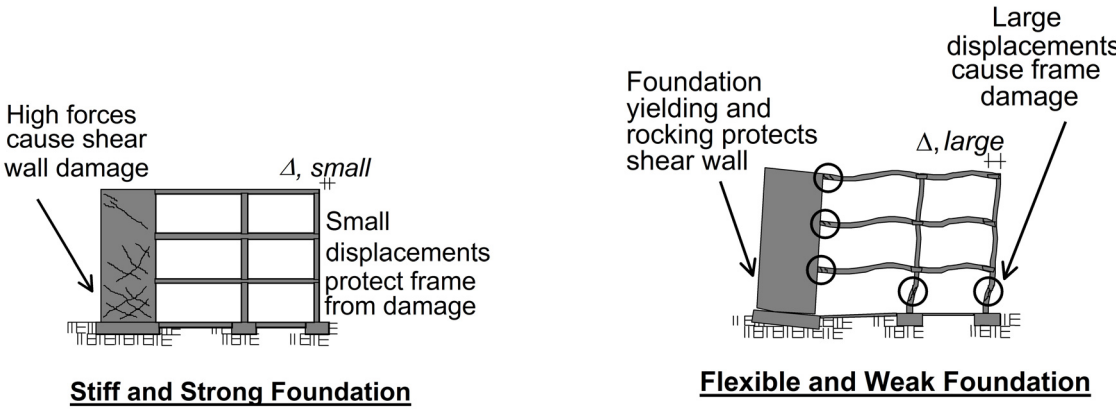

Fig. 5.1 Example components of a combined structural system, where compliance at the foundation level is allowed for (a) a stiff and strong foundation and (b) a soft and flexible foundation, below the rocking superstructure (Courtesy of ATC-40, 1996)

To evaluate the accuracy of simplified design procedures, in this report, simulation results considering foundation rotation and possible uplift are compared with current design methods used to account for the increase in displacement of an equivalent single-degree-of-freedom (SDOF) system when reduced design strength is provided. The basis for the approach is the estimation of a displacement amplification factor C_1, for a system with a prescribed design strength ratio R (C_1-R estimations).

5.2 SEISMIC DISPLACEMENT DEMAND ESTIMATION METHODS

There are a variety of approaches suggested in design codes for estimating seismic displacement demands. Design documents such as FEMA 356 (2000), ATC-40 (1996), and UBC-97 (ICBO 1997) suggest procedures ranging from simple elastic static analyses to nonlinear dynamic analyses. Four analysis methods suggested in current codes for the design or rehabilitation of a building include the linear static procedure (LSP), the capacity spectrum approach (CSA), the nonlinear static procedure (NSP), and the nonlinear dynamic procedure (NDP) (after FEMA 356, 2000). Linear refers to a linear elastic system, and nonlinear refers to systems, which behave nonlinearly or exhibit inelastic response. A static procedure considers response (loads and displacements) from an applied set of monotonic loads or a target floor displacement. A

dynamic procedure may be either linear or nonlinear and includes a full time-history analysis of a representative analytical model considering earthquake motion input.

To apply the nonlinear static procedure, a target displacement at each floor, δ_t, may be calculated:

$$\delta_t = C_0 C_1 C_2 C_3 SA \frac{T_e^{\,2}}{4\pi^2} g \tag{5.1}$$

where:

C_0 = Modification factor to relate spectral displacement of an equivalent SDOF system to the roof displacement of the building MDOF system

C_1 = Modification factor to relate expected maximum inelastic displacements to displacements calculated for linear elastic response

= 1.0 for $T_e \geq T_S$

= $[1.0 + (R-1)T_S / T_e] / R$ for $T_e < T_S$

= 1.5 maximum

T_e = Effective fundamental period of the building

T_S = Characteristic period of the response spectrum

R = Ratio of elastic strength demand to calculated yield strength

C_2 = Modification factor to represent the effects of pinched hysteresis shape, stiffness degradation, and strength deterioration on maximum displacement response (equal to 1 for linear procedure)

C_3 = Modification factor to represent increased displacements due to dynamic $P-\Delta$ effects

SA = Response Spectrum acceleration at the fundamental period and damping ratio of the building

The target displacement at each floor is then used to calculate the resulting forces in the component members, and acceptance or rejection of the design or retrofit results based on the acceptance criteria of the component as a function of the designated target building performance level.

5.2.1 Previous Investigations into Code Prescriptions

There have been a number of investigations evaluating the applicability of simplified-spectral-based design procedures, specifically force reduction-displacement ductility (R-μ_Δ) relation methods. Such works have involved considering the response of systems to pulse-type excitations [Veletsos and Newmark (1960); Veletsos and Newmark (1964); and Cuesta and Aschheim (2000, 2001a–c)], elasto-plastic systems [Newmark and Hall (1973, 1982); Veletsos et

al. (1965); Veletsos (1969); Veletsos and Vann (1971); and Lai and Biggs (1980)], degrading systems [Riddell and Newmark (1979); Al-Sulaimani and Roessett (1984); Riddell et al. (1989); and Vidic et al. (1994)], and softening systems (Hidalgo and Arias 1990), and other important structural behavioral facets deemed to potentially affect the accuracy of these estimations. These studies have improved upon such factors, providing semi-empirically derived values to support increased accuracy [Elghadamsi and Mohraz (1987); Peng et al. (1988); Takada et al. (1988); Nassar and Krawinkler (1991); Miranda (1993); Riddel (1995); Ordaz and Perez-Rocha (1998) and Chopra and Goel (1999)]. To refine the accuracy of the analysis, the force reduction may be presented as a function of ductility, damping, stiffness characteristics, natural and characteristic period and/or site soil-profile type. Miranda and Bertero (1994) provide a review of the evolution of the strength reduction factor R from Newmark and Hall (1973) to the publication date. More recent studies include work by Cuesta et al. (2003), who investigate the relationship between R as a function of μ_Δ and the ratio T/T_S, where μ_Δ is the displacement ductility demand of the system, T is the natural period of the system and T_S is the characteristic ground motion period. Cuesta et al. (2003) found that both the FEMA and ATC methods were appropriate for models with significant stiffness degradation. Fajfar (2000) describes the N2-method, where expected inelastic displacements of an equivalent SDOF system are calculated using inelastic spectra as a function of ductility. The method presented in this study is fundamentally different than the N2 capacity spectrum method as described in Fajfar (2000) in that elastic spectra are used to estimate inelastic displacements as a function of both R and the relative periods of the SDOF and the demand spectrum, similar to current code recommendations, and additionally attempt to include the effect of soil-structure interaction.

Relative to rocking-spectrum analyses, Makris and Konstantinidis (2002) find that rocking structures should not be replaced with SDOF simplifications because of the nonlinear response of the soil-structure interaction and its sensitivity to the input demand. However, the study presented in this report attempts to incorporate the sensitivity of the Winkler model to the characteristics of the input ground motion through (a) the relative magnitude of the soil-structure systems' natural period to the ground motion characteristic period and (b) the relative magnitude of the spectral acceleration of the elastic rocking system to the elastic rocking system with uplift allowed. Therefore, the coupling of demand and response observed by Makris and Konstantinidis (2002), which is lacking in current simplified design approaches and the basis of the argument to abandon simplified methods, is accounted for here.

5.3 SCOPE OF THIS STUDY

The approach in current design codes allows one to compromise between strength and ductility while still attempting to control performance targets, through a displacement-based design procedure. An accurate assessment of these strength and displacement values when evaluating a building for rehabilitation becomes increasingly important due to cost-performance trade-offs. Often the advantage of allowing energy dissipation through the foundation system is of great interest in these situations. However, if a simplified analysis procedure is to be performed, an evaluation of the accuracy of these procedures is warranted. Therefore, in this report a suite of nonlinear dynamic analyses are performed using a Winkler model with a simple lumped mass attached, considering two foundation conditions: (1) elastic springs (rocking system) and (2) elastic springs allowed to uplift (rocking-uplifting system). Nonlinearity in the analysis is introduced through possible uplift for case two. Results from these analyses are compared with design code relations for the strength (R) factors and displacement (C_1) factors to be used in a simplified analysis method. All analyses are performed in the OpenSees (Open System for Earthquake Engineering Simulation) platform, developed by the Pacific Earthquake Engineering Research Center (PEER) at the University of California, Berkeley.

5.3.1 Consistent Definitions C_1-R

Consistent definitions for the quantities C_1 and R must be adopted in the context of the rocking structural system to allow proper comparison with design approaches. In its most basic definition, the R factor is the ratio of elastic demand to the specified yield force in the nonlinear system:

$$R = \frac{SAmg}{H_y} \tag{5.2}$$

where:

SA	=	Response spectrum acceleration at the fundamental period and damping ratio of the building
m	=	Seismic mass
g	=	Acceleration due to gravity
H_y	=	Lateral yield strength

In this work, the yield force for the analysis of structures supported on rocking-uplift foundations (case 2) is defined as the force applied at the top of the superstructure, which just causes separation of the soil-foundation interface, or uplift. The conventional definition of H_y is the intersection between the pre-yield and post-yield stiffness of the pushover analysis, commonly calculated by an equivalent-area bilinear response. This definition can be applied in the current analysis, where the pre-yield and post-yield stiffnesses are defined at the onset of uplift.

For this study, a range of R factors is prescribed and, considering the elastic state of stress, a corresponding vertical factor of safety FS_q against bearing capacity mobilization can be calculated (e.g., Allotey and Naggar 2003). This will define the limits of validity for the current study, such that the soil structure interaction will behave elastically even while uplift may occur. Consider the vertical factor of safety *FSv*, under a purely vertical load. As a footing rotates, the bearing capacity at an extreme end will increase. A variable FS_q can be defined as the ultimate bearing capacity divided by the maximum bearing pressure beneath the footing (at an extreme end). Note that under a purely vertical load, FS_q is equal to FS_V, but FS_q decreases as lateral load is delivered to a system and the footing rotates. This relationship is described graphically in Figure 5.2, and defines the limits of validity of the current study. For a lateral force "*R*" times the yield force H_y (force required to cause incipient uplift), the subgrade will remain elastic for footings with a sufficient FS_V such that the curve does not fall below FS_q=1.0. Note that typical "*R*" values fall in the range of FS_V found in conventional design practice, which is approximately FS_V = 3-4.

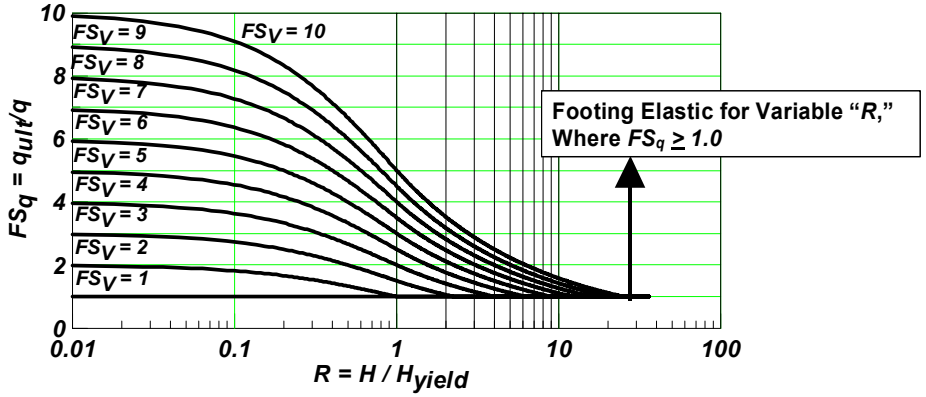

Fig. 5.2 Parameter range for an assumption of a foundation remaining in the elastic range

The second quantity under investigation is C_1, the ratio of displacement demand on an elastic system to the displacement demand on the nonlinear system. C_1 is commonly defined as a function of the natural period of the structure. The analysis presented is an attempt to verify the current code C_1-R functions for a range of periods.

From a numerical standpoint, a robust approach to the problem is to define structures that have an exact R over a range of periods, which are subject to a large collection of earthquakes. The structures defined for this task will be simple in nature; a lumped mass supported by an elastic column and connected to an elastic foundation on an elastic Winkler subgrade. The definition of R over a range of periods and for this simple system must be consistently defined.

Settlement of an elastic foundation of length L, superstructure weight W, and global soil vertical stiffness K_Z may be determined as:

$$s = \frac{W}{K_Z} \tag{5.3}$$

Since in this study the yield point of the system is defined as the point of uplift, this state must be well defined. Psycharis (1981, 1983) gives the critical rotation at incipient uplift, shown in Figure 5.3:

$$\tan(\theta_{cr}) = \frac{2s}{L} \tag{5.4}$$

This assumes the structure above is stable with respect to overturning. Thus, the soil springs are stiff enough to prevent instability due to overturning.

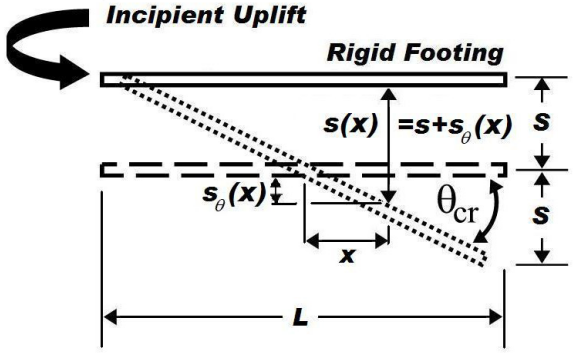

Fig. 5.3 Notation to define critical rotation for an elastic subgrade modulus

The critical moment applied to the base that would just cause uplift, M_{cr}, is found by summing the moments about the center of the footing. The (uniform) vertical displacement at

any point is *s*, and the additional contribution to this value due to rotation is labeled $s_\theta(x)$. Since force is a function of displacement via the vertical stiffness of the system, the critical moment is found by integrating the displacements as a function of distance from the center of the footing, multiplied by stiffness per unit length of footing.

$$M_{cr} = \int_{-L/2}^{L/2} \left(s + s_\theta(x)\right) \frac{K_Z}{L} x dx \tag{5.5}$$

The critical moment can then be simplified to the "kern" assumption:

$$M_{cr} = \frac{K_Z}{12} L^2 \tan(\theta_{cr}) = \frac{WL}{6} \tag{5.6}$$

For these analyses, the beam-column stiffness is taken as sufficiently large, as envisioned for a stiff shear wall. It is therefore reasonable to neglect any contribution of the shear wall to the horizontal displacement of the system, since the variable of interest is foundation rocking and uplift. The assumption of a rigid beam (foundation) and column (shearwall) in the following derivations is accurate to within approximately 0.1% error for even the highest bound of soil stiffnesses given a concrete shear wall as the dominant superstructure element. However, to avoid any contribution of superstructure flexibility to the flexibility of the entire system in general applications, the "beam" element should be sufficiently stiff such that Eb*Ib/(Es*Is) $\geq$ 50 and the "column" element should be sufficiently stiff such that Ec*Ic/(Es*Is) $\geq$ 100, where E and I are elastic modulus and moment of inertia for the beam (subscript "b"), column (subscript "c"), and subgrade (subscript "s").

Continuing with the rigid beam-column assumption, knowing M_{cr} and θ_{cr} at uplift, the two final factors needed to solve for a set of lumped mass models with identical subgrade reactions, which will give a constant line of R for a range of periods, is the magnitude of the lumped mass and the distance "a" from the foundation to the lumped mass (i.e., the lever arm). Solving for H_y from Equation 5.2 and substituting M_{cr} gives the moment arm or effective height "*h*" to the center of mass at the top of the structure:

$$h = \frac{RL}{6SA} \tag{5.7}$$

Given the range of periods through which the line of constant R will sweep, and the range of *h*'s previously defined, a range of lumped masses can be calculated. The elastic period of the structure can be defined using the horizontal stiffness of the system:

$$K_L = \frac{H_y}{\Delta_{top}} = \frac{M_{cr}}{h\Delta_{top}} \tag{5.8}$$

Substituting (a) the lateral stiffness and (b) the displacement of the top of the structure as a function of rotation into (c) the definition of the natural period a structure and solving for mass gives:

$$m = \frac{K_Z}{48}\left(\frac{LT}{h\pi}\right)^2 \tag{5.9}$$

Since the natural period is a function of mass and stiffness, and the R-value is a function of SA and the effective height "*h*"; then for a given R-value with a fixed subgrade modulus and foundation aspect ratio, but over a range of natural periods and further a group of earthquakes, each point on a graph of C_1 versus T will have a different mass and "*h*."

The rocking foundation has several components of displacement that contribute to the overall horizontal displacement of the center of mass. The total horizontal displacement of the system is the sum of foundation rotation and column flexibility.

5.3.2 Ground Motions Selected

A suite of ground motions was chosen to represent a wide range of earthquake characteristics for use as input to the model. In this work, the simulations use the longitudinal components of the 19 unscaled time histories described by Somerville and Collins (2002). Table 5.1 lists the characteristics of interest for the longitudinal directions of the ground motions. These ground motions represent a broad range of peak ground accelerations (PGA), peak ground velocities (PGV) and peak ground displacements (PGD) levels. PGA levels range from 0.13 to 0.75 g's, PGV ranges from 9.1 to 84.8 cm/s, and PGD ranges from 1.2 to 18.7 cm.

The characteristic period T_S in this work is defined as the intersection of the constant acceleration and constant velocity region of the time history (Newmark and Hall 1987). To calculate T_S for each motion, a mean fit through the values of pseudo-acceleration, pseudo-velocity and pseudo-displacement was performed. The range of characteristic periods for these motions is T_S = 0.26 to 0.88 seconds.

Figure 5.4 (a) and (b) shows the mean (μ) and mean ± standard deviation (σ) for all 19 ground motions (longitudinal component) of the spectral acceleration and spectral displacement

versus period, respectively. As evident in the $\mu \pm \sigma$ plots, the suite of motions selected have broad spectral characteristics. Figures 5.4 (c) and (d) shows the mean (μ) and mean ± standard deviation, normalized by the mean, for all 19 ground motions (longitudinal component) of the spectral acceleration and spectral displacement versus period, respectively. These plots further substantiate the broad spectral characteristics of the motions selected.

Table 5.1 Ground motions used in this study (longitudinal component)

EQ Note	Station	Name	Dist[5] (km)	PGA (g)	PGV (cm/s)	PGD (cm)	T_S (sec)
1	Palm Springs Airport	NPS_plma	9.6	0.204	12.1	2.4	0.26
2	Canoga Park, Topanga Canyon Blvd	NR_cnpk	17.7	0.331	31.6	12.6	0.35
2	Encino, Ventura Blvd #1	NR_env1	17.7	0.503	56.6	16.0	0.45
2	Encino, Ventura Blvd #9	NR_env9	17.9	0.247	31.3	8.1	0.48
2	North Hollywood, Lankershim Blvd #1	NR_nhl2	18.4	0.185	27.6	5.5	0.49
2	Arleta, Nordhoff Fire Station	NR_nord	9.4	0.344	40.6	14.6	0.64
2	Northridge, Roscoe #1	NR_nrr1	13.7	0.390	37.4	15.8	0.56
2	Sun Valley, 13248 Roscoe Blvd	NR_rosc	10.8	0.444	38.2	10.0	0.88
2	Sepulveda VA Hospital	NR_spva	9.2	0.753	84.8	18.7	0.58
2	Van Nuys, Sherman Way #1	NR_vns1	12.8	0.375	37.7	9.2	0.68
2	Van Nuys, Sherman Circle #1	NR_vnsc	12.8	0.474	31.4	7.6	0.52
2	Van Nuys -- 7-story hotel	NR_vnuy	11.3	0.469	54.4	11.3	0.42
2	Woodland Hills, Oxnard Street #4	NR_whox	20	0.318	41.8	12.3	0.39
3	Los Angeles, 14724 Ventura Blvd	SF_253	16.3	0.203	21.5	12.3	0.34
3	Los Angeles, 15910 Ventura Blvd	SF_461	16.2	0.151	17.2	8.4	0.76
3	Los Angeles, 15250 Ventura Blvd	SF_466	16.4	0.164	24.1	11.5	0.48
3	Glendale, Muni Bldg, 633 E Broadway	SF_glen	18.8	0.227	32.0	10.0	0.83
3	Van Nuys -- 7-story hotel	SF_vnuy	9.5	0.134	23.3	14.9	0.87
4	Caltech, Braun Athletic Building	WH_athl	16.6	0.149	9.1	1.2	0.41

Notes:

(1) Earthquake Location and Date 1: North Palm Springs, July 8, 1986
(2) Earthquake Location and Date 2: Northridge, January 17, 1994
(3) Earthquake Location and Date 3: San Fernando, February 9, 1971
(4) Earthquake Location and Date 4: Whittier Narrows, October 1, 1987
(5) Distance is defined as the closest surface distance from the fault rupture to the ground motion recording station.

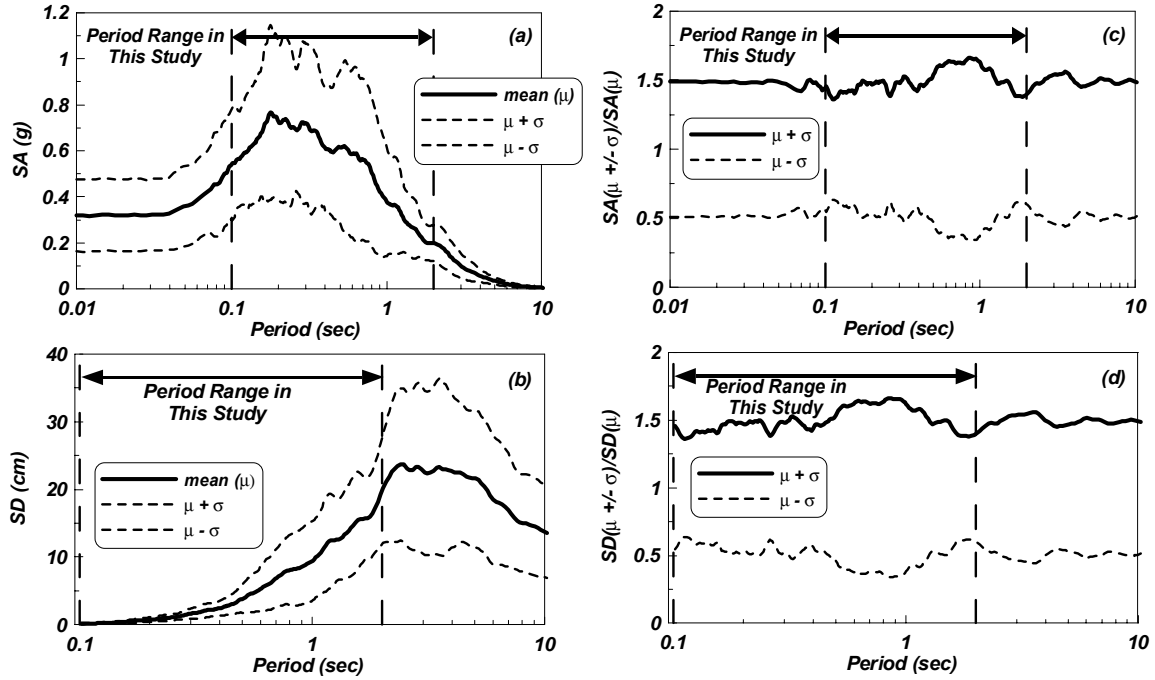

Fig. 5.4 Mean (μ) ± standard deviation (σ) of (a) spectral acceleration (*SA*) vs. period and (b) spectral displacement (*SD*) vs. period for the longitudinal component of the ground motions considered in this study. Also shown are the mean (μ) ± standard deviation (σ) normalized by the mean for (c) spectral acceleration (*SA*) vs. period and (d) spectral displacement (*SD*) vs. period for the longitudinal component of the ground motions considered in this study.

5.4 ANALYSIS RESULTS AND DISCUSSION

Numerical models were constructed considering a range of natural periods (T = 0.1 to 2.0 seconds, at increments of ΔT = 0.2 s) and a range of design R-values (R = 1.5, 2.0, 4.0 and 8.0). Each of these models was subjected to the ground motions listed in Table 5.1. Simulation results for these cases are presented in Figure 5.5, for the condition of R = 4.0. Figure 5.5 shows C_1 values versus normalized period T/T_S, where T_s is the characteristic period noted in Table 5.1. The displacement ratio C_1 in this study is defined as:

$$C_1 = \frac{\Delta_{nonlinear}}{\Delta_{elastic}} \tag{5.10}$$

where $\Delta_{nonlinear}$ is that calculated for the system allowed to uplift, while $\Delta_{elastic}$ results from the system where uplift is not allowed. For comparison, the FEMA 356 recommended value for C_1, as well as a mean fit to the data is shown. ATC-40 suggests a limit of $C_1 = 2.0$ at $T < 0.1$ seconds, whereas FEMA 356 suggests a limit of $C_1 = 1.5$ with the intersection of the curve defined in Equation 5.1. The nonlinear regression to the data is taken as the mean ($C_{1\text{-}ave}$) for $T/T_S < 0.5$, and where $T/T_S \geq 0.5$:

$$C_1 = \frac{1}{1 + Ae^{-B(\frac{T}{T_S} - 0.5)}} \tag{5.11}$$

In order to best fit the data and meet the average value at $T/T_S = 0.5$, $A = \frac{1}{C_{1-ave}} - 1$ and B is varied such that the correlation coefficient between the fit curve and the data points is a maximum.

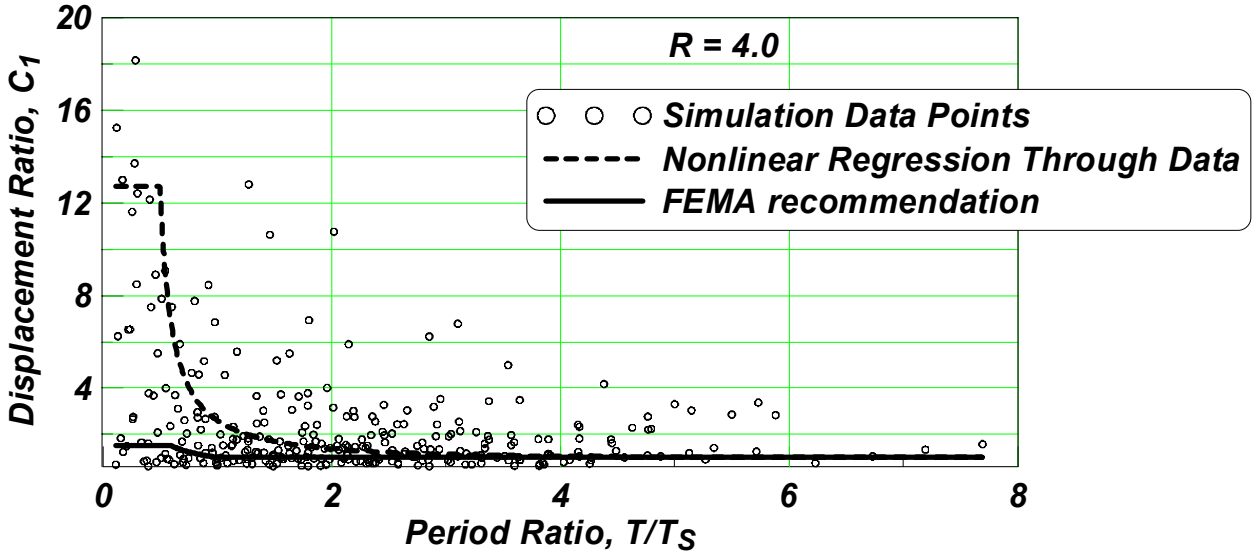

Fig. 5.5 C_1 vs. normalized period for R equal to 4.0 (six data points above $C_1 = 20$)

Figure 5.5 illustrates a large range for the calculated values of C_1 for $R = 4.0$, though a discernible trend is evident. At small period ratios, approximately less than 1.0, C_1 is very large. At larger values, C_1 converges to unity as recognized in design codes. This is consistent with the long period equal displacement principle. Results for other simulations indicate that at smaller R-values ($R = 1.5$), current code recommendations result in a conservative estimate of C_1 for most short period cases ($T/T_S \leq 1.0$). However, as R is increased ($R = 2.0$, 4.0 or 8.0), the recommendations suggested in current code documentation tend to be highly unconservative,

indicating rocking induced transient displacement contributions may be very large. Overall, the results indicate that the current displacement coefficient method (based on recommendations for C_1-R relations) may be unreasonable for estimating rocking induced displacements. An inspection of the data may help assist in alternative forms of C_1-R relations for estimating these inelastic displacement contributions.

Although binning the data by basic ground motion characteristics such as PGA or PGV does not reveal any consistent trends between varying values of R, the data appear to be sensitive to the ratio of the spectral accelerations determined at the periods of the nonlinear and elastic systems, termed $SA_{nonlinear}$ and $SA_{elastic}$, respectively. The term "nonlinear" is used to differentiate the elastic foundation allowed to uplift from the elastic system not allowed to uplift. From the viewpoint of a "pushover" analysis, the load versus displacement curve of the elastic system not allowed to uplift is a straight line, while the elastic system allowed to uplift is linear until uplift is reached, after which the stiffness degrades (note that no hysteresis will be observed with repeated loading since the Winkler springs are elastic). The spectral acceleration for each "elastic" and "nonlinear" system with a defined period T is defined as the peak horizontal acceleration from an input ground motion. A normalizing parameter is defined as a function of these two variables; $\psi_{SA} = SA_{nonlinear} / SA_{elastic}$. The data are binned into three groups of equal number of samples, where the first group all have values of $\psi_{SA} <$ X1, the second group X1 $\leq \psi_{SA} <$ X2, and the third group $\psi_{SA} \geq$ X2. The values of X1 and X2, as well as the maximum and minimum values of ψ_{SA}, for all R cases are listed in Table 5.2.

Table 5.2 Binning results

R	X1	X2	Max ψ_{SA}	Min ψ_{SA}
1.5	0.947	1.000	1.651	0.854
2.0	0.881	0.995	1.556	0.619
4.0	0.679	0.874	1.171	0.417
8.0	0.518	0.760	1.150	0.275

Table 5.3 lists the calculated parameters A and B resulting in the highest correlation coefficient for Equation 5.11, for each value of R and each bin of ψ_{SA}.

Table 5.3 Regression coefficients for Equation 5.11

R	Group	A	B
1.5	I, $\psi_{SA} <$ X1	-0.013	0.01
1.5	II, X1 $\leq \psi_{SA} <$ X2	-0.087	3.89
1.5	III, $\psi_{SA} \geq$ X2	-0.479	0.52
2.0	I, $\psi_{SA} <$ X1	0.051	0.45
2.0	II, X1 $\leq \psi_{SA} <$ X2	-0.259	3.05
2.0	III, $\psi_{SA} \geq$ X2	-0.888	0.56
4.0	I, $\psi_{SA} <$ X1	-0.503	0.01
4.0	II, X1 $\leq \psi_{SA} <$ X2	-0.881	0.12
4.0	III, $\psi_{SA} \geq$ X2	-0.967	0.07
8.0	I, $\psi_{SA} <$ X1	-0.930	0.07
8.0	II, X1 $\leq \psi_{SA} <$ X2	-0.984	0.02
8.0	III, $\psi_{SA} \geq$ X2	-0.971	0.10

Figure 5.6 shows the results of C_1 versus normalized period in binned form with simulation data points for R = 4.0. The recommended curve, as discussed in this report is overlain on the data, as well as a logistic curve similar to the recommended curve but with a regressed function of the form $y = a/\left(1 + be^{-cx}\right)$, where *a*, *b* and *c* are regressed coefficients. The former applies a limit on C1, termed "regression through data (per Equation 5.11)." The later applies no limit in the short period ratio range, termed "Regression Through Data." The recommended curve is typically conservative with respect to the logistic curve for longer period structures. However, the recommended curve provides a more realistic design displacement for shorter period structures ($T/T_S < 0.5$) since only the mean value of C_1 is considered in this range, where the logistic data fit would prescribe an excessively conservative design.

Using the regression analysis presented in Equation 5.11 in conjunction with Tables 5.2 and 5.3 allows one to estimate the lateral design displacement of a rocking-dominated system using a design spectrum approach. Consider for example, a system with a natural period equal to 2.0 seconds and a design ground motion with a characteristic period of 0.4 seconds. First, from the intersection of the model pushover and the design spectrum, say the SA of a nonlinear system is estimated as 0.5 g (for example). Using either a similar analytical model *not* allowed to uplift, or with a lateral stiffness defined by one rotational spring in place of the Winkler model (an

alternative approach suggested in code), an intersection with the design spectrum gives 0.6 g. Therefore, $\psi_{SA} = SA_{nonlinear} / SA_{elastic}$ = 0.5/0.6 = 0.83. Given a target design R value of 4.0, X1 = 0.68 and X2 = 0.87 from Table 5.2. From Table 5.3, the system falls into group II under R = 4.0 because X1 $\leq \psi_{SA} <$ X2, therefore A = -0.881 and B = 0.12. Finally, from Equation 5.11, $C_1 = 1/[1\text{-}0.881e^{-0.12*((2/0.4)-0.5)}] = 2.06$.

In summary, for the range of *R* values studied it appears that at low period ratios and for large values of ψ_{SA}, where the spectral acceleration of the nonlinear system is greater than the spectral acceleration of the linear system, large displacement ratios can result. FEMA 356 uses a limit of C_1 = 1.5 and ATC-40 gives a limit of C_1 = 2.0; much larger displacements are found in this study for the uplifting system for *R* values greater than 1.5, suggesting the current codes may be unconservative for the case of a shallow foundation allowed to uplift.

5.5 ILLUSTRATIVE DESIGN EXAMPLE

An illustrative design example using recommended simplified design procedures is explored, using the suggestions from the calculated C_1-R relations for a rocking shallow foundation allowed to uplift. Additionally, rocking induced lateral displacements and the level of damping are used to estimate accrued settlements based on empirical damping versus distortion comparisons.

The design example foundation structure is modeled as a beam-on-nonlinear-Winkler-foundation, using nonlinear q-z springs based on the formulation presented in Boulanger et al. (1999). Salient Winkler spring system parameters are based on the conclusions stated in Chapter 4 of this report, and graphically shown in Figure 4.7. Recommendations for Winkler spring system modeling were based on evaluation against results from centrifuge testing at UC Davis [Gajan et al. (2004a,b) and Rosebrook and Kutter (2003a,b,c)] and other 1-g test data [Bartlett (1976); Negro et al. (1998); and Weissing (1979)]. The Winkler elements degrade in stiffness prior to reaching ultimate capacity. A parabolic shaped bearing capacity beneath the foundation is recommended to account for the experimentally observed stress distribution. Finally, the study recommends a specific region at the ends of the foundation receive a larger stiffness to account for observed stiffening due to densification of the soil medium associated with rotation of the foundation. Such an approach is similar to procedures outlined in ATC-40 (1996).

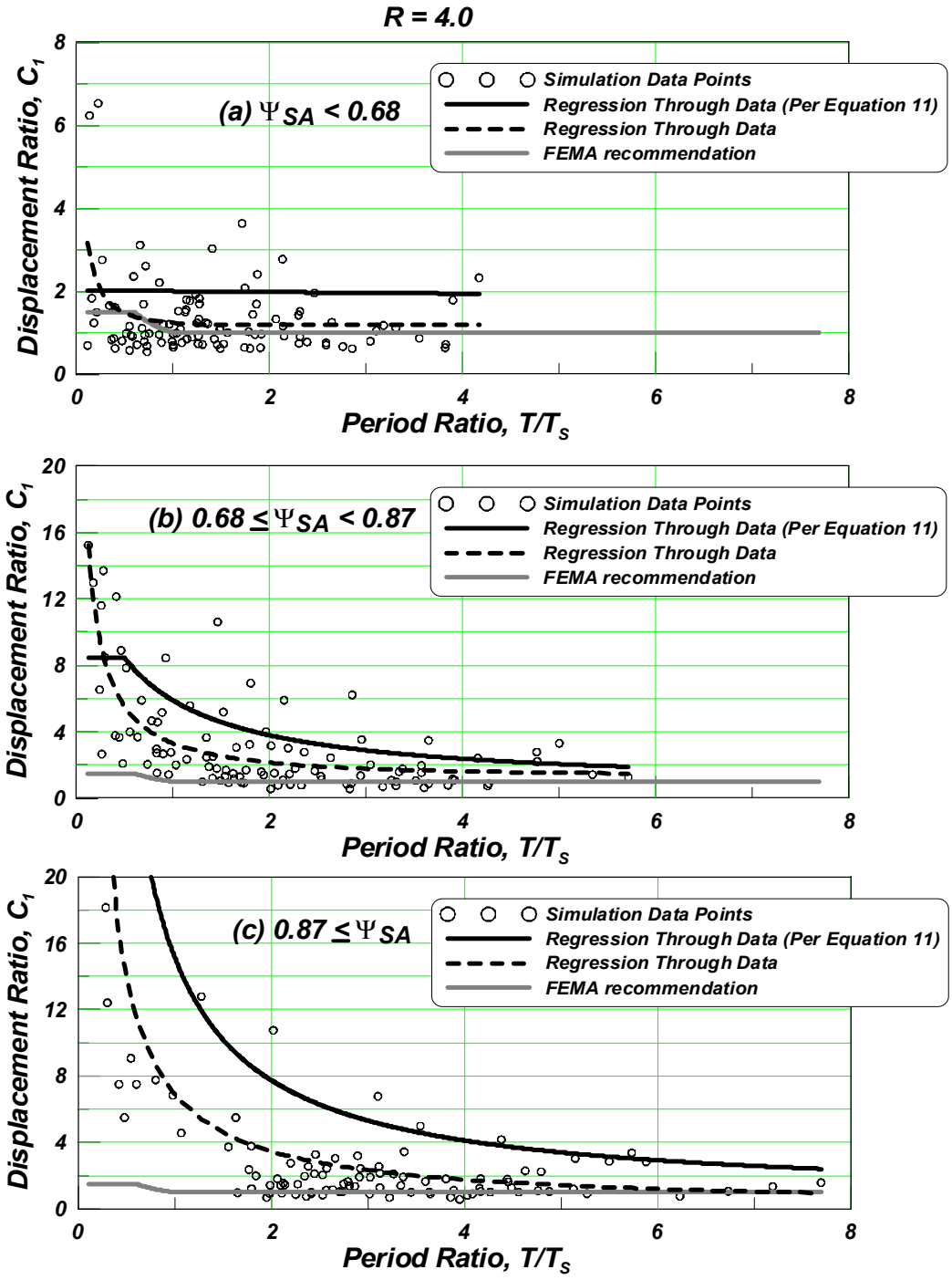

Fig. 5.6 Binned data - C_1 vs. normalized period for R equal to 4.0. Note, 6 data points (6% of binned subset) of outliers with C_1 greater than 20 not shown for (c). The curve "regression through data (per Equation 5.11)" is recommended and defined in conjunction with Tables 5.2 and 5.3.

For this design example, structure aspect ratios of foundation length L to width B of 3.2 (=L/B) and shear wall height H to wall length L_w of 3.0 (= H/L_w) are selected. The geometric configuration shown in Figure 5.7 is selected to result in these aspect ratios, where a 5-story shear wall of dimensions 5 m long by 15 m high is supported on a strip foundation of 8 m by 2.5 m. The design vertical factor of safety, FS_V, for this footing is selected as 4.0. A BNWF model is created to model this elastic shear wall resting on a nonlinear soil, such that only the influence of soil compliance (both uplift and soil nonlinearity) is considered.

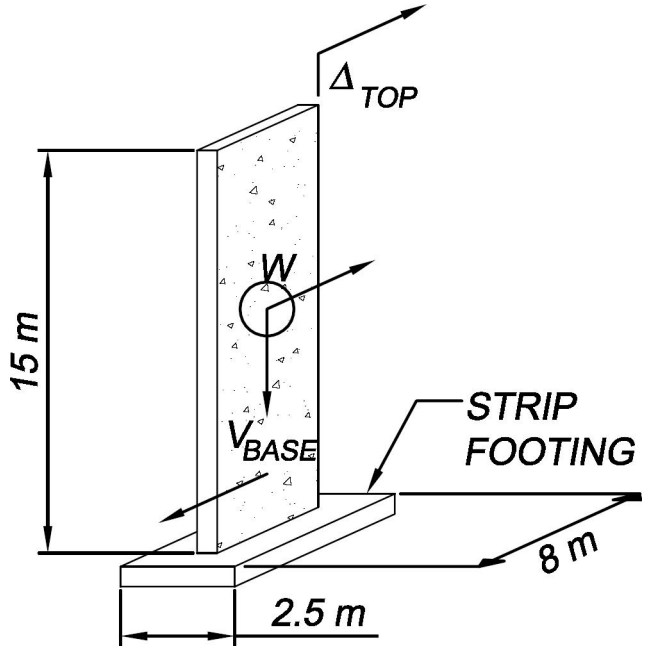

Fig. 5.7 Dimensions of 5-story shear wall – shallow foundation system selected for design example

The soil medium is assumed to be sand at 90% relative compaction, which corresponds to a relative density of 75% (after Lee and Singh, 1971) and $\phi' = 33^o$. The soil properties, structural dimensions and loading used for input into the model are provided in Table 5.4. Assuming the shear wall supports a tributary area of approximately 50 m^2, with a distributed dead and live load of 100 kN (DL = LL = 50 kN) per floor (total DL + LL = 5*100kN = 500 kN), in addition to the self weight of the wall and footing equal to 900 kN, the total vertical load is equal to 1400 kN, or approximately 3% of the compressive strength of the concrete wall.

Table 5.4 BNWF parameters used for design example

SSI property	Value	Reference
Effective Shear Modulus Ratio	$G/G_o = 0.478$	FEMA 356 (2000)
Shear wave velocity	$v_s = 150$ m/s	Das (1993)
Initial Shear Modulus	$G_o = 18100$ kPa	FEMA 356 (2000)
Global Vertical Stiffness	$K_z = 300$ MN/m	Gazetas (1991)
Global Rotational Stiffness	$K_\theta = 3200$ MN-m	Gazetas (1991)
End Length Ratio	$L_e/L = 25\%$	Harden et al. (2004)
Middle Region subgrade reaction	$k_{mid} = 15$ MN/m	Harden et al. (2004)
End Region subgrade reaction	$k_{end} = 85$ MN/m	Harden et al. (2004)
End Tip Resistance	qi = 70%	Harden et al. (2004)
Allowable Bearing	qa = 275 kPA	FEMA 356 (2000)

Five simplified design methods are used to evaluate the displacement demand of the system; the Capacity Spectrum Approach (termed *"Analysis Type 1"*), a method which incorporates rocking based on Housner's (1963) approach (*"Analysis Type 2"*), the Nonlinear Static Procedure with conventional C_1 values (*"Analysis Type 3"*), the Nonlinear Static Procedure with C_1 values modified per this study (*"Analysis Type 4"*) and the Time History method (*"Analysis Type 5"*). Comparison of these design methods for estimating the maximum displacment demand is conducted. Each method is evaluated for the cases of an inelastic subgrade allowed to uplift, an elastic subgrade allowed to uplift and an elastic subgrade fixed against uplift, as well as the fully fixed-base case (i.e., no consideration for soil structure interaction). Note that the case of an elastic subgrade fixed against uplift is identical to a model with a single elastic rotational and vertical spring; this type of analysis is recommended in several design codes and is termed "*method 1*", after FEMA 356 (2000). For the four analytical models used to evaluate the five simplified analysis methods, Table 5.5 lists the natural period of each model from initial stiffness of the various pushover curves. The pushover curves were developed from the model as shown in Figures 4.7 and 5.7, incorporating the parameters as listed in Table 5.4 and the soil structure interaction constraints as mentioned above (i.e. elastic or nonlinear, fixed or allowed to uplift, etc). Note that the system becomes more flexible when elastic soil springs are added, and even more flexible when nonlinear behavior is introduced into the springs. This softening effect can also be seen in the normalized pushover curves of the various models of Figure 5.8. Note that the elastic model and the elastic model with uplift allowed are identical until uplift occurs.

Table 5.5 Natural period of model for simplified analysis methods

	SSI Included (uplift may occur)		SSI Not Included
	Nonlinear Soil Springs	Elastic Soil Springs	Fixed Base
Natural Period, T	0.56	0.42	0.03

The fixed modification factors (Equation 5.1) for the structure described, for use with the analysis are selected as C_0 = 1.4, C_2=1.0, and C_3=1.0. Justification for these values is as follows. The modification factor to relate spectral displacement of an equivalent SDOF system to the roof displacement of the building MDOF system is defined in FEMA 356 (2000) equal to 1.4 for a building of five stories with any load pattern. The BNWF model reasonably displays the hysteresis and strength degredation observed in model test data through emprically calibrated nonlinear foundation elements briefly described above; therefore the value of C_2 which ordinarily would account for these effects in a linear model is set to one. Additionally, the value of C_3 is taken as one because $P-\Delta$ effects are directly accounted for in this design example. The site-specific demand response spectrum for a site in Southern California is created after FEMA 356 (Section 1.6.1.5), based on a 10% probability of exceedance in 50 years. The characteristic period T_S of this spectrum is 0.37 sec. Finally, an effective mass factor Cm, to account for higher mode participation, is required when calculating base shear per Equation 3-10 of FEMA 356 (2000). The effective mass factor C_m is taken as 0.8, as defined in FEMA 356 (2000) for a concrete shear wall system with 3 or more stories.

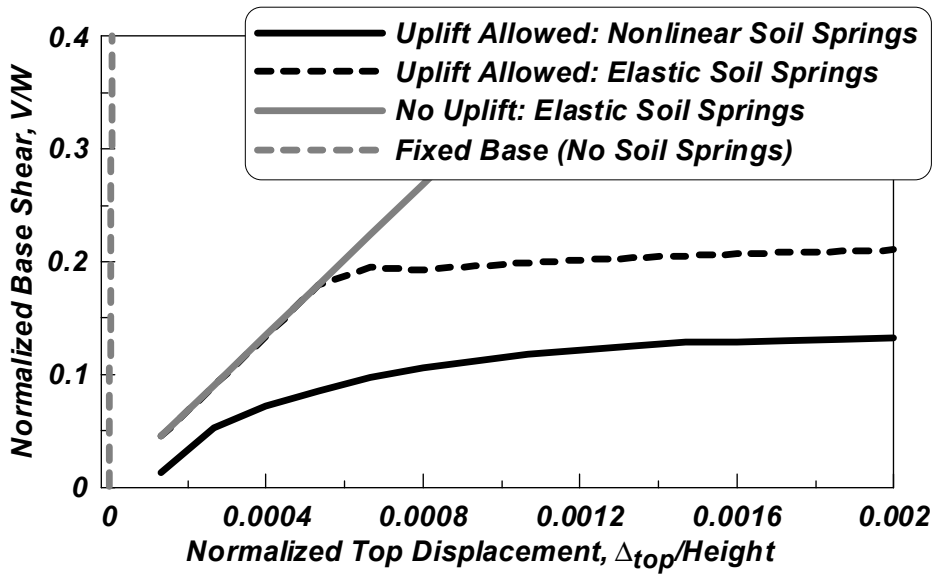

Fig. 5.8 Normalized base shear vs. normalized top displacement for the various models used to evaluate the simplified analysis methods

The five analysis types are described in the following section, with values explicitly described for the beam on a nonlinear Winkler foundation (BNWF) as applicable.

5.5.1 Capacity Spectrum Approach (CSA) — Analysis Type 1

In general, a pushover curve is developed using the BNWF model with the values discussed, and is converted to an SDOF capacity curve, using a modal mass coefficient C_m and the participation factor C_0. The subsitute structure Capacity Spectrum is therefore defined by $SA_{sub} = \frac{H_{PO}}{W}\frac{1}{C_m}g$ and $\Delta_{sub} = \Delta_{top}\frac{1}{C_0}$, where H_{PO} is the base shear. Because the design response spectrum is not reduced for system nonlinearities, the peak displacement is given by the intersection of the design capacity spectrum and the substitute structure capacity spectrum, as shown in Figure 5.9, considering a system with nonlinear and uplifting soil behavior. This is found to be $\Delta_{sub} \cong 200mm$ for the model with nonlinear soil springs. The design displacement is then converted to the actual structure displacement by $\Delta_{top} = \Delta_{sub}C_0$, which in this case is 280 mm for the BNWF substitute structure.

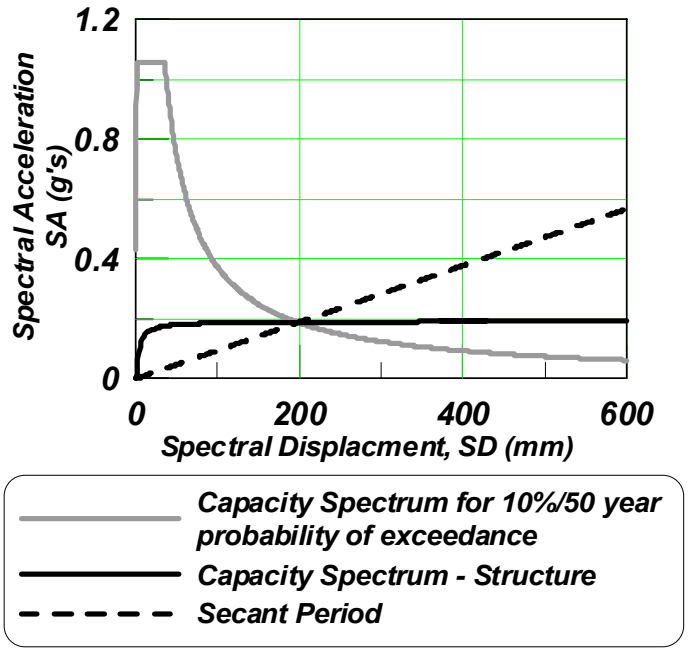

Fig. 5.9 Peak displacement of substitute structure, using capacity spectrum approach and the nonlinear soil model. Analysis Type I.

For this analysis exercise, the estimate of Δ_{top} is not based on iterating the percent of critical damping ξ (T_{secant}) as suggested in other documents. FEMA 356 does not provide critical damping curves, accounting for a rocking foundation in the capacity spectrum approach. For this analysis the percent of critical damping is assumed to be 5%.

5.5.2 Housner Rocking Block Approach — Analysis Type 2

An alternative simplified method to estimate the peak displacement of a rocking shallow foundation is based on the application of Housner's (1963) approach, with slight modifications. For a rocking block as shown in Figure 5.10, the effective viscous damping is a function of the block dimensions, the seismic mass, and the mass moment of inertia. In addition, the rocking will be sensitive to the vertical factor of safety, since this affects the point of rotation through which the block rocks, based on an assumed contact area.

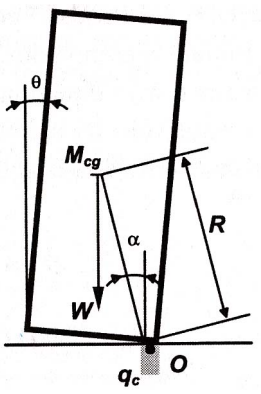

Fig. 5.10 Housner's (1963) rocking block (after FEMA 356 (2000))

Considering the demand displacement of a substitute structure Δ_{sub}, the rocking period of the structure may be calculated as:

$$T = \frac{4}{\sqrt{\frac{WR}{I_O}}} \cosh^{-1}\left(\frac{1}{1-\frac{\theta}{\alpha}}\right), \text{ where } \theta = \frac{\Delta_{sub}}{R\cos(\alpha)} \tag{5.12}$$

Additionally, R and α are functions of the block geometry shown in Figure 5.10, θ is the block rotation and I_O is the mass moment of inertia about one corner. The design displacement may be found through iteration of an assumed displacement or, perhaps the more straightforward approach, at the intersection of a pushover type curve and the design spectrum.

The effective viscous damping (in %) of the rocking block may be calculated as:

$$\xi_{eff} = 40\left(1-\sqrt{r}\right) \tag{5.13}$$

where r is calculated as:

$$r = \left[1-\frac{mR^2}{I_O}\left(1-\cos(2\alpha)\right)\right]^2 \tag{5.14}$$

For the shear wall considered, the effective viscous damping is calculated to be 10%, therefore $\Delta_{sub} \cong 147mm$. The design displacement is then converted to the actual structure displacement by $\Delta_{top} = \Delta_{sub} C_0$, which for the BNWF model is 206 mm.

5.5.3 Nonlinear Static Procedure (NSP) — Analysis Type 3

The nonlinear static procedure is investigated, which estimates the demand displacement using Equation 5.1. From Equation 5.2, the demand spectral acceleration of the elastic system is 0.9g (at the initial period), and the yield force from a bilinear approximation of the pushover curve for the system allowed to uplift is 197 kN. Using these variables, the strength ratio R was found to be 4.0 for the BNWF model; *R = 0.9g*1400kN/(197kN*0.8) = 4.0.* The effective period, 0.56 sec is then calculated through the elastic perfectly-plastic transition of a bilinear approximation to the pushover curve, similar to that described in FEMA 356 (2000) Figure 3-1 with a zero post-yield stiffness. With R and the effective period determined, the design displacement is calculated for the conventional definition of C_1. For this case, C_1 defined by FEMA 356 (2000) is equal to one (Equation 5.1). The design displacement is then calculated directly from Equation 5.1 as $\Delta_{top} \cong 91mm$.

5.5.4 Nonlinear Static Procedure (NSP) with Modified C_1 Values — Analysis Type 4

The nonlinear static procedure is further explored with the modified value of C_1 calculated by the procedure presented in this report. As discussed above, the strength ratio R was found to be 4.0 for the BNWF model, and an effective period of 0.56 sec. The demand spectrum in this example has a characteristic period of 0.37 seconds. The ratio of the elastic period to the characteristic period is 0.56/0.37=1.5, used in the final calculation of C_1. Estimating the force demand from the intersection of the demand spectrum with both the elastic and nonlinear models, the spectral acceleration ratio is calculated as $\psi_{SA} = SA_{nonlinear} / SA_{elastic} = 0.81$. Given that R is equal to 4.0, X1 = 0.68 and X2 = 0.87 from Tables 5.2. From Table 5.3, the system falls into group II under R = 4.0 because X1 $\leq \psi_{SA} <$ X2, therefore A = -0.881 and B = 0.12. Finally, C_1 defined by an elastic shallow foundation allowed to uplift is calculated from Equation 5.11, C_1=1/[1-0.881$e^{-0.12x(1.5-0.5)}$] = 4.6; approximately five times what would be recommended in conventional design codes. The design displacement from Analysis type 3 was calculated to be $\Delta_{top} \cong 91mm$. Incorporating the modified C_1 value in place of the original C_1 value gives a design displacement of $\Delta_{top} \cong 91mm\left(C_1 / C_{1-FEMA}\right) = 91mm\left(4.6/1.0\right) \cong 414mm$.

5.5.5 Time History (TH) Method — Analysis Type 5

Conducting a nonlinear time history analysis should provide for the most realistic estimation of the seismic demands. Using recorded ground motions to assess structural demands, here, three ground motions are selected from the suite of 19 ground motions used to investigate the relation between C_1 and R (See Table 5.1). The longitudinal components of two ground motions from the 1994 Northridge earthquake (Woodland Hills and Van Nuys, Sherman Circle denoted "NR-whox" and "NR-vnsc", respectively) and the longitudinal component of one ground motion from the 1971 San Fernando earthquake (Glendale, Muni Building, denoted "SF-glen") are selected. The longitudinal components of the selected ground motions are assumed parallel to the wall in this design example. The characteristics of these motions best represent the design spectrum for three binned groups of short, medium and long characteristic periods. Figure 5.11 (a) shows the elastic acceleration response spectra for these motions along with the design spectrum. It is recommended to use at least three representative time histories with accelerations scaled such that the average spectral acceleration is at least 1.4 times the design spectrum. Accelerations within the range of 0.2 to 1.5 times the natural period are used to calculate the average spectral acceleration. Figure 5.11(b) shows the three spectra scaled using the aforementioned criteria along with the design spectrum. Figure 5.12 shows the top displacement and settlement time history for the largest PGA ground motion, "NR-vnsc." This ground motion's characteristic period of 0.52 seconds is closest to the BNWF structure period of 0.56 seconds. Top displacements of 385 mm and 102 mm are calculated using these scaled time histories and the Winkler model for the cases of nonlinear and elastic soil, respectively.

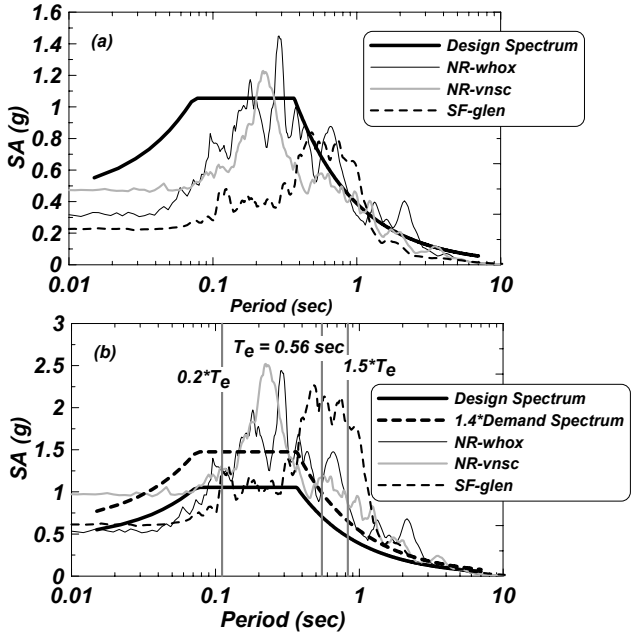

Fig. 5.11 (a) Demand and unscaled ground motion acceleration spectrum at 5% damping (b) demand and scaled design ground motion acceleration spectrum at 5% damping

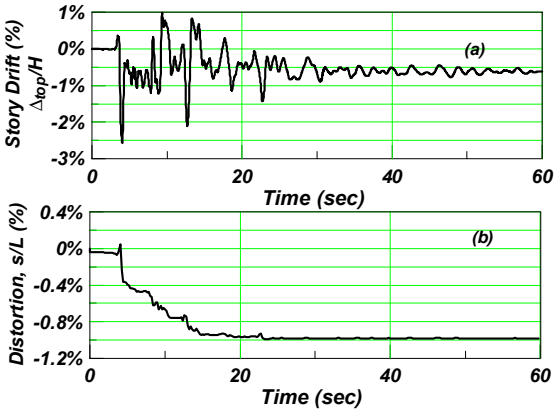

Fig. 5.12 (a) Story drift and (b) settlement time history for nonlinear soil springs

5.5.6 Design Example Results and Discussion

Displacement demands predicted for the three model types and four analysis methods are summarized in Table 5.6. For all analysis methods; the CSA, Housner's model, and NSP with C_1 conventional definition are less conservative than either the time history method or the NSP with modified C_1 values. The NSP with C_1 based on an uplifting elastic foundation finds a result which is conservative with respect to the time history method. This is positive in the sense that using the C_1 values from this study allows a design engineer to include the effects of foundation uplift with current code simplified design methods without performing an overly-rigorous analysis, while still resulting in a conservative demand estimate.

With respect to base shear demand, the NSP with C_1 conventional definition, NSP with modified C_1 values and time history method for a nonlinear subgrade resulted in the least conservative design base shear (Table 5.7). This result is to be expected given the larger displacements observed for these cases, and is a significant benefit of allowing permanent (where

nonlinear springs are used) and transient displacements of the foundation. The fixed-base (No soil springs) analysis provides a valuable contrast to the analyses incorporating some form of soil structure interaction. The design shear is significantly larger than those cases where uplift is allowed, and the target displacements are much smaller — both prohibitive to economic design.

Table 5.6 Design displacement values for the various analysis methods

	Soil Structure Interaction (SSI)			
	Included			*Not Included*
	Uplift Allowed		--	*Fixed Base*
	Nonlinear Soil Springs	*Elastic Soil Springs*	*Method 1*	
Analysis Method Type	u_{top} (mm)	u_{top} (mm)	u_{top} (mm)	u_{top} (mm)
TYPE 1 – CSA	280	178	38	0.14
TYPE 2 – Housner	206	202	202	***NA***
TYPE 3 – NSP (conventional C_1)	91	57	57	0.27
TYPE 4 – NSP (modified C_1)	414	308	62	0.27
TYPE 5 - TH	385	102	237	0.0003

Table 5.7 Design base shear demand for the various analysis methods

	Soil Structure Interaction (SSI)			
	Included			*Not Included*
	Uplift Allowed		--	*Fixed Base*
	Nonlinear Soil Springs	*Elastic Soil Springs*	*Method 1*	
Analysis Method Type	V (kN)	V (kN)	V (kN)	V (kN)
TYPE 1 – CSA	211	331	1181	728
TYPE 2 – Housner	284	291	291	***NA***
TYPE 3 – NSP (conventional C_1)	162	240	1024	793
TYPE 4 – NSP (modified C_1)	170	265	1108	793
TYPE 5 - TH	169	251	4245	1341

Another useful comparison can be made to the Uniform Building Code (UBC), 1997 edition, which allows for a direct calculation of the base shear and maximum displacement, independent of soil structure interaction. Note that a similar comparison can be made with the International Building Code (IBC), 2000 edition, though the UBC is generally more conservative. Assuming worst-case conditions (a fault proximity of less than 2 km and soil type "D") in a Zone 4 location, the UBC static force procedure (Chapter 16) gives a base shear of 514

kN. This is approximately twice the value found when using the simplified analysis methods and with elastic soil springs (recall that the UBC is generally understood as a conservative design document). Based on the height of the building and lateral-force-resisting system, the maximum elastic deflection at the top of the building is calculated as 119 mm, while the maximum inelastic deflection is calculated as 375 mm. Note that for both elastic and nonlinear spring models, all of the analysis methods except the NSP with C_1 conventional definition allow for similar or greater displacements than the UBC allows (a conservative baseline). This highlights to a greater extent the need to account for soil structure interaction in the nonlinear static procedure.

5.5.7 Design Example Settlement Estimation

The displacement of the system evaluated by any of the simplified methods allows one to estimate the settlement using empirical energy dissipation data and the calculated number of cycles from an initial displacement using Housner's (1963) model.

Housner (1963) gives the angle of rotation of a foundation after the n^{th} impact, due to an initial rotation, θ_o, as

$$\theta_n = 1 - \sqrt{1 - r^n \left(1 - \left(1 - \theta_o\right)^2\right)} \tag{5.15}$$

The initial rotation θ_o is estimated from the results for each of the simplified design methods using the top lateral design displacement demand (Table 5.6) or using the direct values from the time history analysis (for Method 5), and where r was previously defined in Equation 5.14.

Using a suite of experimental data, Harden et al. (2004) synthesize results in terms of equivalent viscous damping and distortion level. A sample of these results, for statically moment-loaded footings is shown in Figure 5.13. Distortion here is defined as the settlement normalized by the foundation length per cycle. These data fall both below and above typical foundation design distortion values, as suggested by Duncan and Buchignon (1987), for steel frame and load bearing wall structures. Note however that a dependency on the static factor of safety FS_V is observed, which is not provided in design recommendations. Figure 5.14 shows the magnitude of equivalent viscous damping versus the half amplitude of rotation (i.e., not averaged over cycles of loading) of a footing per cycle. This information will be used to estimate the

amount of equivalent viscous damping mobilized during foundation settlement due to the demand lateral displacement estimated from the simplified design methods.

Nonlinear regression through the data shown in Figure 5.13 results in equivalent viscous damping versus distortion per cycle, for $FS_V \geq 3$ as:

$$s = e^{\frac{\ln(\xi)-4.451}{0.248}} \tag{5.16}$$

Similarly, incorporating the results of shallow foundation model tests shown in Figure 5.14, the relationship for equivalent viscous damping versus half-amplitude of rotation is found through regression for $FS_V \geq 3$ as:

$$\xi_{eq} = e^{0.336\ln(\theta)+3.137} \tag{5.17}$$

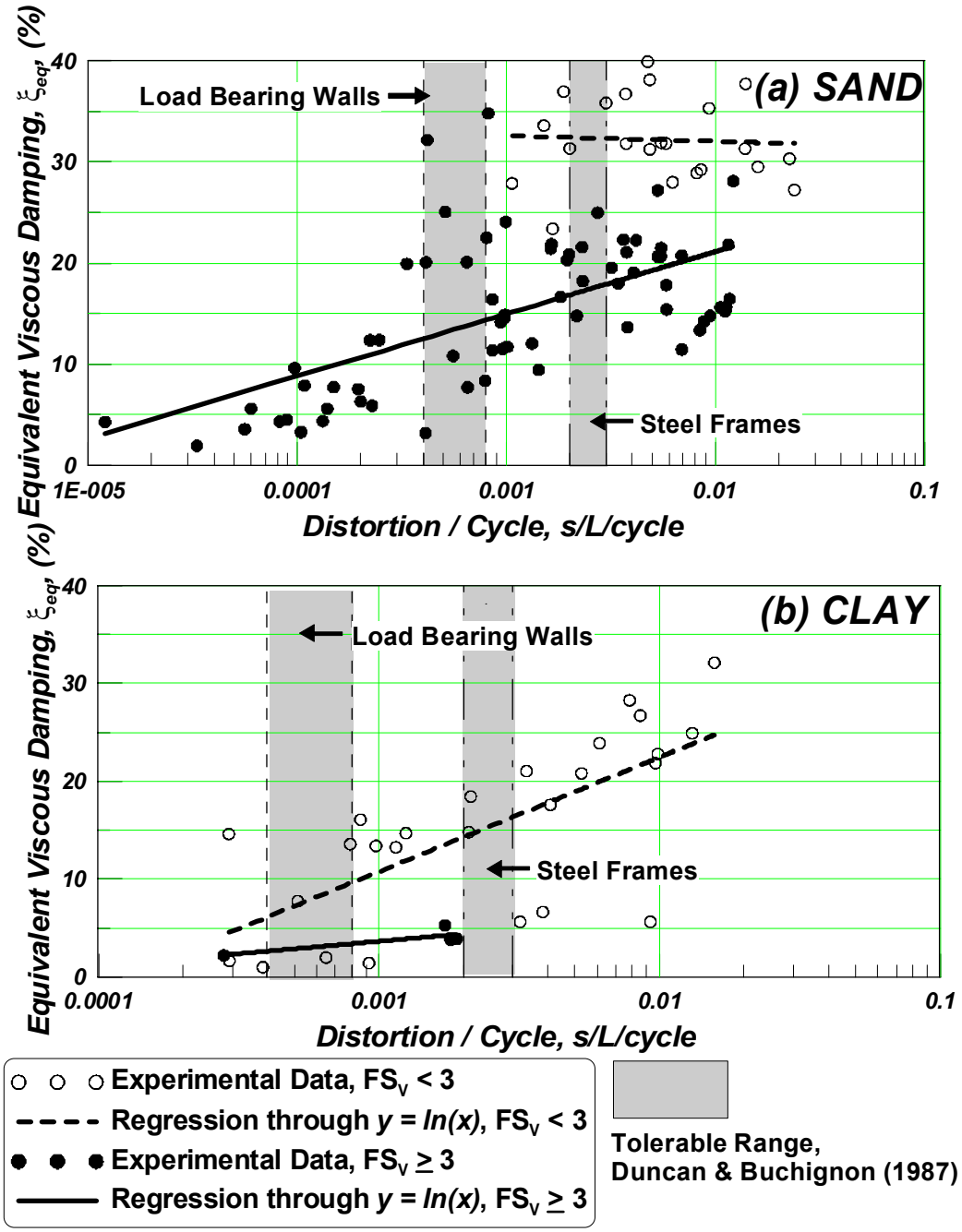

Fig. 5.13 Equivalent viscous damping vs. maximum footing distortion (settlement normalized by footing length per cycle for slow cyclic tests: (a) sand data and (b) clay data. Experimental data sets courtesy of Bartlett (1976), Gajan et al. (2003a, b), Negro et al. (1998), Rosebrook and Kutter (2001a, b, c), and Weissing (1979).

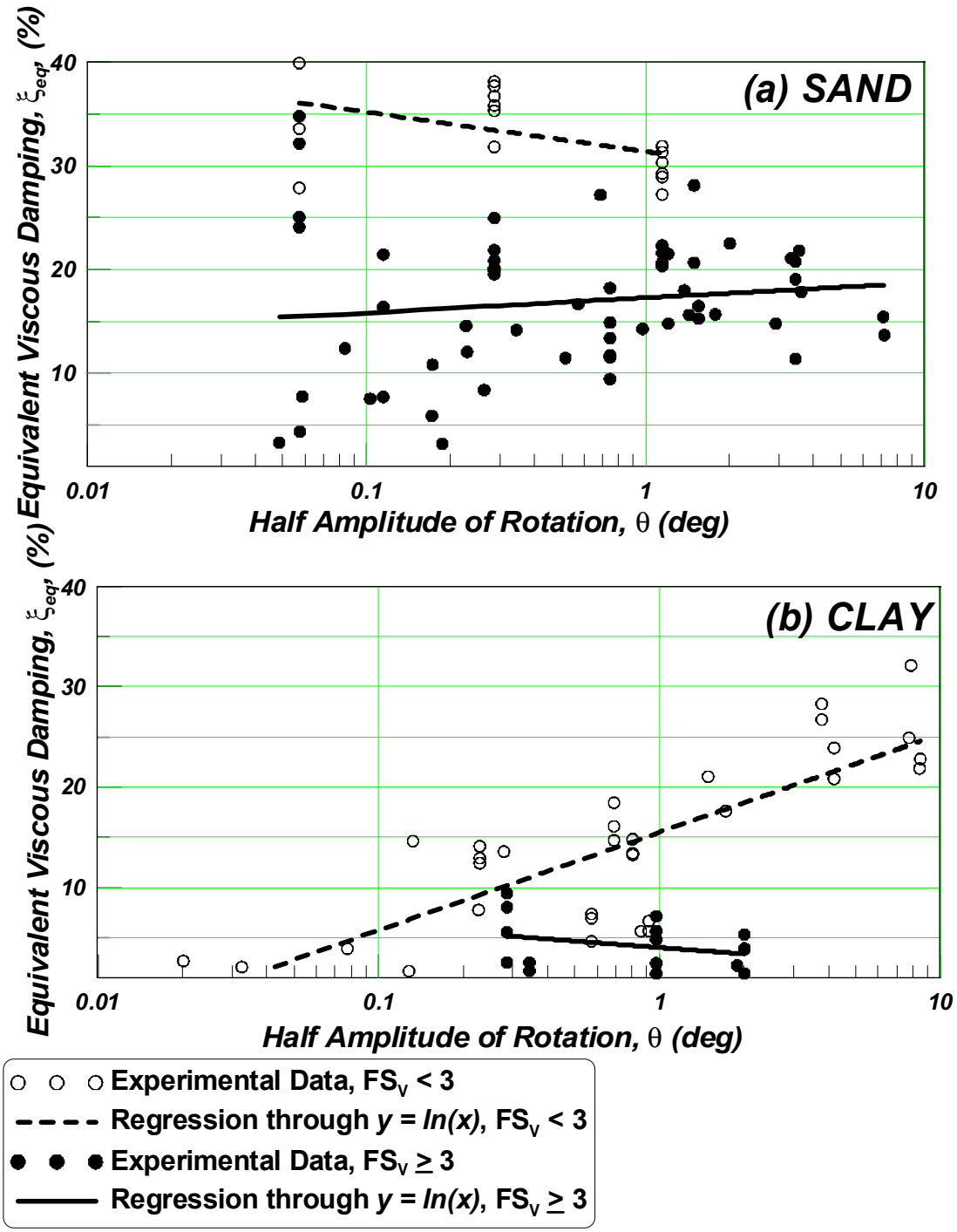

Fig. 5.14 Equivalent viscous damping vs. half amplitude of rotation for slow cyclic tests: (a) sand data and (b) clay data. Experimental data sets courtesy of Bartlett (1976), Gajan et al. (2003a, b), Negro et al. (1998), Rosebrook and Kutter (2001a, b, c), and Weissing (1979).

Using Equations 15 through 17, an iterative approach can be applied until the number of cycles (with two impacts per cycle) forces the rotation amplitude to zero (at rest). The procedure begins with the initial displacement demand calculated by any of the simplified methods previously discussed. The last step of the procedure is to sum the settlements calculated for all cycles. The accumulated settlement values are listed in Table 5.8, calculated using the maximum estimated top displacement values from the simplified procedures.

Table 5.8 Calculated accumulated permanent settlement values

Analysis Method Type	u_{top} (mm) (nonlinear soil spring case)	s (mm)	Total Distortion (s/L) (%)
TYPE 1[1] – CSA	280	56	0.7
TYPE 2[1] – Housner	206	38	0.5
TYPE 3[1] – NSP (conventional C_1)	91	12	0.2
TYPE 4[1] – NSP (modified C_1)	414	96	1.2
TYPE 5[2] - TH	385	86	1.1

Note 1: Estimated based on empirical simplified settlement analysis method.
Note 2: Accrued settlement from BNWF model (time history analysis) with nonlinear soil springs.

The accumulated settlement values are sensitive to the starting value of top displacement. Larger initial horizontal displacements accrue larger settlements. This is an intuitive result; as a higher level of performance is demanded of the system, a larger cost is accrued in settlement. Similarly, using the nonlinear static procedure with values of C_1 calculated from this study gives a conservative result with respect to the CSA, the Housner model and the traditional NSP, though much more comparable to the time history method. Recall from Figure 5.12(b) the maximum settlement from the largest PGA ground motion of the three considered using the time history method was 80 mm. Most notably, the NSP method, using conventional C1 values grossly under predicts the accumulated settlement when compared to the time history method, which is approximately seven times the Type 3 method. The simplified settlement analysis using the initial displacement from the modified NSP gives a value close to the settlement estimated using the initial displacement from the time history method, within 20% on the conservative side. These reasonably close values add credibility to the proposed empirical method of estimating settlement, combined with Housner's rocking block approach, and using the experimentally-regressed ξ_{eq}–distortion curves.

5.6 CONCLUSIONS

The relationship between the strength ratio R and the displacement ratio C_1 was investigated in this report, for shallow foundations allowed to uplift. Compared to current design codes, the displacement ratio was found to be significantly larger in the acceleration sensitive range of the response spectrum ($T/T_S \leq 0.5$), indicating that rocking shallow foundations may be a case where special attention is required when using simplified design procedures. Suggestions for improved C_1-R relations are provided, based on regression through the nonlinear time history data collected in this study.

To illustrate the approach for using the improved C_1-R relation, a design example was presented considering five different methods of analysis. Using the C_1 value from the uplift study provided for a relatively close estimate of peak displacement demand when compared to the time history method. Both methods are conservative with respect to the displacements calculated from the LSP, rocking block analogy and CSA procedures commonly used in design codes. A procedure to estimate settlement based on empirical rocking foundation data was presented and used for each of the simplified design methods. The simplified settlement estimate using an initial displacement from the modified NSP procedure compared well with the accrued settlement calculated from time history analysis using a Winkler foundation with nonlinear soil springs allowed to permanently deform.

6 Conclusions

6.1 SUMMARY REMARKS AND CONCLUSIONS

The scope of this report was to contribute to practical numerical procedures for reasonably capturing the nonlinear response of shallow foundations subjected to combined moment, axial and shear cyclic loading. A simplified beam-on-nonlinear-Winkler-foundation (BNWF) approach is used to model the shallow foundation response. Particular focus is given to capturing the expected consequences (permanent settlement, horizontal displacement) due to the benefits of mobilizing energy dissipation (through M*, H, V)* within the soil. The numerical model is used to study input parameters specific to the Winkler approach, and the results are compared against a suite of shallow foundation experimental data sets available in the literature.

Analysis of the suite of experimental data, including scale footings resting on sand and clay tested at one-g as well as centrifuge (20-g) tests on sand and clay, revealed that a good deal of energy dissipation can be developed from the shallow foundation system. This dissipation of energy can be represented as equivalent viscous damping, ξ_{eq}, and compared against demands of settlement, s, or rotation, θ. In Chapter 2, ξ_{eq} vs. s and ξ_{eq} versus θ curves are generated from the experimental data for use in practical design.

Winkler modeling of the diverse set of data was accomplished using a mesh generator *"BNWFshallow.txt"* written for the OpenSees platform. To provide comparison with the model test data, ideas were introduced to capture the observed failure mechanisms at the soil-structure interface. These parameters include variable stiffness and pressure distribution along the base of the foundation to capture the more heavily loaded (and potentially densified) ends of the footing. Stiffness selection was investigated using the experimental data and published formulae, and it was found that vertical unloading stiffness provides the best result in terms of capturing the combined rotational and vertical stiffness (via a laterally distributed set of springs). To capture the densification observed at the ends of the footing due to rotation, two parameters were

studied; the end length ratio and the end length stiffness. The distribution of bearing capacity of the system was studied and the most suitable distribution (again from comparison with experimental data) was observed to be parabolic. The selection of BNWF model parameters was based on capturing observed global features from the suite of shallow foundation test data, including absolute maximum (positive and negative) moment M, absolute maximum rotation θ, settlement s and horizontal displacement u. Insight into the sensitivity of selection of these parameters was also provided in Chapter 3, and results presented in a normalized fashion as a function of a decision variable for footings with a broad range of vertical factors of safety FS_V. A summary of the numerical modeling results is presented in Chapter 4, as well as a summary of the normalized parameters.

To synthesize the practical aspects of the work, current simplified design methods are investigated in Chapter 5. Using a range of representative values of the strength reduction factor R (R = 1.5, 2.0, 4.0, and 8.0 are studied), numerical models of a stiff shear wall resting on an elastic Winkler foundation both allowed and restrained from uplift were developed across a broad range of natural periods. These models were subjected to 19 earthquake time histories. Results from these nonlinear dynamic analyses are presented in terms of a normalized displacement demand parameter, $C_1 \equiv \Delta_{inelastic} / \Delta_{elastic}$, where $\Delta_{\text{inelastic}}$ is obtained from the uplifting foundation. The C_1 values are shown to be much larger than current practice and regression through the analysis presented suggest modified C_1-T relations to account from uplifting. The empirical relation of ξ_{eq} with settlement found from the suite of shallow foundation model test data (Chapter 2) was combined with the revised C_1-T relation (accounting for the modification required for a system allowed to uplift), and a design example illustrated.

6.2 SUGGESTIONS FOR FUTURE WORK

Although the results illustrated that with suitable parameter selection, the BNWF analysis method is a valuable tool for studying the shallow foundation rocking problem, additional work is needed to further its validity and advance its development as a performance-based design procedure. The following addresses directions for future research.

- The scope of this report included a 2-D BNWF representation of the collection of experimental data sets. Such a 2-D representation effectively lumps stiffness and strength of a volume of soil at a spring. Comparison of these (2-D) modeling approaches

with 3-D (solid) models using the same set of experimental data would provide valuable insight into the validity of this simplification. Similar recommendations such as those made in this report could be made for the 3-D BNWF models to accurately represent capacity and displacement demands.

- An in-depth study including the nonlinearity of the structural elements (shear walls) in the model combined with the BNWF system would provide insight into the combined system response. This will be particularly useful to understand the reduction in structural demands, given the yielding and capacity mobilization at the foundation. Care should be taken to develop study cases which differentiate when the soil subgrade yields exclusively, when the structure yields exclusively, and when both the soil and structure yield together.
- Centrifuge experiments where specific structural "hinges" are incorporated would provide much needed experimental data to validate the above numerical models. Again, care should be taken to select a range of appropriate safety factors and yielding capacities.
- Systems considered in this report comprised structures resting on either sand ($c_u = 0$) or clay ($\phi' = 0$). Numerical models considering the soil medium composed of mixed (c-ϕ) materials would provide insight into a broader range of realistic soil-structure systems. However, physical data sets have yet to be conducted to validate such models; centrifuge experiments could provide important data to this respect.
- It is well known that liquefaction below the foundation results in reduced bearing capacity, and this should be studied in the context of the rocking shallow foundation.
- This report investigated one aspect of current simplified design approaches using the shallow foundation model allowed to uplift on an elastic subgrade. The nonlinearity of both the soil and structure should be incorporated into the simplified methods study. Inclusion of the nonlinear soil could help predict, as a function of strength reduction factor R, the amount of anticipated settlement, as well as the peak structural displacement, which will be different than the elastic model predicted. Recommendations for expected vertical (settlement) and lateral (drift) displacements presented in terms of safety factors, normalized foundation aspect ratios and normalized yield capacities of the subgrade would be valuable to practice. Inclusion of nonlinear

structure in the generation of C_1-T curves will account for redistribution of forces (and thus will be reflected in assessment of demand).

- Finally, 3-D analytical and physical modeling of a whole building structure would be important to investigate the redistribution of loading during a seismic event. Two types of models could be studied; a combined flexible frame and shear wall in addition to a flexible frame combined with an out-of-plane structural system. These combined types of structural systems are very sensitive to the capacity and stiffness of the soil, and thus recommendations from this study would be valuable to practice.

REFERENCES

Allotey, N. and Naggar, H. (2003), "Analytical moment-rotation curves for rigid foundations based on a Winkler model." Journal of Soil Dynamics and Earthquake Engineering, vol. 23, pp. 367-381.

Al-Sulaimani, G.J. and Roessett, J.M. (1984), "Design Spectra for Degrading Systems," J. of Struct. Engrg., ASCE, Vol. 111, No. 12, pp. 2611-2623.

Applied Technolgy Council (ATC) (1996). "Seismic Evaluation and Retrofit of Concrete Buildings ATC-40." Volume 1 and 2 November.

Bartlett, P. E. (1976), "Foundation Rocking on a Clay Soil," M. E. Thesis, University of Auckland, New Zealand.

Bolton, M. D. (1986), "The Strength and Dilatency of Sands," Geotechnique, vol. 36, No. 1, Mar. 1986, pp. 65-78.

Boulanger, Ross W., Curras, Christina J., Kutter, Bruce L., Wilson, Daniel W., and Abghari, Abbas (1999). "Seismic Soil-Pile Structure Interaction Experiments and Analyses," Journal of Geotechnical and GeoEnvironmental Engineering, ASCE. Vol. 125, No. 9.

Boulanger, Ross W. (2000a). "The PySimple1 Material," Document for the OpenSees platform.

Boulanger, Ross W. (2000b). "The QzSimple1 Material," Document for the OpenSees platform.

Boulanger, Ross W. (2000c). "The TzSimple1 Material," Document for the OpenSees platform.

Broms, B.B. (2003). Foundation Engineering. Geo-Forum, Geo Texts and Publications site: http://www.geoforum.com/knowledge/texts/broms/index.asp

Budhu, M. and Al-Karni, A. (1993) "Seismic Bearing Capacity of Soils," Géotechnique 43, No. 1, 181-187.

Caquot, A. and Kérisel, J. (1949). *Traite de mechanique des sols.* Gauthier-Villars, Paris, France (in French).

Chopra, A, and Yim, C. "Earthquake Response of Structures with Partial Uplift on Winkler Foundation," Earthquake Engineering and Structural Dynamics, Vol. 12, 263-281 (1984).

Chopra, A.K. (1995). *Dynamics of Structures – Theory and Application to Earthquake Engineering*. Prentice Hall, New Jersey.

Chopra, A.K. and Yim, S.C. (1985). "Simplified earthquake analysis of structures with foundation uplift." *ASCE Journal of Structural Engineering*. 111(4): 906-930.

Chopra, A. and Goel, R. (1999) "Capacity-Demand-Diagram Methods for Estimating Seismic Deformation of Inelastic Structures: SDF Systems," Report No. PEER-1999/02, University of California, Berkeley.

Coduto, Donald P.(2001). *Foundation Design: Principles and Practices*. Prentice Hall, New Jersey.

Cuesta, I, and Aschheim, M.A. (2000). "Waveform Independence of R-Factors," Paper No. 1246, 12th World Conf. on Earthquake Eng., Auckland, New Zealand.

Cuesta, I, and Aschheim, M.A. (2001a). "Using Pulse R-Factors to estimate structural response to earthquake ground motions," MAI Center Report Series CD release 01-03, University of Illinois at Urbana-Champaign, IL, March.

Cuesta, I, and Aschheim, M.A. (2001b). "Isoductile Strengths and Strength Reduction Factors of Elasto-Plastic SDOF Systems Subjected to Simple Waveforms," Earthquake Eng. Struct. Dyn. 30 (7), July.

Cuesta, I, and Aschheim, M.A. (2001c). "Inelastic Response Spectra Using Conventional and Pulse R-factors," J. Struct. Eng. 127 (9), 1013-1020.

Cuesta, I, Aschheim, M., and Fajfar, P. (2003). "Simplified R-Factor Relationships for Strong Ground Motions," Earthquake Spectra, vol 19, No. 1.

Das, Braja M. (1999). *Principles of Foundation Engineering*. Brooks/Cole Publishing Company, California

DeBeer, E.E. (1970). "Experimental Determination of the Shape Factors and Bearing Equation Factores of Sand, "Geotechnique, Vol. 20, No. 4, pp 387-411.

Duncan, J. M., Byrne, P., Wong, K. S., and Mabry, P. (1980). Strength, Stress-Strain and Bulk Modulus Parameters for Finite Element Analyses of Stresses and Movements in Soil Masses, Report No. UCB/GT/80-01, August, Department of Civil engineering, University of California, Berkeley, California.

Elghadamsi, F.E. and Mohraz, B. (1987), "Inelastic Earthquake Spectra," Earthquake Engineering and Structural Dynamics, Vol. 15, pp. 91-94.

Fajfar, P. (2000). “A Nonlinear Analysis Method for Performance-Based Seismic Design,” Motions,” Earthquake Spectra, vol 16, No. 3.

EPRI (1990) Manual on Estimating Soil Properties for Foundation Design. Electric Power Research Institute, Palo Alto, California.

Fang, Hsai-Yang, ed. (1991) “Foundation Engineering Handbook” Van Nostrand Reinhold, New York.

FEMA 356 (2000). *Prestandard and Commentary for the Seismic Rehabilitation of Buildings.* American Society of Engineers, Virginia.

Gadre, A. and Dobry, R. (1998). “Lateral Cyclic Loading Centrifuge Tests on Square Embedded Footing,” Journal of Geotechnical and Geoenvironmental Engineering, ASCE. Vol. 124, No. 11. 1128-1138

Gajan, S., Phalen, J.D. and Kutter, B.L. (2003a). “Soil-Foundation Structure Interaction: Shallow Foundations. Centrifuge Data Report for the SSG02 Test Series," Center for Geotechnical Modeling Data Report UCD/CGMDR-03/01.

Gajan, S., Phalen, J.D. and Kutter, B.L. (2003b). “Soil-Foundation Structure Interaction: Shallow Foundations. Centrifuge Data Report for the SSG03 Test Series," Center for Geotechnical Modeling Data Report UCD/CGMDR-03/02.

Gazetas, G. (1991). *Foundation Engineering handbook*, Fang, H.Y. edit. Van Nostrand Rienhold, 40 pp.

Gazetas, G. and Tassoulas, J. L. (1987). “Horizontal stiffness of arbitrary shaped embedded foundations.” Journal of Geotechnical Engineering, ASCE, 113(5), 440-457.

Gazetas, G. “Displacement and Soil-Structure Interaction Under Dynamic and Cyclic Loading,” Proceedings of the Tenth European Conference on Soil Mechanics and Foundation Engineering, Florence, May 1991.

Georgiadis, M. and Butterfield, R. “Displacements of Footings of Sand Under Eccentric and Inclined Loads,” Canadian Geotechnical Journal, Vol. 25, 1988.

Gulkan, P. and Sozen, M.A. (1974). “Inelastic responses of reinforced concrete structures to earthquake motions.” *ACI Journal,* Title No. 71-41, 604-610.

Hanna, A. M. and Meyerhoff, G.G. (1981). "Experimental Evaluation of Bearing Capacity of Footings Subjected to Inclined Loads," *Canadian Geotechnical Journal,* Vol. 18, No. 4, pp. 599-603.

Hansen, J. B. (1970). "A Revised and Extended Formula for Bearing Capacity," Danish Geotechnical Institute, *Bulletin* 28, Copenhagen.

Hidalgo, P.A. and Arias, A. (1990), "New Chilean Code for Earthquake-Resistant Design of Buildings," Proc. 4th U.S. Nat. Conf. Earthquake Engrg, Palm Springs, California, Vol. 2, pp 927-936.

Hausmann M. R. (1990). *Engineering Principles of Ground Modification,* McGraw-Hill Publishing Company.

Housner (1963) "The Behavior of Inverted Pendulum Structures During Earthquakes," Bulletin of the Seismic Society of America, v. 53, 2, 403-417.

Ho, M. and Lopes, R. (1969). "Contact Pressure of a Ridid Circular Foundation," Journal of the Soil Mechanics and Foundations Division, Proceedings of the American Society of Civil Engineers, Vol. 93, No. SM3.

Hucklebridge, A.A. and Clough, R.W. (1978). "Seismic response of uplifting building frame." *ASCE Journal of the Structural Division*. 104(ST8): 1211-1229.

Hudson, D.E. (1965). "Equivalent viscous friction for hysteretic systems with earthquake-like excitations." *Proceedings 3rd World Conference on Earthquake Engineering*, Vol. II, 185-202.

Hutchinson, T. (2001) "Energy Dissipated and Associated Consequences of Rocking Shallow Foundations Systems," University of California, Irvine.

Jennings P.C. (1968). "Equivalent viscous damping for yielding structures." *Journal of Engineering Mechanics Division,* ASCE, 94(1): 103-116.

Jones, Allen L., Kramer, Steven K., and Arduino, Pedro (2001). "Estimation of Uncertainty in Geotechnical Properties for Performance-Based Earthquake Engineering," Report No. PEER-2001/03, University of California, Berkeley.

Kerr, A. D. (1989). "Tests and analyses of footings on a sand base." Japanese Society of Soil Mechanics and Foundation Engineering, Vol. 29(3), 83-94.

Kowalsky, M.J., Priestley, M.J.N., and MacRae, G.A. (1995). "Displacement-based design of RC bridge columns in seismic regions." *Earthquake Engineering and Structural Dynamics*, 24: 1623-1643.

Kutter, B., Martin, G., Hutchinson, T., Harden, C., Sivapalan, G., Phalen, J. "Status Report on Study of Modeling of Nonlinear Cyclic Load-Deformation Behavior of Shallow Foundations" PEER Workshop March 5, 2003 Documentation

Kutter, Bruce L. (1997), "Dynamic Centrifuge Modeling of Geotechnical Structures," Transportation Research Record, Department of Civil Engineering, University of California, Davis.

Lai, S. and Biggs, J. (1980), "Inelastic Response Spectra for Aseismic Building Design," J. Struct. Div., ASCE, Vol. 106, No. ST6, pp 1295-1310.

Lambe, William T. and Whitman, Robert V. (1969). Soil Mechanics. John Wiley & Sons, Inc. New York. 553 pp.

Lee, P.Y. and Singh, A. (1971), "Relative Density and Relative Compaction," Journal of the Soil Mechanics and Foundations Division, ASCE, Vol. 97, No. SM7, 1049-1052.

Martin, G., Yan, L, and Lam, I. (1997) "Development and Implementation of Improved Seismic Design and Retrofit Procedures for Bridge Abutments," University of Southern California.

Martin, G, and Yan, L. (1999) "Simulation of Moment Rotation Behavior of a Model Footing," FLAC and Numerical Modeling in Geomechanics, Detournay and Hart (eds), Balkema, Rotterdam.

Matyas, E, and Taylor, B. "Influence Factors for Settlement Estimates of Footings on Finite Layers," Canadian Geotechnical Journal, Vol. 20, 832-835 (1983).

Mazzoni, Silvia, McKenna, Frank, Scott, Michael H., Fenves, Gregory L., and Jeremic, Boris. (2003). "OpenSees Users Manual, version 2.0" http://peer.berkeley.edu/~silvia/OpenSees/manual/html/

Miranda, E. (1993), "Site-Dependent Strength Reduction Factors," J. of Struct. Engrg., ASCE, Vol. 119, No. 12.

Murzenko, Yu. N. (1965). "Experimental results on the distribution of normal contact pressure on the base of a rigid foundation resting on sand." Journal of Soil Mechanics and Foundation Engineering, Proceedings of the American Society of Civil Engineers, Vol 2(2), 69-73.

Meyerhoff, G. G. (1951). "The Ultimate Bearing Capacity of Foundations," Géotechnique, vol. 2, pp. 301.

Miranda, E. and Bertero, V. (1994). "Evaluation of Strength Reduction Factors for Earthquake-Resistant Design," Earthquake Spectra, vol 10, No. 2.

Montrasio, L. and Nova, R. (1997) "Settlements of Shallow Foundations on Sand: Geometrical Effects," Géotechnique 47, No. 1, 49-60.

Muller, G. U. (1996) "Photoelastic Determination of Contact Stresses of Foundations." Journal of Geotechnical Engineering, vol 122, No. 8.

Nakaki, D.K. and Hart, G.C. (1987). "Uplifiting response of structures subjected to earthquake motions. U.S.-Japan Coordinated Program for Masonry Building Research. Report No. 2.1-3. Ewing, Kariotis, Englekirk and Hart.

Nassar, A.A. and Krawinkler, H. (1991), "Seismic Demands for SDOF and MDOF Systems," Report No. 95, The John A. Blume Earthquake Engineering Center, Stanford University, Stanford, California.

Negro, P., Verzeletti, G., Molina, J., Pedretti, S., Lo Presti, D., and Pedroni, S. (1998), "Large-Scale Geotechnical Experiments On Soil-Foundation Interaction: (TRISEE Task 3)," European Commission, Joint Research Center, Special Publication No. I.98.73.

Newmark, N., and Hall, W. (1973). "Seismic Design Criteria for Nuclear Reactor Facilities," *Report No. 46*, Practices for Disaster Mitigation, National Bureau of Standards, U.S. Department of Commerce, pp. 209-236.

Newmark, N., and Hall, W. (1987). *Earthquake Spectra and Design,* EERI Monograph Series, Earthquake Engineering Research Institute, Oakland, California.

OpenSees (Open System for Earthquake Engineering Simulation) platform, developed by the Pacific Earthquake Engineering Research Center (PEER), at the University of California, Berkeley. http://opensees.berkeley.edu/

Ordaz, M. and Perez-Rocha, L.E. (1998) "Estimation of Strength-Reduction Factors for Elasto-Plastic Systems: A New Approach," Earthquake Eng. Struct. Dyn. 27, 889-901.

Paolucci, R. "Simplified Evaluation of Earthquake-Induced Permanent Displacements of Shallow Foundations," Journal of Earthquake Engineering Vol. 1, No. 3 (1997) 563-579.

Peng, M.-H., Elghadamsi, F.E. and Mohraz, B. (1988), "A Stochastic Procedure for Nonlinear Response Spectra," Proc. 9th World Conf. on Earthquake Engrg., Tokyo-Kyoto, Japan, Vol. V, pp. 1069-1074.

Phalen, J. D. (2003). "Physical Modeling of the Soil-Foundation Interaction of Spread Footings Subjected to Lateral Cyclic Loading," M.S. Thesis, University of California Davis

Paolucci, R. and Pecker, A. (1997). "Seismic bearing capacity of shallow strip foundations on dry soils." *Soils and Foundations*. Japanese Geotechnical Society. 37(3): 95-105.

Poulos, H. G., "Settlement of Isolated Foundations", in Soil Mechanics - Recent Developments, Eds. S. Valliapan, S. Hain, and I. K. Lee, William H. Sellen Pty., Zetland, 1975, pp. 181-212.

Psycharis, I. (1983) "Dynamics of Flexible Systems with Partial Lift-Off," Earthquake Engineering and Structural Dynamics, Vol. II, 501-521.

Psycharis, Ioannis N. (1981). "Dynamic Behavior of Rocking Structures allowed to Uplift," PhD Thesis, California Institute of Technology.

Reese, L.C., and O'Neill, M. W. (1988) "Field Load Tests of Drilled Shafts," Proceedings, Deep Foundations on Bored and Auger Piles, Ed. W. F. Van Impe, Balkema, Rotterdam, 1988, pp. 145-192.

Richards, R., Elms, D., and Budhu, M. "Seismic Bearing Capacity and Settlements of Foundations," Journal of Geotechnical Engineering, Vol. 119, No. 4, April, 1993.

Riddell, R. and Newmark, N. (1979), "Statistical Analysis of the Response of Nonlinear Systems Subjected to Earthquakes," Structural Research Series No. 468, Dept. of Civ. Engrg., University of Illinois, Urbana.

Riddell, R., Hidalgo, P., and Cruz, E. (1989), "Response Modification Factors for Earthquake Resistant Design of Short Period Structures," Earthquake Spectra, Vol. 5, No. 3, pp. 571-590.

Riddell, R. (1995), "Inelastic Design Spectra Accounting for Soil Conditions," Earthquake Engineering and Structural Dynamics, vol 24:1491-1510.

Rosebrook, Key R. (2001), "Moment Loading on Shallow Foundations: Centrifuge Test Data Archives," M.S. Thesis, University of California, Davis.

Rosebrook, K. R. and Kutter, B.L. (2001a), "Soil-Foundation Structure Interaction: Shallow Foundations. Centrifuge Data Report for the KRR01 Test Series," Center for Geotechnical Modeling Data Report UCD/CGMDR-01/01.

Rosebrook, K. R. and Kutter, B.L. (2001b), "Soil-Foundation Structure Interaction: Shallow Foundations. Centrifuge Data Report for the KRR02 Test Series," Center for Geotechnical Modeling Data Report UCD/CGMDR-01/01.

Rosebrook, K. R. and Kutter, B.L. (2001c), "Soil-Foundation Structure Interaction: Shallow Foundations. Centrifuge Data Report for the KRR03 Test Series," Center for Geotechnical Modeling Data Report UCD/CGMDR-01/01.

Rutenberg, A., Jennings, P.C. and Housner, G.W. (1982). "The response of Veterans Hospital Building 41 in the San Fernando Earthquake." *Earthquake Engineering and Structural Dynamics*. Vol. 10.

Sarma, S. and Iossifelis, I. "Seismic Bearing Capacity Factors of Shallow Strip Footings," Géotechnique 40, No. 2, 265-273.

Schultz, E. and Ing (1961), "Distribution of Stress Beneath a Rigid Foundation," Proceedings of the Fifth International Conference on Soil Mechanics and Foundation Engineering, Dunod, Paris. Vol. 1, Division 1-3A.

Selvadurai, A. and Rabaa, S. (1983). "Some Experimental Studies Concerning the Contact Stresses Beneath Interfering Rigid Strip Foundations Resting on a Granular Stratum," Canadian Geotechnical Journal, Vol. 20, No. 3.

Smoltczyk, H. (1967), "Stress Computation in Soil Media," Journal of the Soil Mechanics and Foundations Division, Proceedings of the American Society of Civil Engineers, Vol. 93, No. SM2.

Somerville, Paul and Collins, Nancy (2002). "Ground Motion Time Histories for the Van Nuys Building," Prepared for the PEER Methodology Testbeds Project. http://www.peertestbeds.net/van%20nuys.htm

Spanier, J. and Oldham, K (1987). *An Atlas of Functions*. Hemisphere Publishing Corporation, Washington.

Takada, T., Hwang, H.H.M. and Shinozuka, M. (1988), "Response Modification Factor for Multiple-Degree-of-Freedom Systems," Proc. 9th World Conf. on Earthquake Engrg., Tokyo-Kyoto, Japan, Vol. V, pp. 129-134.

Taylor, P.W., Bartlett, P.E. and Weissing, P.R. (1981). "Foundation rocking under earthquake loading." *In the Proceedings of the 10th International Conference on Soil Mechanics and Foundation Engineering*. Vol. 3: 313-322.

Terzaghi, Karl (1943). *Theoretical Soil Mechanics*. J. Wiley, New York. 510 pp.

Veletsos, A.S. and Newmark, N.M. (1960), "Effects of Inelastic Behavior on the Response of Simple Systems to Earthquake Ground Motions," Proc. 2nd World Conf. Earthquake Engrg., Japan, Vol. II, pp 895-912.

Veletsos, A.S. and Newmark, N.M. (1964), *Design Procedures for Shock Isolation Systems of Underground Protective Structures*, Air Force Weapons Laboratory, New Mexico, Technical Documentary Report No. RTD TDR-63-3096, III.

Veletsos, A.S., Newmark, N.M. and Chelapati, C.V. (1965), "Deformation Spectra for Elastic and Elastoplastic Systems Subjected to Ground Shock and Earthquake Motions," Proceedings 3rd World Conf. Earthquake Engrg., Wellington, New Zealand, Vol. 2, pp.663-680.

Veletsos, A.S. (1969), "Maximum Deformations of Certain Nonlinear Systems," Proc. 4th World Conf. Earthquake Eng., Santiago Chile, 2, 155-170.

Veletsos, A.S. and Vann, W.P. (1971), "Response of Ground-Excited Elasto-Plastic Systems," J. Struct. Div., ASCE 97, No. ST4, 1257-1281.

Vidic, T., Fajfar, P. and Fischinger, M. (1992), "A procedure for Determining Consistent Inelastic Design Spectra," Proc. Workshop on Nonlinear Seismic Analysis of RC Structures, Bled, Slovenia.

Ugural, A. C. and Fenster, S. K. (1995). *Advanced Strength and Applied Elasticity*. Prentice Hall, New Jersey.

Vijayvergiya, V. N. (1977). "Load-Movement Characteristics of Piles," Proceedings, Ports 77 Conference, American Society of Civil Engineers, Long Beach, California, March.

Wallace, J.W., Moehle, J.P. and Martinez-Cruzado, J. (1990). "Implications of the design of shear wall buildings using data from recent earthquakes." *In the Proceedings of the 4th National Conference on Earthquake Engineering*. Palm Springs, California.

Wang, Shaomin, Kutter, Bruce L., Chacko, Jacob M., Wilson, Daniel W., Boulanger, Ross W. and Abghari, Abbas (1998). “Nonlinear Seismic Soil-Pile Structure Interaction” Earthquake Spectra, Volume 14, No. 2.

Welch, Brent. B. (2000). Practical Programming in Tcl and Tk. Prentice Hall, New Jersey, third ed.172 pages.

Wiessing, P. R. (1979), "Foundation Rocking on Sand," School of Engineering Report No. 203, Universtiy of Auckland, New Zealand.

Yan, Liping (1998) "Nonlinear Load-Deformation Characteristics of Bridge Abutments and Footings under Cyclic Loading." Ph.D Dissertation, University of Southern California, December.

Yim, S.C. and Chopra, A.K. (1985). “Simplified earthquake analysis of multistory structures with foundation uplift.” *ASCE Journal of Structural Engineering*. 111(12): 2708-2731.

Winkler, E. (1867). Die Lehre von der Elasticitaet und Festigkeit. Prag, Dominicus.

Zeng, X. and Steedman, R. S. (1998) “Bearing capacity failure of shallow foundations in earthquakes,” Géotechnique 48, No. 2, 235-256.

Appendix A BNWF Mesh Generator Files: BNWFShallow.txt and BNWF_MAT.txt

Notes: BNWFShallow.txt is a mesh generator which creates a specified number of nodes, beam elements and zero-length elements to model the soil-structure interaction of a shallow foundation, as shown in the figure below. The structural foundation is also created through this process, as the zero-length elements are directly connected. After BNWFShallow has been run to create the foundation and soil-structure-interaction elements, a superstructure can be created, with a connection to the foundation at the central node of the foundation. The number of this node is globally created from the BNWFShallow and named "sn" for "starting node." BNWF_MAT.txt is called by BNWFShallow.txt throughout the creation process in order to create the proper subgrade finite element materials.

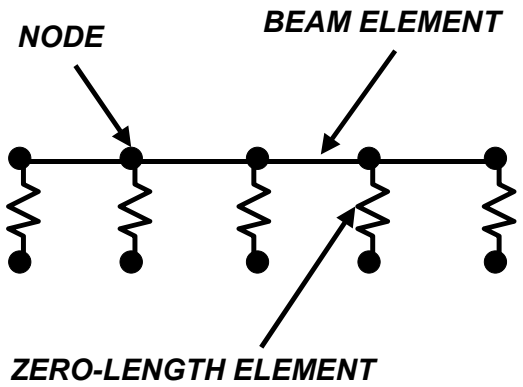

BNWFShallow.txt

```
##########################################################################
# FOR MORE INFORMATION ON BNWFShallow, please see the text:
# Harden, C. (2003).  Numerical modeling of the nonlinear cyclic response of shallow foundations.  C. Harden, T. Hutchinson, G. R. Martin, and B. L. Kutter. PEER report 2005/04. Berkeley, Calif.: Pacific Earthquake Engineering Research Center, University of California.
# PROPER REFERENCE TO THE ABOVE TEXT SHALL BE GIVEN IF THESE FILES
# ARE USED FOR ANY RESEARCH OR DESIGN PUBLICATION
##########################################################################
# ARGUMENTS -
## VERTICAL WINKLER MESH ARGUMENTS
# qult -- Ultimate Bearing Capacity of the foundation, in units of Force per Unit Area (F/L2)
# Kzm -- Vertical Global Stiffness of the foundation for a unit subgrade reaction of the middle region, in units of Force per unit Length (F/L)
# Kze -- Vertical Global Stiffness of the foundation for a unit subgrade reaction of the end region, in units of Force per unit Length (F/L)
# L -- Total Length of foundation, in units of Length (L)
# B -- Total Width of foundation, in units of Length (L)
# type -- Type of Ultimate Bearing Capacity Contact Pressure Distribution
#         -- 1 = Uniform, 2 = Triangular, 3 = Trapezoidal, 4 = Parabolic
# qip -- End Tip Resistance Ratio, which controls the shape of the Ultimate Bearing Capacity Contact Pressure Distribution
#    --  entered as a decimal ratio
# Lep -- End Length Percentage, entered as a decimal ratio
# TP -- percent tension capacity, entered as a decimal ratio of Qult
# ratiom -- spacing ratio for the middle region, entered as a decimal
# ratioe -- spacing ratio for the end region, entered as a decimal
# FEmat -- Material Type: 8 = ENT, 9 = Elastic, 10 = Qz Material, 11 = Parallel Hysteretic Material, 12 = ElasticPPGap material
# z50 -- displacement at which 50% of the load is mobilized
# soiltype -- indicates either sand or clay.  1 = clay, 2 = sand
## SLIDING CONSTANTS
# Cr -- Percent of Ultimate load at which the material changes from elastic to plastic behavior
# sn -- VALUE OF STARTING NODE FOR MESH GENERATOR.  SHOULD BE LARGER THAN ALL OTHER NODES IN THE MODEL
# FSECTION -- Previously Created Foundation Section Number (enter 0 for elastic, extremely rigid section
# Kf -- Sliding Stiffness due to friction (put 0 to omit), in units of Force per unit Length (F/L)
# Qf -- Sliding Capacity due to friction (put 0 to omit), in units of Force (F)
# KPEP -- Sliding Stiffness due to Passive Earth Pressure (put 0 to omit), in units of Force per unit Length (F/L)
# QPEP -- Sliding Capacity due to Passive Earth Pressure (put 0 to omit), in units of Force (F)
# crad -- value of radiation damping

proc BNWFShallow {qult Kzm Kze L B type qip Lep TP ratiom ratioe FEmat soiltype z50 Cr sn FSECTION Kf Qf KPEP QPEP crad cradx } {

    set depth 0
    global eletext
    global nodetext

    # CALCULATIONS FOR SPRING SPACING
    ########################################
    set Lmp [expr 1-2*$Lep]
    set nodesm [expr int(pow($ratiom,-1))+1]
    set Lmid [expr $Lmp*$L]
    set Aratiom [expr $ratiom*$Lmid*pow($L,-1)] ;# changed 03-0131 [expr $Lmid*pow($L*($nodesm-1),-1)]
```

```
    set nodese [expr int(pow($ratioe,-1))]
    set Lend [expr ($L-$Lmid)*0.5]
    set Aratioe [expr $ratioe*$Lend*pow($L,-1)] ;# [expr $Lend*pow($L*$nodese,-1)]
    set nodes [expr $nodesm+2*$nodese]
    set Aratio $Aratiom
    puts "middle nodes = $nodesm, end nodes = $nodese"
    puts "L = $L, Lmid = $Lmid, Lend = $Lend"
    if {$Lmp == 1} {
        puts "Zero end region"
        set nodes $nodesm
    }
    set remtest [expr $nodesm*0.5-int($nodesm*0.5)]
    if {$remtest == 0} { ;# even nodes
        puts "even nodes, rem = $remtest"
        set nodetest  [expr 0.5*$nodes]
        set nodetestm [expr 0.5*$nodesm]
    } elseif {$remtest == 0.5} { ;# odd nodes
        puts "odd nodes, rem = $remtest"
        set nodetest [expr 0.5*($nodes-1)]
        set nodetestm [expr 0.5*($nodesm-1)]
    }
    # FOUNDATION SECTION
    if {$FSECTION == 0} {
        # section Elastic $E $A $Iz
        set Efoundation [expr (1E10)]
        section Elastic 100 $Efoundation [expr pow($L,2)] [expr pow($L,3)]
        set FSECTION 100
    }
    # CREATE NODES AND ELEMENTS FROM CENTER OF FOOTING OUT
    ##########################################
    # INITIALIZE FOR MIDDLE REGION
    set Qtotal 0
    set ktotal 0
    # set z50i $z50globalZ
    set Ki $Kzm
    set i 0
    set node1 [expr $sn+1+10]
    set node2 [expr $sn+10]
    set flength [expr $ratiom*$Lmid]
    ###### START - BNWF_MAT : CALL FOR INDIVIDUAL SPRING STRENGTH AND STIFFNESS
###############
    set x 0
    set mcount 0
    source BNWF_MAT.txt
    ###### END - BNWF_MAT #################
    set testeven 1
    node $sn    [expr 0.5*$L]  [expr $depth]
    set eletext " "
    set nodetext " "
    set lengthtext " "
    ############################################################
    if {$remtest == 0.5} {
        #For ODD number of MIDDLE nodes this IF statement works
        set nodemn [expr $sn-7]
        node $nodemn    [expr 0.5*$L]  $depth
        fix $nodemn 1 1 1
        element zeroLength [expr 2*$i+$sn-2] $nodemn $sn -mat $mati -dir 2
```

```
        set eletext [expr 2*$i+$sn-2]
        set nodetext $sn
        set lengthtext 0
        set Qtotal $Qultx
        set ktotal $kzi
        puts "Qi = $Qultx, Qtotal = $Qtotal, ki = $kzi, ktotal = $ktotal"
        set MC 0  ;# MOMENT CALCULATION #############
        puts "created central element"
    }
    ####################
    set mcount 1
    set lastnoderight $sn
    set lastnodeleft $sn

    while {$i < $nodetest} {
        set x [expr $flength+$x]
        if {$i == 0} {
            if {$remtest == 0.5} {
                set x $flength
                puts "odd nodes"
            } elseif {$remtest == 0.0} {
                set x [expr 0.5*$flength]
                puts "even nodes"
            }
        }
        ############ START - BNWF_MAT ##############
        set mcount [expr $mcount+1]
        if {$i == [expr ($nodetest-1)]} {
            set Aratio [expr 0.5*$Aratioe]
        }
         if {$i == [expr ($nodetestm-1)]} {
            set Aratio [expr 0.5*$Aratiom+0.5*$Aratioe]
        }

        source BNWF_MAT.txt
        set Qtotal [expr $Qtotal+2*$Qultx]
        set ktotal [expr $ktotal+2*$kzi]
        # puts "Qi = $Qultx, Qtotal = $Qtotal, 2*ki = [expr 2*$kzi], ktotal = $ktotal"
        ############ END - BNWF_MAT ##############
        node [expr 2*$i+$node1]  [expr 0.5*$L+$x] $depth
        node [expr 2*$i+$node2]  [expr 0.5*$L+$x] $depth
        fix [expr 2*$i+$node1] 1 1 1

        element zeroLength [expr 2*$i+$sn] [expr 2*$i+$node1]  [expr 2*$i+$node2] -mat $mati -dir 2
        node [expr 2*$i+$node1+$nodes]  [expr 0.5*$L-$x] $depth
        node [expr 2*$i+$node2+$nodes]  [expr 0.5*$L-$x] $depth
        fix [expr 2*$i+$node1+$nodes] 1 1 1
        element zeroLength [expr 2*$i+$sn+$nodes] [expr 2*$i+$node1+$nodes]  [expr 2*$i+$node2+$nodes] -mat
$mati -dir 2

        set eletext "[expr 2*$i+$sn+$nodes] $eletext [expr 2*$i+$sn]"
        set nodetext "[expr 2*$i+$node2+$nodes]  $nodetext [expr 2*$i+$node2]"
        set lengthtext "-$x $lengthtext $x"

global ASF
global ES
global If
```

```
        element elasticBeamColumn  [expr 2*$i+$sn-1] [expr 2*$i+$node2] $lastnoderight $ASF $ES $If 1
        element elasticBeamColumn  [expr 2*$i+$sn+$nodes-1] [expr 2*$i+$node2+$nodes] $lastnodeleft $ASF $ES
$If 1

        set lastnoderight [expr 2*$i+$node2]
        set lastnodeleft [expr 2*$i+$node2+$nodes]

        incr i
        if {$i >= $nodetestm} { ;# changed 03-0121 $nodetestm-1
            puts "End region generation started"
            set flength [expr $ratioe*$Lend]
            set Aratio $Aratioe
            set Ki $Kze ;# added 03-0125
        }
    }

    puts "Last two nodes created for [expr $nodes] node set, node [expr 2*($i-1)+$sn] (right) and node [expr 2*($i-
1)+$sn+$nodes] (left)."
    puts "2*x = [expr 2*$x], L = [expr $L]"

    ######## ADD ELEMENT(S) FOR SLIDING ####################
    if {($Qf == 0 & $QPEP == 0) || ($Kf == 0 & $KPEP == 0)} {
        fix $sn  1 0 0 ;#FREE FOR ZEROLENGTH ELEMENTS WITH LATERAL CAPACITY
        puts "base fixed against lateral movement"
    } else {
        global nodebs
        global eleBS
        global eleKP
        set nodebs [expr $sn-10]
        set eleBS $nodebs
        set eleKP [expr $sn-9]
        node $nodebs  [expr 0.5*$L]  [expr $depth]
        fix $nodebs 1 1 1
        # element for sliding
        if {$Qf != 0} {
            element zeroLength $eleBS $sn $nodebs -mat 5 -dir 1
            puts "sliding element created"
         }
        # element for earth pressure
        if {$QPEP != 0} {
            element zeroLength $eleKP $sn $nodebs -mat 6 -dir 1
            puts "passive earth pressure element created"
        }
    }

    puts "Qult = [expr $qult*$L*$B], sum of elements Qsum = $Qtotal"
    puts "KZ = [expr $Kzm], sum of elements Ktotal = $ktotal"
    puts "elements: $eletext"
    puts "nodes: $nodetext"
}
```

BNWF_MAT.txt

```
# THIS FILE IS CALLED FROM BNWFShallow.txt, in order to create the
# material models at each iteration of the mesh generator

##########################################################################
# FOR MORE INFORMATION ON BNWF_MAT, PLEASE SEE THE TEXT:
# Numerical modeling of the nonlinear cyclic response of shallow foundations.  C. Harden, T. Hutchinson, G. R. Martin, and B. L. Kutter. PEER report 2005/04. Berkeley, Calif.: Pacific Earthquake Engineering Research Center, University of California.
# PROPER REFERENCE TO THE ABOVE TEXT SHALL BE GIVEN IF THESE FILES
# ARE USED FOR ANY RESEARCH OR DESIGN PUBLICATION
##########################################################################

set qi [expr $qip*$qult]

if {$type == 1} {  ; #UNIFORM DISTRIBUTION
set qx $qult
}
if {$type == 2} {  ; #TRIANGULAR DISTRIBUTION
set a [expr -4*($qult-$qi)*pow($L,-1)]
set h [expr 2*$qult-$qi]
set qx [expr $h+$a*$x]
}
if {$type == 3} {  ; #TRAPEZOIDAL DISTRIBUTION
set TLm [expr $TLmp*$L]
set a [expr -4*$L*($qult-$qi)*pow((pow($L,2)-pow($TLm,2)),-1)]
set h [expr 2*$L*($qult-$qi)*pow(($L+$TLm),-1)]
set b [expr $qi+2*pow($L,2)*($qult-$qi)*pow((pow($L,2)-pow($TLm,2)),-1)]
    set xtest [expr $TLm*0.5*$L] ;#added *$L 052302
    if {$x <= $xtest} {
    set qx [expr $qi+$h]
    }
    if {$x > $xtest} {
    set qx [expr $a*$x+$b]
    }
}
if {$type == 4} { ; #PARABOLIC DISTRIBUTION
set a [expr -6*($qult-$qi)*pow(pow($L,2),-1)]
set h [expr 1.5*($qult-$qi)]
set qx [expr $qi+$h+$a*pow($x,2)]

}
if {$type == 5} {  ; #INVERSE PARABOLIC DISTRIBUTION
set a [expr 12*($qult-$qi)*pow(pow($L,2),-1)]
set qx [expr $qi+$a*pow($x,2)]
}

if {$qx == 0} {
set qx 0.0001
puts "qx zero, set to 0.0001-- x = [expr $x], type [expr $type], mat [expr $FEmat], nodes [expr $nodes]"
}
if {$qx < 0} {
set qx 0.0001
puts "qx negative, set to 0.0001-- x = [expr $x], type [expr $type], mat [expr $FEmat], nodes [expr $nodes]"
}
```

```
set Qultx [expr $L*$B*$Aratio*$qx]

#########################################################################
#########################################################################
# CONSTANT MATERIALS (STEEL, FRICTION, LATERAL EARTH PRESSURE) Kf Qf KPEP QPEP
if {$x == 0} {
     if {$Qf != 0 & $Kf != 0} {
        if { $soiltype == 1 } { set zt50 [expr 0.708*$Qf*pow($Kf,-1)] }
        if { $soiltype == 2 } { set zt50 [expr 2.05*$Qf*pow($Kf,-1)] }
        uniaxialMaterial TzSimple1 5 $soiltype $Qf $zt50 $cradx
    }
    if {$QPEP != 0 & $KPEP != 0 } {
        if { $soiltype == 1 } { set y50 [expr 8*$QPEP*pow($KPEP,-1)] }
        if { $soiltype == 2 } { set y50 [expr 0.542*$QPEP*pow($KPEP,-1)] }
        uniaxialMaterial PySimple1 6 2 $QPEP $y50 0
    }
}

#########################################################################
# SFSI MATERIALS

set kzi [expr $Ki*$Aratio]

if { $FEmat == 8} {
    uniaxialMaterial ENT [expr 1000+$mcount] $kzi
    set mati [expr 1000+$mcount]
}
if {$FEmat == 9} {
    uniaxialMaterial Elastic [expr 1000+$mcount] $kzi
    set mati [expr 1000+$mcount]
}

########################################
# Q-Z MATERIAL CONSTANTS
if {$soiltype == 1} {
    # clay soil
    set c 0.35
    set n 1.2
    set Kfar 0.525
} elseif { $soiltype == 2 } {
    # sand soil
    set c 12.3
    set n 5.5
    set Kfar 1.39
}
########################################

#####################################
# QZ MATERIAL
#####################################
if {$FEmat == 10} {
    set QultQZ [expr $Qultx]
    set z50i [expr $Kfar*$Qultx*pow($kzi,-1)]

    uniaxialMaterial QzSimple1 [expr 1000+$mcount] $soiltype $QultQZ $z50i $TP $crad

    set mati [expr 1000+$mcount]
```

```
}

#######################################
# PARALLEL HYSTERETIC MATERIAL
#######################################
if { $FEmat == 11} {
    set c 0.952
    set n 0.851
    set Cr 0.1
    set count 1
    set qti 0
    set qzi 0
    set qtotal 0

    set BETA 0
    set C 0.99
    set 1ofn [expr -1*pow($n,-1)]
    set zo [expr $Cr*$z50]
    set zqo [expr $c*$z50*(-1+pow(1-$Cr,$1ofn))]
    set pinchx 1 ;# 1
    set pinchy 0 ;# 0.1

    set Cpr 1
    set zmax 10001
    set zlast 10000
    set zlastT $zlast
    set ksum 0
    set ksumT 0

# CALCULATE CUTOFF VALUE
#########################################################
set Cpr 0.8
set Cpri 0.7
set zmax [expr $z50*pow(0.037,-1)]
set countX 0
while {$Cpr != $Cpri && $countX < 1000} {
    set Cpri $Cpr
    set initialz [expr $Cr*$Qultx*pow(2*$kzi,-1)]
    set qz [expr $Cpr*$Qultx]
    set qratio [expr (1-$qz*pow($Qultx,-1))*pow(1-$Cr,-1)]
    set zatq [expr $initialz+$c*$z50*(-1+pow($qratio,$1ofn))]
    if { $zatq > $zmax } { set Cpr [expr $Cpr*(1-0.01*($zatq-$zmax)*pow($zmax,-1))] }
    if { $zatq < $zmax } { set Cpr [expr $Cpr*(1+0.01*($zmax-$zatq)*pow($zmax,-1))] }
if {$Cpr >= 1 || $Cpr < 0 } {set Cpr [expr 1.01*$Cr] }
incr countX
}
puts "count = $countX"
puts "Cpr = $Cpr"
set zmax 10000
set CrMax [expr 0.99*$Cpr]
#######################

    set mp1 [expr $Cr+($CrMax-$Cr)*0.999]
    set mp2 [expr $Cr+($CrMax-$Cr)*0.99]
    set mp3 [expr $Cr+($CrMax-$Cr)*0.98]
    set mp4 [expr $Cr+($CrMax-$Cr)*0.975]
    set mp5 [expr $Cr+($CrMax-$Cr)*0.95]
```

```
    set mp6 [expr $Cr+($CrMax-$Cr)*0.925]
    set mp7 [expr $Cr+($CrMax-$Cr)*0.9]
    set mp8 [expr $Cr+($CrMax-$Cr)*0.8]
    set mp9 [expr $Cr+($CrMax-$Cr)*0.7]
    set mp10 [expr $Cr+($CrMax-$Cr)*0.6]
    set mp11 [expr $Cr+($CrMax-$Cr)*0.4]
    set mp12 [expr $Cr+($CrMax-$Cr)*0.2]
    set mp13 [expr 2*$Cr*pow(3,-1)]
    set mp14 [expr 1*$Cr*pow(3,-1)]
set mpall "$mp1 $mp2 $mp3 $mp4 $mp5 $mp6 $mp7 $mp8 $mp9 $mp10 $mp11 $mp12 $Cr 0"
    foreach {C} { $mp1 $mp2 $mp3 $mp4 $mp5 $mp6 $mp7 $mp8 $mp9 $mp10 $mp11 $mp12 $Cr 0 } {

        # CYCLE 1: FIRST PASS - CALCULATE STIFFNESS
        ###################################
        # DEFINE POINTS ALONG CURVE
        ###########################

        set initialz [expr $Cr*$Qultx*pow(2*$kzi,-1)]
        set qz [expr $C*$Qultx]
        set qzi [expr $Cpr*$Qultx-$qz]
        set qzT [expr $TP*$qz]
        set qziT [expr $TP*$qzi]

        if {[expr $C] > $Cr} {
            set qratio [expr (1-$qz*pow($Qultx,-1))*pow(1-$Cr,-1)]
            set zatq [expr $initialz+$c*$z50*(-1+pow($qratio,$1ofn))]
        }


        if {[expr $C] == $Cr} { set zatq $initialz }
        if {[expr $C] == 0} { set zatq 0 }

        set zatqT [expr -1*$z50*0.5*(1+($TP*$Qultx)*pow($qzT-$TP*$Qultx,-1))]

        # CALCULATE STIFFNESS TO MATCH CURVE
        ################################################

        set kmatch [expr ($qzi)*pow(($zlast-$zatq),-1)]
        set kC [expr $kmatch-$ksum]
        set qnew [expr $kC*$zlast]
        set kmatchT [expr ($qziT)*pow(($zlastT-$zatqT),-1)]
        set kCT [expr $kmatchT-$ksumT]
        set qnewT [expr $kCT*$zlastT]
        uniaxialMaterial ElasticPPGap [expr 1000*(1+$mcount)+$count] $kC -$qnew 0
        set ksum [expr $ksum+$kC]
        set ksumT [expr $ksumT+$kCT]
        set zlast $zatq
        set zlastT $zatqT
        set Cpr $C
        if {$count == 1} { set matTEXT [expr 1000*(1+$mcount)+$count]}
        if {$count > 1} { set matTEXT "$matTEXT [expr 1000*(1+$mcount)+$count]"}

        set count [expr $count+1]
        set qtotal [expr $qtotal+$qzi]
    }
    uniaxialMaterial Parallel [expr 200+$mcount] [expr 1000*(1+$mcount)+1] [expr 1000*(1+$mcount)+2] [expr
1000*(1+$mcount)+3] [expr 1000*(1+$mcount)+4] [expr 1000*(1+$mcount)+5] [expr 1000*(1+$mcount)+6] [expr
```

```
1000*(1+$mcount)+7] [expr 1000*(1+$mcount)+8] [expr 1000*(1+$mcount)+9] [expr 1000*(1+$mcount)+10]
[expr 1000*(1+$mcount)+11] [expr 1000*(1+$mcount)+12] [expr 1000*(1+$mcount)+13] [expr
1000*(1+$mcount)+14] ;# [expr 1000*(1+$mcount)+15] [expr 1000*(1+$mcount)+16] ;#
    uniaxialMaterial Elastic  [expr 400+$mcount] [expr 2*$kzi]
    uniaxialMaterial Series [expr 600+$mcount] [expr 200+$mcount] [expr 400+$mcount]
    set mati [expr 600+$mcount]
    # puts "Qx = $Qultx, Qsumi = $qtotal"
}

if {$FEmat == 12} {
    uniaxialMaterial ElasticPPGap [expr 1000+$mcount] $kzi -$Qultx 0
    set mati [expr 1000+$mcount]
}

puts "mcount = $mcount"
```

Appendix B Static Simulation Comparisons

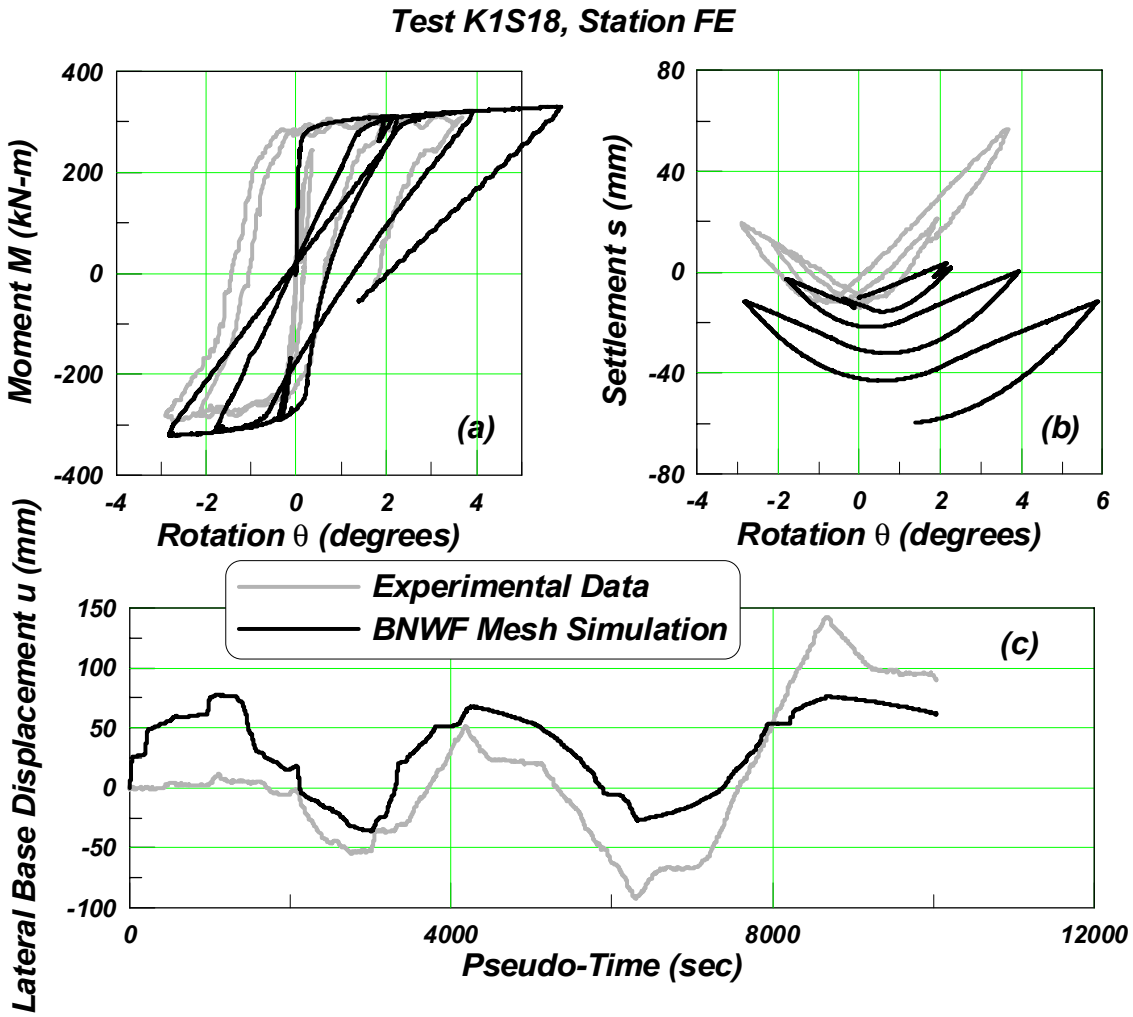
Test K1S18, Station FE
Moment M (kN-m)
400
200
0
-200
-400
-4
-2
0
2
4
Rotation θ (degrees)
(a)
Settlement s (mm)
80
40
0
-40
-80
-4
-2
0
2
4
6
Rotation θ (degrees)
(b)
Experimental Data
BNWF Mesh Simulation
Lateral Base Displacement u (mm)
150
100
50
0
-50
-100
0
4000
8000
12000
Pseudo-Time (sec)
(c)

Test K2S21, Station AE

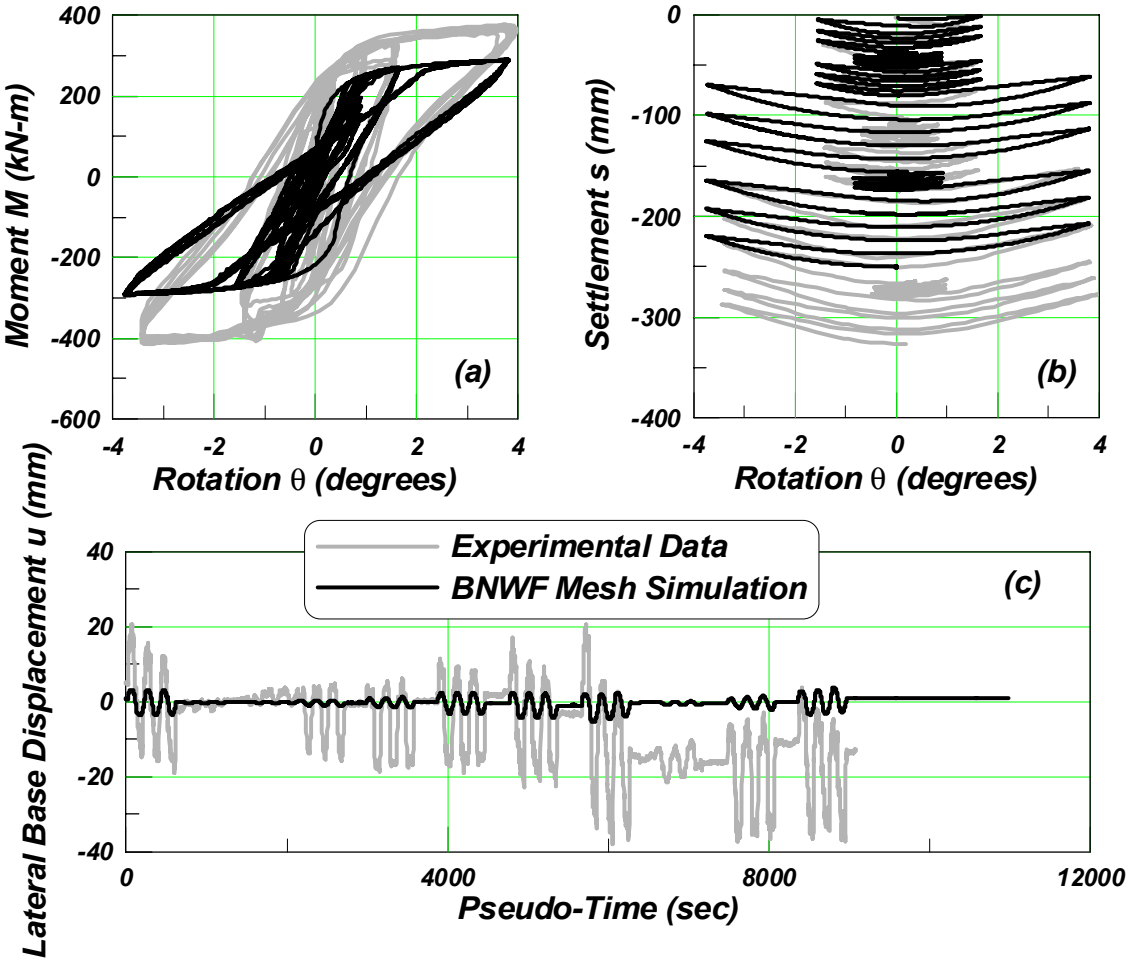

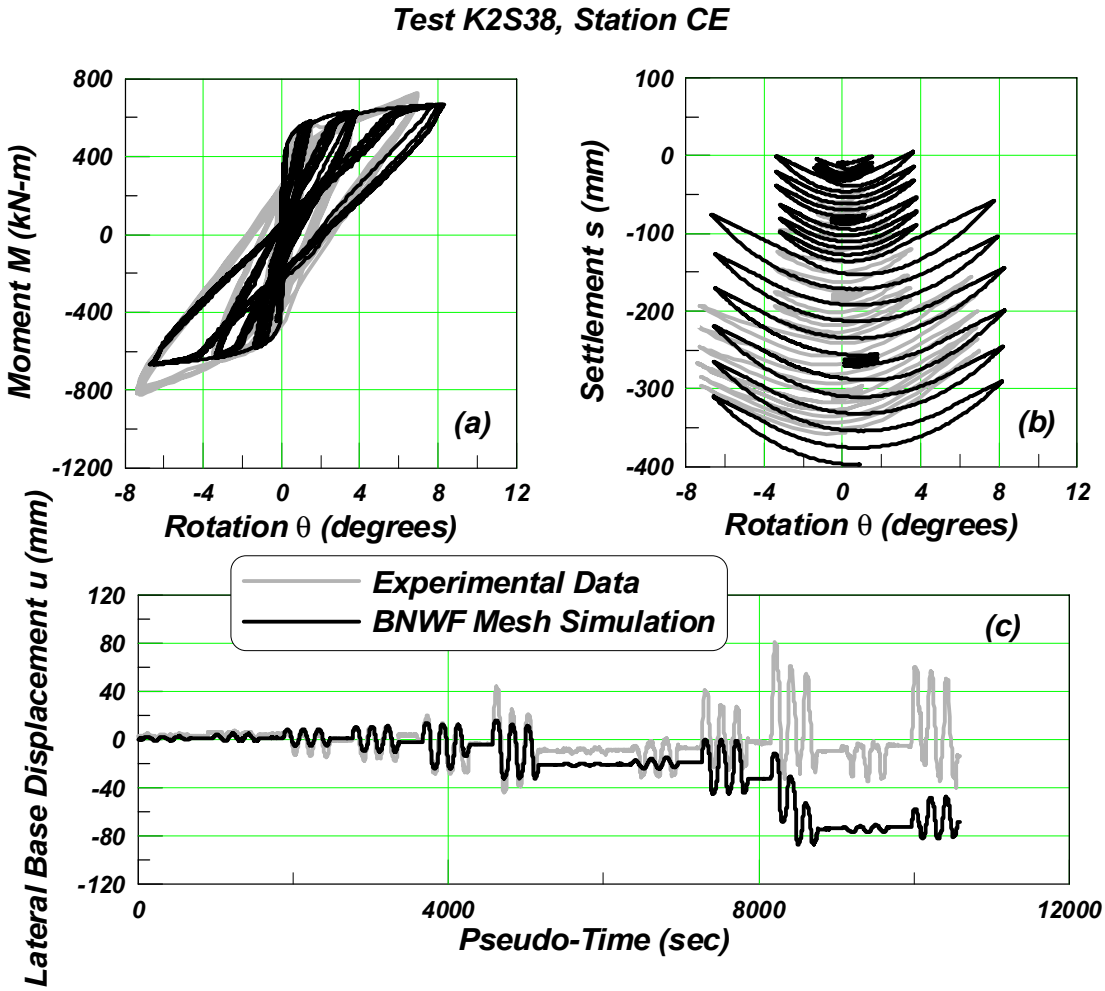
Test K2S38, Station CE
Moment M (kN-m)
800
400
0
-400
-800
-1200
-8
-4
0
4
8
12
Rotation θ (degrees)
(a)
Settlement s (mm)
100
0
-100
-200
-300
-400
Rotation θ (degrees)
(b)
Experimental Data
BNWF Mesh Simulation
Lateral Base Displacement u (mm)
120
80
40
0
-40
-80
-120
0
4000
8000
12000
Pseudo-Time (sec)
(c)

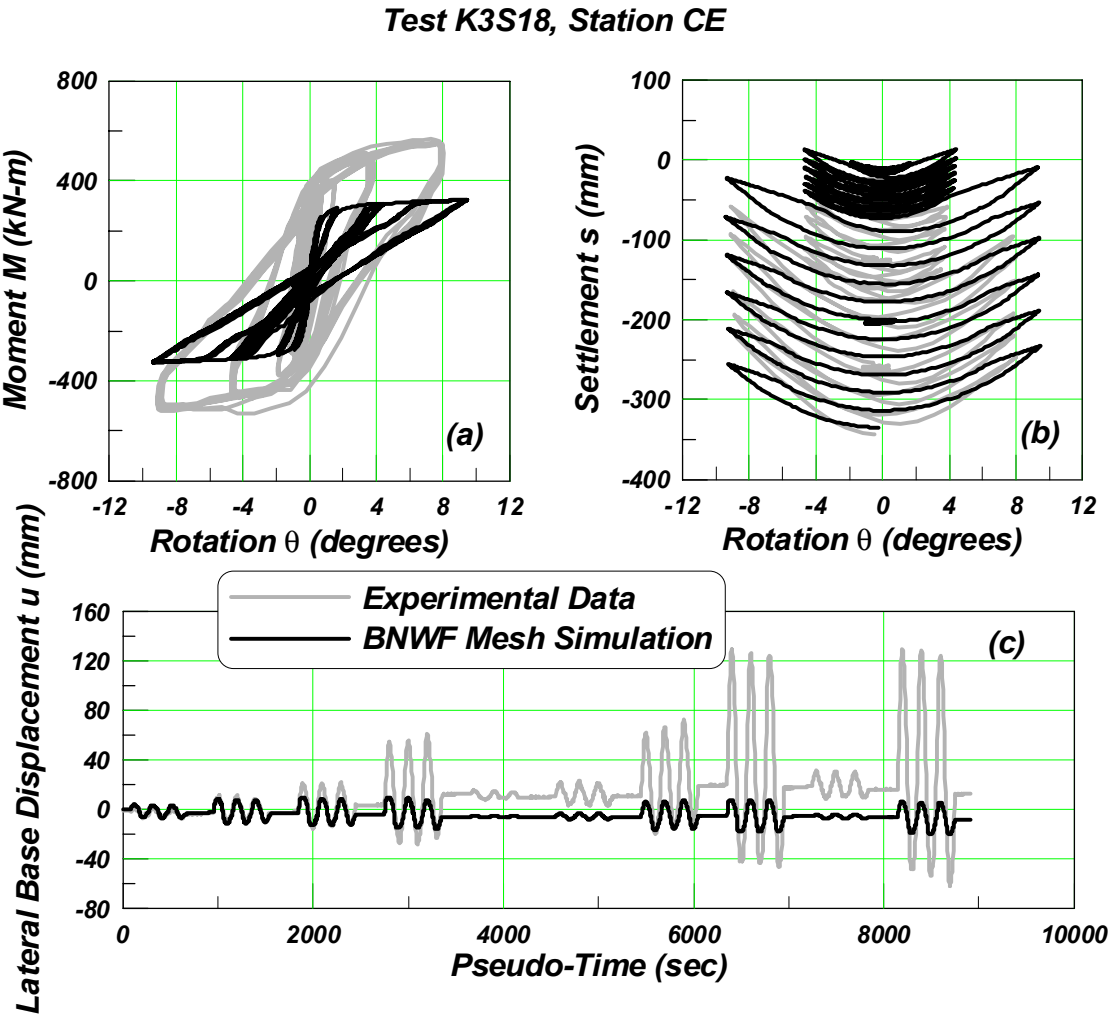
Test K3S18, Station CE
Moment M (kN-m)
800
400
0
-400
-800
-12
-8
-4
0
4
8
12
Rotation θ (degrees)
(a)
Settlement s (mm)
100
0
-100
-200
-300
-400
Rotation θ (degrees)
(b)
Experimental Data
BNWF Mesh Simulation
Lateral Base Displacement u (mm)
160
120
80
40
0
-40
-80
0
2000
4000
6000
8000
10000
Pseudo-Time (sec)
(c)

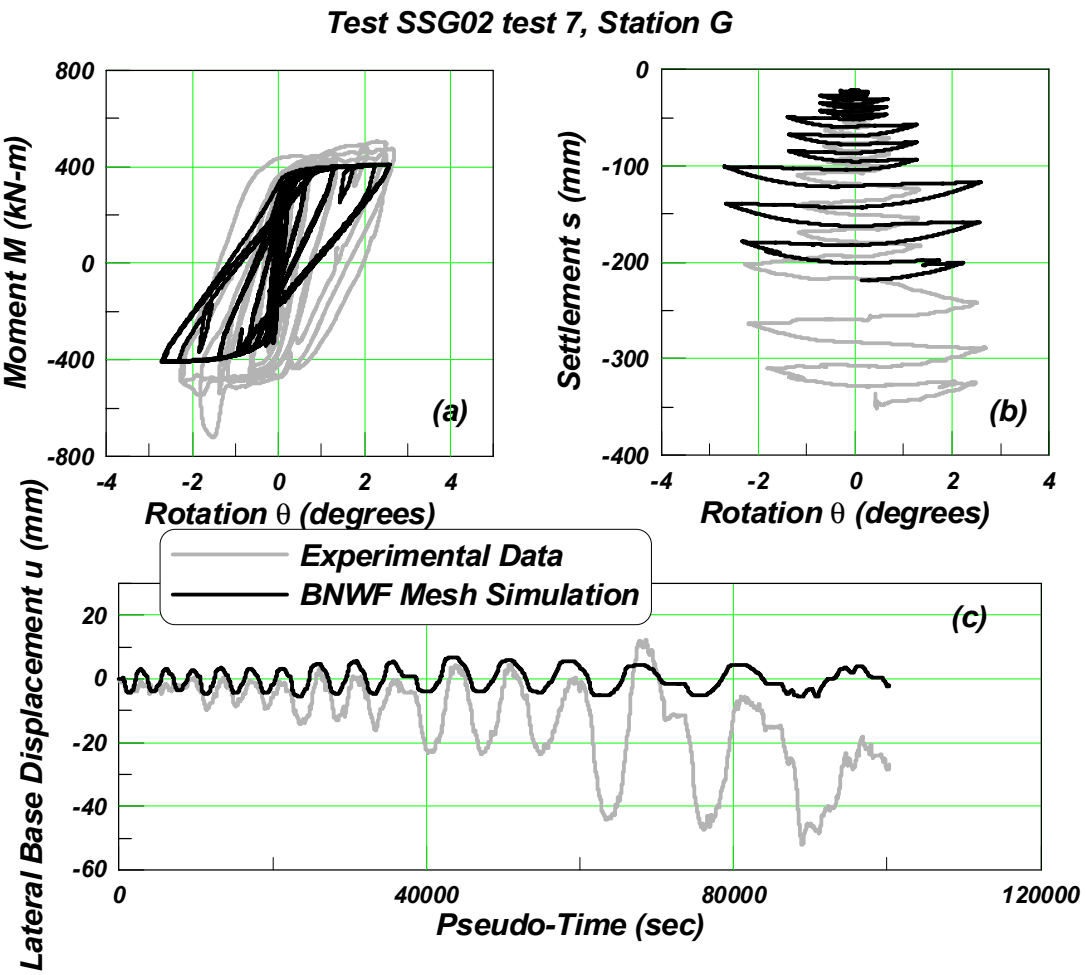
Test SSG02 test 7, Station G
Moment M (kN-m)
800
400
0
-400
-800
-4
-2
0
2
4
Rotation θ (degrees)
(a)
Settlement s (mm)
0
-100
-200
-300
-400
Rotation θ (degrees)
(b)
Experimental Data
BNWF Mesh Simulation
Lateral Base Displacement u (mm)
20
0
-20
-40
-60
0
40000
80000
120000
Pseudo-Time (sec)
(c)

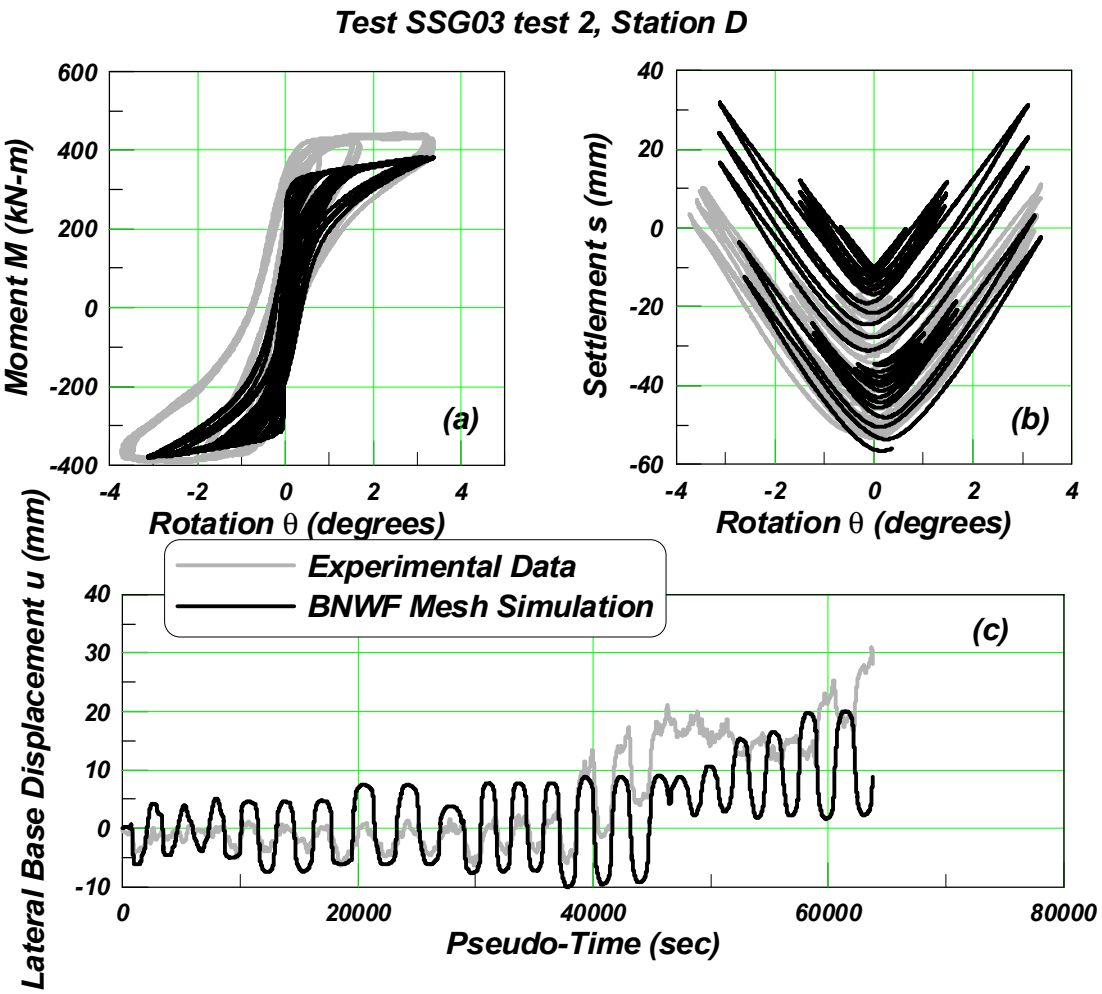
Test SSG03 test 2, Station D
Moment M (kN-m)
600
400
200
0
-200
-400
-4
-2
0
2
4
Rotation θ (degrees)
(a)
Settlement s (mm)
40
20
0
-20
-40
-60
-4
-2
0
2
4
Rotation θ (degrees)
(b)
Experimental Data
BNWF Mesh Simulation
Lateral Base Displacement u (mm)
40
30
20
10
0
-10
0
20000
40000
60000
80000
Pseudo-Time (sec)
(c)

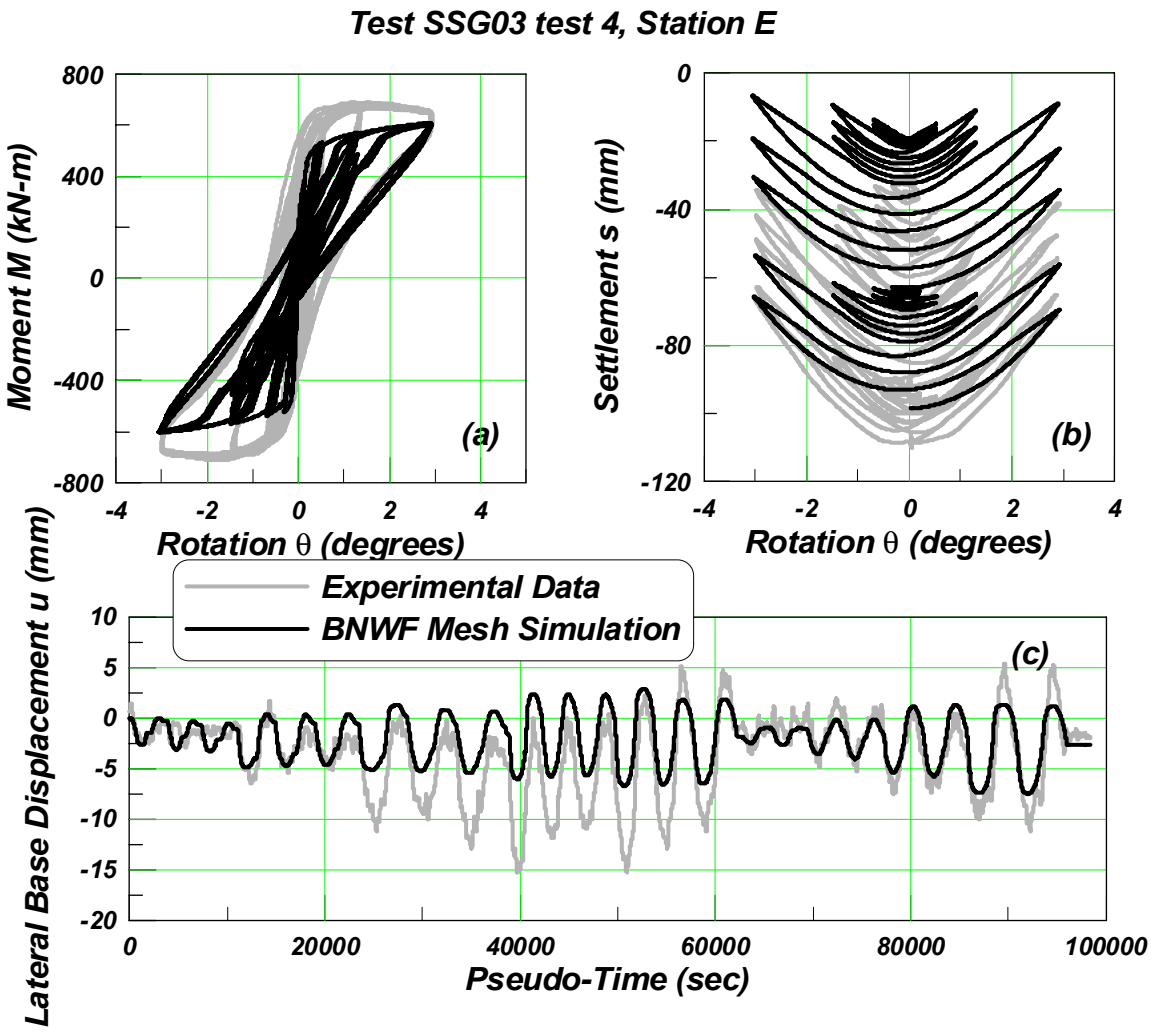
Test SSG03 test 4, Station E
Moment M (kN-m)
800
400
0
-400
-800
-4
-2
0
2
4
Rotation θ (degrees)
(a)
Settlement s (mm)
0
-40
-80
-120
Rotation θ (degrees)
(b)
Experimental Data
BNWF Mesh Simulation
Lateral Base Displacement u (mm)
10
5
0
-5
-10
-15
-20
0
20000
40000
60000
80000
100000
Pseudo-Time (sec)
(c)

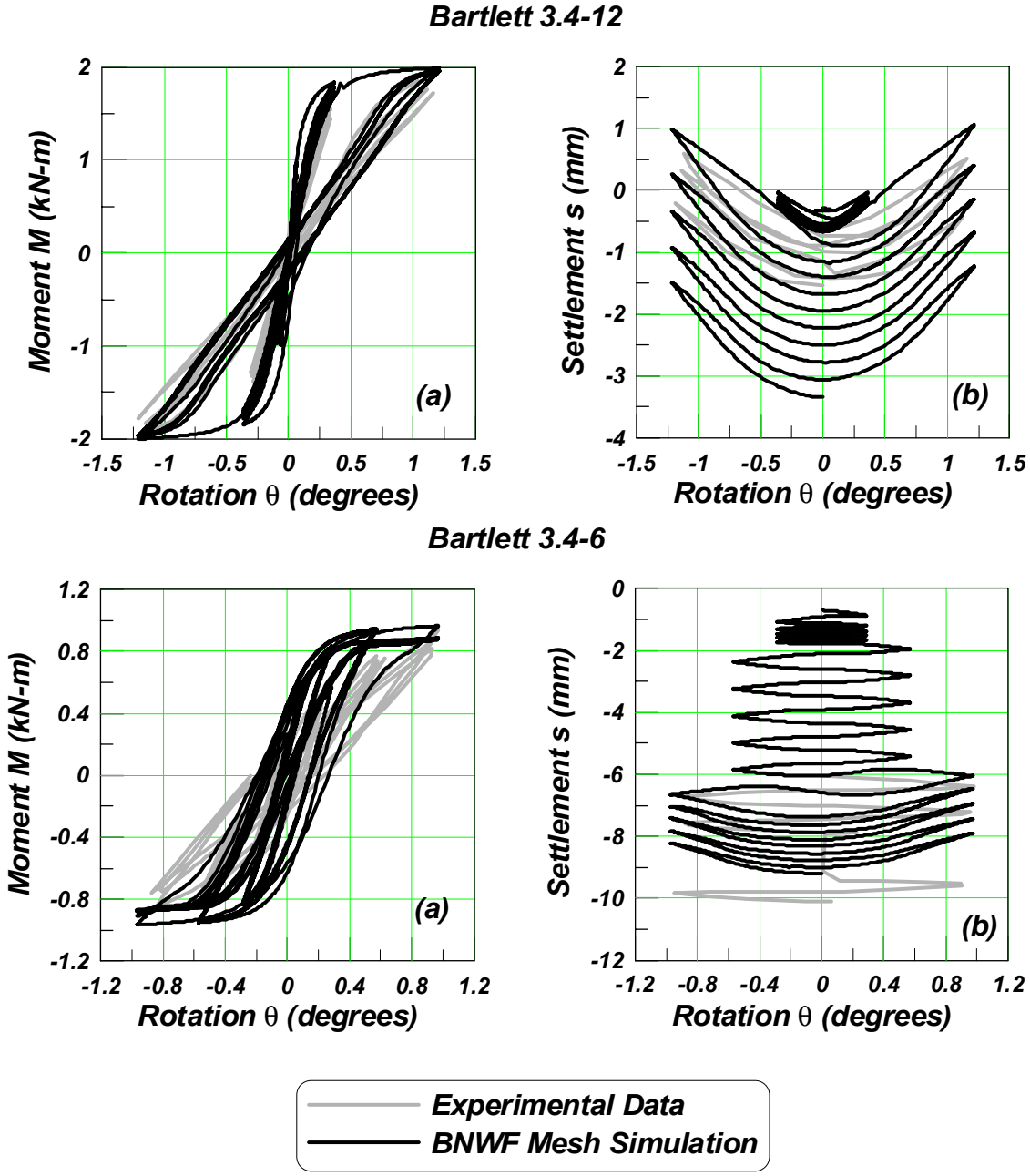
Bartlett 3.4-12
Moment M (kN-m)
Rotation θ (degrees)
(a)
Settlement s (mm)
Rotation θ (degrees)
(b)
Bartlett 3.4-6
Moment M (kN-m)
Rotation θ (degrees)
(a)
Settlement s (mm)
Rotation θ (degrees)
(b)
Experimental Data
BNWF Mesh Simulation

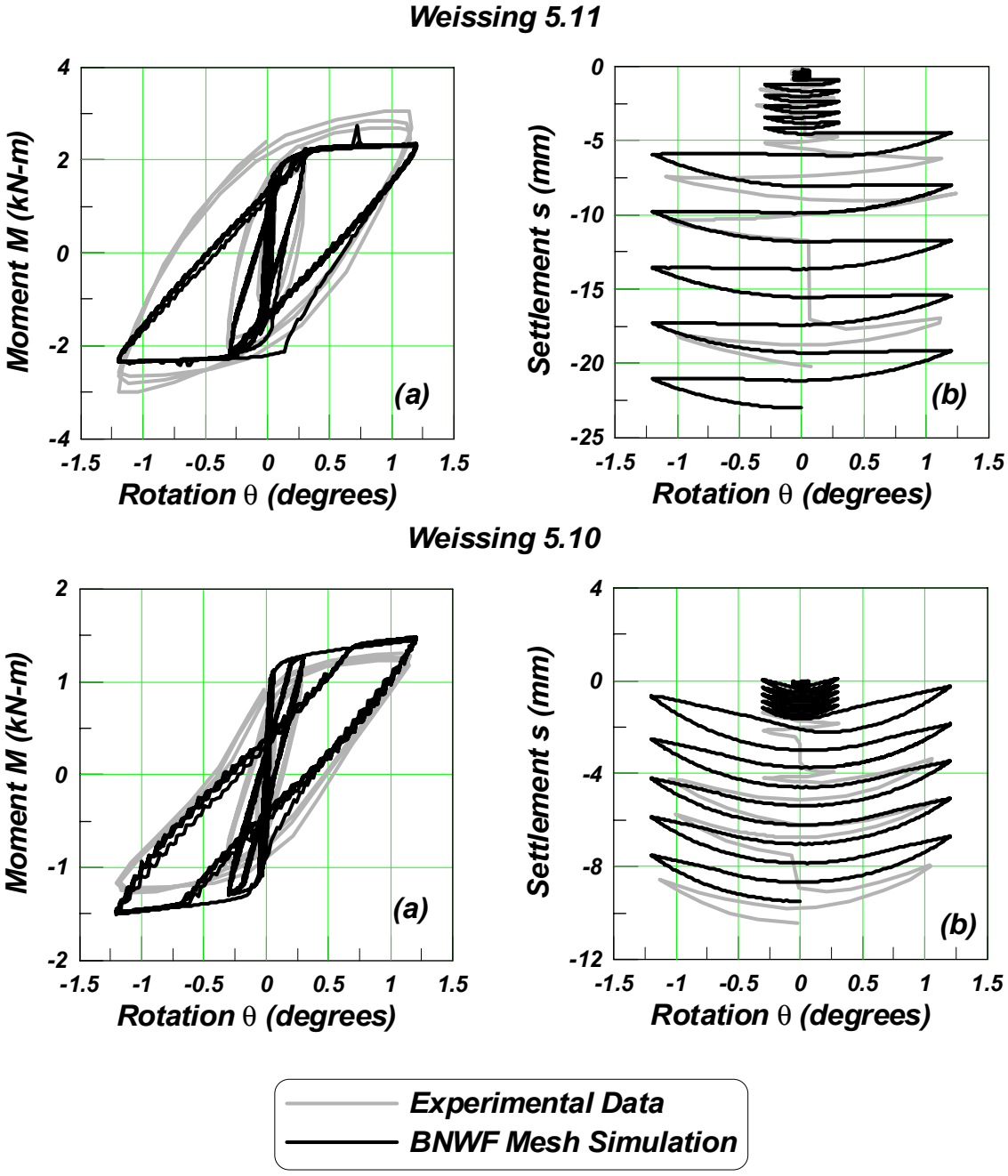
Weissing 5.11
Moment M (kN-m)
Rotation θ (degrees)
(a)
Settlement s (mm)
Rotation θ (degrees)
(b)
Weissing 5.10
Moment M (kN-m)
Rotation θ (degrees)
(a)
Settlement s (mm)
Rotation θ (degrees)
(b)
Experimental Data
BNWF Mesh Simulation

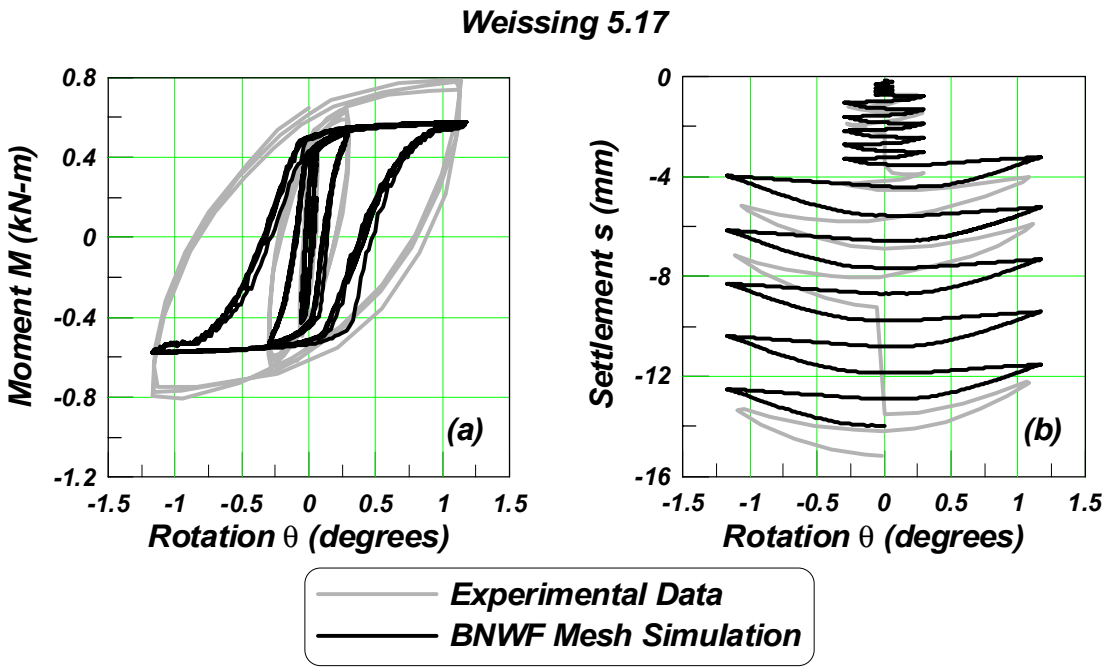
Weissing 5.17
Moment M (kN-m)
0.8
0.4
0
-0.4
-0.8
-1.2
-1.5
-1
-0.5
0
0.5
1
1.5
Rotation θ (degrees)
(a)
Settlement s (mm)
0
-4
-8
-12
-16
Rotation θ (degrees)
(b)
Experimental Data
BNWF Mesh Simulation

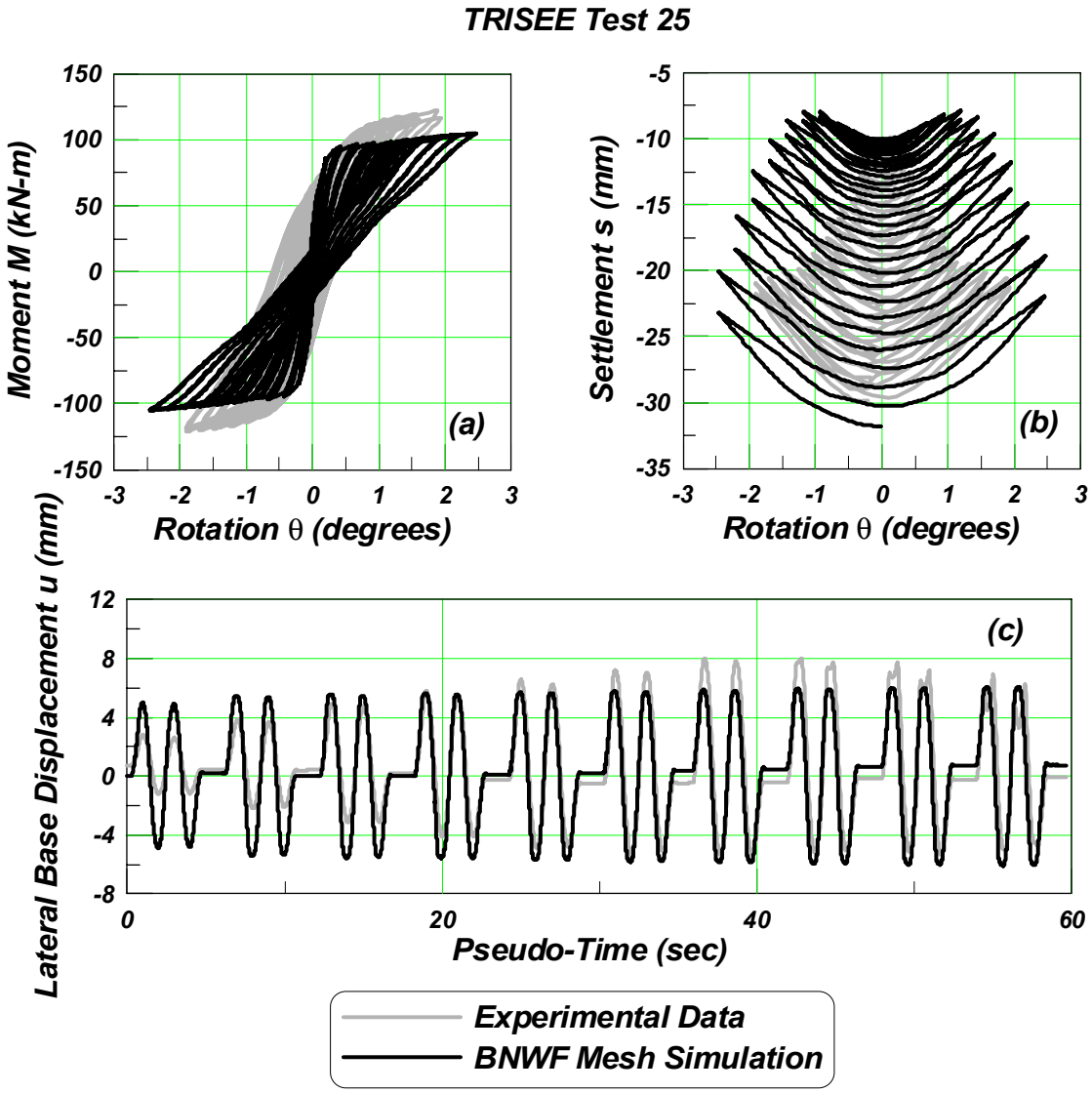
TRISEE Test 25
Moment M (kN-m)
150
100
50
0
-50
-100
-150
-3
-2
-1
0
1
2
3
Rotation θ (degrees)
(a)
Settlement s (mm)
-5
-10
-15
-20
-25
-30
-35
Rotation θ (degrees)
(b)
Lateral Base Displacement u (mm)
12
8
4
0
-4
-8
0
20
40
60
Pseudo-Time (sec)
(c)
Experimental Data
BNWF Mesh Simulation

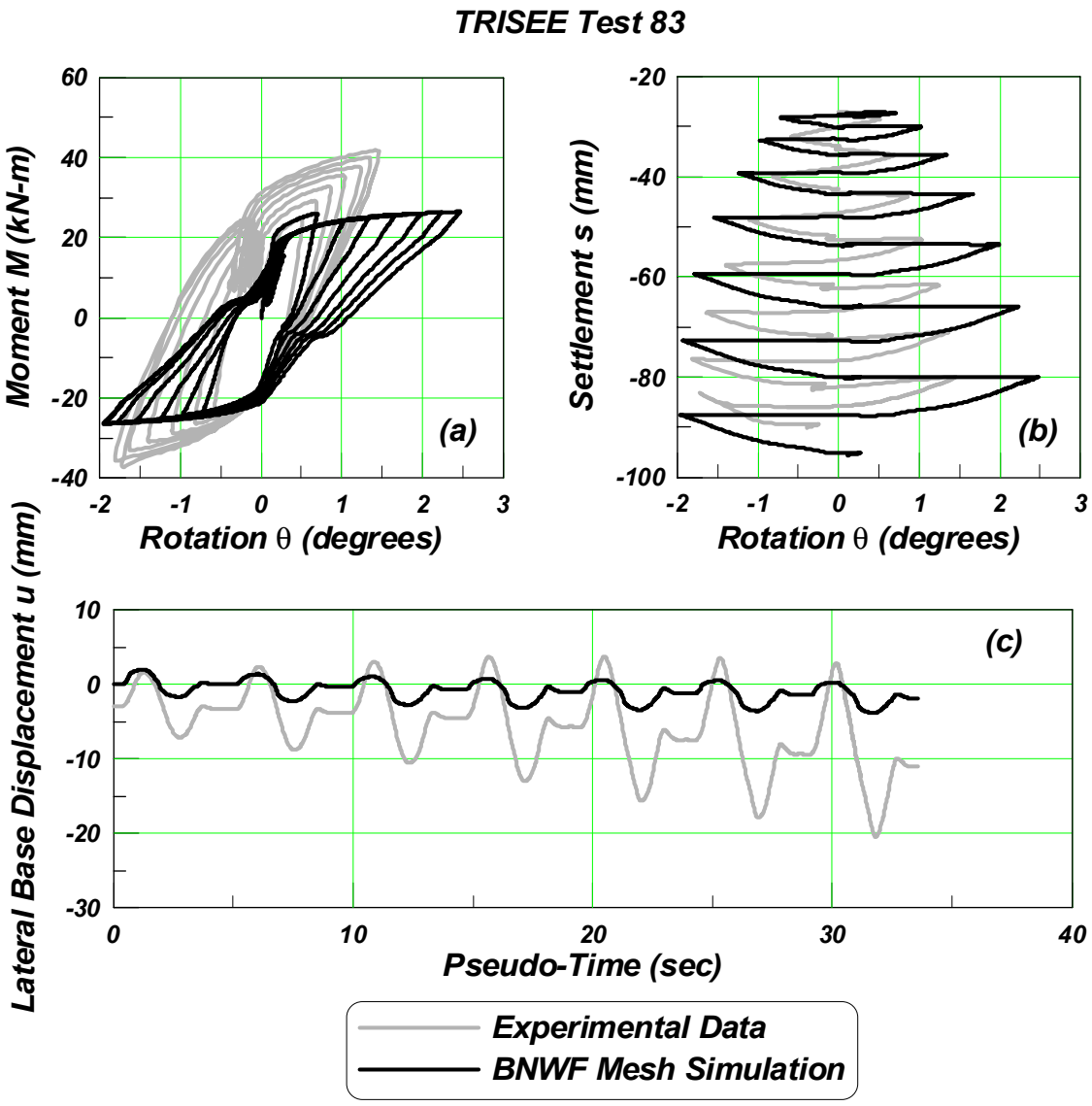
TRISEE Test 83
Moment M (kN-m)
60
40
20
0
-20
-40
-2
-1
0
1
2
3
Rotation θ (degrees)
(a)
Settlement s (mm)
-20
-40
-60
-80
-100
Rotation θ (degrees)
(b)
Lateral Base Displacement u (mm)
10
0
-10
-20
-30
0
10
20
30
40
Pseudo-Time (sec)
(c)
Experimental Data
BNWF Mesh Simulation

Appendix C Dynamic Simulation Comparisons

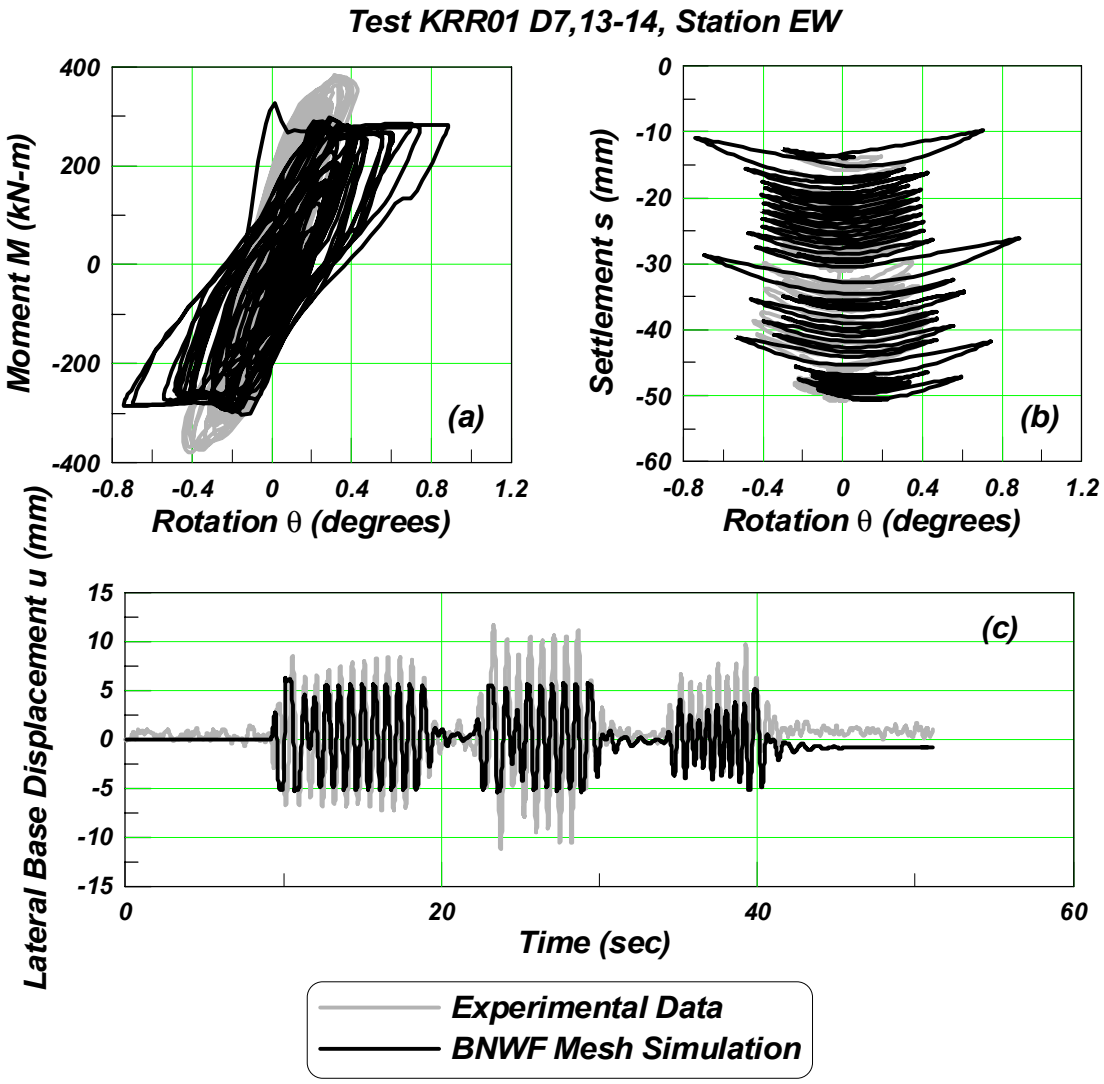
Test KRR01 D7,13-14, Station EW
Moment M (kN-m)
400
200
0
-200
-400
-0.8
-0.4
0
0.4
0.8
1.2
Rotation θ (degrees)
(a)
Settlement s (mm)
0
-10
-20
-30
-40
-50
-60
Rotation θ (degrees)
(b)
Lateral Base Displacement u (mm)
15
10
5
0
-5
-10
-15
0
20
40
60
Time (sec)
(c)
Experimental Data
BNWF Mesh Simulation

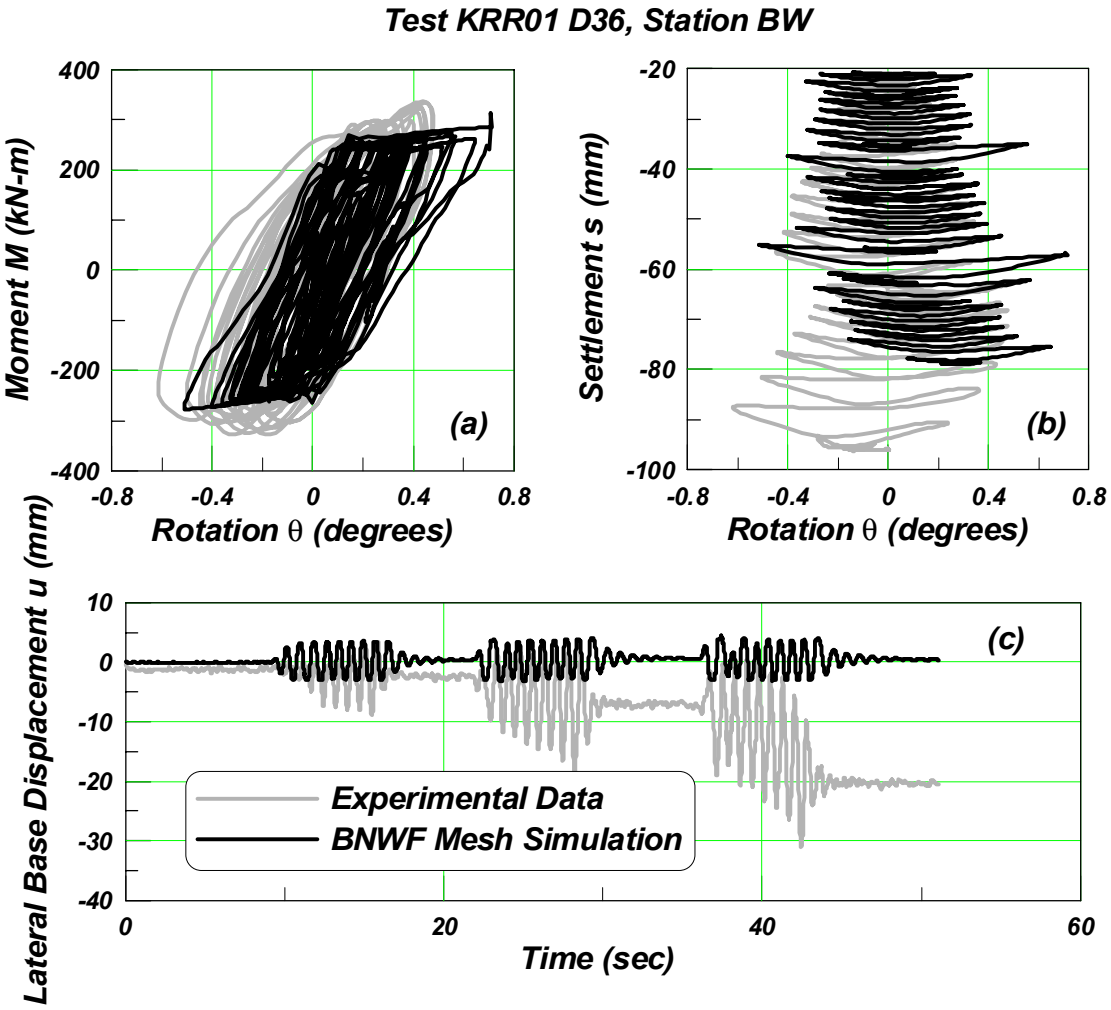
Test KRR01 D36, Station BW
Moment M (kN-m)
400
200
0
-200
-400
-0.8
-0.4
0
0.4
0.8
Rotation θ (degrees)
(a)
Settlement s (mm)
-20
-40
-60
-80
-100
Rotation θ (degrees)
(b)
Lateral Base Displacement u (mm)
10
0
-10
-20
-30
-40
0
20
40
60
Time (sec)
(c)
Experimental Data
BNWF Mesh Simulation

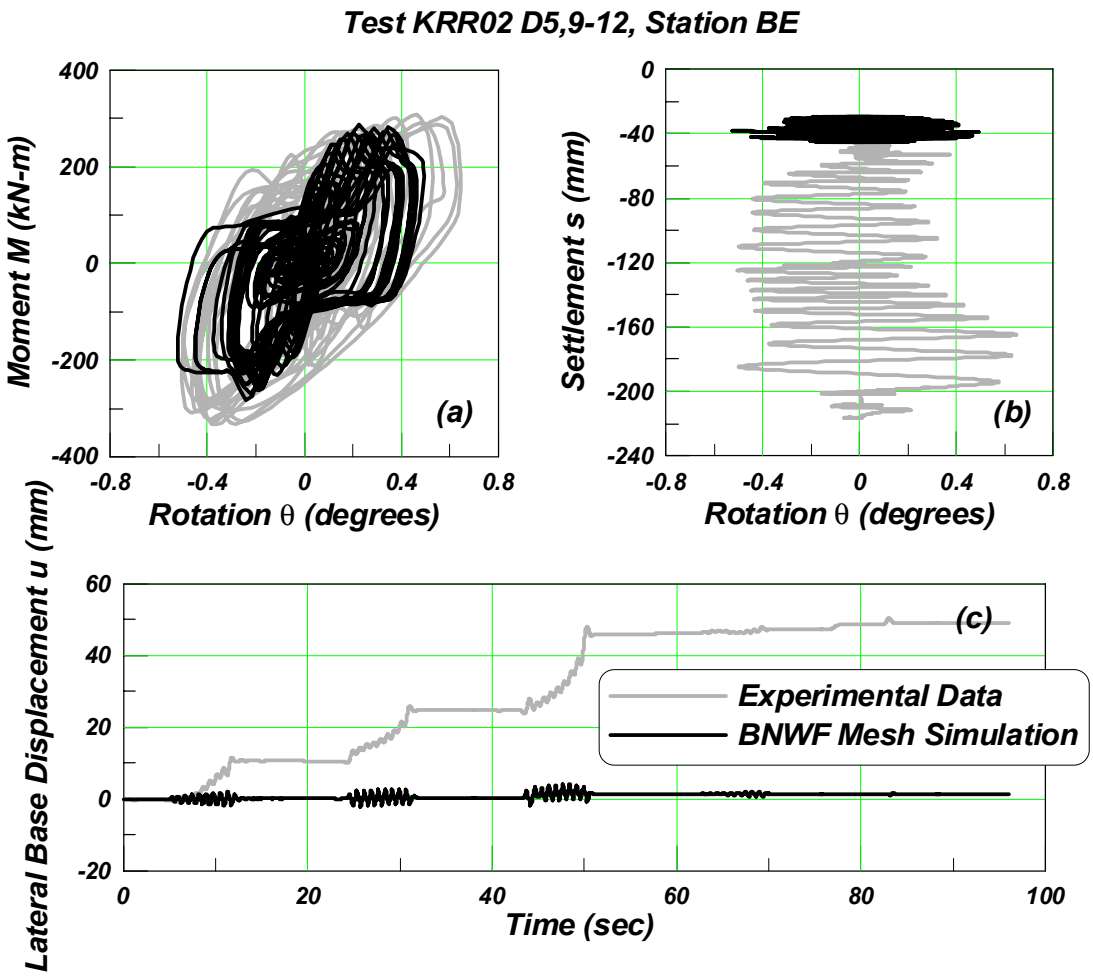
Test KRR02 D5,9-12, Station BE
Moment M (kN-m)
400
200
0
-200
-400
-0.8
-0.4
0
0.4
0.8
Rotation θ (degrees)
(a)
Settlement s (mm)
0
-40
-80
-120
-160
-200
-240
-0.8
-0.4
0
0.4
0.8
Rotation θ (degrees)
(b)
Lateral Base Displacement u (mm)
60
40
20
0
-20
0
20
40
60
80
100
Time (sec)
(c)
Experimental Data
BNWF Mesh Simulation

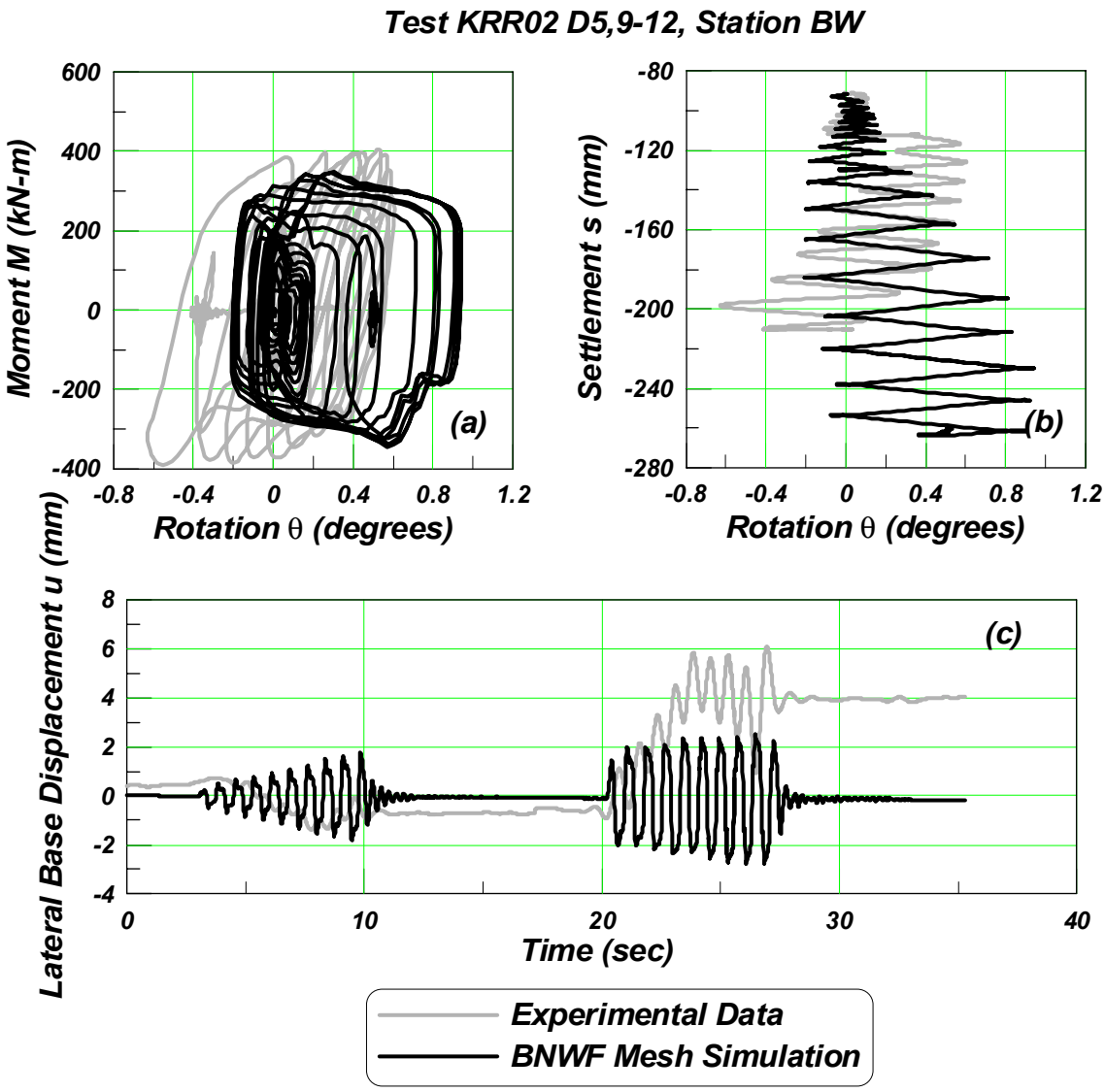
Test KRR02 D5,9-12, Station BW
Moment M (kN-m)
600
400
200
0
-200
-400
-0.8
-0.4
0
0.4
0.8
1.2
Rotation θ (degrees)
(a)
Settlement s (mm)
-80
-120
-160
-200
-240
-280
Rotation θ (degrees)
(b)
Lateral Base Displacement u (mm)
8
6
4
2
0
-2
-4
0
10
20
30
40
Time (sec)
(c)
Experimental Data
BNWF Mesh Simulation

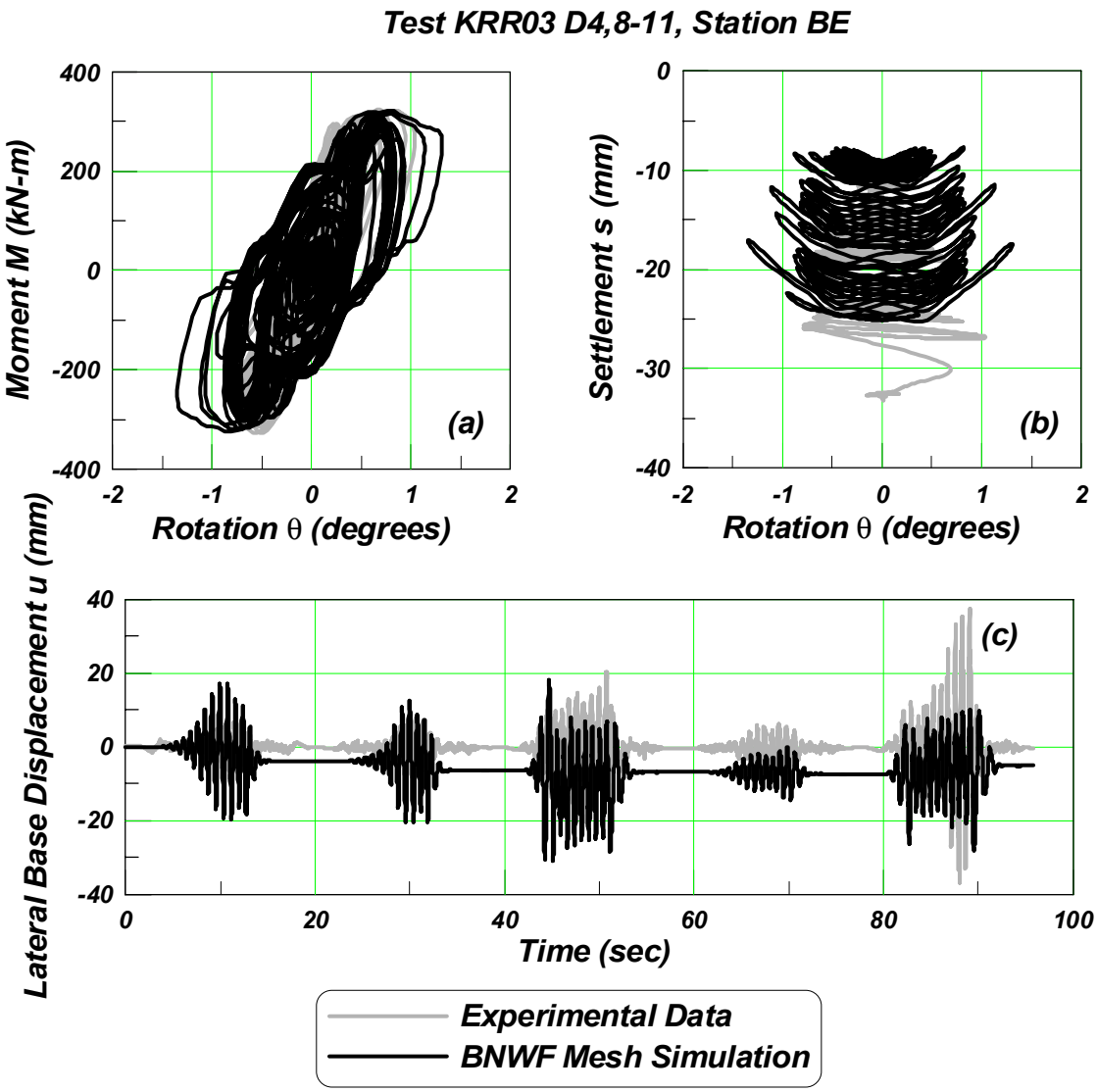
Test KRR03 D4,8-11, Station BE
Moment M (kN-m)
400
200
0
-200
-400
-2
-1
0
1
2
Rotation θ (degrees)
(a)
Settlement s (mm)
0
-10
-20
-30
-40
-2
-1
0
1
2
Rotation θ (degrees)
(b)
Lateral Base Displacement u (mm)
40
20
0
-20
-40
0
20
40
60
80
100
Time (sec)
(c)
Experimental Data
BNWF Mesh Simulation

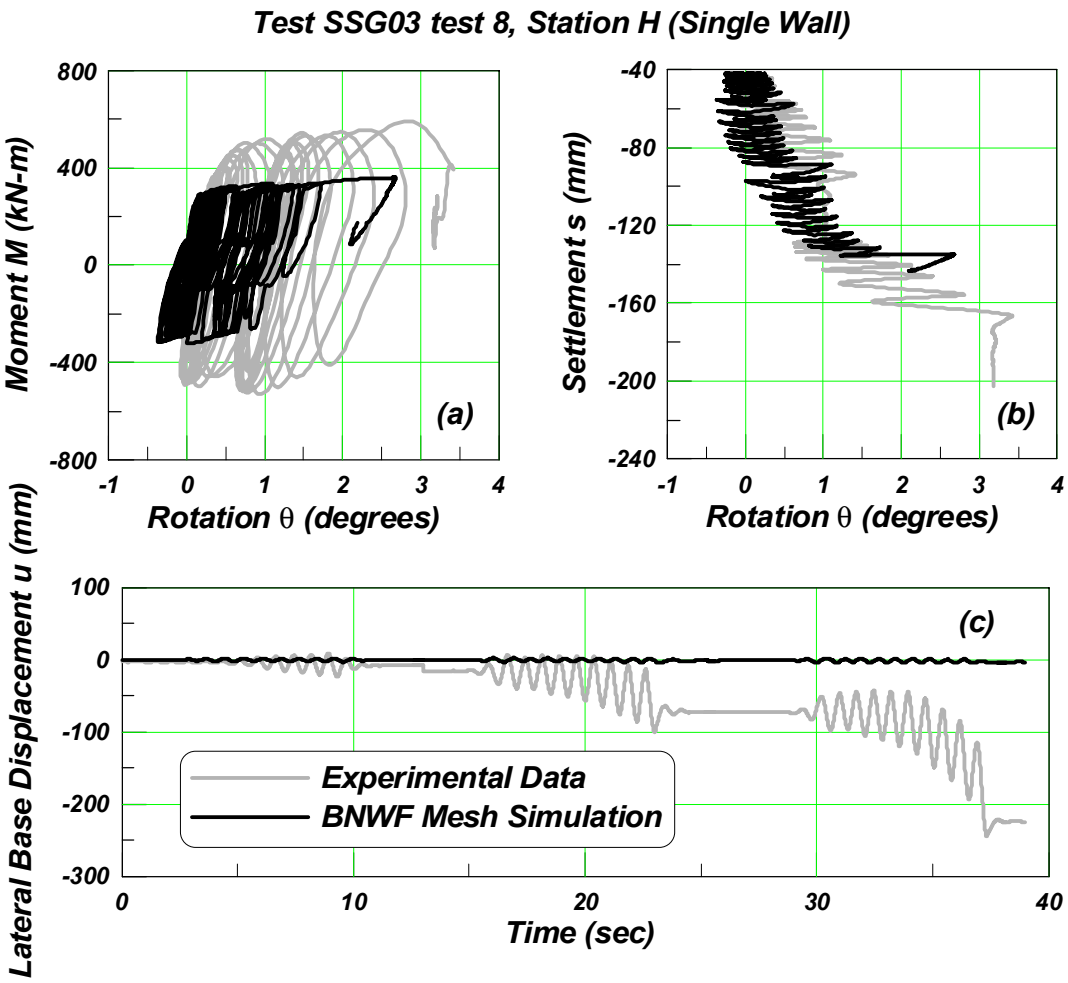
Test SSG03 test 8, Station H (Single Wall)
Moment M (kN-m)
800
400
0
-400
-800
-1
0
1
2
3
4
Rotation θ (degrees)
(a)
Settlement s (mm)
-40
-80
-120
-160
-200
-240
Rotation θ (degrees)
(b)
Lateral Base Displacement u (mm)
100
0
-100
-200
-300
0
10
20
30
40
Time (sec)
(c)
Experimental Data
BNWF Mesh Simulation

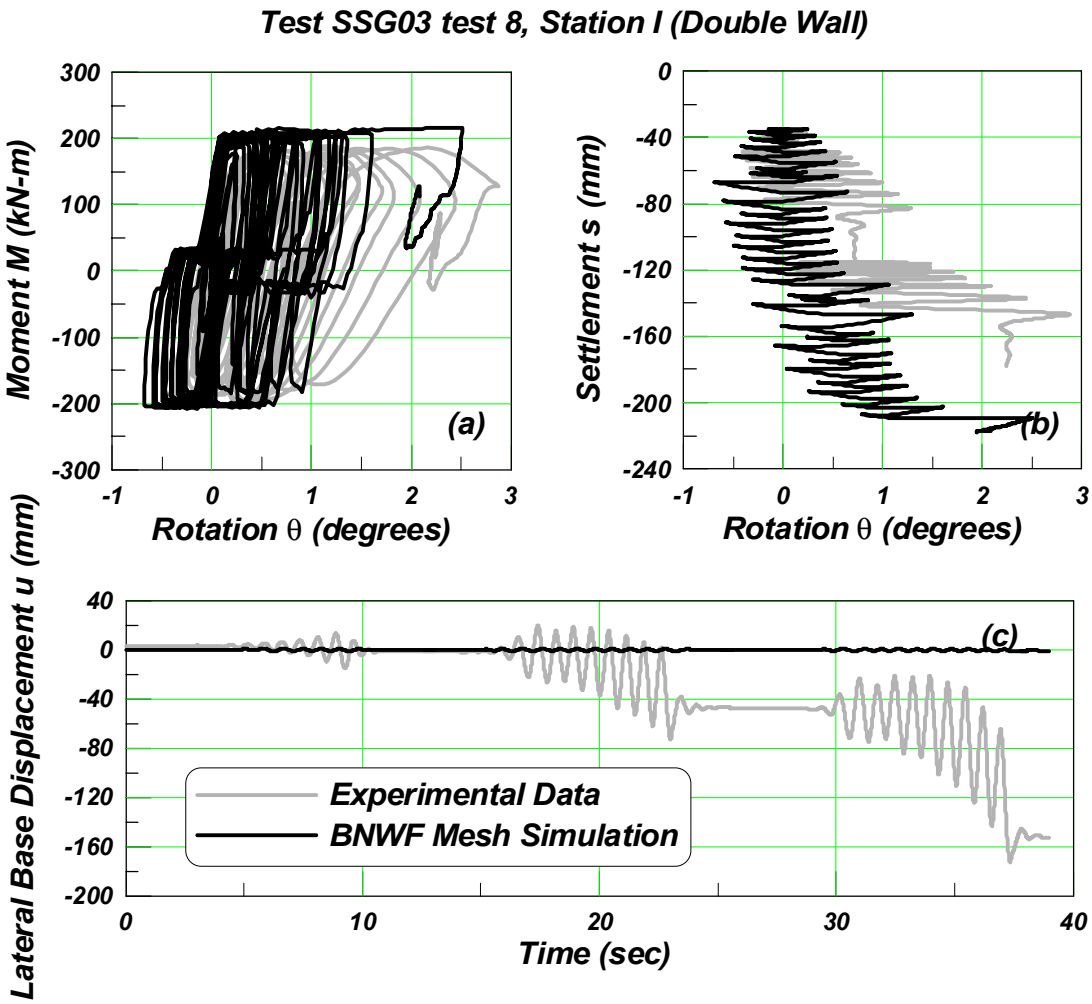
Test SSG03 test 8, Station I (Double Wall)
Moment M (kN-m)
Rotation θ (degrees)
(a)
Settlement s (mm)
Rotation θ (degrees)
(b)
Lateral Base Displacement u (mm)
Time (sec)
(c)
Experimental Data
BNWF Mesh Simulation

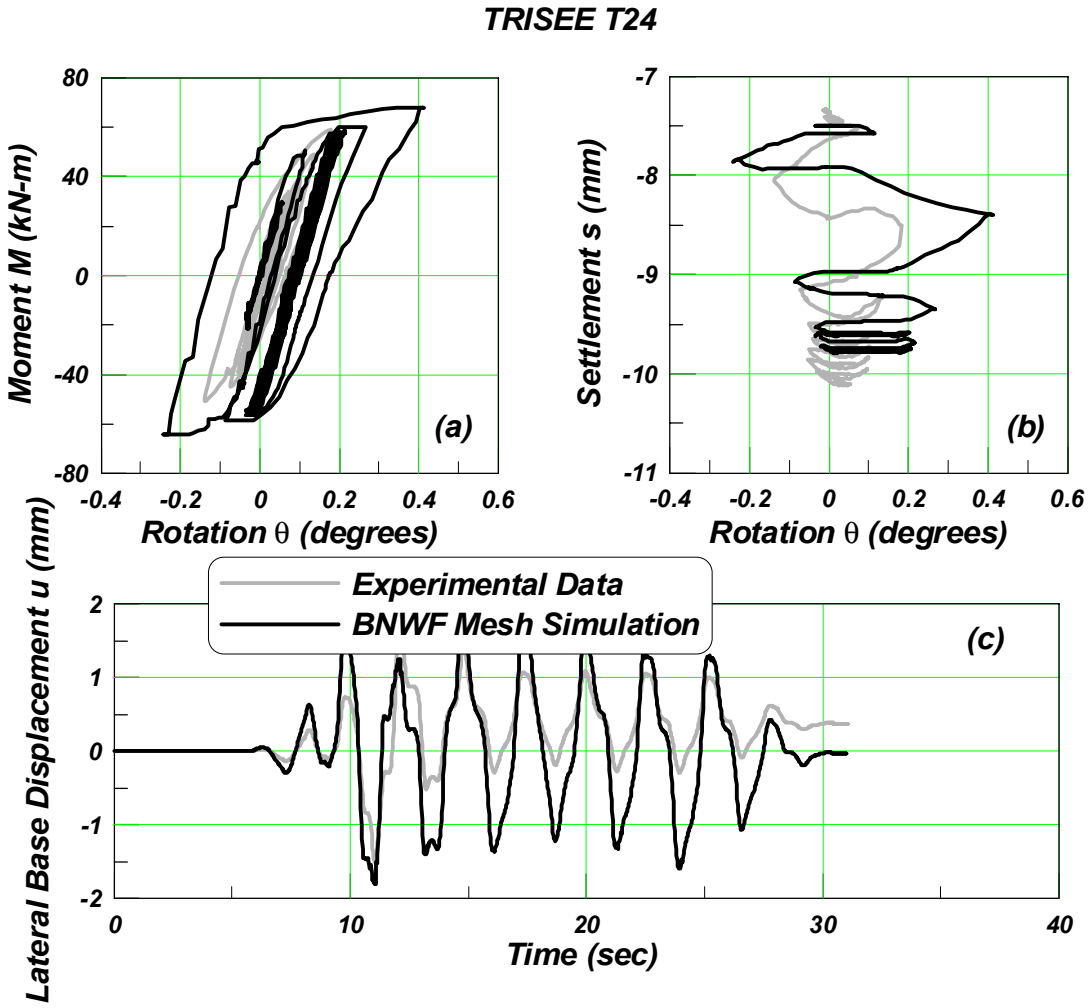
TRISEE T24
Moment M (kN-m)
80
40
0
-40
-80
-0.4
-0.2
0
0.2
0.4
0.6
Rotation θ (degrees)
(a)
Settlement s (mm)
-7
-8
-9
-10
-11
Rotation θ (degrees)
(b)
Experimental Data
BNWF Mesh Simulation
Lateral Base Displacement u (mm)
2
1
0
-1
-2
0
10
20
30
40
Time (sec)
(c)

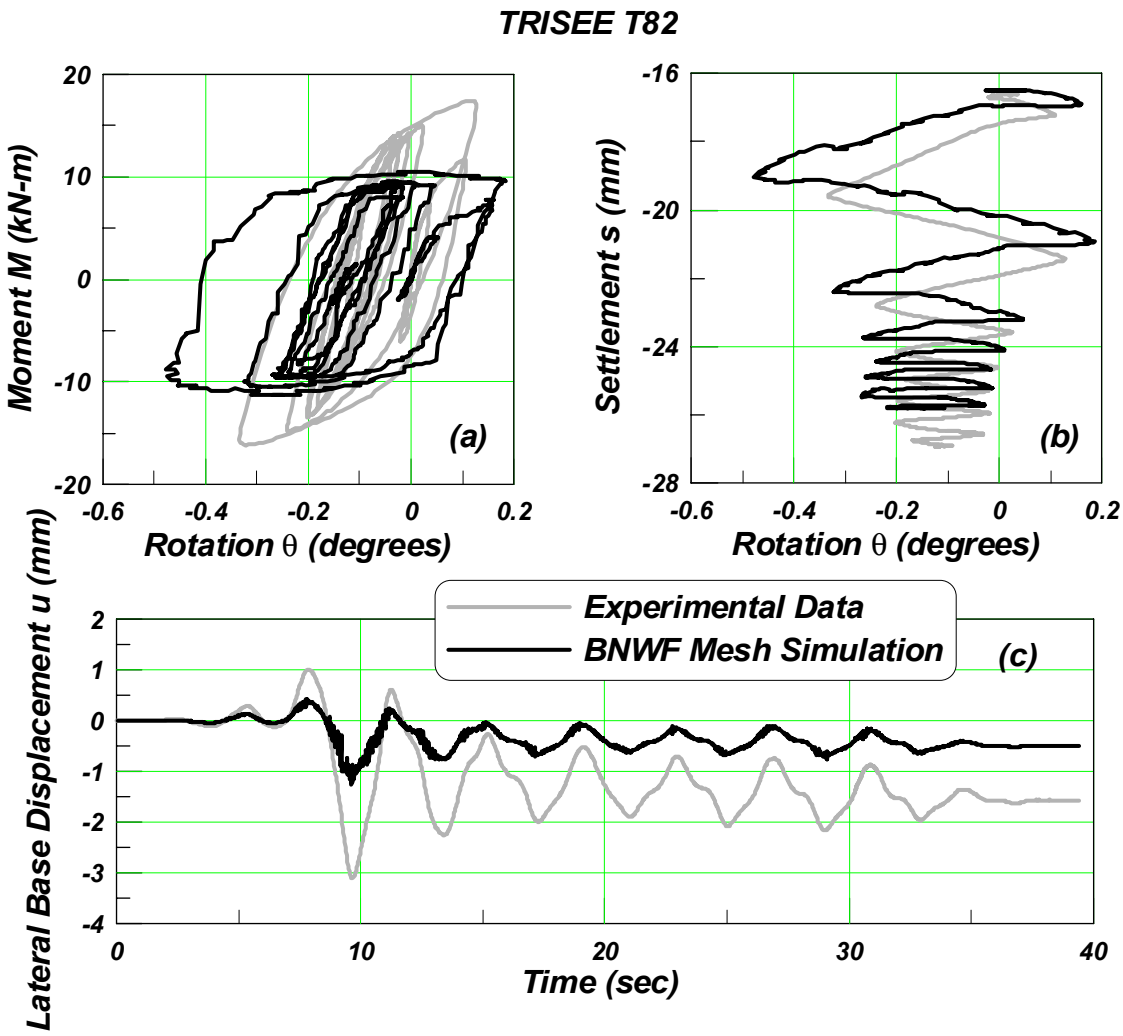
TRISEE T82
Moment M (kN-m)
20
10
0
-10
-20
-0.6
-0.4
-0.2
0
0.2
Rotation θ (degrees)
(a)
Settlement s (mm)
-16
-20
-24
-28
-0.6
-0.4
-0.2
0
0.2
Rotation θ (degrees)
(b)
Lateral Base Displacement u (mm)
Experimental Data
BNWF Mesh Simulation
(c)
2
1
0
-1
-2
-3
-4
0
10
20
30
40
Time (sec)

Appendix D Ground Motion Characteristics for Code Parameters Study

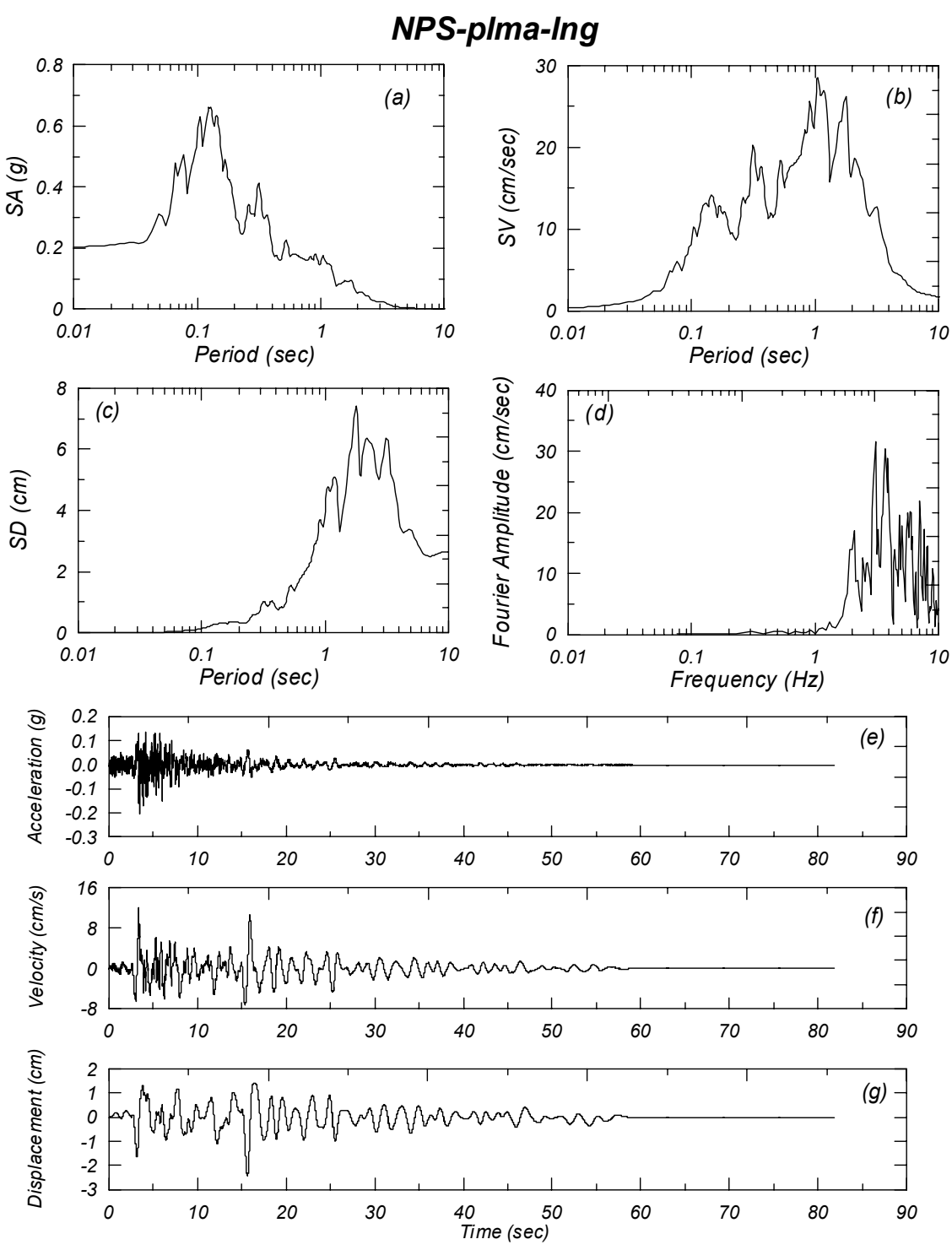

ζ = 5% response spectrum for (a) acceleration, (b) velocity and (c) displacement, (d) Fourier spectrum. Time histories for (e) acceleration, (f) velocity, and (g) displacement.

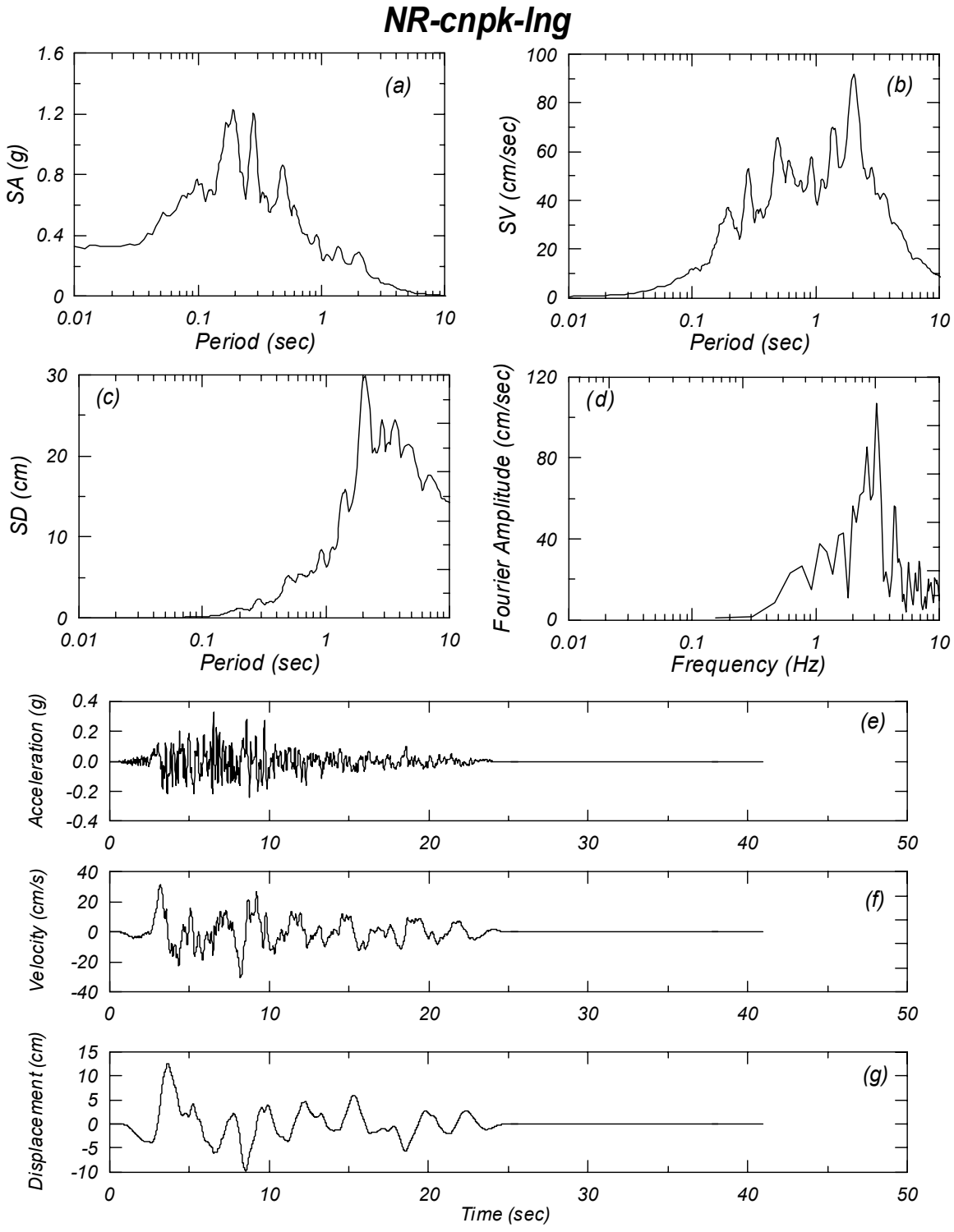

ζ = 5% response spectrum for (a) acceleration, (b) velocity and (c) displacement, (d) Fourier spectrum. Time histories for (e) acceleration, (f) velocity, and (g) displacement.

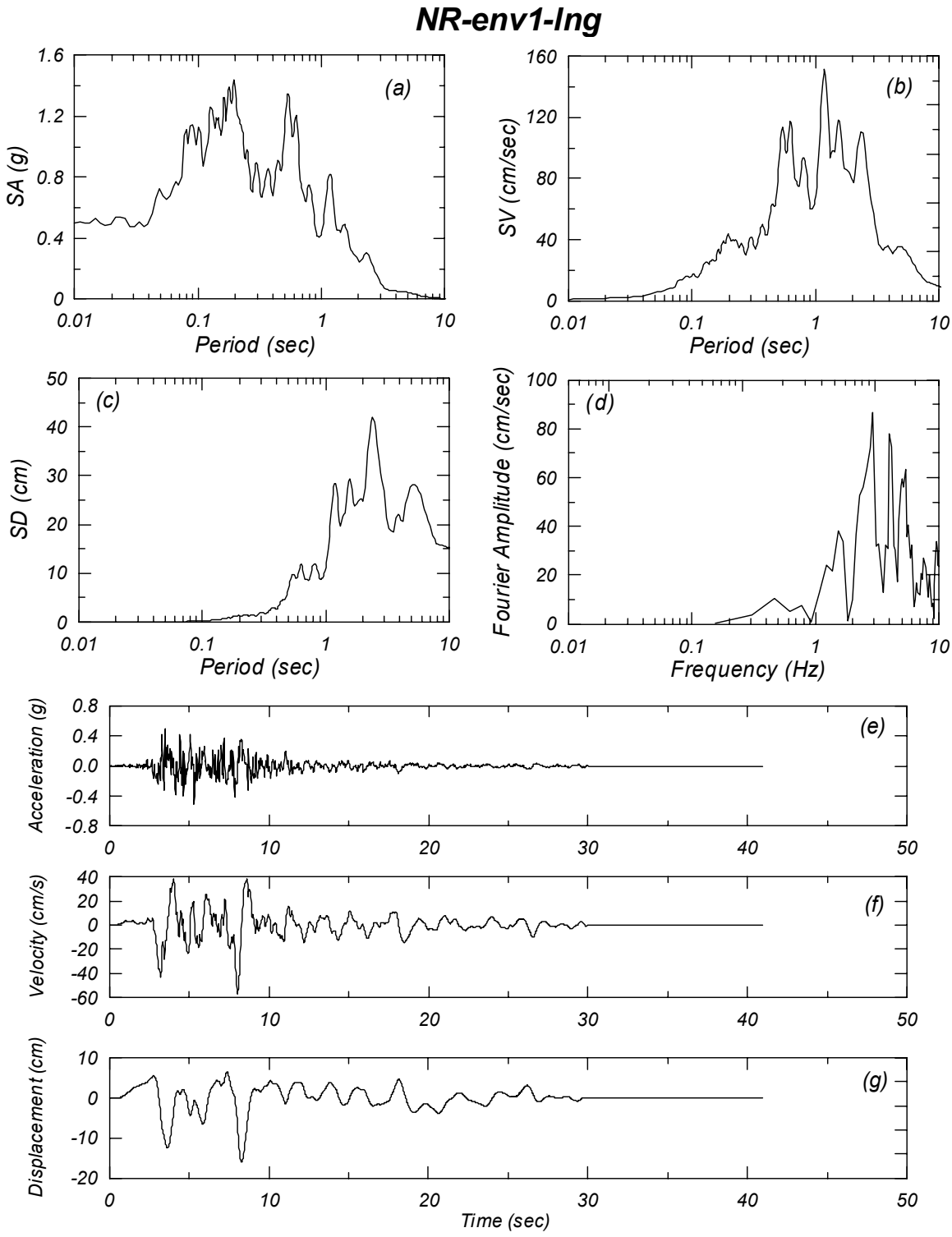

ζ = 5% response spectrum for (a) acceleration, (b) velocity and (c) displacement, (d) Fourier spectrum. Time histories for (e) acceleration, (f) velocity, and (g) displacement.

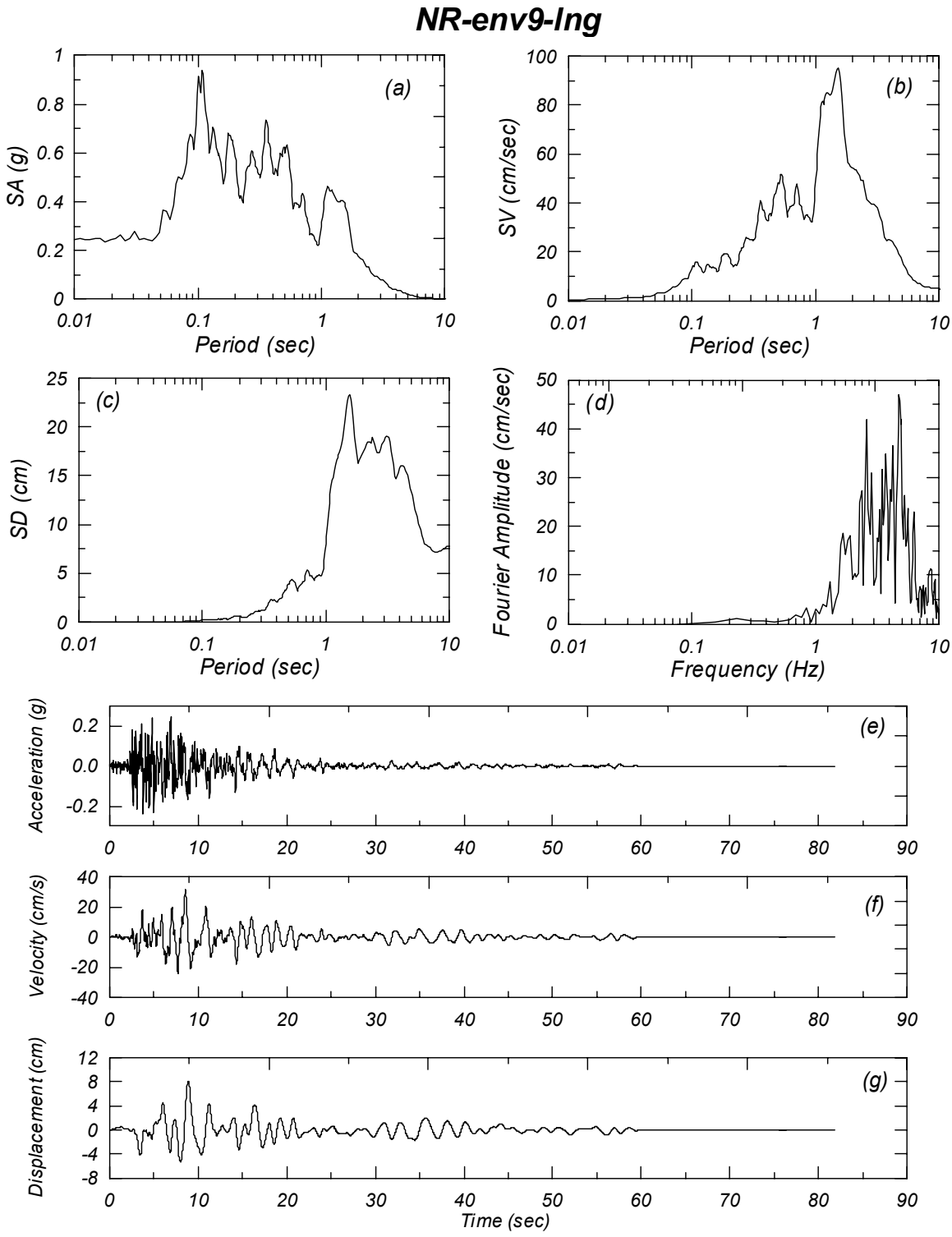

ζ = 5% response spectrum for (a) acceleration, (b) velocity and (c) displacement, (d) Fourier spectrum. Time histories for (e) acceleration, (f) velocity, and (g) displacement.

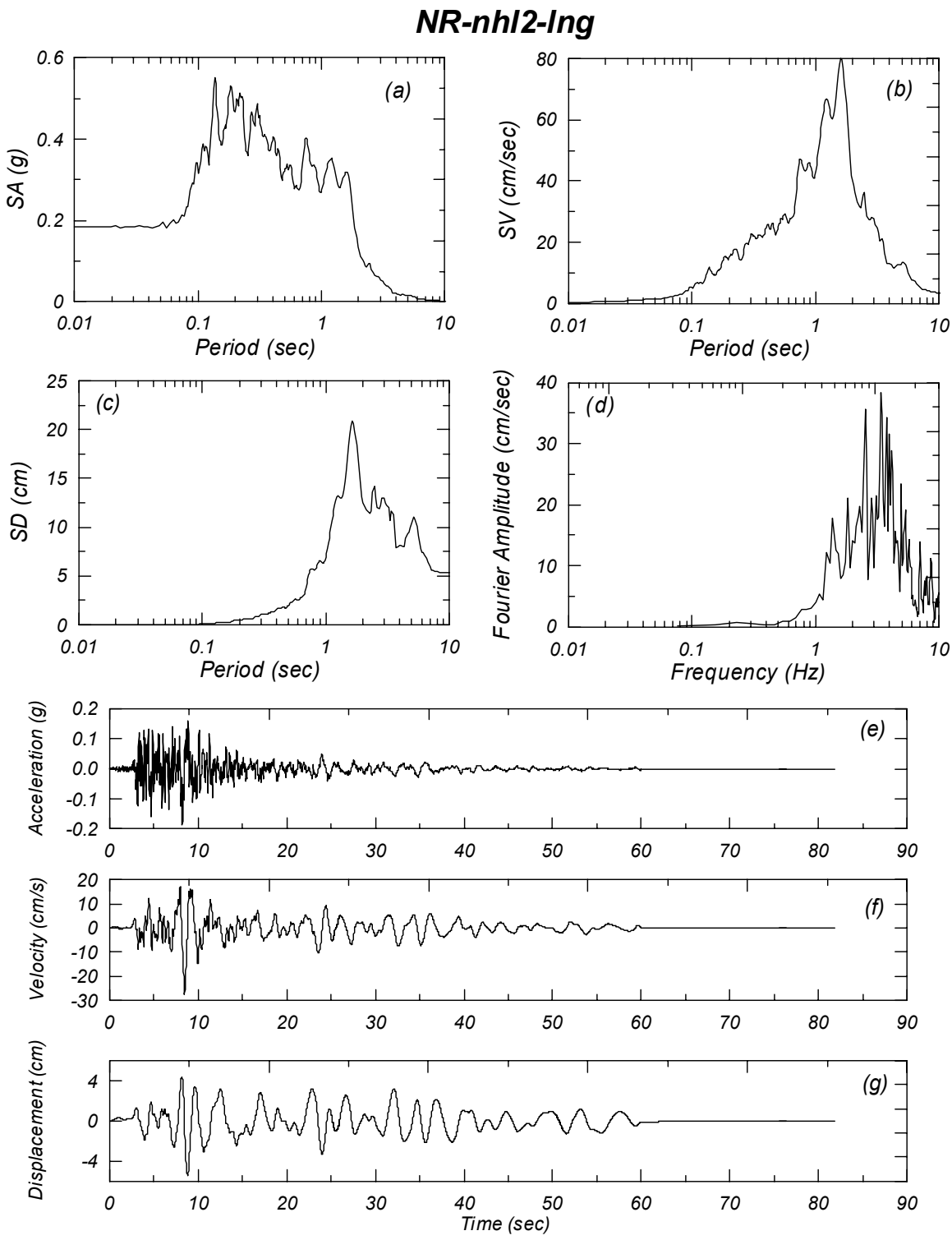

ζ = 5% response spectrum for (a) acceleration, (b) velocity and (c) displacement, (d) Fourier spectrum. Time histories for (e) acceleration, (f) velocity, and (g) displacement.

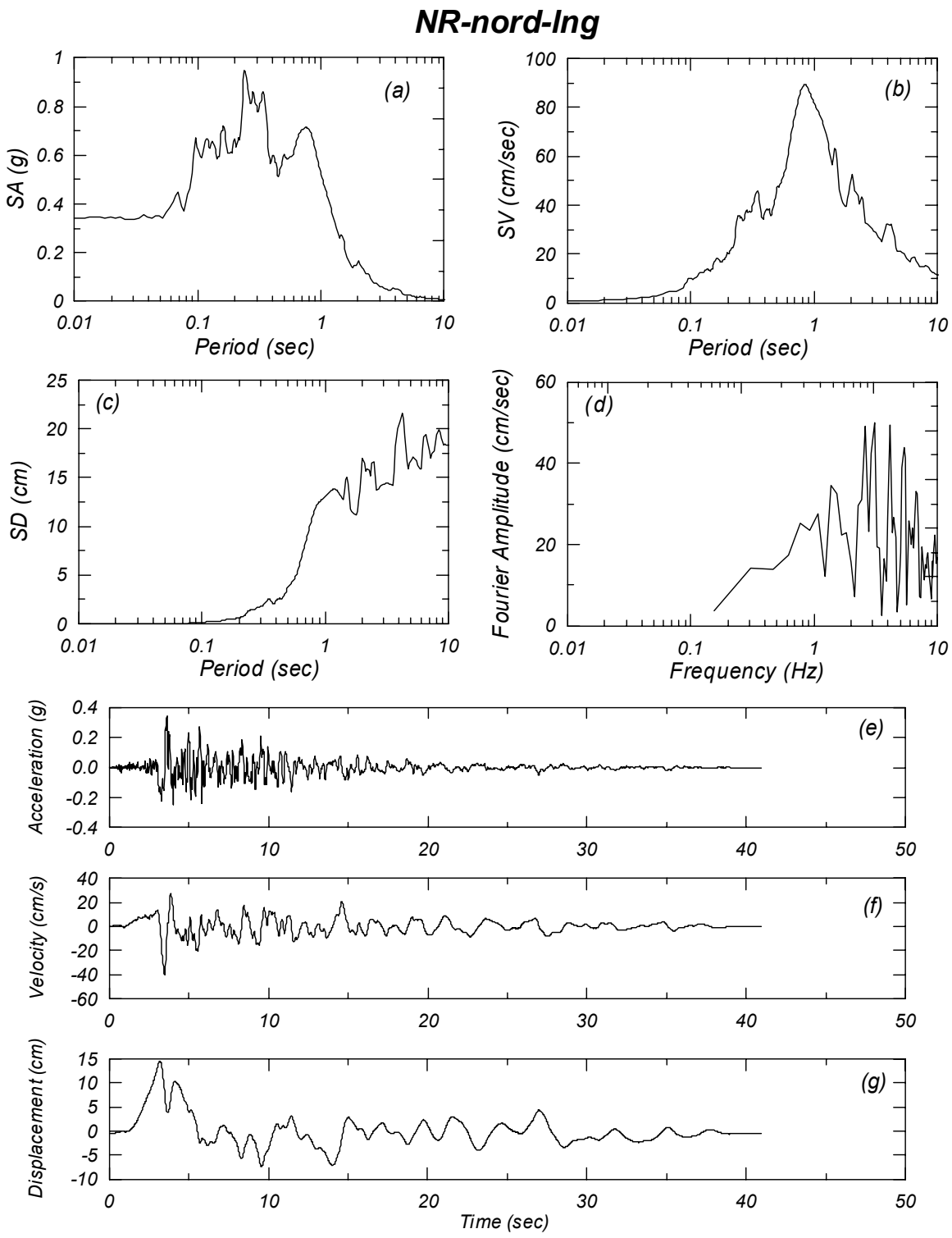

ζ = 5% response spectrum for (a) acceleration, (b) velocity and (c) displacement, (d) Fourier spectrum. Time histories for (e) acceleration, (f) velocity, and (g) displacement.

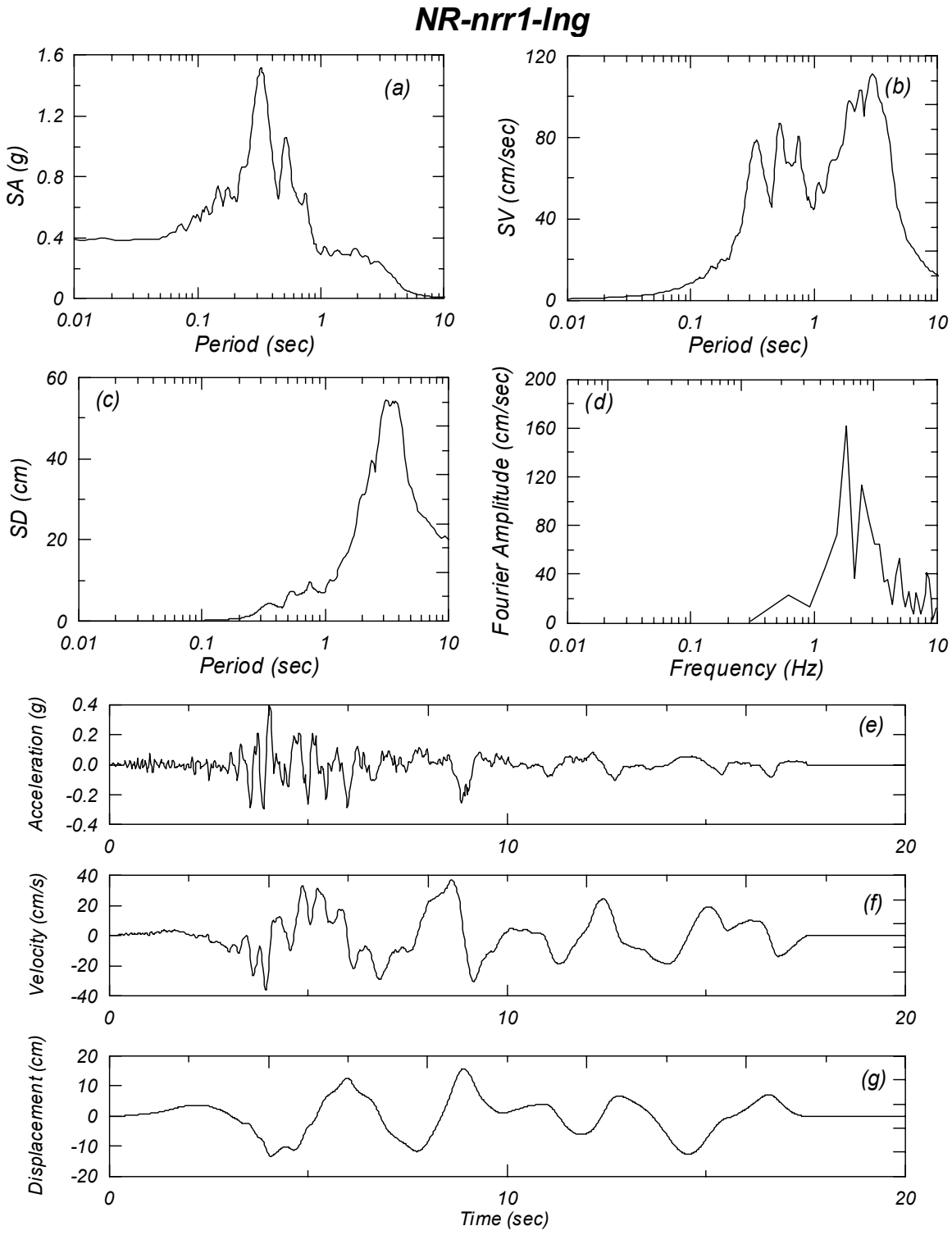

ζ = 5% response spectrum for (a) acceleration, (b) velocity and (c) displacement, (d) Fourier spectrum. Time histories for (e) acceleration, (f) velocity and (g) displacement.

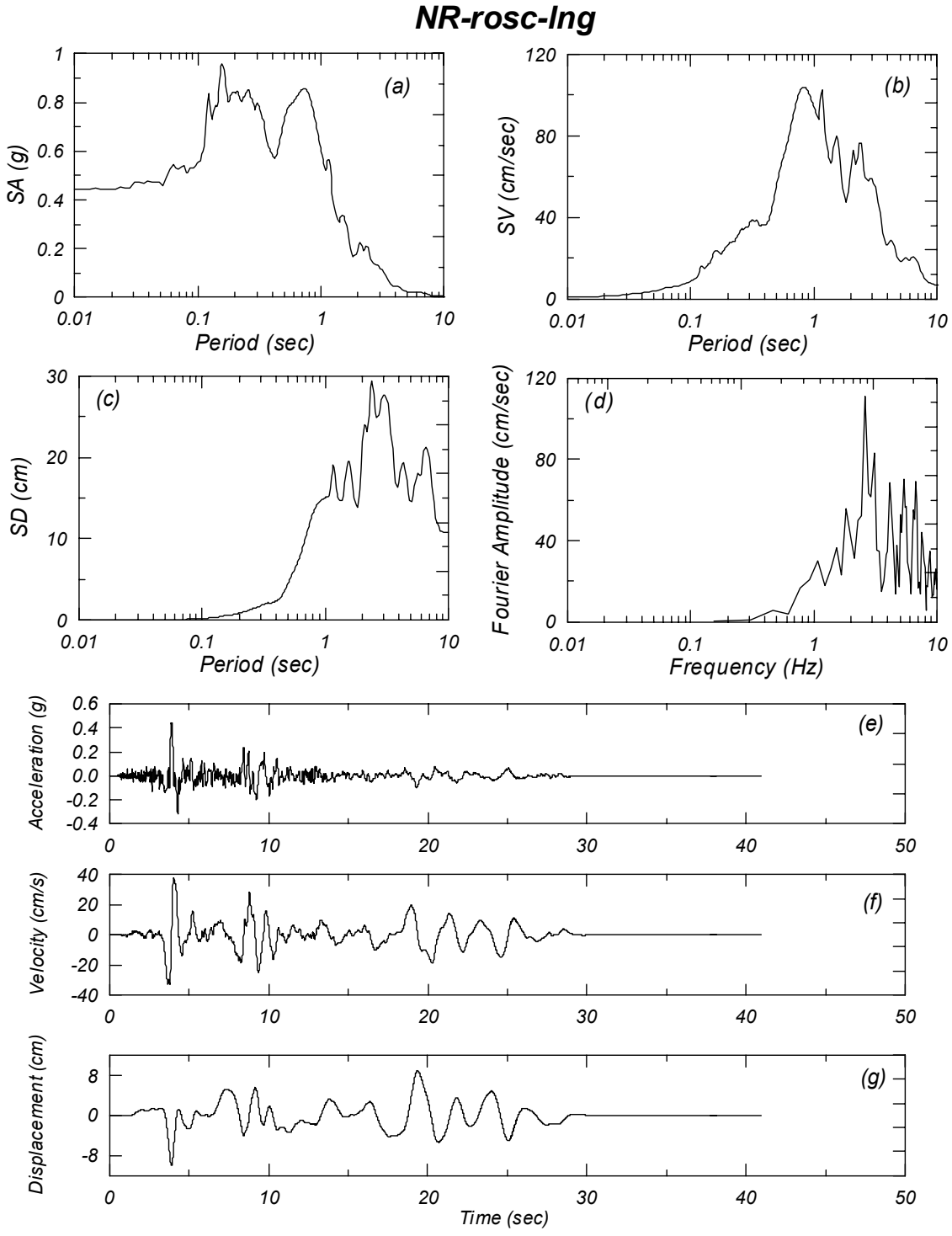

ζ = 5% response spectrum for (a) acceleration, (b) velocity and (c) displacement, (d) Fourier spectrum. Time histories for (e) acceleration, (f) velocity and (g) displacement.

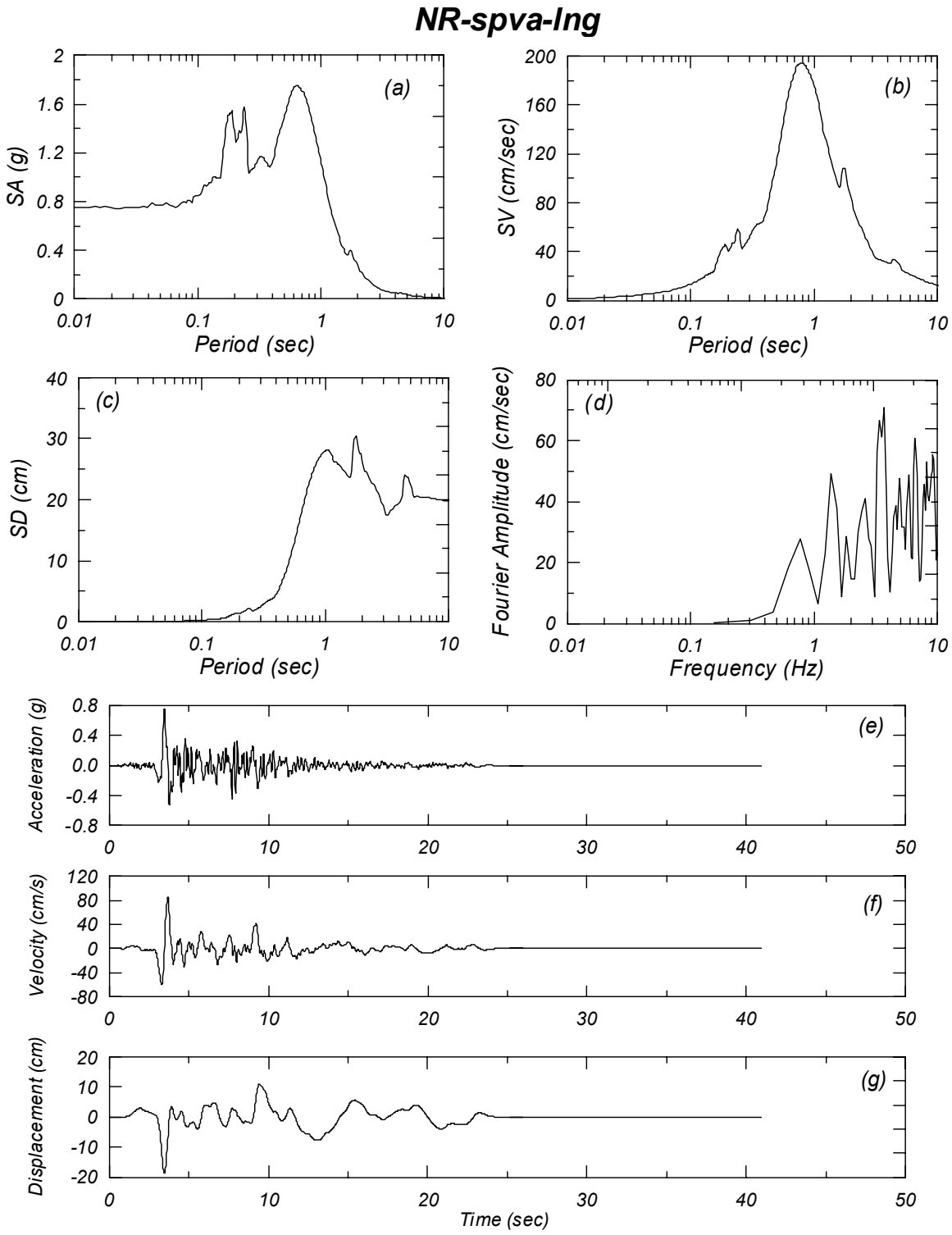

ζ = 5% response spectrum for (a) acceleration, (b) velocity and (c) displacement, (d) Fourier spectrum. Time histories for (e) acceleration, (f) velocity and (g) displacement.

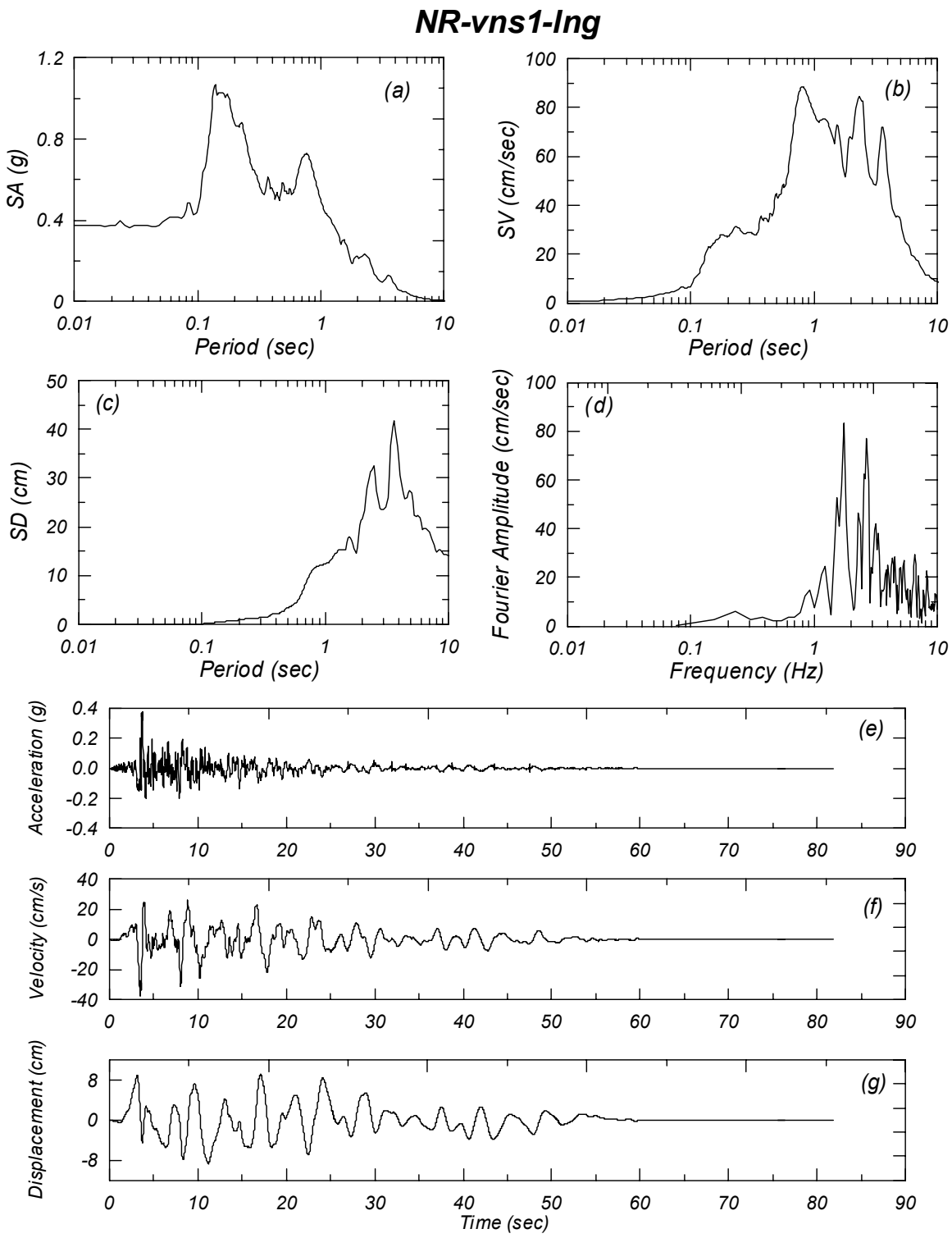

ζ = 5% response spectrum for (a) acceleration, (b) velocity and (c) displacement, (d) Fourier spectrum. Time histories for (e) acceleration, (f) velocity and (g) displacement.

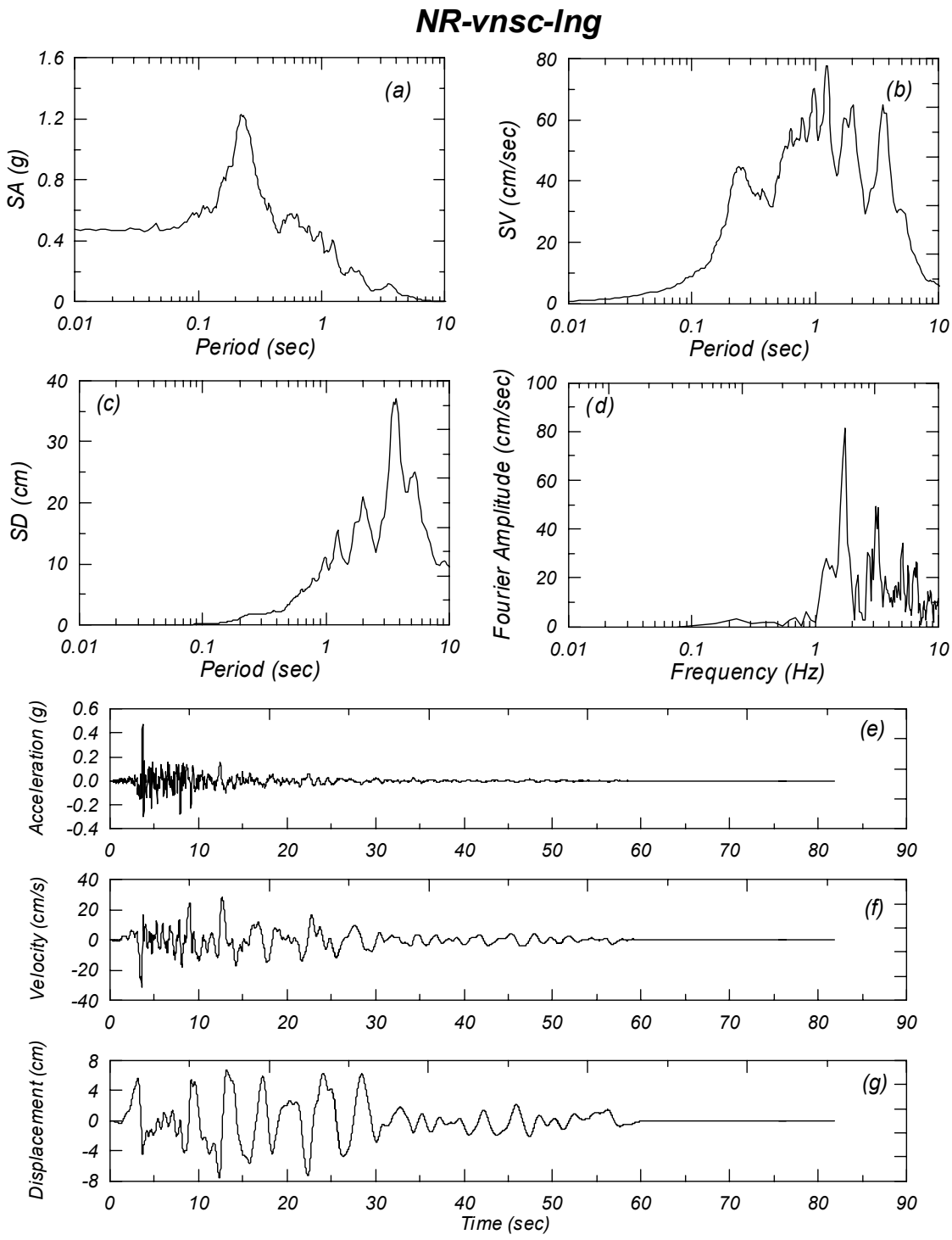

ζ = 5% response spectrum for (a) acceleration, (b) velocity and (c) displacement, (d) Fourier spectrum. Time histories for (e) acceleration, (f) velocity and (g) displacement.

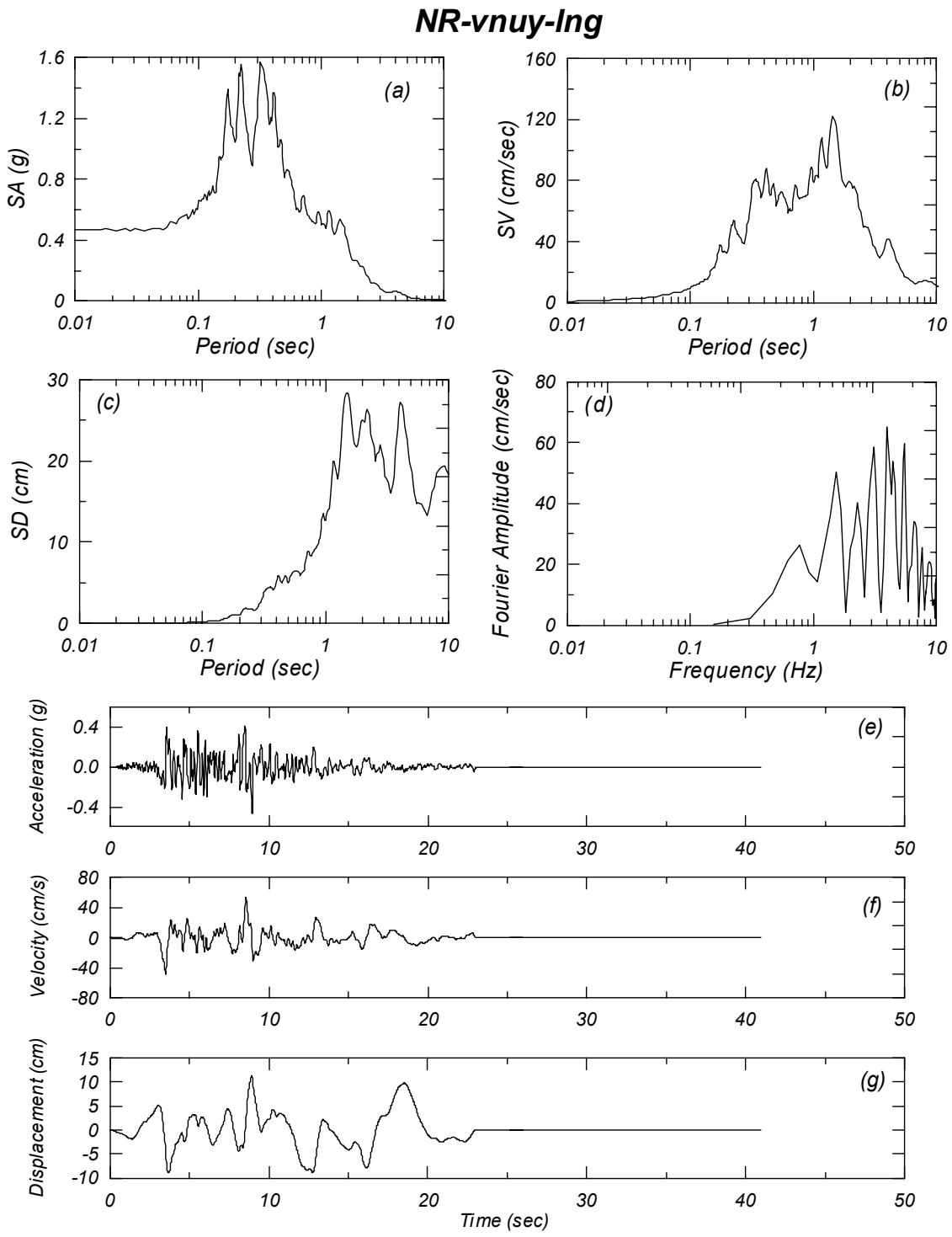

ζ = 5% response spectrum for (a) acceleration, (b) velocity and (c) displacement, (d) Fourier spectrum. Time histories for (e) acceleration, (f) velocity and (g) displacement.

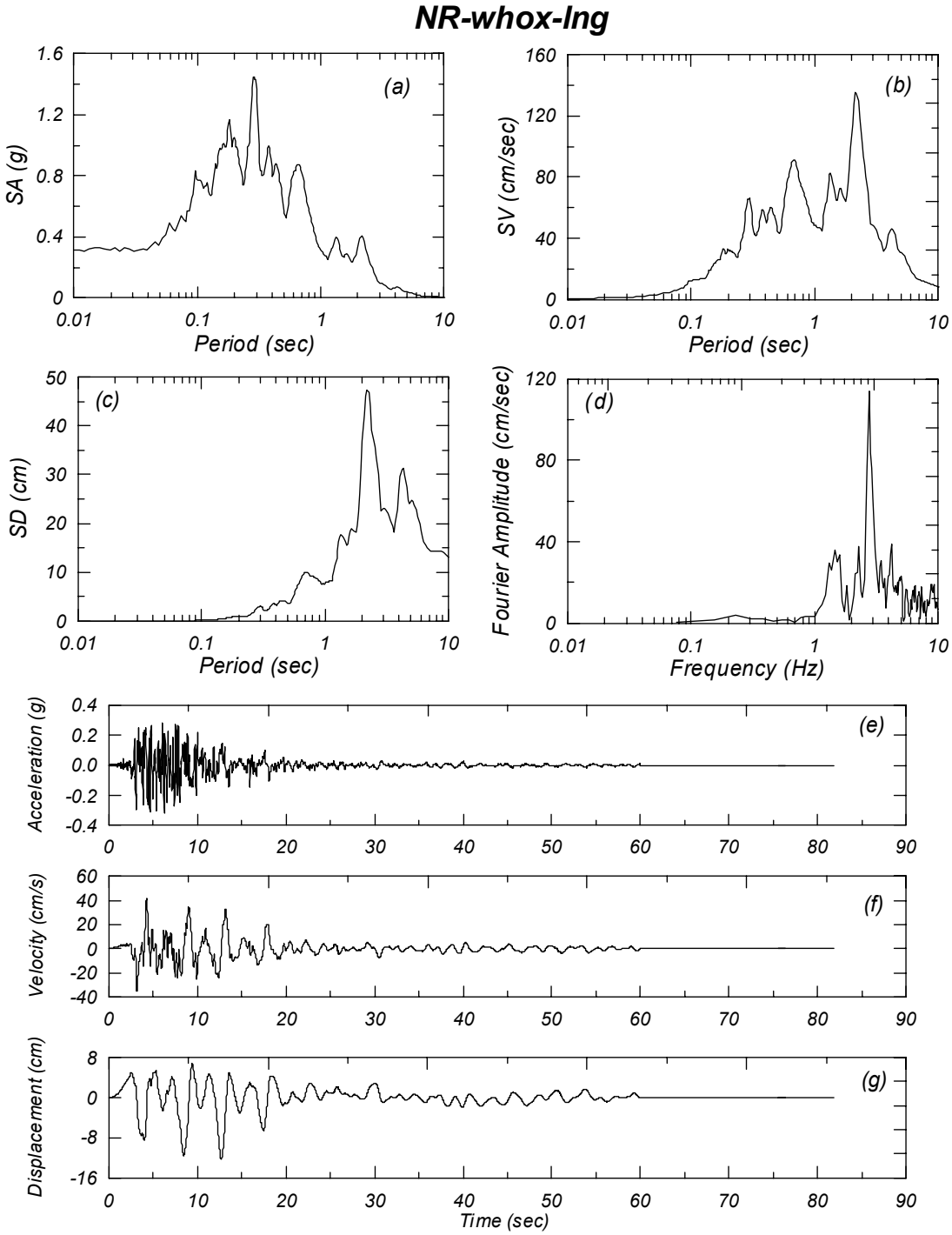

ζ = 5% response spectrum for (a) acceleration, (b) velocity and (c) displacement, (d) Fourier spectrum. Time histories for (e) acceleration, (f) velocity and (g) displacement.

PEER REPORTS

PEER reports are available from the National Information Service for Earthquake Engineering (NISEE). To order PEER reports, please contact the Pacific Earthquake Engineering Research Center, 1301 South 46th Street, Richmond, California 94804-4698. Tel.: (510) 231-9468; Fax: (510) 231-9 461.

PEER 2005/12 *PEER Testbed Study on a Laboratory Building: Exercising Seismic Performance Assessment.* Mary C. Comerio, editor. November 2005.

PEER 2005/11 *Van Nuys Hotel Building Testbed Report: Exercising Seismic Performance Assessment.* Helmut Krawinkler, editor. October 2005.

PEER 2005/10 *First NEES/E-Defense Workshop on Collapse Simulation of Reinforced Concrete Building Structures.* September 2005.

PEER 2005/06 *Global Collapse of Frame Structures under Seismic Excitations*. Luis F. Ibarra and Helmut Krawinkler. September 2005.

PEER 2005/04 *Numerical Modeling of the Nonlinear Cyclic Response of Shallow Foundations.* Chad Harden, Tara Hutchinson, Geoffrey R. Martin, and Bruce Kutter. August. 2005.

PEER 2005/02 *Fragility Basis for California Highway Overpass Bridge Seismic Decision Making*. Kevin R. Mackie and Bozidar Stojadinovic. June 2005.

PEER 2005/01 *Empirical Characterization of Site Conditions on Strong Ground Motion.* Jonathan P. Stewart, Yoojoong Choi, and Robert W. Graves. June 2005.

PEER 2004/09 *Electrical Substation Equipment Interaction: Experimental Rigid Conductor Studies.* Christopher Stearns and André Filiatrault. February 2005.

PEER 2004/08 *Seismic Qualification and Fragility Testing of Line Break 550-kV Disconnect Switches.* Shakhzod M. Takhirov, Gregory L. Fenves, and Eric Fujisaki. January 2005.

PEER 2004/07 *Ground Motions for Earthquake Simulator Qualification of Electrical Substation Equipment.* Shakhzod M. Takhirov, Gregory L. Fenves, Eric Fujisaki, and Don Clyde. January 2005.

PEER 2004/06 *Performance-Based Regulation and Regulatory Regimes.* Peter J. May and Chris Koski. September 2004.

PEER 2004/05 *Performance-Based Seismic Design Concepts and Implementation: Proceedings of an International Workshop.* Peter Fajfar and Helmut Krawinkler, editors. September 2004.

PEER 2004/04 *Seismic Performance of an Instrumented Tilt-up Wall Building.* James C. Anderson and Vitelmo V. Bertero. July 2004.

PEER 2004/03 *Evaluation and Application of Concrete Tilt-up Assessment Methodologies.* Timothy Graf and James O. Malley. October 2004.

PEER 2004/02 *Analytical Investigations of New Methods for Reducing Residual Displacements of Reinforced Concrete Bridge Columns.* Junichi Sakai and Stephen A. Mahin. August 2004.

PEER 2004/01 *Seismic Performance of Masonry Buildings and Design Implications.* Kerri Anne Taeko Tokoro, James C. Anderson, and Vitelmo V. Bertero. February 2004.

PEER 2003/18 *Performance Models for Flexural Damage in Reinforced Concrete Columns.* Michael Berry and Marc Eberhard. August 2003.

PEER 2003/17 *Predicting Earthquake Damage in Older Reinforced Concrete Beam-Column Joints.* Catherine Pagni and Laura Lowes. October 2004.

PEER 2003/16 *Seismic Demands for Performance-Based Design of Bridges.* Kevin Mackie and Božidar Stojadinovic. August 2003.

PEER 2003/15 *Seismic Demands for Nondeteriorating Frame Structures and Their Dependence on Ground Motions.* Ricardo Antonio Medina and Helmut Krawinkler. May 2004.

PEER 2003/14 *Finite Element Reliability and Sensitivity Methods for Performance-Based Earthquake Engineering.* Terje Haukaas and Armen Der Kiureghian. April 2004.

PEER 2003/13 *Effects of Connection Hysteretic Degradation on the Seismic Behavior of Steel Moment-Resisting Frames.* Janise E. Rodgers and Stephen A. Mahin. March 2004.

PEER 2003/12 *Implementation Manual for the Seismic Protection of Laboratory Contents: Format and Case Studies.* William T. Holmes and Mary C. Comerio. October 2003.

PEER 2003/11 *Fifth U.S.-Japan Workshop on Performance-Based Earthquake Engineering Methodology for Reinforced Concrete Building Structures.* February 2004.

PEER 2003/10 *A Beam-Column Joint Model for Simulating the Earthquake Response of Reinforced Concrete Frames.* Laura N. Lowes, Nilanjan Mitra, and Arash Altoontash. February 2004.

PEER 2003/09 *Sequencing Repairs after an Earthquake: An Economic Approach.* Marco Casari and Simon J. Wilkie. April 2004.

PEER 2003/08 *A Technical Framework for Probability-Based Demand and Capacity Factor Design (DCFD) Seismic Formats*. Fatemeh Jalayer and C. Allin Cornell. November 2003.

PEER 2003/07 *Uncertainty Specification and Propagation for Loss Estimation Using FOSM Methods.* Jack W. Baker and C. Allin Cornell. September 2003.

PEER 2003/06 *Performance of Circular Reinforced Concrete Bridge Columns under Bidirectional Earthquake Loading*. Mahmoud M. Hachem, Stephen A. Mahin, and Jack P. Moehle. February 2003.

PEER 2003/05 *Response Assessment for Building-Specific Loss Estimation.* Eduardo Miranda and Shahram Taghavi. September 2003.

PEER 2003/04 *Experimental Assessment of Columns with Short Lap Splices Subjected to Cyclic Loads*. Murat Melek, John W. Wallace, and Joel Conte. April 2003.

PEER 2003/03 *Probabilistic Response Assessment for Building-Specific Loss Estimation.* Eduardo Miranda and Hesameddin Aslani. September 2003.

PEER 2003/02 *Software Framework for Collaborative Development of Nonlinear Dynamic Analysis Program.* Jun Peng and Kincho H. Law. September 2003.

PEER 2003/01 *Shake Table Tests and Analytical Studies on the Gravity Load Collapse of Reinforced Concrete Frames.* Kenneth John Elwood and Jack P. Moehle. November 2003.

PEER 2002/24 *Performance of Beam to Column Bridge Joints Subjected to a Large Velocity Pulse.* Natalie Gibson, André Filiatrault, and Scott A. Ashford. April 2002.

PEER 2002/23 *Effects of Large Velocity Pulses on Reinforced Concrete Bridge Columns.* Greg L. Orozco and Scott A. Ashford. April 2002.

PEER 2002/22 *Characterization of Large Velocity Pulses for Laboratory Testing.* Kenneth E. Cox and Scott A. Ashford. April 2002.

PEER 2002/21 *Fourth U.S.-Japan Workshop on Performance-Based Earthquake Engineering Methodology for Reinforced Concrete Building Structures*. December 2002.

PEER 2002/20 *Barriers to Adoption and Implementation of PBEE Innovations.* Peter J. May. August 2002.

PEER 2002/19 *Economic-Engineered Integrated Models for Earthquakes: Socioeconomic Impacts.* Peter Gordon, James E. Moore II, and Harry W. Richardson. July 2002.

PEER 2002/18 *Assessment of Reinforced Concrete Building Exterior Joints with Substandard Details.* Chris P. Pantelides, Jon Hansen, Justin Nadauld, and Lawrence D. Reaveley. May 2002.

PEER 2002/17 *Structural Characterization and Seismic Response Analysis of a Highway Overcrossing Equipped with Elastomeric Bearings and Fluid Dampers: A Case Study.* Nicos Makris and Jian Zhang. November 2002.

PEER 2002/16 *Estimation of Uncertainty in Geotechnical Properties for Performance-Based Earthquake Engineering.* Allen L. Jones, Steven L. Kramer, and Pedro Arduino. December 2002.

PEER 2002/15 *Seismic Behavior of Bridge Columns Subjected to Various Loading Patterns.* Asadollah Esmaeily-Gh. and Yan Xiao. December 2002.

PEER 2002/14 *Inelastic Seismic Response of Extended Pile Shaft Supported Bridge Structures.* T.C. Hutchinson, R.W. Boulanger, Y.H. Chai, and I.M. Idriss. December 2002.

PEER 2002/13 *Probabilistic Models and Fragility Estimates for Bridge Components and Systems.* Paolo Gardoni, Armen Der Kiureghian, and Khalid M. Mosalam. June 2002.

PEER 2002/12 *Effects of Fault Dip and Slip Rake on Near-Source Ground Motions: Why Chi-Chi Was a Relatively Mild M7.6 Earthquake.* Brad T. Aagaard, John F. Hall, and Thomas H. Heaton. December 2002.

PEER 2002/11 *Analytical and Experimental Study of Fiber-Reinforced Strip Isolators*. James M. Kelly and Shakhzod M. Takhirov. September 2002.

PEER 2002/10 *Centrifuge Modeling of Settlement and Lateral Spreading with Comparisons to Numerical Analyses***.** Sivapalan Gajan and Bruce L. Kutter. January 2003.

PEER 2002/09 *Documentation and Analysis of Field Case Histories of Seismic Compression during the 1994 Northridge, California, Earthquake.* Jonathan P. Stewart, Patrick M. Smith, Daniel H. Whang, and Jonathan D. Bray. October 2002.

PEER 2002/08 *Component Testing, Stability Analysis and Characterization of Buckling-Restrained Unbonded Braces™.* Cameron Black, Nicos Makris, and Ian Aiken. September 2002.

PEER 2002/07 *Seismic Performance of Pile-Wharf Connections.* Charles W. Roeder, Robert Graff, Jennifer Soderstrom, and Jun Han Yoo. December 2001.

PEER 2002/06 *The Use of Benefit-Cost Analysis for Evaluation of Performance-Based Earthquake Engineering Decisions*. Richard O. Zerbe and Anthony Falit-Baiamonte. September 2001.

PEER 2002/05 *Guidelines, Specifications, and Seismic Performance Characterization of Nonstructural Building Components and Equipment*. André Filiatrault, Constantin Christopoulos, and Christopher Stearns. September 2001.

PEER 2002/04 *Consortium of Organizations for Strong-Motion Observation Systems and the Pacific Earthquake Engineering Research Center Lifelines Program: Invited Workshop on Archiving and Web Dissemination of Geotechnical Data, 4–5 October 2001*. September 2002.

PEER 2002/03 *Investigation of Sensitivity of Building Loss Estimates to Major Uncertain Variables for the Van Nuys Testbed.* Keith A. Porter, James L. Beck, and Rustem V. Shaikhutdinov. August 2002.

PEER 2002/02 *The Third U.S.-Japan Workshop on Performance-Based Earthquake Engineering Methodology for Reinforced Concrete Building Structures*. July 2002.

PEER 2002/01 *Nonstructural Loss Estimation: The UC Berkeley Case Study.* Mary C. Comerio and John C. Stallmeyer. December 2001.

PEER 2001/16 *Statistics of SDF-System Estimate of Roof Displacement for Pushover Analysis of Buildings.* Anil K. Chopra, Rakesh K. Goel, and Chatpan Chintanapakdee. December 2001.

PEER 2001/15 *Damage to Bridges during the 2001 Nisqually Earthquake.* R. Tyler Ranf, Marc O. Eberhard, and Michael P. Berry. November 2001.

PEER 2001/14 *Rocking Response of Equipment Anchored to a Base Foundation.* Nicos Makris and Cameron J. Black. September 2001.

PEER 2001/13 *Modeling Soil Liquefaction Hazards for Performance-Based Earthquake Engineering.* Steven L. Kramer and Ahmed-W. Elgamal. February 2001.

PEER 2001/12 *Development of Geotechnical Capabilities in OpenSees.* Boris Jeremi . September 2001.

PEER 2001/11 *Analytical and Experimental Study of Fiber-Reinforced Elastomeric Isolators*. James M. Kelly and Shakhzod M. Takhirov. September 2001.

PEER 2001/10 *Amplification Factors for Spectral Acceleration in Active Regions.* Jonathan P. Stewart, Andrew H. Liu, Yoojoong Choi, and Mehmet B. Baturay. December 2001.

PEER 2001/09 *Ground Motion Evaluation Procedures for Performance-Based Design.* Jonathan P. Stewart, Shyh-Jeng Chiou, Jonathan D. Bray, Robert W. Graves, Paul G. Somerville, and Norman A. Abrahamson. September 2001.

PEER 2001/08 *Experimental and Computational Evaluation of Reinforced Concrete Bridge Beam-Column Connections for Seismic Performance*. Clay J. Naito, Jack P. Moehle, and Khalid M. Mosalam. November 2001.

PEER 2001/07 *The Rocking Spectrum and the Shortcomings of Design Guidelines.* Nicos Makris and Dimitrios Konstantinidis. August 2001.

PEER 2001/06 *Development of an Electrical Substation Equipment Performance Database for Evaluation of Equipment Fragilities*. Thalia Agnanos. April 1999.

PEER 2001/05 *Stiffness Analysis of Fiber-Reinforced Elastomeric Isolators.* Hsiang-Chuan Tsai and James M. Kelly. May 2001.

PEER 2001/04 *Organizational and Societal Considerations for Performance-Based Earthquake Engineering.* Peter J. May. April 2001.

PEER 2001/03 *A Modal Pushover Analysis Procedure to Estimate Seismic Demands for Buildings: Theory and Preliminary Evaluation.* Anil K. Chopra and Rakesh K. Goel. January 2001.

PEER 2001/02 *Seismic Response Analysis of Highway Overcrossings Including Soil-Structure Interaction.* Jian Zhang and Nicos Makris. March 2001.

PEER 2001/01 *Experimental Study of Large Seismic Steel Beam-to-Column Connections.* Egor P. Popov and Shakhzod M. Takhirov. November 2000.

PEER 2000/10 *The Second U.S.-Japan Workshop on Performance-Based Earthquake Engineering Methodology for Reinforced Concrete Building Structures.* March 2000.

PEER 2000/09 *Structural Engineering Reconnaissance of the August 17, 1999 Earthquake: Kocaeli (Izmit), Turkey.* Halil Sezen, Kenneth J. Elwood, Andrew S. Whittaker, Khalid Mosalam, John J. Wallace, and John F. Stanton. December 2000.

PEER 2000/08 *Behavior of Reinforced Concrete Bridge Columns Having Varying Aspect Ratios and Varying Lengths of Confinement.* Anthony J. Calderone, Dawn E. Lehman, and Jack P. Moehle. January 2001.

PEER 2000/07 *Cover-Plate and Flange-Plate Reinforced Steel Moment-Resisting Connections.* Taejin Kim, Andrew S. Whittaker, Amir S. Gilani, Vitelmo V. Bertero, and Shakhzod M. Takhirov. September 2000.

PEER 2000/06 *Seismic Evaluation and Analysis of 230-kV Disconnect Switches.* Amir S. J. Gilani, Andrew S. Whittaker, Gregory L. Fenves, Chun-Hao Chen, Henry Ho, and Eric Fujisaki. July 2000.

PEER 2000/05 *Performance-Based Evaluation of Exterior Reinforced Concrete Building Joints for Seismic Excitation.* Chandra Clyde, Chris P. Pantelides, and Lawrence D. Reaveley. July 2000.

PEER 2000/04 *An Evaluation of Seismic Energy Demand: An Attenuation Approach.* Chung-Che Chou and Chia-Ming Uang. July 1999.

PEER 2000/03 *Framing Earthquake Retrofitting Decisions: The Case of Hillside Homes in Los Angeles.* Detlof von Winterfeldt, Nels Roselund, and Alicia Kitsuse. March 2000.

PEER 2000/02 *U.S.-Japan Workshop on the Effects of Near-Field Earthquake Shaking.* Andrew Whittaker, ed. July 2000.

PEER 2000/01 *Further Studies on Seismic Interaction in Interconnected Electrical Substation Equipment.* Armen Der Kiureghian, Kee-Jeung Hong, and Jerome L. Sackman. November 1999.

PEER 1999/14 *Seismic Evaluation and Retrofit of 230-kV Porcelain Transformer Bushings*. Amir S. Gilani, Andrew S. Whittaker, Gregory L. Fenves, and Eric Fujisaki. December 1999.

PEER 1999/13 *Building Vulnerability Studies: Modeling and Evaluation of Tilt-up and Steel Reinforced Concrete Buildings.* John W. Wallace, Jonathan P. Stewart, and Andrew S. Whittaker, editors. December 1999.

PEER 1999/12 *Rehabilitation of Nonductile RC Frame Building Using Encasement Plates and Energy-Dissipating Devices.* Mehrdad Sasani, Vitelmo V. Bertero, James C. Anderson. December 1999.

PEER 1999/11 *Performance Evaluation Database for Concrete Bridge Components and Systems under Simulated Seismic Loads.* Yael D. Hose and Frieder Seible. November 1999.

PEER 1999/10 *U.S.-Japan Workshop on Performance-Based Earthquake Engineering Methodology for Reinforced Concrete Building Structures.* December 1999.

PEER 1999/09 *Performance Improvement of Long Period Building Structures Subjected to Severe Pulse-Type Ground Motions*. James C. Anderson, Vitelmo V. Bertero, and Raul Bertero. October 1999.

PEER 1999/08 *Envelopes for Seismic Response Vectors.* Charles Menun and Armen Der Kiureghian. July 1999.

PEER 1999/07 *Documentation of Strengths and Weaknesses of Current Computer Analysis Methods for Seismic Performance of Reinforced Concrete Members.* William F. Cofer. November 1999.

PEER 1999/06 *Rocking Response and Overturning of Anchored Equipment under Seismic Excitations.* Nicos Makris and Jian Zhang. November 1999.

PEER 1999/05 *Seismic Evaluation of 550 kV Porcelain Transformer Bushings.* Amir S. Gilani, Andrew S. Whittaker, Gregory L. Fenves, and Eric Fujisaki. October 1999.

PEER 1999/04 *Adoption and Enforcement of Earthquake Risk-Reduction Measures.* Peter J. May, Raymond J. Burby, T. Jens Feeley, and Robert Wood.

PEER 1999/03 *Task 3 Characterization of Site Response General Site Categories*. Adrian Rodriguez-Marek, Jonathan D. Bray, and Norman Abrahamson. February 1999.

PEER 1999/02 *Capacity-Demand-Diagram Methods for Estimating Seismic Deformation of Inelastic Structures: SDF Systems*. Anil K. Chopra and Rakesh Goel. April 1999.

PEER 1999/01 *Interaction in Interconnected Electrical Substation Equipment Subjected to Earthquake Ground Motions.* Armen Der Kiureghian, Jerome L. Sackman, and Kee-Jeung Hong. February 1999.

PEER 1998/08 *Behavior and Failure Analysis of a Multiple-Frame Highway Bridge in the 1994 Northridge Earthquake*. Gregory L. Fenves and Michael Ellery. December 1998.

PEER 1998/07 *Empirical Evaluation of Inertial Soil-Structure Interaction Effects.* Jonathan P. Stewart, Raymond B. Seed, and Gregory L. Fenves. November 1998.

PEER 1998/06 *Effect of Damping Mechanisms on the Response of Seismic Isolated Structures.* Nicos Makris and Shih-Po Chang. November 1998.

PEER 1998/05 *Rocking Response and Overturning of Equipment under Horizontal Pulse-Type Motions.* Nicos Makris and Yiannis Roussos. October 1998.

PEER 1998/04 *Pacific Earthquake Engineering Research Invitational Workshop Proceedings, May 14–15, 1998: Defining the Links between Planning, Policy Analysis, Economics and Earthquake Engineering.* Mary Comerio and Peter Gordon. September 1998.

PEER 1998/03 *Repair/Upgrade Procedures for Welded Beam to Column Connections.* James C. Anderson and Xiaojing Duan. May 1998.

PEER 1998/02 *Seismic Evaluation of 196 kV Porcelain Transformer Bushings.* Amir S. Gilani, Juan W. Chavez, Gregory L. Fenves, and Andrew S. Whittaker. May 1998.

PEER 1998/01 *Seismic Performance of Well-Confined Concrete Bridge Columns.* Dawn E. Lehman and Jack P. Moehle. December 2000.